SPECTRAL CHARACTERIZATION OF DIELECTRIC MATERIALS USING TERAHERTZ MEASUREMENT SYSTEMS

by

Jeffrey M. Seligman

A Dissertation Submitted to the Faculty of the

DEPARTMENT OF ELECTRICAL AND COMPUTER ENGINEERING

In Partial Fulfillment of the Requirements
For the Degree of

DOCTOR OF PHILSOPHY

In the Graduate College

THE UNIVERSITY OF ARIZONA

2015

THE UNIVERSITY OF ARIZONA
GRADUATE COLLEGE

As members of the Dissertation Committee, we certify that we have read the dissertation prepared by Jeffrey M. Seligman, titled Spectral Characterization of Dielectric Materials using Terahertz Measurements Systems and recommend that it be accepted as fulfilling the dissertation requirement for the Degree of Doctor of Philosophy.

_____ Date: May 28, 2015
Christopher K. Walker

_____ Date: May 28, 2015
Steven L. Dvorak

_____ Date: May 28, 2015
Ben K. Sternberg

_____ Date: May 28, 2015
Olgierd A. Palusinski

Final approval and acceptance of this dissertation is contingent upon the candidate's submission of the final copies of the dissertation to the Graduate College.

I hereby certify that I have read this dissertation prepared under my direction and recommend that it be accepted as fulfilling the dissertation requirement.

_____ Date: May 28, 2015
Dissertation Director: Christopher K. Walker

STATEMENT BY AUTHOR

This dissertation has been submitted in partial fulfillment of the requirements for an advanced degree at the University of Arizona and is deposited in the University Library to be made available to borrowers under rules of the Library.

Brief quotations from this dissertation are allowable without special permission, provided that an accurate acknowledgement of the source is made. Requests for permission for extended quotation from or reproduction of this manuscript in whole or in part may be granted by the head of the major department or the Dean of the Graduate College when in his or her judgment the proposed use of the material is in the interests of scholarship. In all other instances, however, permission must be obtained from the author.

SIGNED: Jeffrey M. Seligman

ACKNOWLEDGEMENTS

Writing this dissertation has been the most challenging experience of my life. It was a goal since my original graduate program was interrupted years ago and I was not able to return to complete it until now. I thank my Ph. D committee, the ECE and Astronomy Departments, and Tami Whelan, the ECE graduate coordinator. Thanks to my family, and my friends for supporting me in this effort. Special thanks to Prof. Walker for his project suggestion and his encouragement and guidance and to Steward Observatory for the use of their facilities. Thanks to Prof. Palusinski, Prof. Sternberg, and Prof. Dvorak for providing me with insight into the nature of materials and modern measurement and analysis techniques. Thanks to my staff members at the City of Tucson for their support. Thanks to Christopher Green who provided many hours of support.

The project was funded in part by Raytheon Missile Systems, a DURIP Grant, Rogers Incorporated, the UA Lunar & Planetary Laboratory, and the Arizona Research Laboratory. Thanks to my co-workers at the IT department at the City of Tucson.

Thanks to my industrial and academic affiliates for providing the equipment and resources needed to manufacture the test precision fixture and the samples for this project including the Steward Instrument Shop (Brian Love), Universal Cryogenics (Kirby Hnat, Paul Schickling and Mick), Prototron, Inc, and also to Prof. Jay Quade, UA Geosciences, and UA LPL staff for sample fabrication techniques. Jeff Hesler at Virginia Diodes Inc. provided the use of their THz measurement system, the UA College of Optical Sciences numerous resources, the UA UITS Research Computing Department for analysis support, the UA Physics Department for the use of their TDS system, and to Prof. Gehm, ECE Dept, for providing me with the polymer samples.

A big thanks to Prof. Lisa Zurk at the NEAR Lab, at Portland State University who gave me access to their high resolution T-Ray 4000 TDS and the THz VNA needed to obtain much of the data for this project. I was assisted there by Sam Henry and Gabe Kniffin.

Additional recognition to Dr.'s Craig Kulesa, William Peters, Mark Borgstrom, John McCloy, Prof. Gervasio, Prof. Murray Sargent, and also to Abe Young. Thanks to Mrs. Elsie Lamb, and Rob Kingston for their invaluable suggestions and assistance and to Jefferson Harman, Pima College, for his assistance modifying and aligning the optical control system for Beckman FTS machine.

MEMORIUM

It was an honor to work with the late Prof. Willis E. Lamb, Jr., UA Regents Professor, and Nobel Laureate. He was a confidant, a sponsor, and a friend. I would also like to honor the memory of Prof. John L. Prince, former Committee Chair, and Prof E. S. Gillespie, my M.S. Advisor, who encouraged me to pursue the program at the University of Arizona.

Table of Contents

Table of Figures

Table of Tables

ABSTRACT

The performance of modern high frequency components and electronic systems are often limited by the properties of the materials from which they are made. Over the past decade, there has been an increased emphasis on the development of new, high performance dielectrics for use in high frequency systems. The development of these materials requires novel broadband characterization, instrumentation, and extraction techniques, from which models can be formulated. For this project several types of dielectric sheets were characterized at terahertz (THz) frequencies using quasi-optical (free-space) techniques. These measurement systems included a Fourier Transform Spectrometer (FTS, scalar), a Time Domain Spectrometer (TDS, vector), a Scalar Network Analyzer (SNA), and a THz Vector Network Analyzer (VNA). Using these instruments the THz spectral characteristics of dielectric samples were obtained. Polarization based anisotropy was observed in many of the materials measured using vector systems. The TDS was the most informative and flexible instrument for dielectric characterization at THz frequencies. To our knowledge, this is the first such comprehensive study to be performed. Anisotropy effects within materials that do not come into play at microwave frequencies (e.g. ~10 GHz) were found, in many cases, to increase measured losses at THz frequencies by up to an order of magnitude.

The frequency dependent properties obtained during the course of this study included loss tangent, permittivity (index of refraction), and dielectric constant. The results were largely consistent between all the different systems and correlated closely to manufacturer specifications over a wide frequency range (325 GHz-1.5 THz). Anisotropic behavior was observed for some of the materials. Non-destructive evaluation and testing (NDE/NDT) techniques were used throughout. A precision test fixture was developed to accomplish these measurements. Time delay, insertion loss, and S-parameters were measured directly, from which loss tangent, index of refraction, and permittivity was extracted.

The test materials were low-loss dielectric slabs ranging in thickness from 1-60 mils. The substrate sheets were PTFE, fiberglass, and epoxy-ceramic composite substrates. The other group was polyethylene plastic sheets (LDPE/HDPE/UMHW) and 3D printer Photopolymers. The results were verified by using several online THz spectral databases and compared to manufacturer data sheets.

Permittivity and loss of some of the test samples varied as a function of polarization angle. 0 - 90 degrees of rotation were tested (i.e., H-V, and 45 degrees polarization). Inter-molecular scattering in the composite materials raised the loss considerably. This effect was verified. Standard, well documented, material types were selected for the project for best comparison. These techniques can also be applied to analyze newer substances such as nanodielectrics.

1. INTRODUCTION

The electrical properties of materials are key elements of any new system design. Dielectrics can be characterized using broadband analyzers or spectrographic systems, as was done in this project. There are also narrowband resonator type systems in use, such as those at the National Institute of Standards (NIST) and the Institute for Printed Circuits (IPC).

At lower frequencies, broadband material characteristics are observed using Vector Network Analyzers (VNA/PNA), Scalar Network Analyzers (SNA), or Material Analyzers (scalar, MNA). Some of these systems operate natively up to about 60 GHz and may use transmission line methods (broadband and narrowband), waveguides, or capacitive techniques. They rely on close coupling or direct contact with the material under test (MUT). Newer methods consider measuring negative permittivity materials.

Millimeter wave, sub-millimeter wave, and far infrared THz measurements are best done spatially using quasi-optical (non-contacting) spectrometers. These systems include Time Domain Spectrometers (TDS), Fourier Domain Transform Spectrometer/FTSIR, Vector (VNA) and Scalar Analyzers (SNA) with Frequency Extender Units. The analyzers used in this project all had frequency extenders made by Virginia Diodes, Inc., (VDI) Charlottesville, VA.

THz waves interact with the lattice, molecular, electronic structures, and physical imperfections (inhomogeneity) and, sometimes, regions of anomalous dispersion occur. Some of the test materials were found to have anisotropic characteristics for different wave polarizations.

The specific measurement systems used, included a Beckman Fourier Transform Spectrometer (FTS/FTIR), two different Picometrix Time Domain Spectrometers (TDS), a terahertz Vector Network Analyzer (a Rohde-Schwarz ZVA40 Analyzer with two different Virginia Diodes Extenders), and an experimental VDI Scalar THz sub-millimeter wave system (DURIP program).

The scalar analyzer was a Virginia Diodes custom standalone heterodyne system operating from 140-850 GHz (5 bands). It included a THz transmitter/up-converter and THz receiver/down-converter, a pair of synthesizers, a reference source, and a detector. The FTS system has a Michelson interferometer, broadband source, a lock-in amplifier, a cryogenically cooled silicon bolometer detector (IR Labs), and control software. The Vector Analyzer systems used a Rohde-Schwarz ZVA 40 network analyzer with two different VDI THz Extender Units, covering two bands, 325-500 GHz and 500-750 GHz.

The measurements were in the Transmission mode only. Calibration procedures for these different systems used combinations of Short-Open-Line-Through (SOLT), rather than Through-Reflect-Line (TRL), Through-Reflect-Match (TRM), or Gated-Reflect-Line

(GRL) techniques. This project also used a combination of waveguide SOLT calibration kits made by VDI. Both the VDI calibration and a free space calibration were done with shorts and open circuits.

The measurement range for the TDS was about 200GHz to 1.5 THz, and for the FTS, it was about 200 GHz – 3 THz. Non-contacting techniques were used throughout.

At Terahertz frequencies, materials can exhibit unique spectral signatures due to molecular interactions that do not exist at lower frequencies as a result of the higher energy levels and the shorter wave lengths of T-Ray (THz) radiation. Molecular polarization is one type of spectral related interaction. Three common polarization mechanisms are dipolar relaxation, atomic polarization, and electronic polarization, which are functions of structure, frequency, and temperature. Regions of anomalous dispersion may occur at the transition boundaries between these zones and also near (relaxation) resonances. This type of dispersion results when the index of refraction decreases with increasing frequency or when the group velocity and phase velocity are in reverse relative directions.

1.1 Motivation and Applications of THz Material Measurement Systems

1.1.1 Motivation

As a result of advancements in technology, the performance of future systems is limited by the properties of the materials used in their electronic components, rather than by the circuit or system design. Technology has been consistently approaching the physical limits of nature and thus more detailed knowledge about materials is required to get better models to achieve performance improvements. Modern analyzers and spectrometers are being developed to meet these needs. New material thickness determination equipment is also being developed. Many of these new systems operate at THz frequencies. At this time, there does not appear to be another comprehensive study comparing so many instruments used to perform Terahertz material characterization and also observing anisotropy for different wave polarizations as was done in this project.

Important security related uses of these systems include detection of weapons, illicit drugs, controlled substances, biohazards, and explosives. Another use is the characterization and identification of new types of materials (e.g., nanomaterials and nanodielectrics, and carbon nanotubes). Improved scanning and analysis techniques allow more rapid results. Better definition is achieved using high resolution imaging schemes and spectral analysis.

Biotech and medical applications include screening for irregular cell growth, examining the opacity of the cornea, and monitoring consistency of pharmaceutical products and pill coatings.

Better quality control of manufacturing processes such as monitoring material uniformity used solar cells and semiconductors, as well as accurately measuring the thickness and consistency of dielectric coatings is now possible by using terahertz based metrology. Efficient detection algorithms and software analysis tools are needed to complement these systems. Development of high energy density materials also needs these techniques.

Free space measurements eliminate stripline type conductors and their associated losses.

1.1.2 Applications

Some applications of microwave and millimeter wave (mmw/THz) grade materials are radio astronomy receivers and detectors, semiconductor substrates and devices, component (integrated circuit) package design, studying propagation properties of the atmosphere, analog RF and high speed digital integrated circuit design and control of related fabrication processes, cellular phone components and antennas, Wi-Fi devices, TV and satellite antennas, GPS receivers, antenna radomes, medical imaging systems, avionics equipment, roadside threat detection, and precision missile/drone guidance.

More specific THz applications include:

1. Characterization and electric modeling of dielectric materials, including absorption (loss), permittivity/refractive index, dispersion, and permeability. This data can be used for microwave and millimeter wave component and packaging designs for communications equipment, power generation monitoring equipment, green electric technology (including solar cells), semiconductors, and device coatings.
2. Material identification and classification for security purposes: explosives, biohazards, and illicit drugs
3. Quality control: measuring electrical and mechanical uniformity of materials. Macro and microscopic properties of materials are measured using spectroscopic techniques, some of which rely on inelastic scattering, to observe vibrational and rotational modes.
4. THz Imaging (Pulsed, CW, FM, and Doppler). A CW scanning system can only show one level, a pulsed system add a depth profile. Both reflection and transmission modes are exploited when possible.
5. Medical Applications and Biogenic Materials
6. Analysis of pharmaceuticals- e.g., pill coating thickness
7. In vivo THz imaging for organic matter and to examine cell irregularities, and defects or check for carcinoma, without disturbing the sample.
8. THz wave surface depth measurements and observation
9. Mapping and examination of eye tissue irregularities
10. Analysis of Dental enamel finish and sub-surface defects
11. Examine polarization and reflection of cells.

12. Near Field techniques and Atomic Force Microscope (AFM) measurements can be used to extend limits of detail resolution (microscopic).
13. Examination New Materials
14. Nano Technology
15. AFM analysis for precise outline details
16. Macroscopic and microscopic examination of nanomaterials and nano-machines
17. Metamaterials – structure behavior analysis (transmission and reflection) negative dielectric constant and invisibility. [Ziolkowski:209]
18. Characterization of Single Walled Graphene and Carbon Nanotubes - (SWCNT)
19. Nanodielectrics; Multi-component nanostructures are used to alter the dielectric constant by changing the charge distribution.
20. Nanoparticles and Nanowires
21. Automotive Applications
    - 21.1.1. Uniformity analysis of plastics used throughout vehicle
    - 21.1.2. Analysis of tire sidewalls for damage and defects
    - 21.1.3. Examination of fluids and fuel used therein
    - 21.1.4. THz Radar and Imaging for vehicular positioning
    - 21.1.5. Coating thickness analysis for glass

1.2 Spectral Instrumentation and Basic Equipment Description

The instruments used in this project are classified as a function of frequency and their characteristics are compared in Table 2 (manufacturer) and Table 3 (this project).

1.2.1 Fourier Transform Spectrometer (FTIR, a Scalar System)

The FTS used for this project is a Beckman FS720, which consists of an adjustable Michelson interferometer (i.e., a fixed mirror, a moving mirror, and a beam splitter), a broadband CW arc lamp source with a parabolic mirror, a chopper, a detector, a lock-in amplifier, vacuum pumps, and support instrumentation. The FTS can operate up to 3.0 THz. The system uses an electro-optical mechanical servo delay and translation mechanism and an arc-lamp source. This source is not polarized, so that type of anisotropy could not be observed. Scattering, absorption, and reflection were detected for certain samples, depending their on thickness and dielectric constant.

By using a broadband high intensity source in the FTS, noise figure and speed improvements are realized due to the Fellgett (Multiplex) [6] Advantage, the Jacquinot [14] (Energy or Throughput) Advantage, and the Connes [87] (frequency accuracy) Advantage. These factors allow improved spectral processing techniques [Bell:84, 85], [Han:11].

1.2.2 Time Domain Spectrometer (TDS)

The Time Domain Spectrometer at the University of Arizona is a Picometrix T-Ray 2000 was used for preliminary measurements, but this unit it did not have the accuracy required for parameter extraction and its source was unstable and eventually stopped operating. Thus most of the TDS measurements were performed on a new high resolution Picometrix T-Ray 4000 located at the (Northwest Electromagnetic and Acoustic Research) NEAR Lab at Portland State University. The Picometrix TDS systems are pulsed and they use a femtosecond laser, a fiber to THz E/O conversion system (a transmitter, a receiver/detector, antennas, and Auston switch), optical lens collimators, a grating dispersion compensator, a translating stage, a control unit, a laser supply, a PC, a cooler, and support equipment. The T-Ray 4000 is completely integrated making it much faster and more accurate than the T-Ray 2000 which had separate components. These systems operate up to about 1.5 THz. A lock-in amplifier is not required, but can be used for better performance. These systems will be discussed in more detail in a later chapter.

1.2.3 Network Analyzers (Scalar and Vector):

These instruments consist of broadband synthesized sources and companion receivers. Vector analyzers also have matched balanced couplers, mixers, down converters, and tracking receivers. The vector system is phase coherent. By using sophisticated calibration techniques, vector information (i.e., magnitude and phase) and is obtained, in the form of complex s-parameters. The scalar system can only yield relative insertion loss of the test samples.

In general, dielectric materials operating at frequencies below 100 GHz do not exhibit intermolecular behavioral anomalies. Their responses are smooth, except for relaxation effects (i.e., dipolar resonances). At millimeter wave (mmw) and terahertz (THz) frequencies however, there are wave interactions that produce unique spectral signatures which are associated with the material lattice, molecular arrangement, and/or the atomic structure (See Table 1). These interactions are more pronounced at THz bands due to the shorter wavelengths and higher energies of these waves. Some of these effects are very narrow band, such as water lines. However, they are very important for astronomers and scientists. On the other hand, broadband macroscopic effects, such as dispersion and loss, need to be incorporated into engineering models.

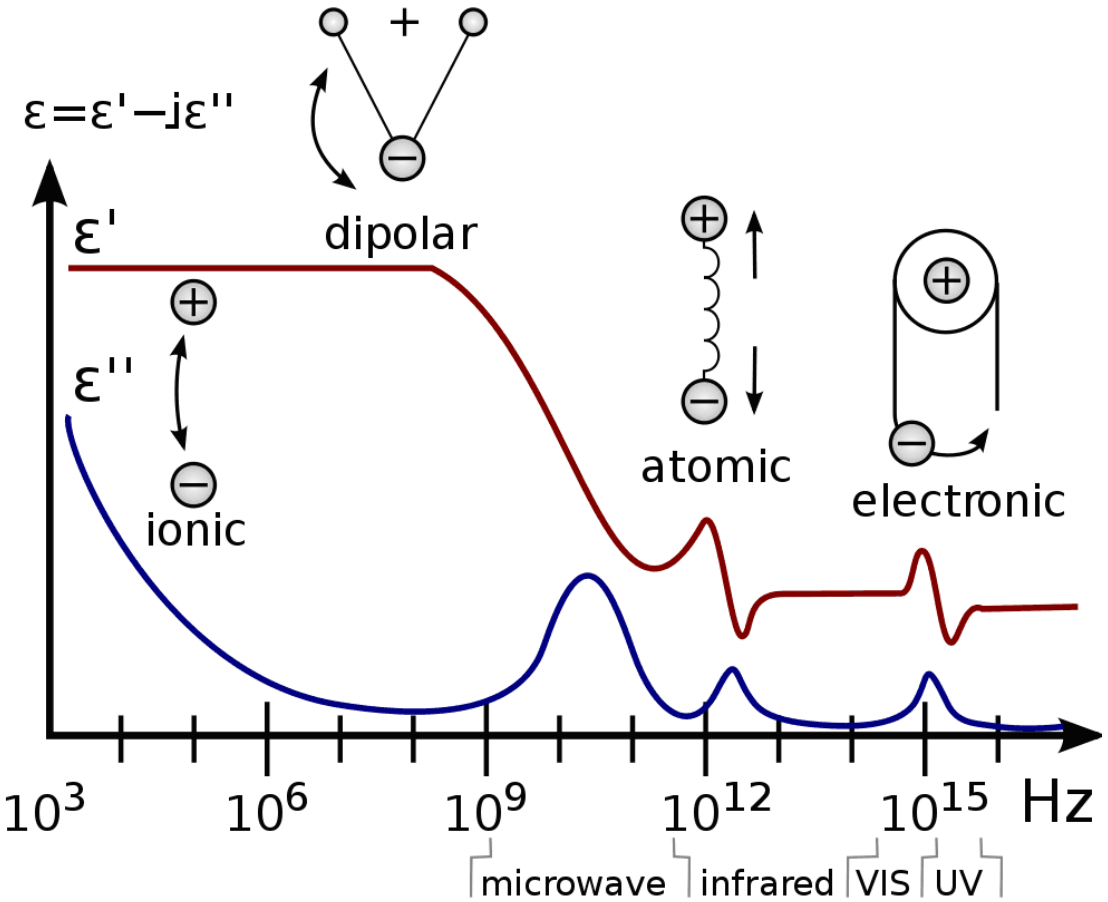

DIELECTRIC MECHANISMS vs FREQUENCY RESPONSE

MEASUREMENT TECHNOLOGY			
HF **1000-10^8 Hz,** **($3x10^5$m-3m)**	**Microwave/MMW** **0.1-100 GHz** **(3 mm to 3000 mm)**	**Sub-MMW-far IR** **100 GHz-10 THz** **(3 mm to 0.03mm)**	**IR-Light-UV** **10^{13}-10^{16} Hz** **(30 µm-0.03µm)**
MA, SNA, VNA	**SNA, VNA, PNA/X, FTMS**	**FTS, TDS, VNA/PNA + THz Extender**	**FTIR/FTS**
Legend: MA/MNA = Materials Analyzer SNA = Scalar Network Analyzer VNA = Vector Network Analyzer PNA = Precision Network Analyzer MMW=millimeter wave		FTMS = Fourier Transform Microwave Spectrometer FTS = Fourier Transform Spectrometer TDS = Time Domain Spectrometer FTIR = Fourier transform infrared spectroscopy HF=High Frequency, THz=Terahertz	

Table 1: Dielectric Mechanisms and Measurement Technologies vs. Frequency and are detailed in section 1.3. (Adapted from Wikipedia, Dr. Ken Mauritz)

1.3 DIELECTRIC MECHANISMS RELATED TO FREQUENCY

(See Table 1), [Potter:195, Balanis:130]

Dielectric polarization of a material varies with applied electric field intensity and direction, frequency, temperature, and the state of the material. Dielectric Relaxation is the result of (delayed) movement of dipoles and electric charges due to an applied alternating field and is usually in the frequency range of $10^2 – 10^{10}$ Hz. Relaxation mechanisms are slow compared to electronic, atomic, or molecular vibrations/transitions which occur at frequencies > 10^{12} Hz. These mechanisms result in variations of the refractive index, and therefore effects absorption and transmission. The materials characterized in this project are solids that are linear, mostly isotropic and homogeneous at microwave frequencies below 60 GHz. Dielectrics have several different behavioral regions: Ionic and/or Dipolar Polarization (lowest frequency), Atomic Polarization (mid-range, microwave frequencies), and Electronic Polarization (THz). The transitions in Table 1 joining these domains may be anomalous. Figure 1 shows the relative position of THz radiation in the electromagnetic spectrum and the associated measurements techniques available.

Ionic Polarization-Relaxation: Occurs in ionic materials. Small space charge shifts occur when an electric field is applied. This effect dominates at lower frequencies, < 10^6 Hz. Interfacial relaxation can occur when charge carriers are trapped, 10^3-10^6 Hz.

Dipole Relaxation (Dipolar 'orientation' polarization): Polar covalent molecules with permanent and induced dipoles align in response to an applied electric field otherwise the dipoles are not aligned due to thermal noise and relaxation. Dipole relaxation is temperature dependent. This is a low-mid frequency effect, 10^6-10^9 Hz.

Atomic Polarization: Electronic cloud deformation results from an applied field and a negative and positive space charge region is formed. This is a resonant process that happens at microwave frequencies, 10^9-10^{12} Hz.

Electronic Polarization occurs when an applied electric field displaces electronic density relative to the nucleus. This is a very fast effect, and is usually observed at frequencies above 10^{12} Hz.

FREQUENCY RANGE	INSTRUMENT TYPE	RESOLUTION	TECHNOLOGY
0.1-100 GHz (1 THz with Extender Unit)	**Vector Network Analyzer** (VNA/PNA/ZVA; *Agilent, R&S*)	1 kHz	Coax, stripline, coplanar and standard waveguide
0.140-1.0 THz	**Scalar THz Network Analyzer** (*VDI/Agilent*)	~10 KHz	Waveguide and free space
0.60-4.5 THz	**Time Domain Spectrometer** (TDS: *API -Picometrix*)	78 fs (time) ~1-3 GHz (freq)	Free space, pulsed femtosecond laser, mixer, E/O transducer, Auston Switch
THz band	**THz Time Domain Reflectometer** (**TDR:** *Agilent, TeraView*)	Fault Resolution, <10 microns (3MHz)	THz pulsed proprietary system
900 GHz	**CW-THz Spectrometer**, (*TeraView)*	High spectral intensity, and narrow THz linewidth (proprietary)	Optical heterodyne technique, (CW-THz LT-GaAs photomixer device at difference frequency of 2 CW optical beams)
0.2 THz – 30 THz (10um)	**Fourier Transform Spectrometer** (FTS/FTIR)	~1 GHz	Free space Michelson, Interferometer

Table 2 Instrument Technology Classified by Frequency and Manufacturer

FREQUENCY RANGE	INSTRUMENT TYPE	RESOLUTION	TECHNOLOGY
0.140-1.0 THz (300um)	**VDI Scalar Network Analyzer** (DURIP program)	**~10 KHz**	**Scalar**: Quasi-optical, frequency domain analyzer using synthesizer, multipliers, heterodyne mixers, waveguide, bolometric sensor and Golay cell detectors
0.20-4.5 THz	**Time Domain Spectrometer (TDS),** T-Ray series	**~1 GHz**	**Vector:** free space femtosecond pulsed laser, mixer, optics, Auston Switch E/O converter
0.20THz-3.0 THz (100um)	**Fourier Transform Spectrometer** (FTS/FTIR)	**~1 GHz**	**Scalar:** Free space, broadband source and Michelson interferometer
0.01-110 GHz	**Basic Vector Network Analyzer: ZVA-40/VNA**	**<1 KHz**	**Vector:** Coax, W/G, stripline, frequency domain heterodyne system, tracking receiver, precision coupler)
200 GHz-1 THz	**VNA/RSA ZVA-40 + VDI Extender Unit**	**<1 KHz**	**Vector:** Frequency domain heterodyne system (amplitude and phase)
Terahertz Measurement Systems Characterized by Frequency that were used for this Project			

Table 3 Terahertz Measurement Systems Characterized by Frequency

THz INSTRUMENTATION COMPARED			
	THz-TDS	**Far-IR FTS (FT_IR)**	**SNA/VNA/PNA**
Domain	Time domain	Frequency domain	Frequency domain
Transmission/ Reflection Measurements	Both available	Both available	Measured simultaneously
Phase Measurement	Available (Vector)	Limited (Scalar)	Available for VNA/PNA
Dynamic Range for Power	10^{8} (<3 THz)	~ 300 (<3 THz)	10^{19} @ 200 GHz 10^{6} @ 700 GHz
Typical Resolution	3 GHz	3 GHz	10 kHz
Peak Power	1 mW (Integrate over the bandwidth)	0.1 uW (Integrate over the bandwidth)	1.3 mW@200 GHz 0.001 mW@600 GHz
Bandwidth	Tens of 10 GHz to 4-5 THz	100 GHz to visible	8 GHz to 1 THz, with THz Extender
Noise Equivalent Power	10^{-16} W/rtHz (<3 THz)	8^{-10} W/rtHz (<3 THz)	10^{-12} W/rtHz (min)
Source Reliability	Good	Not good	Good
THz Development	Initial stages	Mature	Formative
Degeneracy Parameter	~ 10^{5}	~1	n/a
Data Acquisition Time	Minutes	Minutes: Multiplex Fellgett advantage, Throughput Jacquinot advantage	seconds-minutes
Uniqueness	Time Gated Coherent pulse (femtosecond laser)	Broader spectrum	Yes
Drawbacks	Repeatability & sensitivity to THz optical alignment	Instrument line function (beam splitter), scalar.	Limited frequency range

Table 4 Comparison of THz Instrumentation (Degeneracy parameter is the number of photons in a coherence volume, or TDS pulse [Han:155])

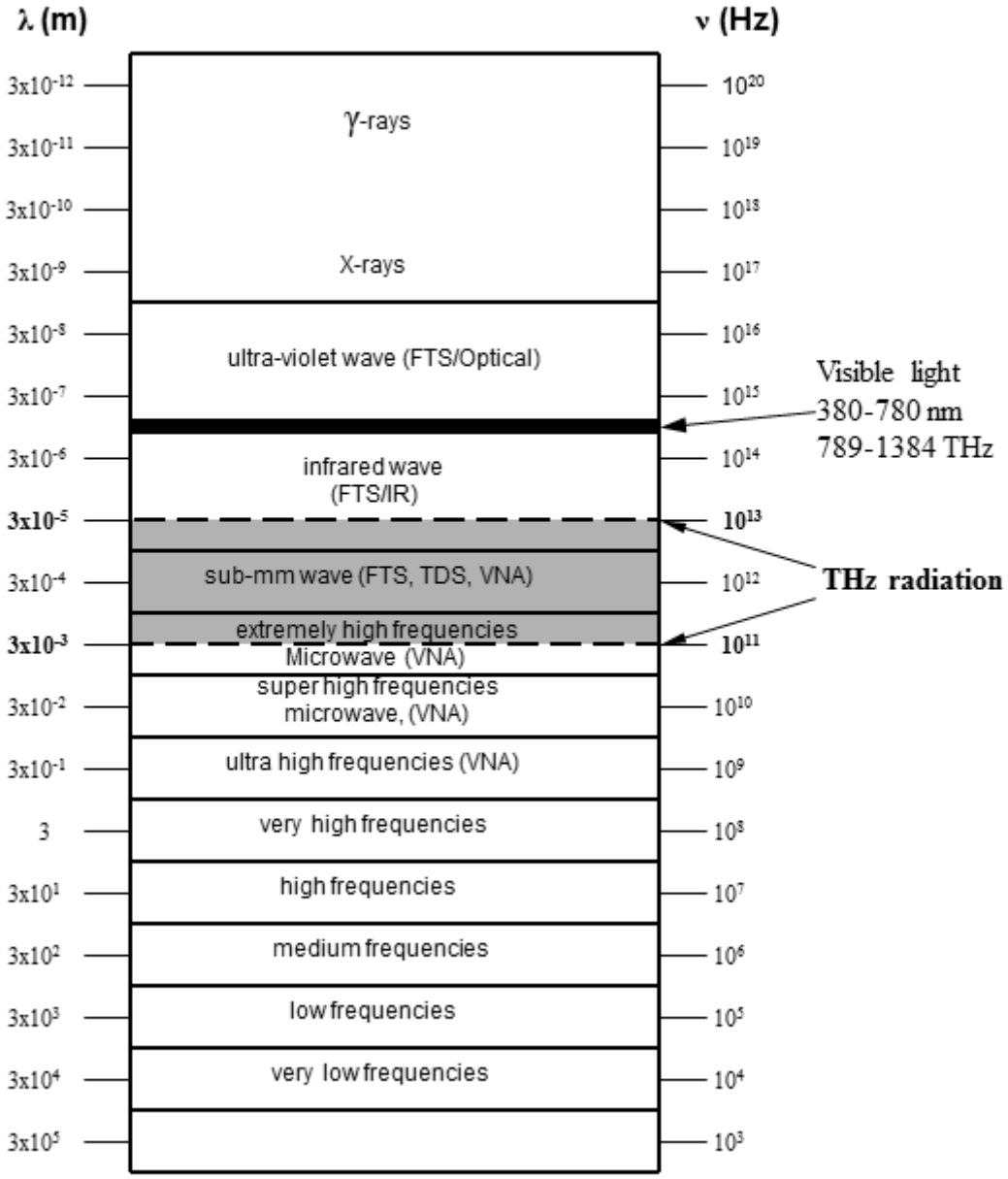

Figure 1 THz Radiation in the Electromagnetic Spectrum. This table shows relative position of THz radiation in the electromagnetic spectrum and the associated measurements techniques available.

2 THz SYSTEMS AND MEASUREMENT TECHNIQUES

There are two broad categories of material measurement techniques: destructive and non-destructive. Destructive testing means physically permanently altering the test material in some way to examine an observable property such as hardness or loss. Various aspects of these systems are compared in Tables 4-6. Each system has their own unique characteristics that will be discussed in detail in the following sections.

The FTS is the widest band instrument (up 30 THz) but it is not a vector system, while the VNA is narrower band but has the highest resolution, and the TDS has wider bandwidth than the VNA and is vector based and is stable and has extensive averaging. The source in THz time-domain spectroscopy has much better stability than the mercury lamp used in Fourier transform spectroscopy. *This project shows that the TDS is the best instrument of choice for Terahertz characterization of dielectric materials.*

Non-destructive testing and evaluation (NDT/NDE) implies using a noninvasive form of observation to analyze the material for a desired property, without making any permanent change in the material itself. An NDT example would be probing a sample with electromagnetic waves, as is done with a spectrometer or a network analyzer. Other NDT systems use ultrasonic sound waves, magnetic-particles, liquid penetrants, radiographic systems (digital and optical imaging), lasers, MRI, X-rays, and magnetic induction (eddy-current) testing methods. For circuit board substrate material there is a commonly used method entitled, IPC-TM-650 (2.5.5.5, Stripline Test for Permittivity and Loss Tangent,

Dielectric Constant and Dissipation Factor at X-Band, 10GHz typical). This method is set forth by the Institute for Interconnecting and Packaging Electronic Circuits (ipc.org).

Although the material under test is machined in order to fit into a test fixture or made into include a transmission line, this is not considered to be a destructive technique since the physical material properties are not altered. In a spatial measurement, there is no direct contact with the material, but the sample may still need to be shaped to fit into a test fixture.

The frequency dependent dispersive properties of materials are needed to determine parameters for models that are then used in numerous applications such as semiconductor packages. These techniques can be broken down into several categories:

1. Spectrographic Analyzers (TDS, FTS)
2. Network Analyzers (THz Scalar and VNA, all free space)
3. Contacting and non-contacting test fixtures and probe stations
    3.1. Test fixtures with connectors/launchers
    3.2. Placing the sample between frames or wave guides, thus passing EM wave though the MUT
4. Transmission lines, waveguide systems, or coaxial systems
5. Resonators (stripline, cavity, cylinder, or split type).

The electrical properties of dielectric materials that are of most interest are index of refraction (scalar and complex dielectric constant), insertion loss, loss tangent, dispersion, dissipative loss, and reflectivity. Permeability is one for most dielectrics and the ones in this experiment. Some of these are parameters are related atomic structure, electronic structure, molecular arrangement (polar and non-polar), and lattice. Near field TDS systems are in development (presently there are Atomic Force Microscopes, AFM) and they can measure microscopic properties. However, the other systems (FTS/VNA/TDS) measure macroscopic properties which may include s-parameters, permittivity, loss tangent, uniformity, and homogeneity.

Spectral analysis can reveal a combinations of atomic and molecular structures, polarization (chirality), and (dielectric, dipolar) relaxation properties.

2.1 Measurement Techniques Sorted by Frequency (Tables 4-6)

These tables show various instrument properties as a function of frequency.

FREQUENCY RANGE	INSTRUMENT TYPE	RESOLUTION	Interconnect Technology
0.1-100 GHz	Network Analyzer (VNA/PNA)	1 kHz	Coax, stripline, coplanar and waveguide
0.145-1.0 THz	Scalar THz Network Analyzer (VDI/Agilent)	~10 KHz	Waveguide and free space (quasi-optical)
0.60-4.5 THz	Time Domain Spectrometer THz-TDS	~1 GHz	Free space, Pulsed femtosecond laser, E/O transducer
0.20THz-30THz (10um)	Fourier Transform Spectrometer (FTS/FTIR)	~1 GHz	Free space, Michelson Interferometer

FREQUENCY RANGE	INSTRUMENT TYPE	RESOLUTION	INSTRUMENT TECHNOLOGY
0.145-1.0 THz	Scalar Network Analyzers (DURIP program-VDI, Agilent)	~10 KHz	Frequency domain scalar instrument using synthesizers, multipliers, and waveguide
0.20-4.5 THz	Time Domain Spectrometer TDS	~1 GHz	Vector: femto-second laser and semiconductors THz transducer (pulsed/vector)
0.20THz-3.0THz (100um)	Fourier Transform Spectrometer (FTS/FTIR)	~1 GHz	Modified broadband Michelson Interferometer
0.01-110GHz; 2THz w/VDI Extender	Vector Analyzers: VNA, ZVA-40	<1KHz	Vector Frequency Domain Analyzers (amplitude and phase)

Table 5 Terahertz (Material) Measurement Systems vs Frequency

Table 5 shows instrument and interconnection technology as a function of frequency. Coax and waveguides are used for microwave and quasi-optical for THz eliminating conductor loss.

THz INSTRUMENTATION OPERATIONAL COMPARISON			
Parameter vs Instrument	**THz-TDS**	**Far-IR FTS (FT_IR)**	**SNA/VNA/PNA**
Domain	Time domain	Frequency domain	Frequency domain
Transmission/ Reflection Measurements	Both available	Both available	Measured simultaneously
Phase Measurement	Available (Vector)	Limited (Scalar)	Available for VNA/PNA
Dynamic Range for Power	10^{8} (<3 THz)	~ 300 (<3 THz)	10^{19} @ 200 GHz 10^{6} @ 700 GHz
Typical Resolution	1-3 GHz	1-3 GHz	10 kHz
Peak Power	1 mW (Integrate over the bandwidth)	0.1 uW (Integrate over the bandwidth)	1.3 mW@200 GHz 0.001 mW@600 GHz
Bandwidth	Tens of 10 GHz to 4-5 THz	100 GHz to visible	8 GHz to 1 THz, with THz Extender
Noise Equivalent Power	10^{-16} W/rtHz (<3 THz)	8^{-10} W/rtHz (<3 THz)	10^{-12} W/rtHz (min.)
Source Reliability	Good	Not good	Good
THz Development	Initial stages	Mature	Formative
Degeneracy Parameter	~ 10^{5}	~1	n/a
Data Acquisition Time	Seconds-Minutes	Minutes: Multiplex Fellgett advantage, Throughput Jacquinot advantage	seconds-minutes
Uniqueness	Time Gated Coherent pulse (femtosecond laser)	Broader spectrum	Yes
Drawbacks	Repeatability & sensitivity to THz optical alignment	Instrument line function (beam splitter)	Limited frequency range

Table 6 THz Instrumentation Compared

Table 6 shows detailed instrument operational characteristics as a function of frequency. These parameters allow the best choice of equipment for a desired task.

2.1.1 LOWER FREQUENCY SYSTEMS (110 GHz and below)

2.1.1.1 Resonator Techniques (narrow band - spot measurement)

Resonator techniques are commonly used and include the dielectric-post resonator, circular-cylindrical cavity, split-cylinder resonator, and the whispering-gallery mode resonators. There are also the IPC compliant systems using stripline resonators. All these measurements are narrow band and near the resonator center frequency. They can be done at different frequencies, but require precise machining of each resonator assembly for each. They are not practical at Terahertz frequencies since the wavelengths are so small.

2.1.1.2 Method of Multiple Reflections (broad band up to 10 GHz)

This technique is wideband, 10 or more octaves, and uses a stripline test structure to measure reflections in terms of complex s-parameters from which dispersion and permittivity can be computed [Abernethy:50], [Green:47]. The methodology is based on the Kramers-Kronig relationship, which relates material loss and energy storage, for materials of arbitrary shapes. Exact structure dimensions are not needed as long as all the sources of loss can be accounted for and the MUT (material under test) thickness and stripline length are accurately known, and all the fields are contained within the test structure. This system uses a VNA, a variable load-pull system, and de-embedding

software. Its accuracy is limited by the requirement to have a significant portion of a wavelength inside the MUT, and at the same time we must know accurately time delay (length) and the reflection coefficient (s-parameters, VNA). It is best not to have too many wavelengths inside the MUT or interference and cancellations will occur. Since multiple passes are made through the MUT assembly, a matched load is not needed. In fact, large reflections are helpful as long as the load impedance is known. The higher the frequency, the harder it is to use this method, due to the dimensional limitations in a contacting type system. Presently, no MMR systems have been made at millimeter wave frequencies.

2.1.1.3 Several Commercial THz Materials Measurement Systems exist

2.1.1.3.1.1 FilmTek™ Thin Film Thickness and Refractive Index Measurement Systems

2.1.1.3.1.2 Wide Band Spectrographic Techniques: Time Domain Reflectometer System (TDS) and Fourier Transform Spectrometer (FTS)

2.1.1.3.1.3 RF Impedance/Material Analyzers (Agilent 4291, E4991)

These are dedicated scalar system that measures permittivity and loss of dielectric materials and some options also measure permeability of magnetic materials. It operates at frequencies up to several GHz and it uses coaxial, stripline, or capacitive type test contacting fixtures.

2.1.1.3.2 *THz Quasi-Optical Vector Measurement Systems*

There are several THz VNA/PNA/ZVA vector systems (Agilent and Rhode-Schwarz + THz Extender Units). VDI, Keating, and OML make Extension units for the analyzers. Complete integrated vector systems are now available, including the parameter extraction software operating up to 1.5 THz.

There are both dedicated THz (scalar and vector) and multipurpose systems available that can be used primarily for material analysis made by VDI, Agilent, Rhode-Schwarz, and Teraview. Additionally there are application specific FTS systems available from Nicolet and some of those systems are even field portable.

2.2 APPROACH AND DESCRIPTION OF TERAHERTZ INSTRUMENT SYSTEMS

2.2.1 THz SCALAR NETWORK ANALYZER INSTRUMENT

(Defense University Research Instrumentation Program, DURIP, made by Virginia Diodes, Inc.)

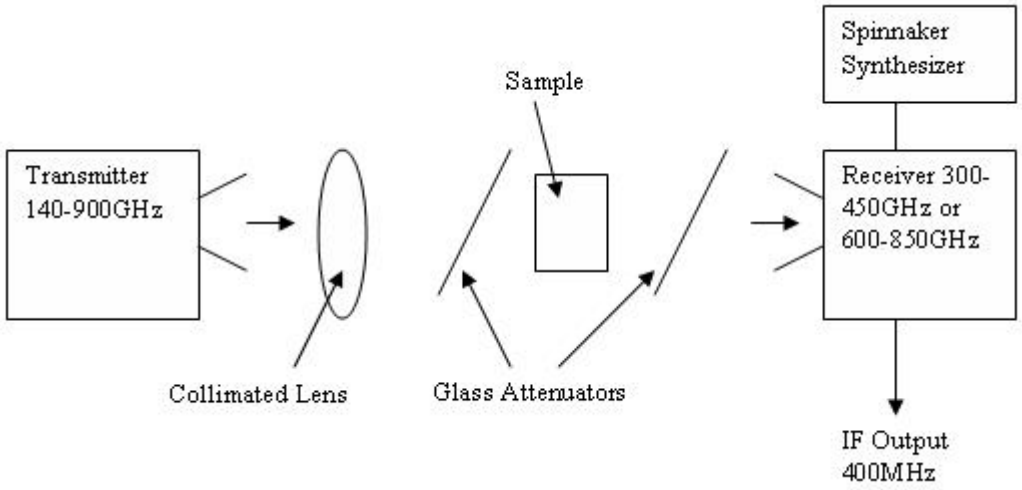

Figure 2 Basic Free Space Scalar Analyzer (Durip program/VDI system)

2.2.1.1 Durip system operational summary

This instrument is a coherent super heterodyne system which consists a THz receiver (down converter), and a THz transmitter (up converter). Both units require a separate mixer, LO multiplier chain, common reference and synthesizer, followed by a detector, and related support equipment and optics. The operating region is divided into five MMW bands from ranging from 200-900 GHz, as shown in Figures 3-11.

A translation stage plus an extensive shielding housing assembly were added to the setup to reduce reflection interference and this was a successful improvement, but it was implemented after my measurements were completed.

Operation: A signal would first pass through a reference sample (or air) and then on a sweep/second pass, it would go through the Test sample and then these results were divided to get the final normalized results. See Figure 3 for a block diagram.

At the time that this setup was used for this project, the reflections were still dominant and the translation stage and shielding assembly were not yet constructed. I was able however, to make simple relative measurements, but they were not always consistent, due to reflection, thus leading to the upgrade. Figure 4 shows the laboratory setup including both up and down converters. Figure 5 shows the beam path and layout for the direct conversion detector system using a Microtech Instruments Golay cell (Appendix 9).

A lot of time and effort was put into getting this system operational even though my final measurements were made on other systems. These measurements provided me the practical and conceptual understanding to migrate to the FTS and later the TDS and the VNA. Further my initial measurements were the basis for future improvements.

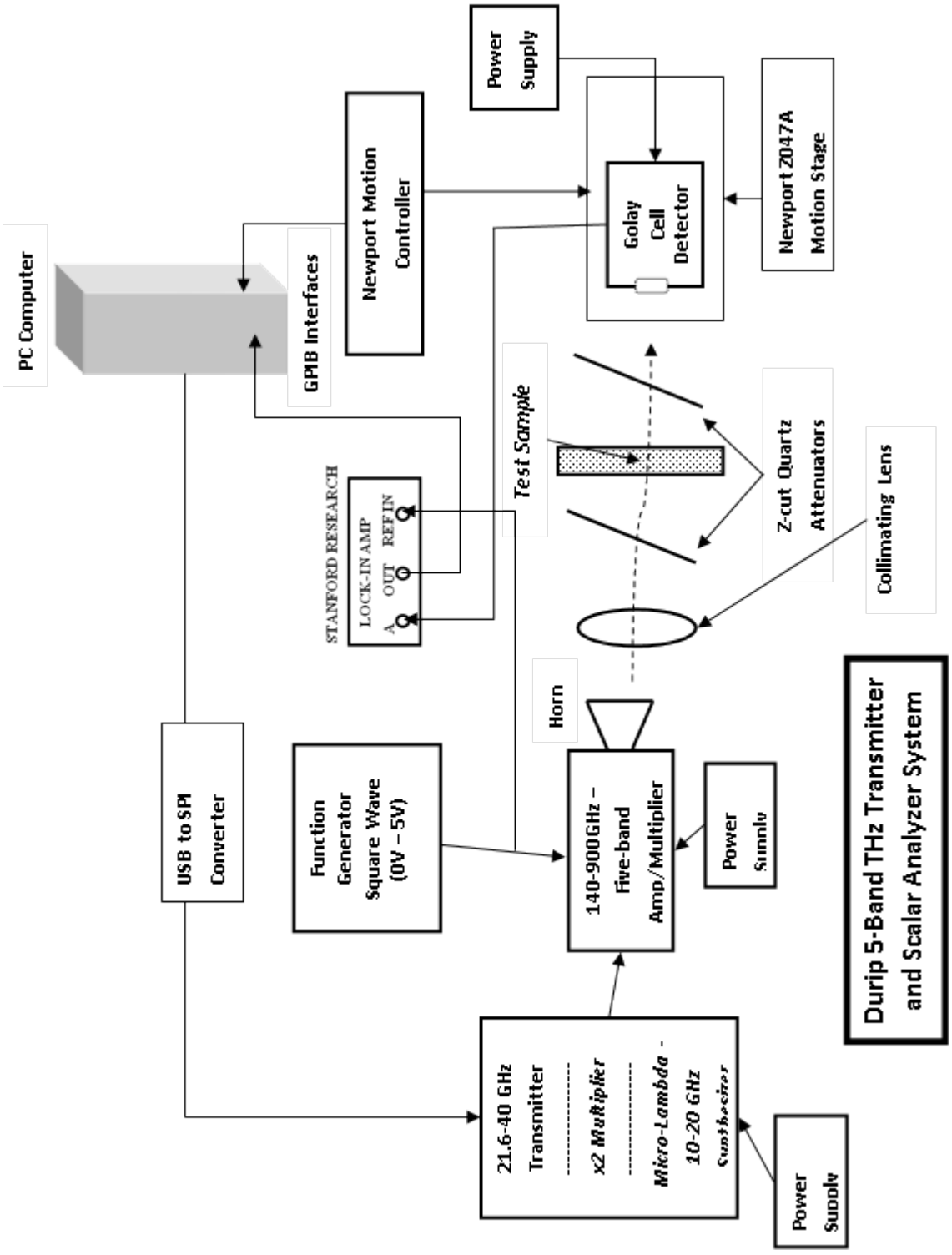

Figure 3 Detailed Scalar Analyzer System Block Diagram: The detector was replaced by a Golay Cell.

Figure 4 Scalar Analyzer System Laboratory Setup

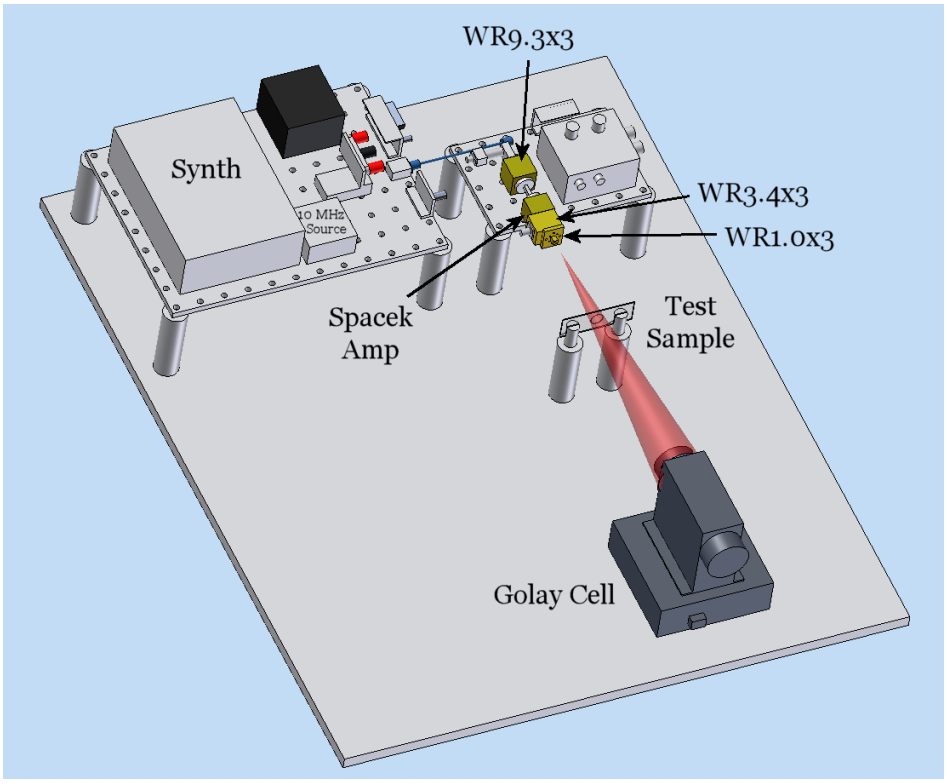

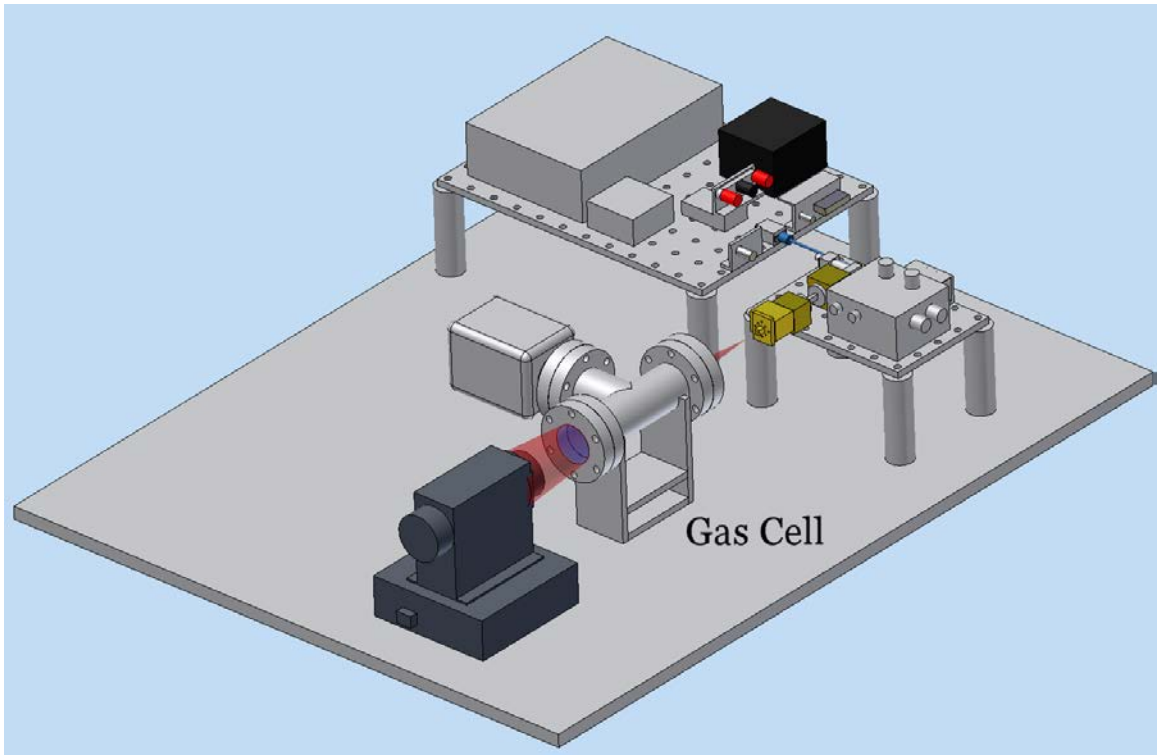

Figure 5 Physical Layout of Scalar VDI Analyzer

2.2.1.2 The VDI THz Transmitter/Multiplier System consists of a number of subsystems including a 21-40 GHz Driver, a Synthesizer, and a 140-900GHz Multi-band Amplified Multiplier Chain. (DURIP Program)

2.2.1.2.1 *VDI 21.6-40GHz Transmitter Driver*

System Components: Micro Lambda MLSE-synthesizer; RLC switch/splitter; Marki AD1020P X2 multiplier; Wenzel 10MHz reference; VDI Power Box and Cables as per Figures 6-7.

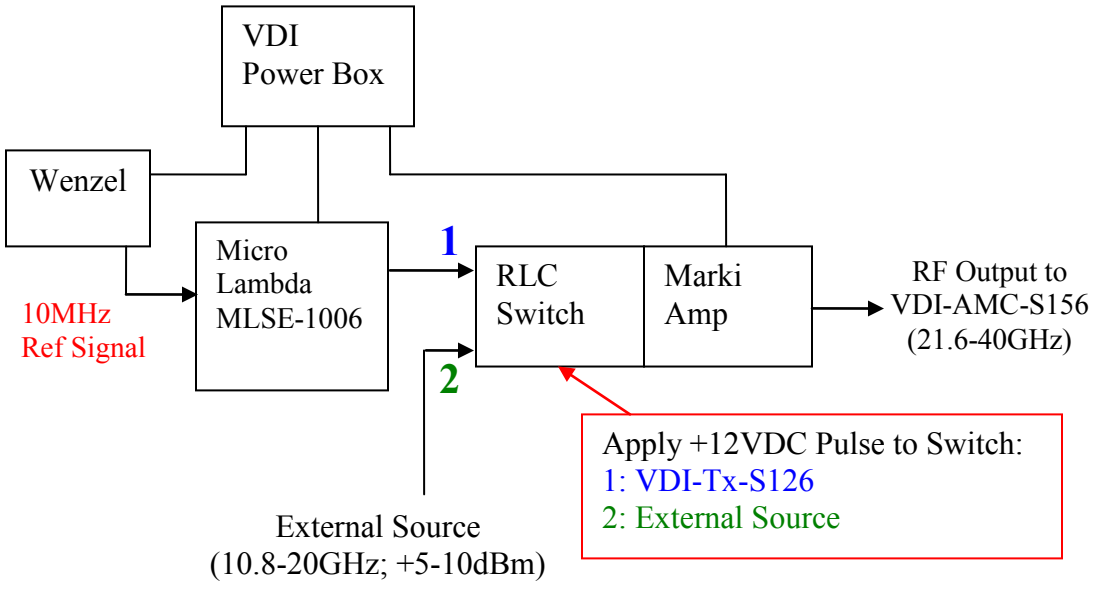

Figure 6 The 20-40 GHZ Driver/Transmitter (courtesy of Virginia Diodes, Inc)

Figure 7: The 20-40 GHZ Synthesizer-Driver-Transmitter (courtesy of Virginia Diodes, Inc.)

2.2.1.3 VDI 140-900 GHz Multi-band Amplified Multiplier Chain

Components: VDI-WR Series Multipliers (with integrated diagonal horn), VDI Power Box; Marki Microwave driver; Spacek Labs amplifier; conical Custom Microwave Horns; for each band and WR VDI Diagonal Horns, see Figure 8 and 9.

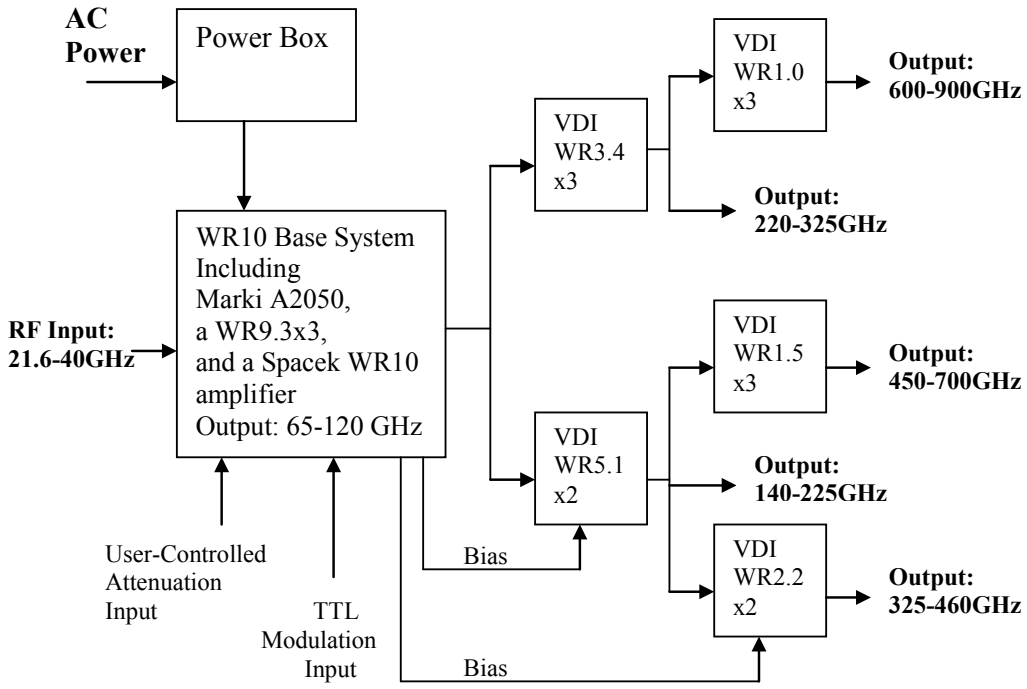

Figure 8: The 140-900GHz Five Band Transmitter Layout (courtesy of Virginia Diodes, Inc.)

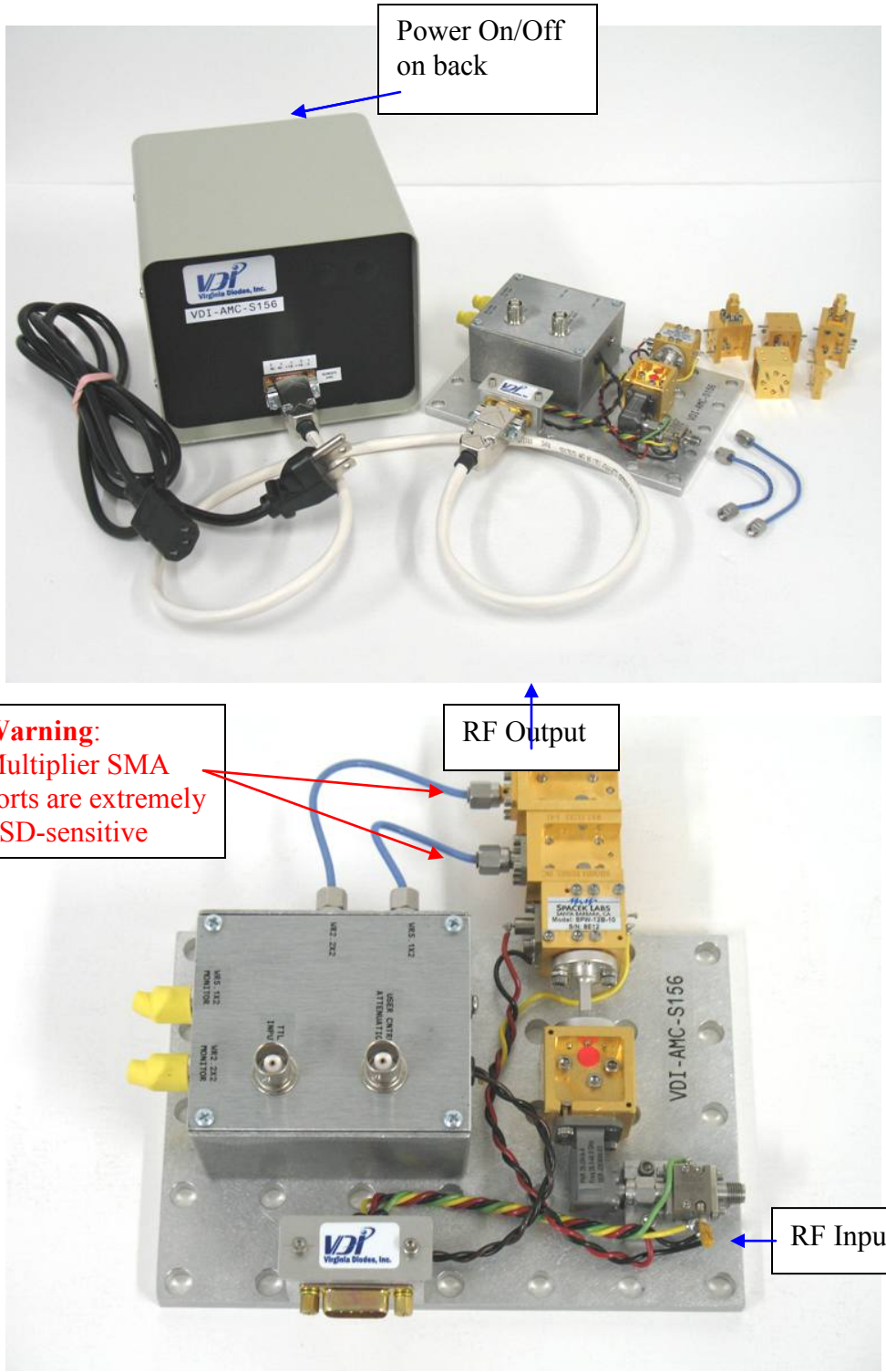

Figure 9: THz Transmitter Assembly using the WR5.1x2 and the WR2.2x2 (horns are not shown) (Courtesy of Virginia Diodes, Inc.)

2.2.1.4 VDI Receiver: 280-450GHz and 750-900GHz Receiver System (DURIP)

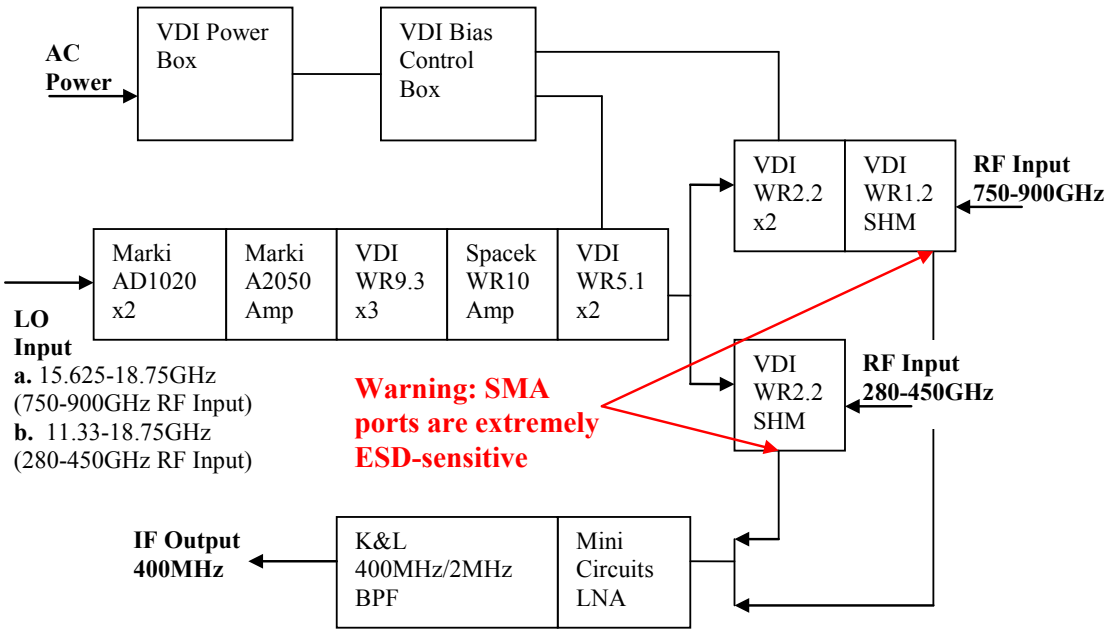

Figure 10 VDI (DURIP) Receiver: 280-450GHz and 750-900GHz Receiver System Diagram

Receiver Components:

VDI-WR series multipliers, mixers, down converters, (Spinnaker) synthesizer, diagonal horns, VDI Bias Control Box, VDI Power Box; Amplifiers, Filters (including a lock-in amplifier). For some measurements, a *Golay Cell detector and lock-in amplifier* replaced the receiver for direct (incoherent) detection measurements. This eliminated the need for a second synthesizer as per Figure 5.

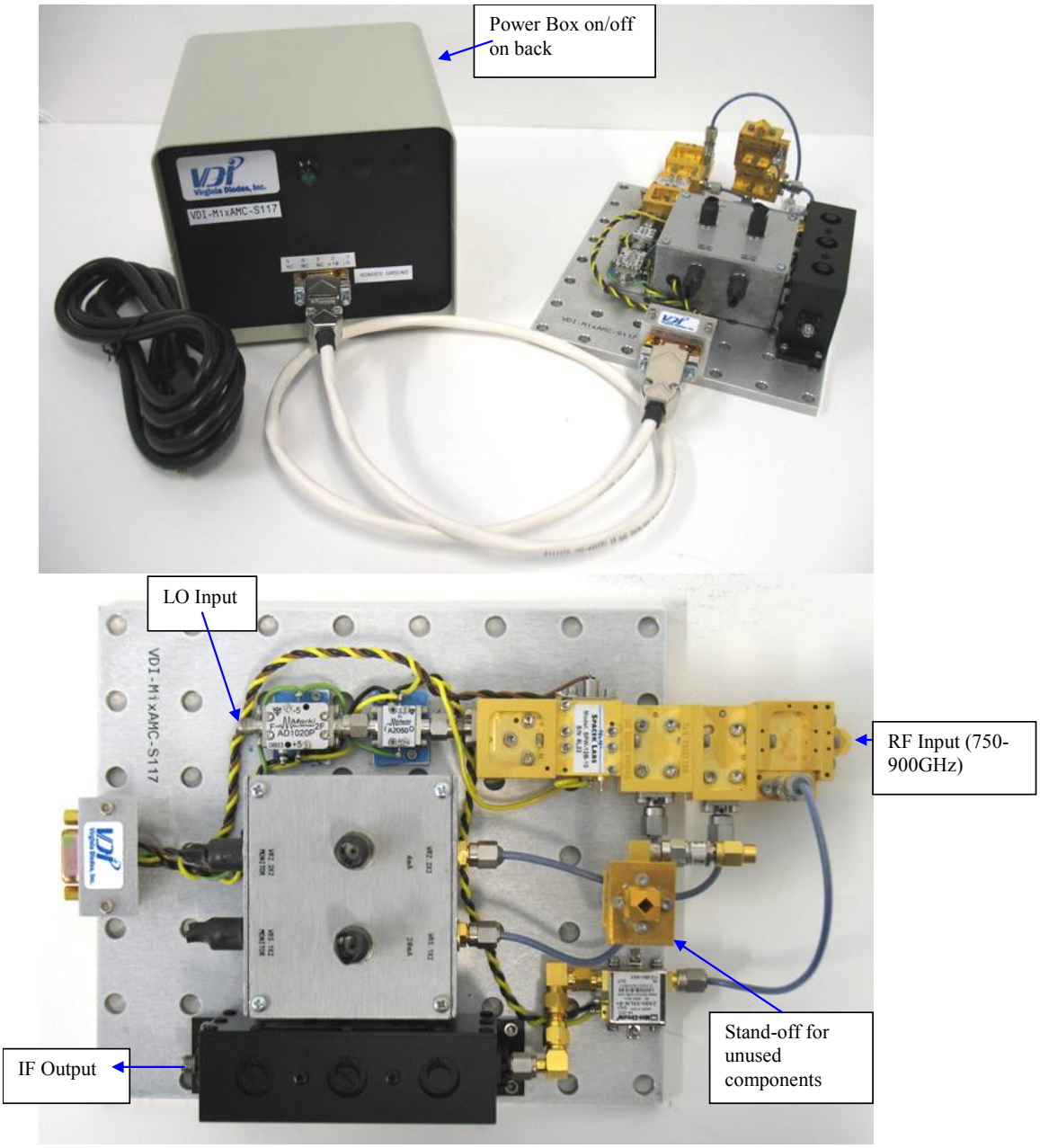

Figure 11 VDI DURIP Receiver: 280-450GHz and 750-900GHz Receiver System

Above is two of the five receiver band converter modules made by Virginia Diodes.

2.2.2 Vector Network Analyzer (VNA)

2.2.2.1 VNA System Basics

The heart of most microwave vector measurements systems is the Vector Network Analyzer (VNA). There are also new high-end systems and called Precision Network Analyzer (PNA, Agilent) and a ZVA (Rohde-Schwarz). These vector systems measure amplitude and phase over multi-octave frequency ranges.

The VNA is a linear, 2 port, frequency domain instrument that operates up to 110 GHz, natively and the data output is in s-parameter format. Some specialized systems can have up to 6-ports, and have nonlinear capability (NVNA/PNA-X) combined with X-parameters, and they also may have time domain (TDR) measurement capability by using an FFT transformation software package. The frequency range of a VNA is increased to the THz region by using Frequency Extender Units, which are sophisticated up and down converters manufactured by several companies. This project used VDI extenders.

S-parameters (Agilent Technology) are used to relate forward and reflected waves, input/output reflection coefficients, along with forward and reverse transmission coefficients. There is also a reference signal path available for normalization and leveling.

A VNA is depicted and is made of up the following components:

a pair of matched precision dual directional couplers, a multiport microwave switch to reverse the direction of test ports to measure all four s- parameters, a receiver/detector system, a synthesized signal generator, firmware to support equipment operation and calibration and analysis routines, plus an on board processor/display and a computer. This is shown in the block diagram and the internal details are in Figures 12-13.

Also required is a calibration system consisting of external hardware (Short, Open, loads, and calibrated delay lines) and firmware/software is needed. A pair of precision coax cables or waveguides is also needed to connect to the test samples and they must be part of the calibration.

Forward, reverse and reflected signals must be measured to compute all four s-parameters. Typical measurements consist of 1-port or -2-port devices, but there are multiple port systems available at NIST.

Once the system is calibrated, the Device under Test (DUT) is inserted between the test cables, and its s-parameters are produced. Then extraction routines can be run to get desired device parameters from the s-parameters.

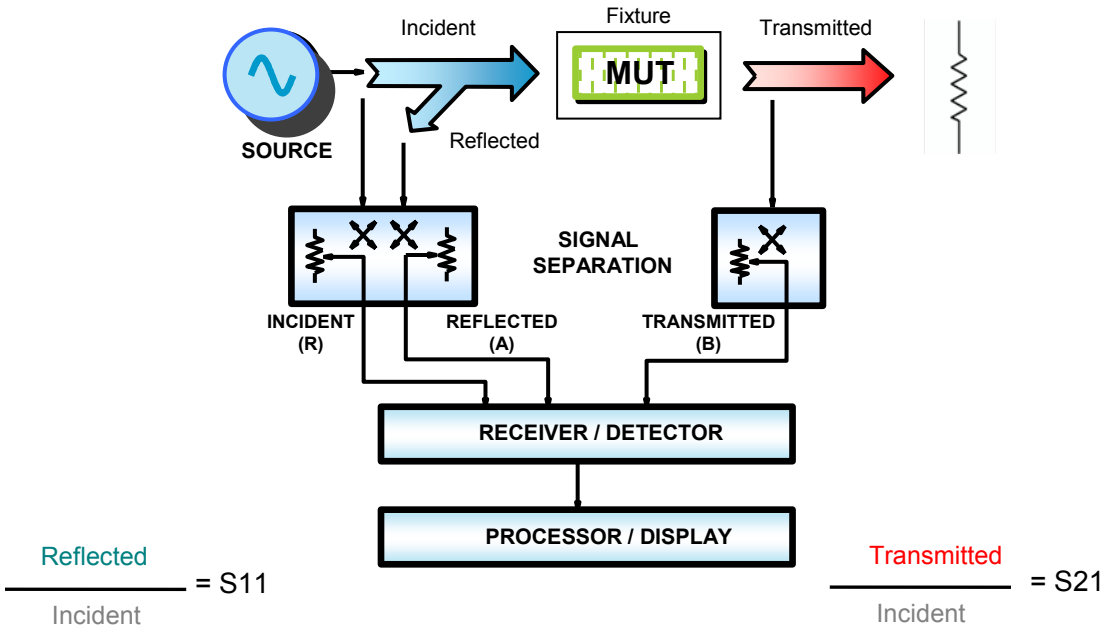

Figure 12 Vector Network Analyzer Block Diagram (adapted Courtesy Keysight Technology:[44])

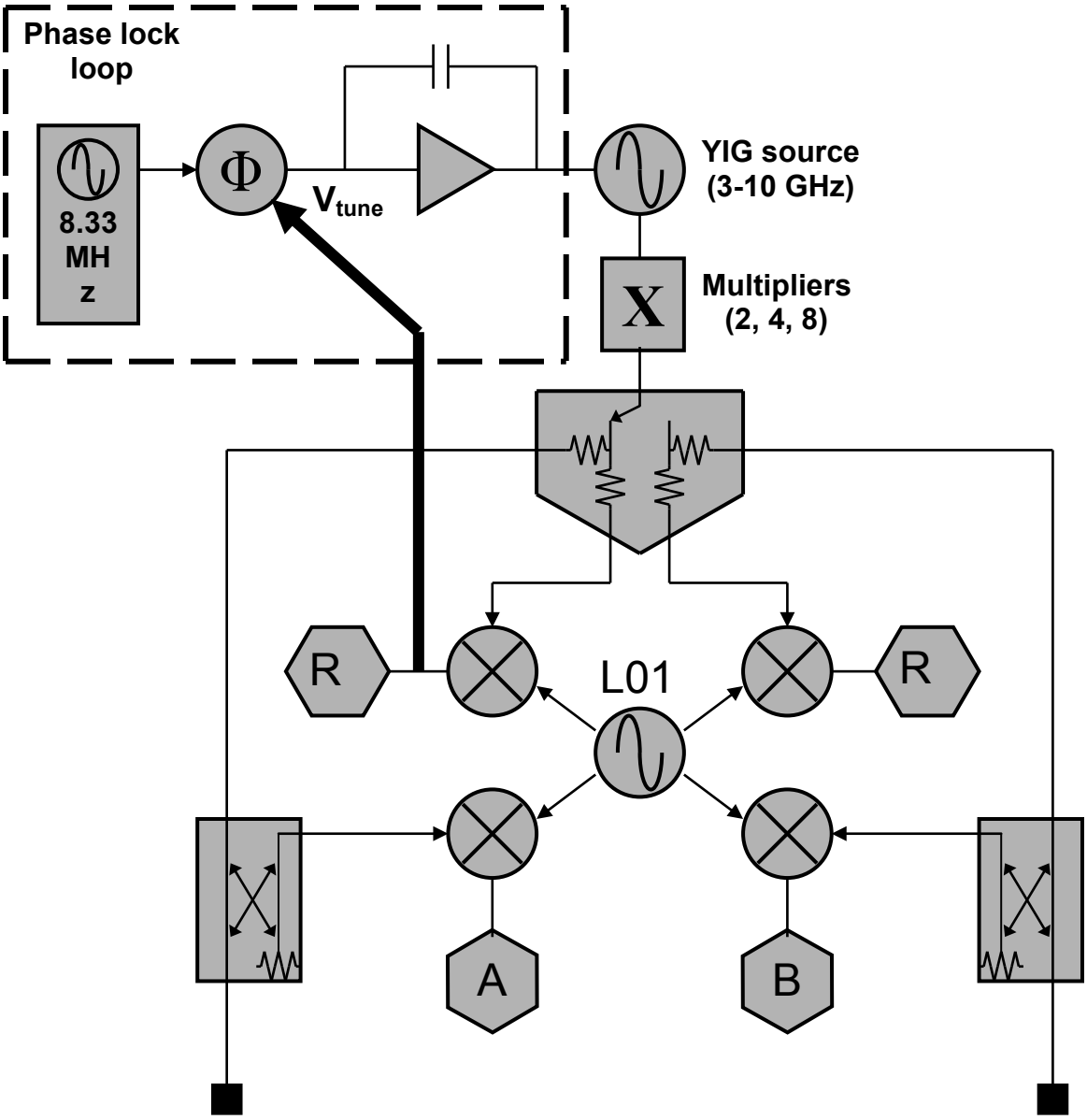

Figure 13 Block Diagram of an Agilent Precision Vector Network Analyzer ™

Above is a layout for the advanced Agilent Precision analyzer (PNA). The more complicated source and reference is present but it still depends on a pair of precision matched couplers.

2.2.3 Terahertz Vector Network Analyzer System using a THz Frequency Extender (Virginia Diodes, Inc.)

There are presently two approaches to making a Terahertz VNA. The first is to make an entire integrated MMW system , but the more common approach is by adding a Frequency Extender Unit to a microwave VNA. A THz Extender is MMW up/down heterodyne converter which translates the THz signals to a band within the native capability of the VNA. Figures 14 and 15 show the VDI Extender system and its interconnection to the VNA. Figure 16 shows the WR waveguide calibration kit.

The Extender approach makes the full capability of a standard VNA available to the THz user. The other approach (ELVA-1 Millimeter Wave Division) is fully integrated system and therefore may have greater sensitivity and dynamic range, but has limited signal processing capability and is not band selectable.

These systems use free space, or waveguide calibration kits and software are required. The calibration may be also combination of multiple techniques to achieve the better speed and accuracy. For example SOLT, TRL, or TRM, can be used to calibrate the VNA and cables, and an SOLT or GRL technique is used for the free space calibration of the antennas and fixture. In Figure 17, absorbers surround the source and detector and Figure 18 shows the waveguide local calibration. Figure 19 shows the entire system.

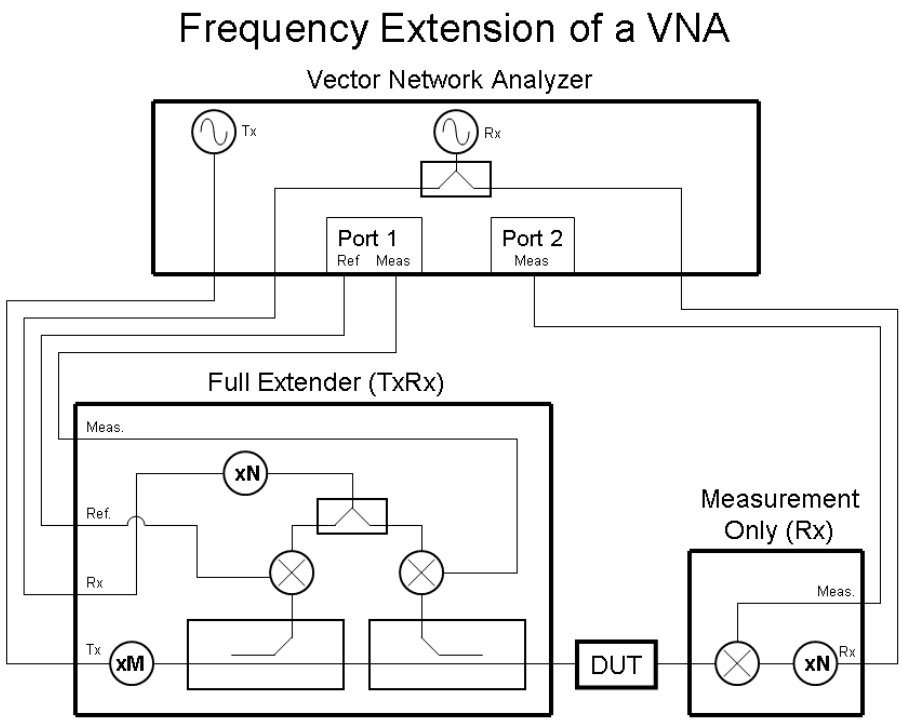

Figure 14 Block Diagram of VNA with Extender (adapted from VDI guide)

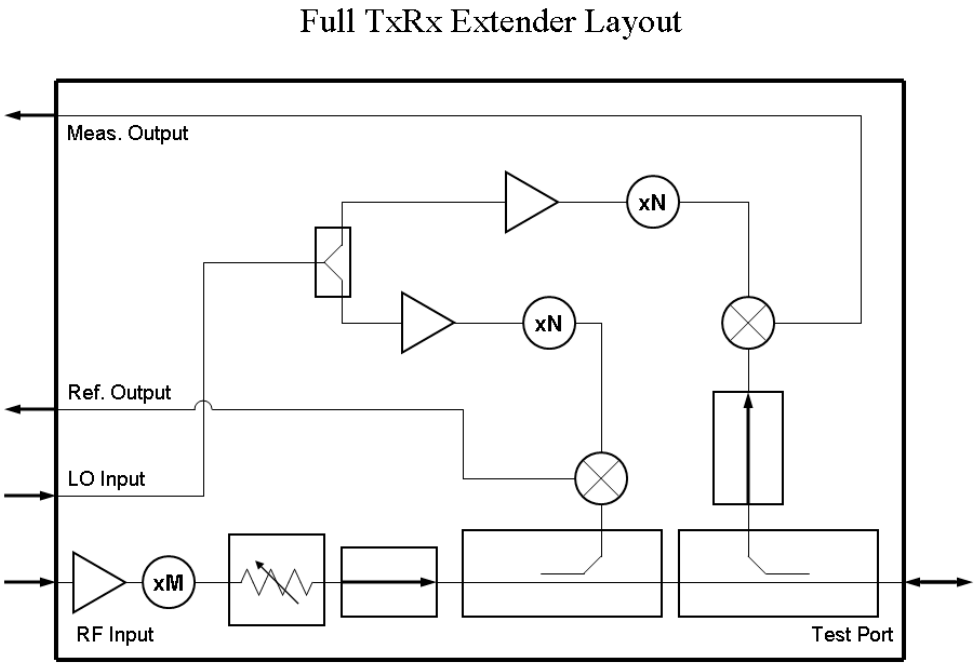

Figure 15 THz Extender Block Diagram (adapted from VDI guide)

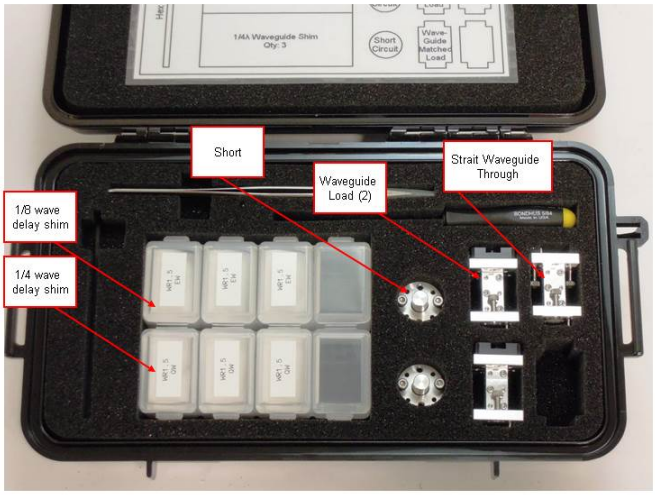

Figure 16 VDI Waveguide Calibration Kit

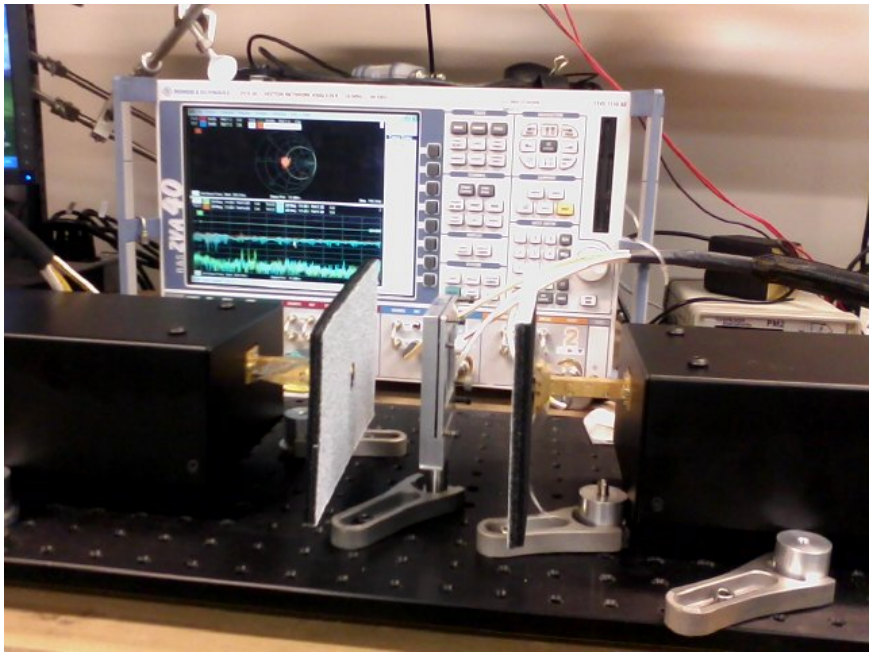

Figure 17 VDI THz VNA System with test sample and absorbing sheets. This equipment was located at Virginia Diodes facility and used for 500-850 GHz measurements.

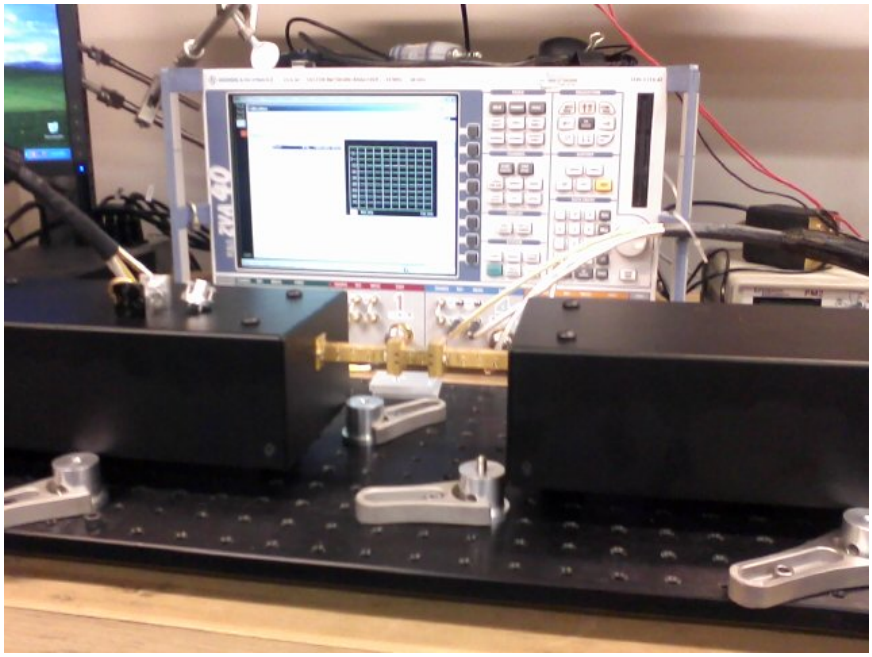

Figure 18: Calibration of THz VNA System at Virginia Diodes

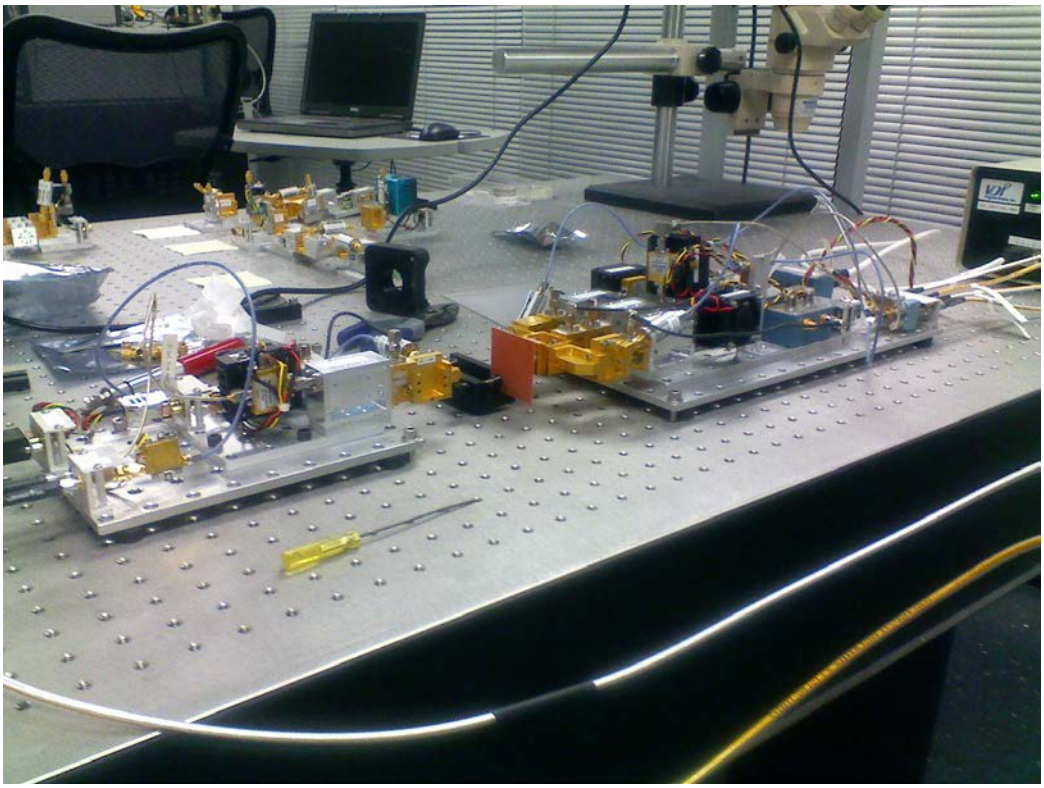

Figure 19 THz VNA at PSU NEAR Lab with test sample

2.2.4 THz Time Domain Spectrometer (THz-TDS, Vector, Transmission mode used, best overall system for the measurements in this project)

Time domain spectroscopy is a technique incorporating pulsed signal generation (and detection) radiation equipment using lasers, optics, and E/O converters to analyze properties of materials. The terahertz pulses are generated by mixing and converting a femtosecond pulsed laser or a combination of lasers to THz radiation via an Auston switch. TDS systems provide vector measurements, while traditional FTS systems only provide relative scalar amplitude information. (Figure 22, ff. shows various elements of a TDS).

Additional advantages of THz-TDS systems, is when materials are transparent to THz waves (e.g., biological samples, art works such as Shroud of Turin, packaging, paper, and clothing), they are not disturbed by low power bursts of THz radiation (non-ionizing radiation, as compared to ionizing for x-rays). THz images are well resolved (<1mm). Many controlled substances including explosives, certain pharmaceutical ingredients, and narcotics, have distinct signatures in the THz region and are easily identifiable. The TDS has high resolution, stable operation, and has higher sensitivity (5 orders of magnitude over FTS, NEP=10^{-16}W $Hz^{1/2}$). This is in a largely due to system coherence.

Terahertz radiation can penetrate many materials that are opaque to light. THz-TDS has a big advantage over conventional Fourier-transform spectroscopy (FTS), in that it is sensitive to both amplitude and phase (vector) and does not require cooling. Some unique applications of TDS are probing controlled materials including explosives, pharmaceutical ingredients, illicit substances (narcotics), and biological tissue samples. Note that terahertz non-ionizing radiation is relatively safe for biological materials.

There are two common type of TDS measurement schemes depicted in Figures 21 and 22, reflection and transmission. Transmission measurements were used for this project with incidence kept angles at 90 degrees. Reflection techniques can be used when penetration is limited, however oblique incidence requires more calculation as two types of reflection and propagation must be taken into account since there is still some transmission. Figure 22 shows a basic block diagram of a TDS [155].

The TDS system at University of Arizona is a T-Ray 2000, (Figures 23, and ff.) was manufactured by Picometrix, Inc. (now API, Inc.). It is excited by a Coherent Vitesse laboratory grade femto-second pulsed laser. It uses an Auston switch type of detector. This early type of system proved to be inadequate for material parameter extraction. It lacked the stability and positional accuracy required for this type of measurement. Hence, most of the TDS measurements were performed using a Picometrix T-Ray 4000, on site, at the NEAR at Portland State University, graciously provided by Prof. Lisa Zurk, via their Electrical and Computer Engineering Department. This system had excellent

results. The measuring equipment and block diagrams are shown in Figures 23-26. Note the high accuracy positioning system and test fixture in Figure 27. This instrument also had internal self-calibrated components and averaged over 6000 times per sweep as compared to 3X for the older T-Ray 2000. The software was considerably more evolved.

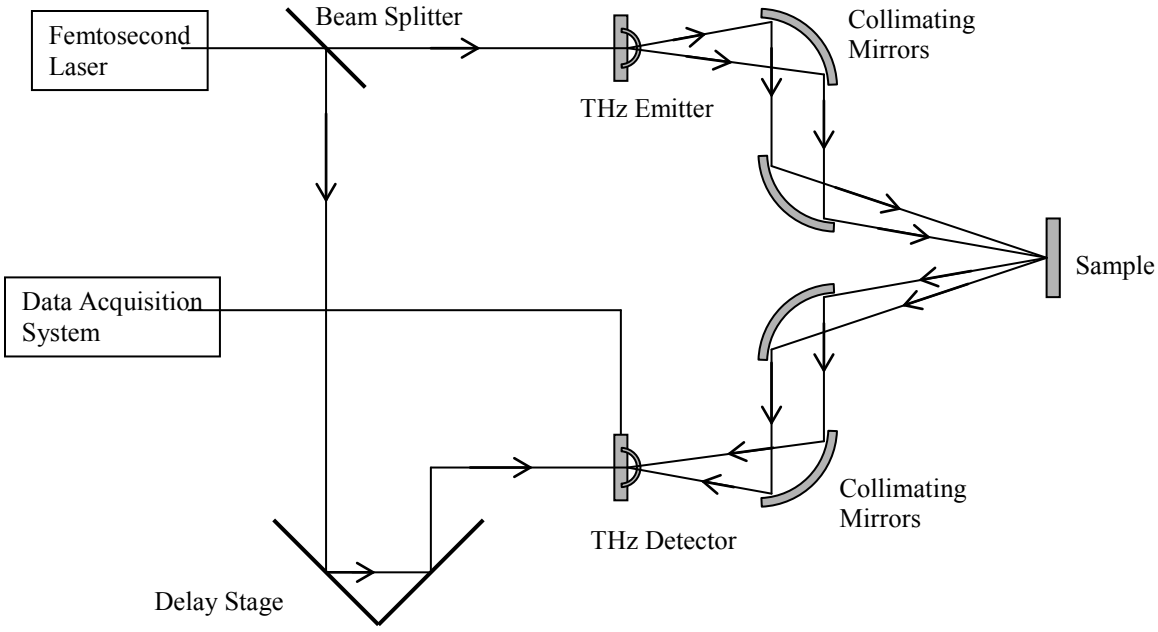

Figure 20 A TDS Reflective Measurement, can be used when samples are not very transparent or with reflector behind sample

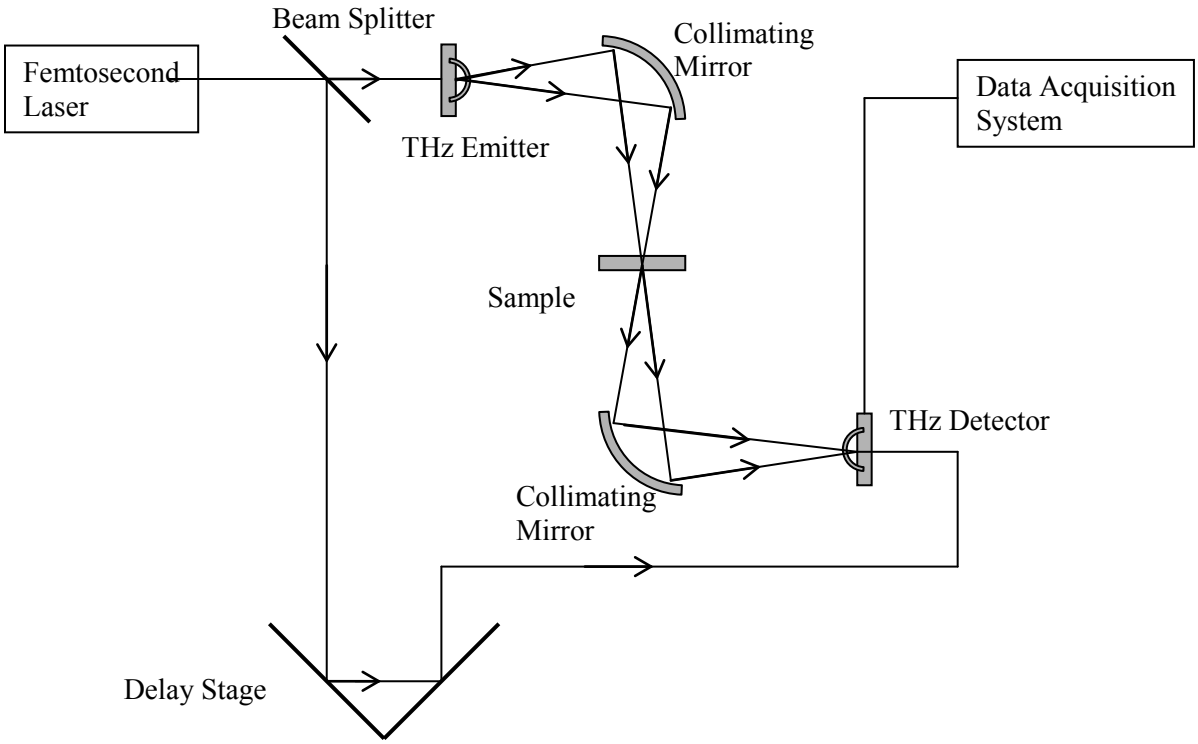

Figure 21 TDS Transmission Measurement for transmission samples – as used for this project.

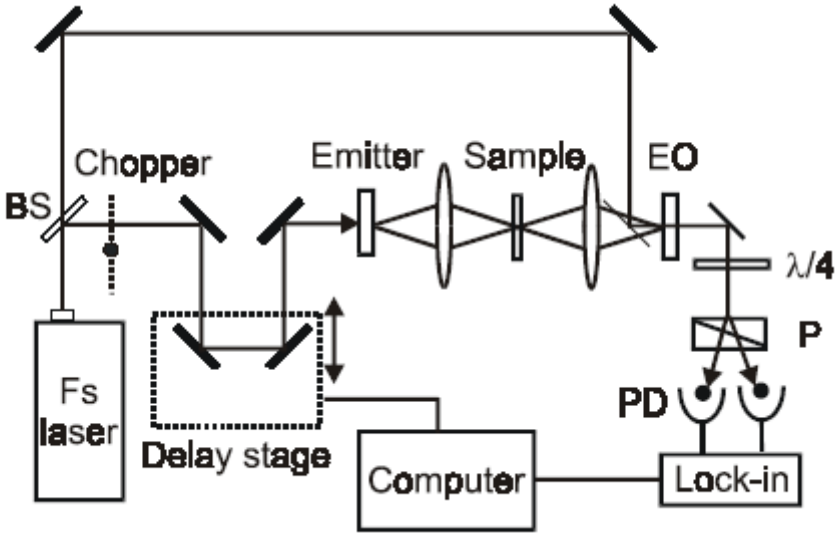

Figure 22 The Basic Elements of Quasi-optical TDS System [P Y Han, X-C Zhang:213]. These components include a source, fast laser, chopper, delay stage, and lock-in amplifier. The T-Ray system did not require all of these components.

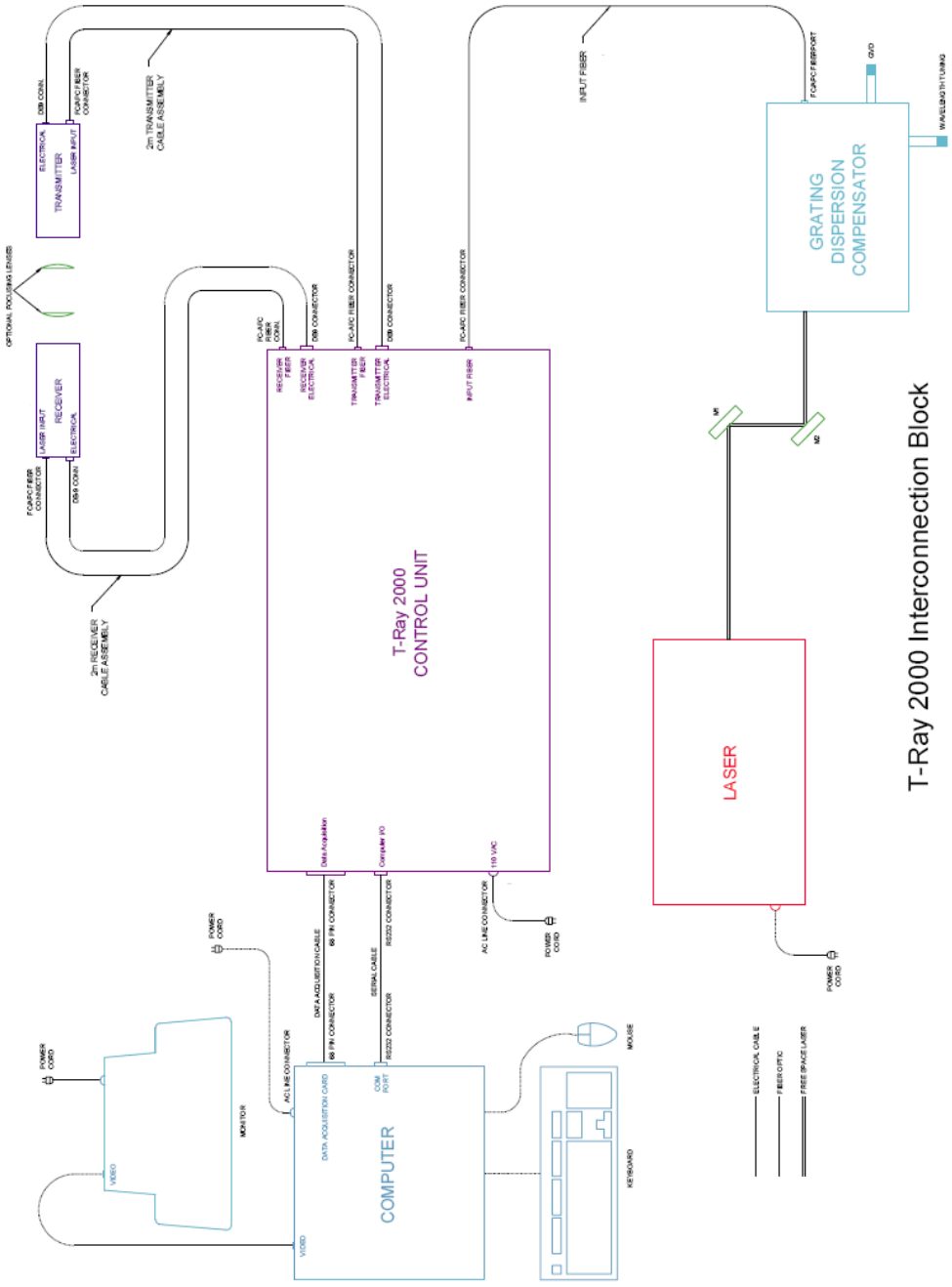

Figure 23 U of AZ T-Ray2000 Interconnection Blocks (Picometrix, Inc.)

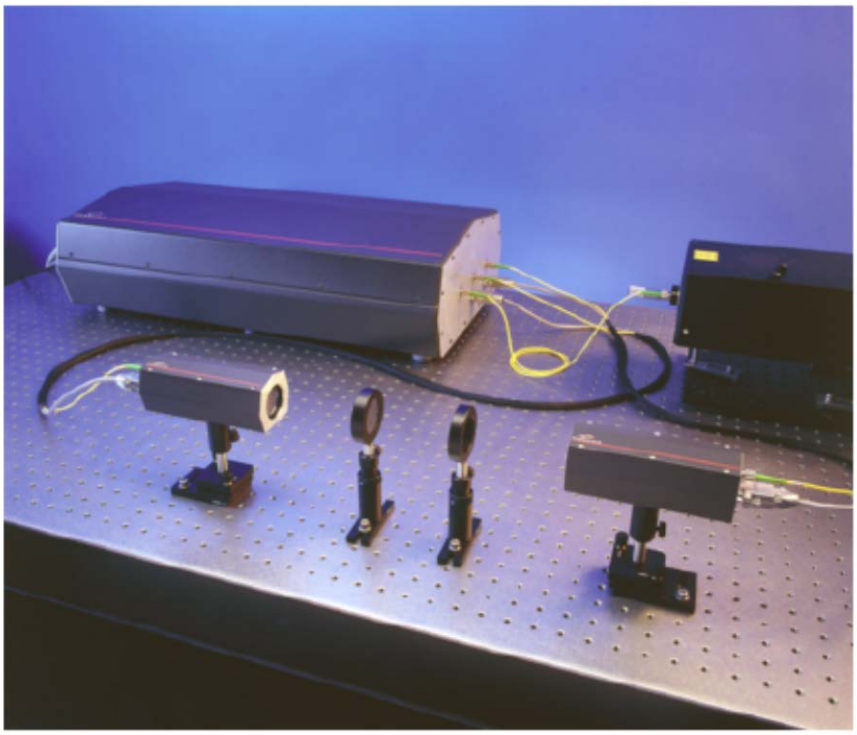

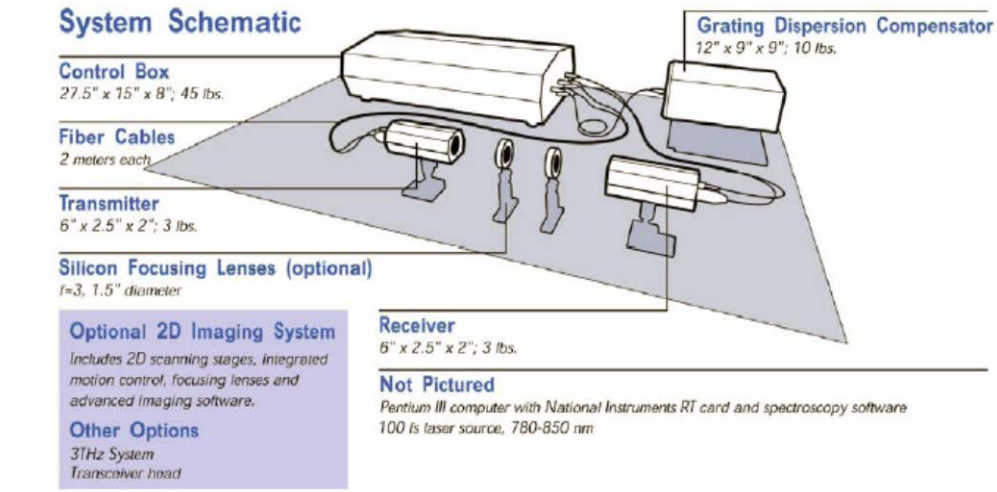

Figure 24: System view of T-Ray 2000 System at University of Arizona (Courtesy, Picometrix, Inc.)

Figure 25: The T-Ray 4000 System at Portland State University (Picometrix, Inc.)

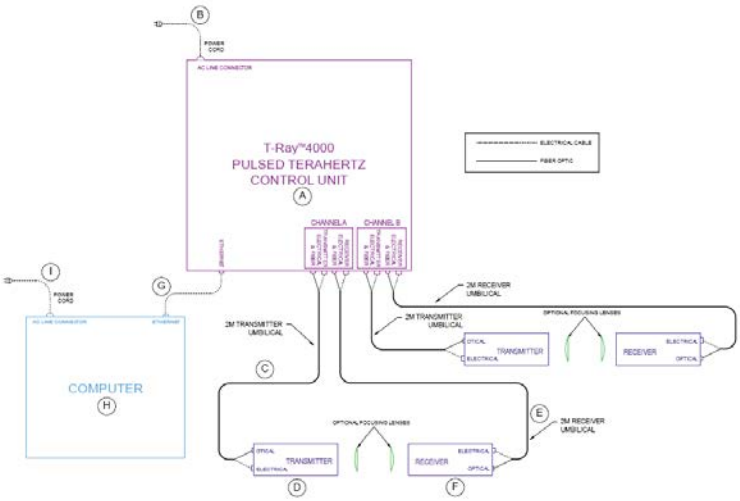

Figure 26 T-Ray 4000 Block Diagram, (Courtesy, Picometrix, Inc.). This figure shows the modern, streamlined arrangement.

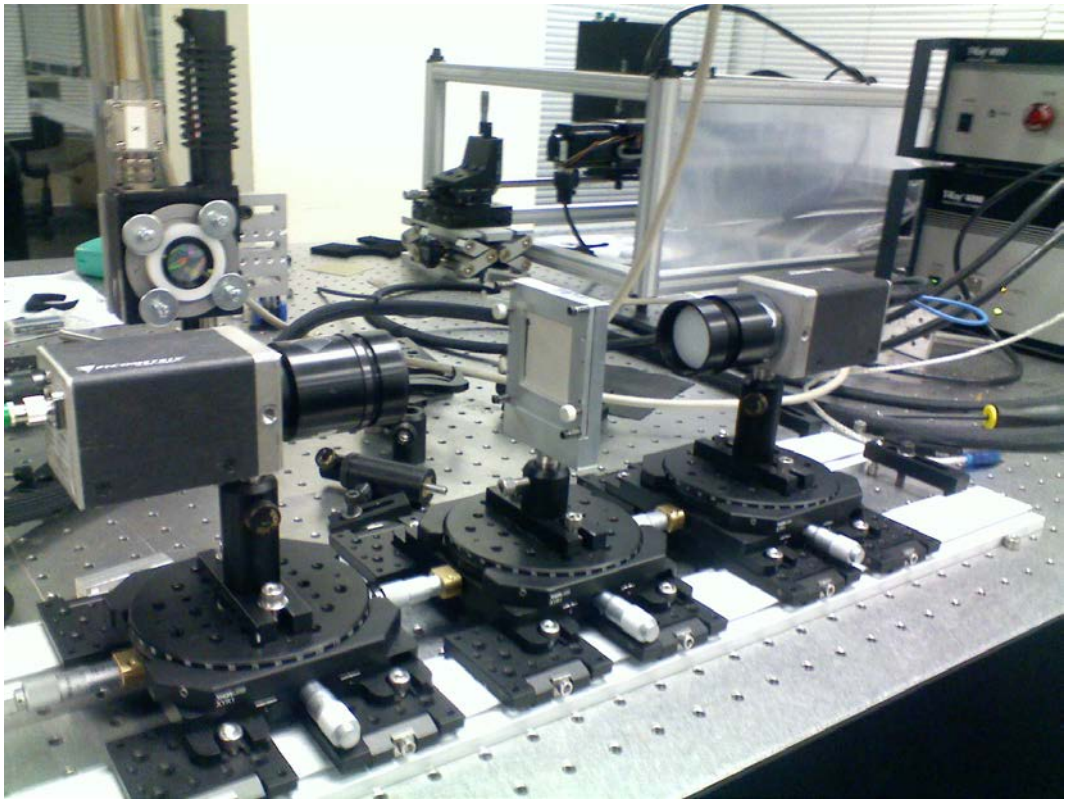

Figure 27 Transmission Sample Measurements on the T-Ray 4000 at Portland State University. This is the actual setup used with test sample and test fixture.

2.2.5 FOURIER TRANSFORM SPECTROMETER (FTS)

2.2.5.1 FTS Section Fourier Transform Spectrometer -Theory and Operation

A Fourier Transform Spectrometer (FTS) system consists of an interferometer, a collimated source, a collimated detector, lock-in amplifier, and a computer to process data and control the phase delay system.

A typical FTS laboratory system (University of Arizona) has a Michelson Interferometer, and its path length changing element is a linearly translating mirror located on one port of the instrument, which produces a variable spatial interference pattern at the output port, where the test sample and detector is located. (See figure 28.) This pattern is picked up by the detector and is transformed into a spectral response curve by a computer using a Fast Fourier Transform tool (FFT). The FTS makes a wideband, scalar measurement, rather than a vector measurement. Figure 29 shows a more detailed breakdown of the system including all the mirrors required.

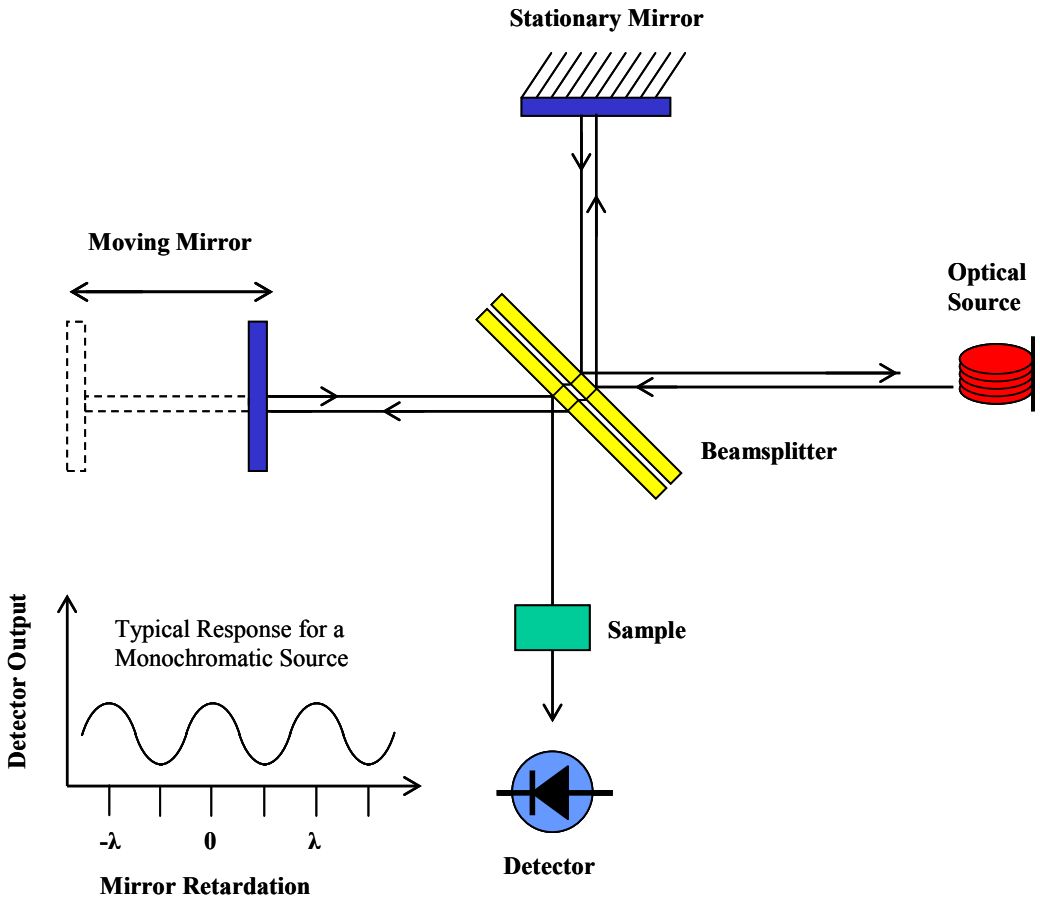

Figure 28 A Basic Fourier Transform Spectrometer

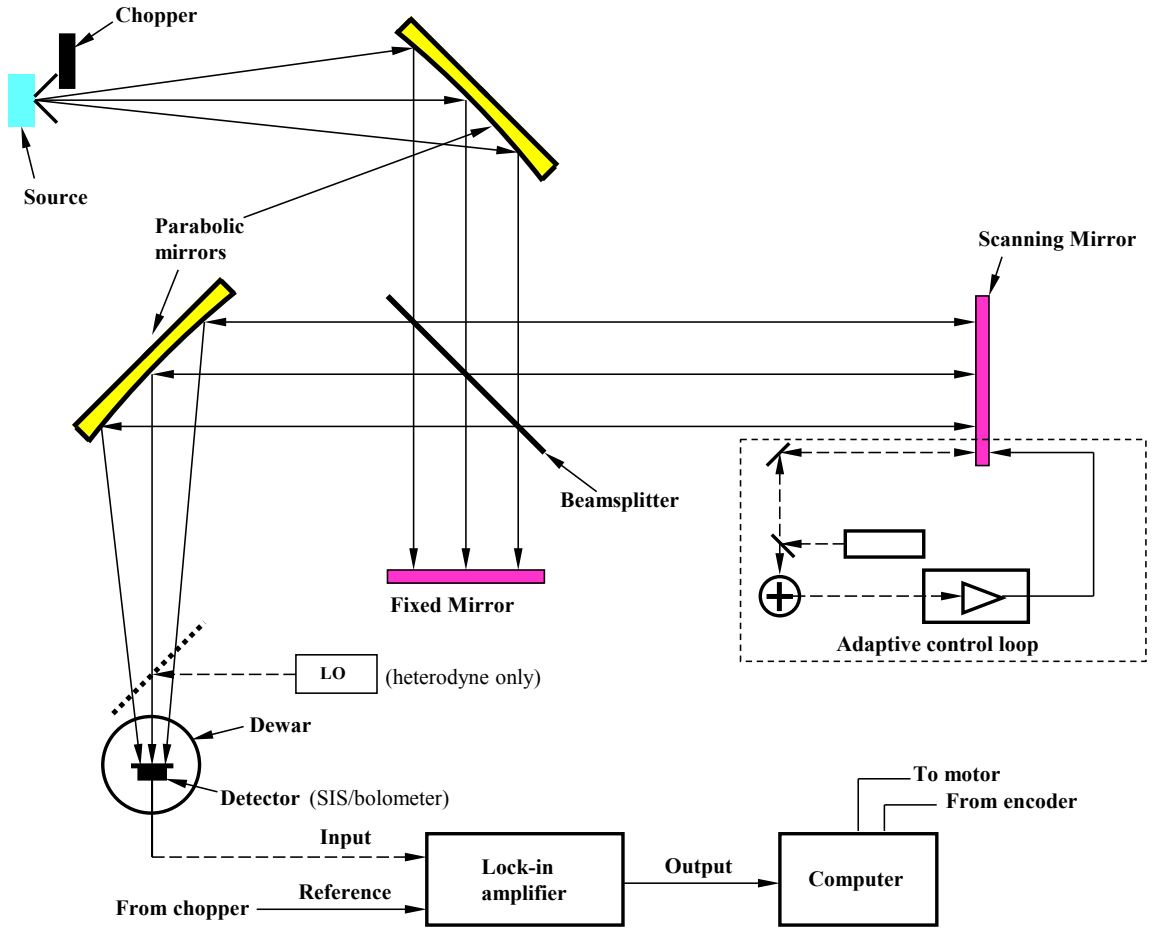

Figure 29 A Block Diagram of an FTS System: with a broadband source and chopper, focusing mirror, interferometer (mirrors, beam splitter, stage controller), a detector, and support equipment.

Transmission or reflection measurements can be made depending on the transmittance of the Material under Test (MUT). For a highly transparent material, we would measure its properties by passing the test signal through the sample before it reaches the detector. For a highly reflective material, the signal would be bounced off the MUT, at an angle, and then collimated into the detector. For some materials, both measurements may be performed.

Another type of FTS (FTMW) uses a pulsed microwave source and a Fabry-Perot cavity interferometer to measure various rotational properties of gasses [Ziurys:177].

For this project, the electrical properties of solid dielectric materials, included permittivity (ε) and index of reflection (n), loss (scalar and also tan δ), and dispersion were measured using an FTS with a Michelson interferometer. FTS systems are very broadband and can operate at frequencies from MHz (10^6 Hz)–THz (10^{12} Hz). A typical FTS operating range is 0.10-3 THz and some go to up to 30 THz. Liquid samples can be measured with the same type of system as solids, but they must be held in a functionally transparent container. FTS-IR systems are also used at infrared and optical frequency bands. An FTS system can also be used for measuring the vibrational properties of solids. To measure the rotational properties of a gas, there is a system is employing a Fabry-Perot cavity interferometer and it operates at microwave or millimeter wave frequencies (100 MHz to several hundred GHz). This system is called a Fourier Transform Microwave/millimeter wave Spectrometer (FTMS) which uses a source that may be swept and/or pulsed.

There are several types of FTS systems are at the University of Arizona. The FTS system used for this project is a model FS-720 FT-IR Michelson interferometer system, manufactured by Research and Industrial Instruments Company. (R.I.I.C.) of London and distributed by Beckman Instruments, Inc., vintage 1978.

Test samples may be cooled, kept at room temperature, or heated or in a vacuum. The measurements performed on this project are done at room temperature with standard atmospheric conditions. The FTS is evacuated by a series of vacuum pumps along with a dedicated lamp cooling pump. This is done to suppress water lines and variations in humidity. The beam splitter must be chosen for the specific band of operation and if the splitter has in band nulls more than one measurement sweep may be necessary. The MUT properties may change slightly due to the time involved in changing out the splitter, recalibrating, and repeating the measurement. Multiple sweeps may be required for calibration and reference levels.

The FS-720 has two perpendicular mirrors, and a polyethylene membrane type beam splitter placed at the vertex, which is oriented at 45 degrees relative to the mirrors, as shown in Figures 30-31. The signal source is a water cooled, stabilized 90-100 watt quartz jacketed, high pressure broadband mercury lamp with a D.C. arc. This is followed by a 15-100 Hz chopper, and a collimator mirror. The lamp has several fixed apertures (3, 5, and10mm diameter) which must be selected. The chopper is a three blade unit resulting in a 15 Hz chopping rate driven by a synchronous motor. The moveable mirror is driven by a positioning system which allows the mirror to travel up to 5 cm on either side of zero path difference point, which sets the resolution (R=1/D). The detector can be a Golay Cell, a high performance (cooled) silicon bolometer, a Hot Electron Bolometer (HEB), or a cooled SIS mixer operating in the detection mode. Some of the

considerations for the detector chosen are sensitivity, dynamic range, bandwidth, frequency band, and stability. A Golay cell is less stable and less sensitive, but requires no cooling and it is wideband and allows easy setup of the system. The runs were performed by using a cooled Silicon Bolometer made by IR Labs (Appendix 10).

The interferometer's optical system (Figure 30) uses surfaced aluminized mirrors. Light from the Arc Lamp source passes through the chopper and is reflected by the off axis paraboloid mirror and is directed to the beam splitter. The collimated beam then is diverted to the moving plane mirror and is then sent to fixed plane mirror (4). The recombined beam is condensed by the off axis paraboloid mirror (5) and is reflected by the plane mirror (6) to the sampling point (7). The beam is further condensed, optionally, by the black polyethylene field lens (8) and the light cone (9) before reaching the window of the detector (10).

The entire FTS system resides at Steward Observatory at U of A and is shown fully configured in Figures 31-32. It requires vacuum pumps, cooling for the source and detectors, a large power supply for the source, the electronics, and the stage motion system. A Stanford Instruments Lock-in amplifier was used and an oscilloscope was required to adjust the chopper pulse/sample rate.

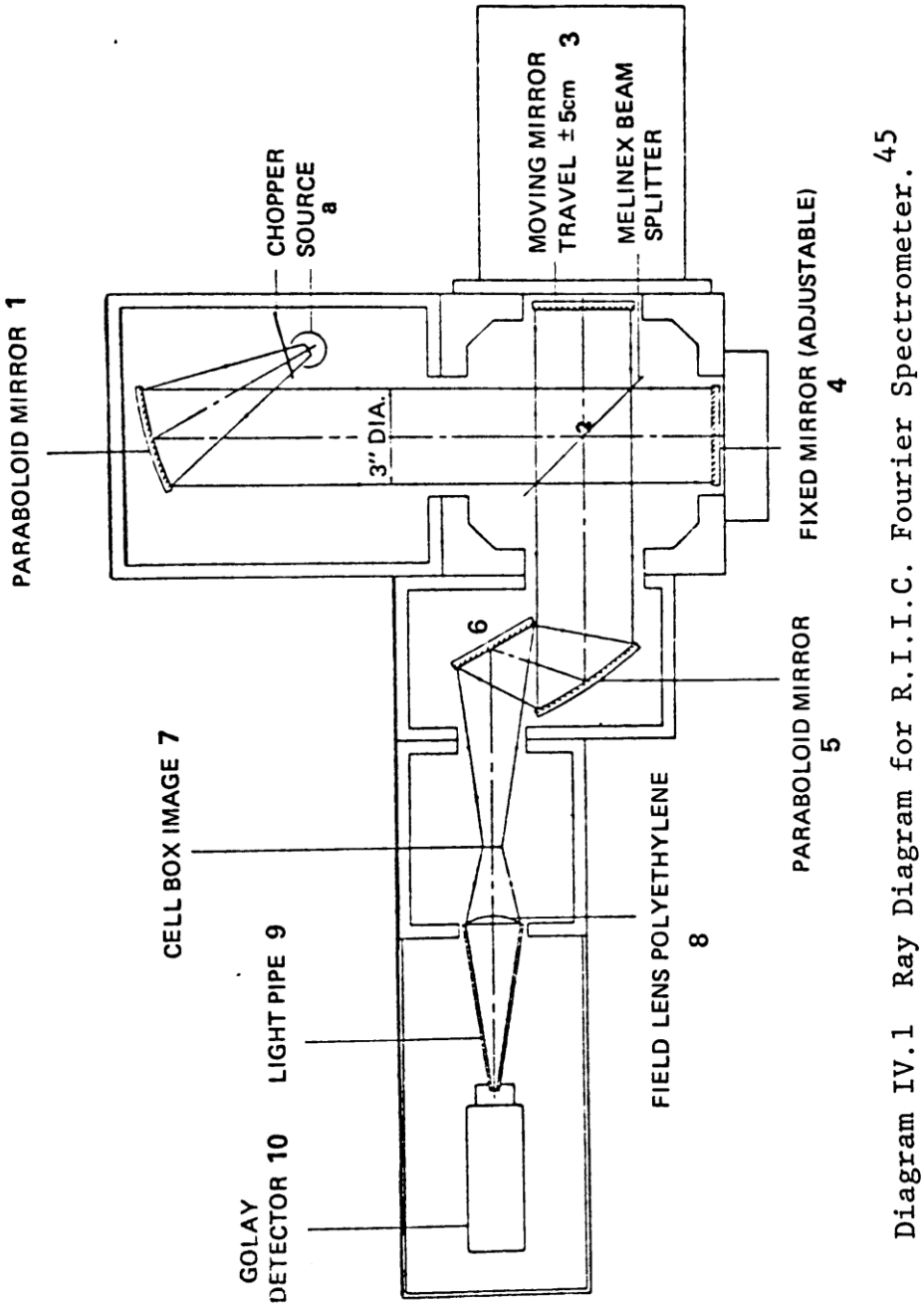

Figure 30 Diagram of RIIS Beckman FTS 720 Machine (RIIC Manual)

One mirror is fixed and the other mirror is on a linearly translating stage which varies the path length (delay) as it moves. This motion generates a spatially varying interference pattern at the sample/output port. (Resolution=1/D). The test material (MUT) is placed between with the output port and the detector (see detail) thereby modifying the signal. A computer is used to for the FFT computations. An important limitation of an FTS is the fact that it will yield only scalar data on the however, it is very broadband with high resolution.

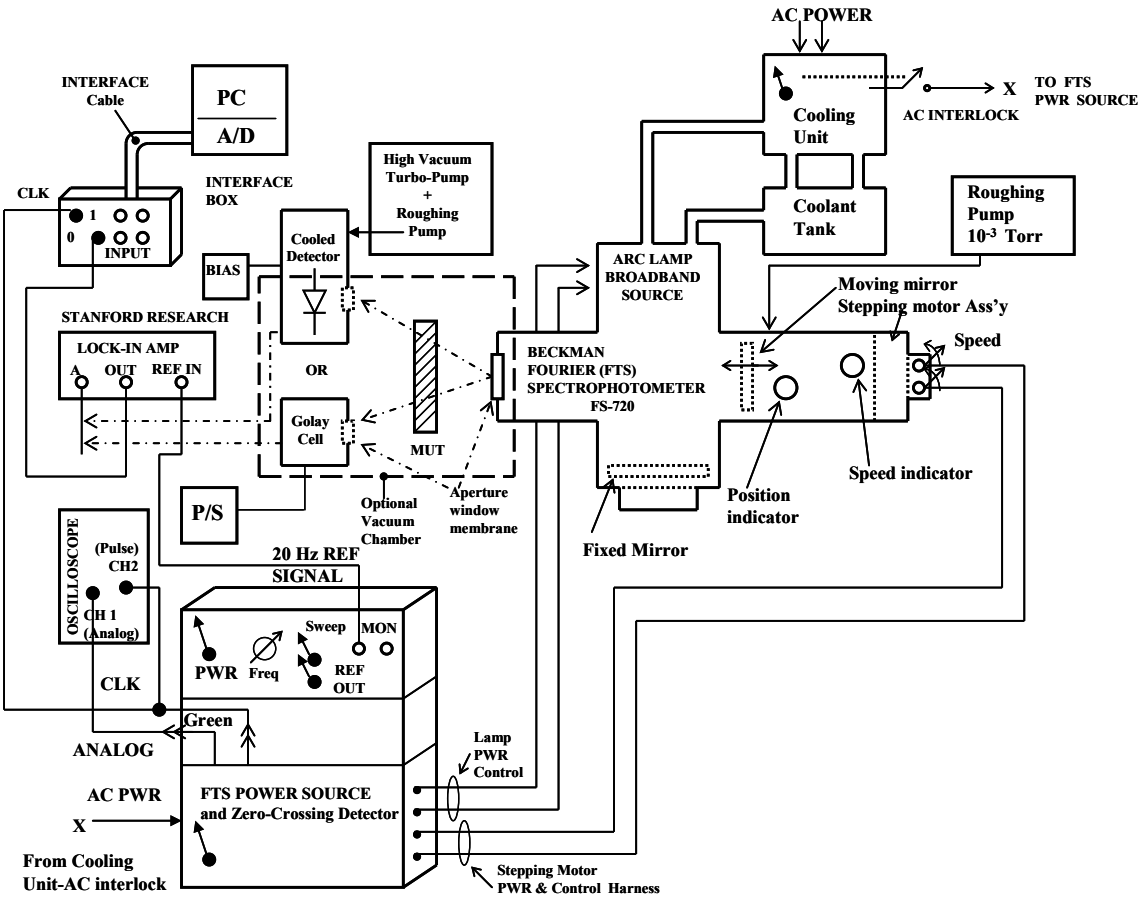

Figure 31 Block Diagram of the Entire FTS-IR System at U of A, Including Vacuum and Cooling Pumps

Figure 32 FTS System Photo with Cooled Silicon Bolometer Detector

The Fast Fourier transform (FFT) computations were done using the MIT FFTW (Fastest Fourier Transform in the West) package based on the Cooley-Tukey algorithm [http://www.fftw.org/].

Transmission or reflection measurements can be made with a Michelson type FTS. The choice depends on the characteristics of the sample, the source, and the detector sensitivity. A translucent dielectric sample may be characterized by transmission or reflection, or both, depending on its relative permittivity compared to air (or measurement medium) and its loss. For a highly transmissive sample (i.e., relative permittivity close air, n=1-10, and/or low loss), transmission type measurements are the best choice, since a reflected signal may be too small to measure. For a highly reflective sample (high permittivity compared to air, or a highly reflective surface) the reflection method may a good alternative as a transmission measurement may not be practical. In both cases, there are surface and internal reflections should to be accounted for and will vary with the angle of incidence as well as the difference in index of refraction (Fresnel, Fabry Perot, Brewster angle). Normal incidence transmission measurements were used in this project which simplified transmission measurements, but is subject to inline reflections producing standing waves.

Figure 33 shows another type of FTS at University of Arizona, that is used for analyzing an atmospheric gas samples, (rotational and vibrational properties) is an FTMS (Fourier Transform Microwave Spectrometer) which contains a Fabry-Perot interferometer which is a swept monochromatic system. [Ziurys:155].

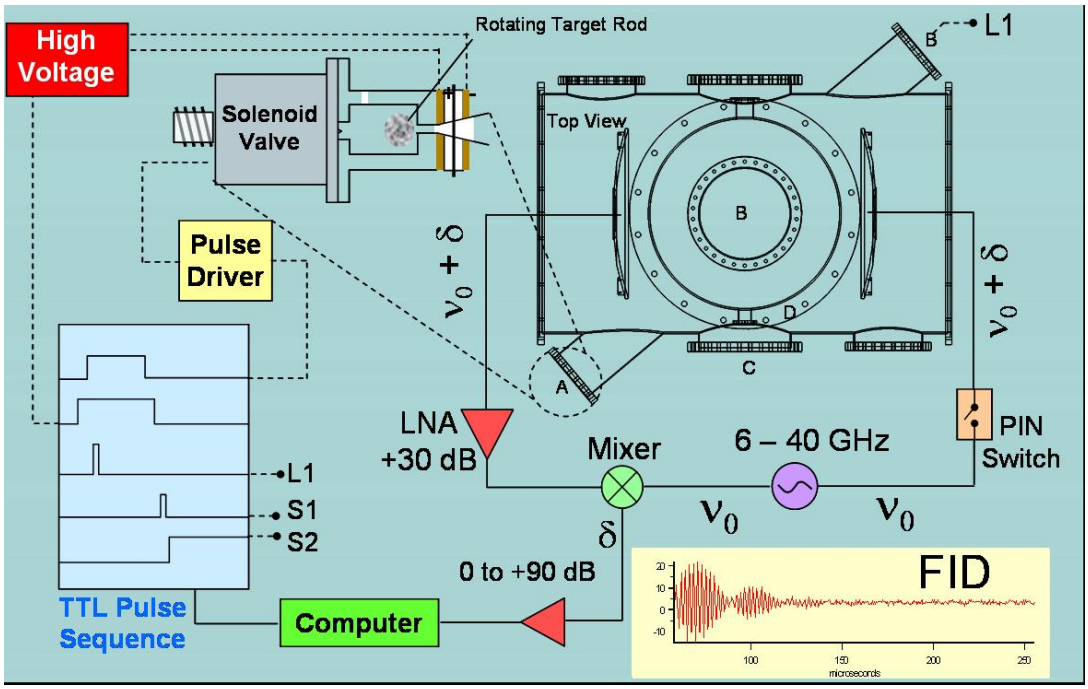

Figure 33 A Monochromatic FTS for Gas Measurement using Fabry-Perot Cavity
(Courtesy Ziurys Group of Steward Observatory, U of A)

The Beckman FS720, used in this project, has a broadband arc lamp source and Michelson interferometer and the output will be the Fourier transform of the spatial interference pattern. Applying an FFT then gives the desired results. For a Fabry-Perot FTMS system, a swept and/or pulsed monochromatic source is used. The output signal will be a modulated sine wave and the hence the data must be swept and taken point by

point at each frequency to construct the entire pattern and a low noise system and processing time is required.

One important benefit of a broadband interferometer FTIR-FTS is the Fellgett (circa 1949) or multiplex advantage. This improvement in spectroscopic techniques is realized when a broadband interferometer system is used instead of a monochromator. It states that Fourier transform spectroscopy will produce a gain of the order of the square root of ***m*** in the signal-to-noise ratio of the resulting spectrum, when compared with an equivalent scanning monochromator (***m*** is the number of elements comprising the resulting spectrum when the measurement noise is dominated by detector noise). The multiplex FTS method requires a good broadband source. It is especially beneficial when the measurement noise is dominated by detector noise. There is also the fact that radiation passes directly through a broadband system; while it is partially absorbed by an inline monochromator system, thus decreasing performance. The result is that the wideband (Michelson FTS) will produce an improvement in signal to noise ratio which is proportional to the square root of the number of sample elements in the spectrum, when compared with an equivalent scanning monochromator system. The disadvantage is that the signal fluctuations will be masked. *[Fellgett:82, 88*]

2.3 Detectors

2.3.1 Description of Incoherent detectors used for this project

Two different incoherent (direct) detectors were used in the scalar measurement systems and their detailed specifications are in the Appendix. For the FTS, a sensitive cooled silicon bolometer, made by Infrared Labs, Inc., Tucson, AZ, was used. This device is brought to 4.2K with liquid helium inside of a nitrogen cooled Dewar. The VDI THz Scalar Analyzer used a Golay Cell detector, distributed by Microtech Instruments, Eugene, OR, and it operates at room temperature. The data sheets for these devices have been included in the appendix.

By comparison, the VDI system was also equipped with a coherent down converter receiver detector, described elsewhere. The TDS (uses Auston switch) and VNA (uses synchronous tracking receiver) have their own coherent detection systems.

A Golay cell [Golay:8] is a direct detection, gas filled, pneumatic device. It has a very wide band of operation and high dynamic range. Since it is uncooled, it has lower sensitivity and a slower response time (25 ms) than cooled detectors. It is mechanically sensitive to outside movement and also tends to drift over time. Hence, it is followed by a lock-in amplifier which removes unwanted electrical and vibrational noise. This

detector has a responsivity of about $8x10^3$ [V/W] and its NEP is about 10^{-10} [W/√Hz]. The Golay cell was used for room temperature measurements.

The IR Labs Silicon Bolometer is cooled to 4.2K (He) and uses also direct detection. It has a higher sensitivity and a faster response time (1 ms) than the Golay Cell. Once it has reached operating temperature, the bolometer is quite stable, but its bandwidth was less than the Golay Cell. As mentioned, this bolometer was used with the FTS spectrometer with a lock-in amplifier. Its responsivity is about $1.5\ x10^4$ [V/W] and its NEP is about $2x10^{-12}$ [W/√Hz]. The Golay cell was found not to be sensitive enough for the FTS application.

2.3.1.1 Detector Types – and Background

Figure 34 shows the two basic types of detection schemes used in Terahertz and Millimeter wave receivers. *Coherent (indirect) detectors* are usually heterodyne systems that use various types of nonlinear elements such as Hot Electron Bolometer (HEB) mixers, Schottky diode mixers, and superconductor insulator superconductor (SIS) mixers. The other type of detectors are *direct (incoherent)* devices which also can use bolometers (usually, Silicon, Germanium, or InSb), Golay cells, Schottky diodes, and Transition Edge Sensors (TES, a superconducting bolometer), and superconducting quantum interference devices (SQUID). No heterodyne carrier source is required for direct detectors.

Coherent detectors respond to both *field amplitude and phase* (E-field/voltage) changes while direct detectors respond to intensity (power) changes and have no phase coherence. Another division among detectors relates to their operating temperature. There are ambient room temperature detectors (uncooled), and there are cryogenically cooled detectors, which have lower noise figure and better sensitivity.

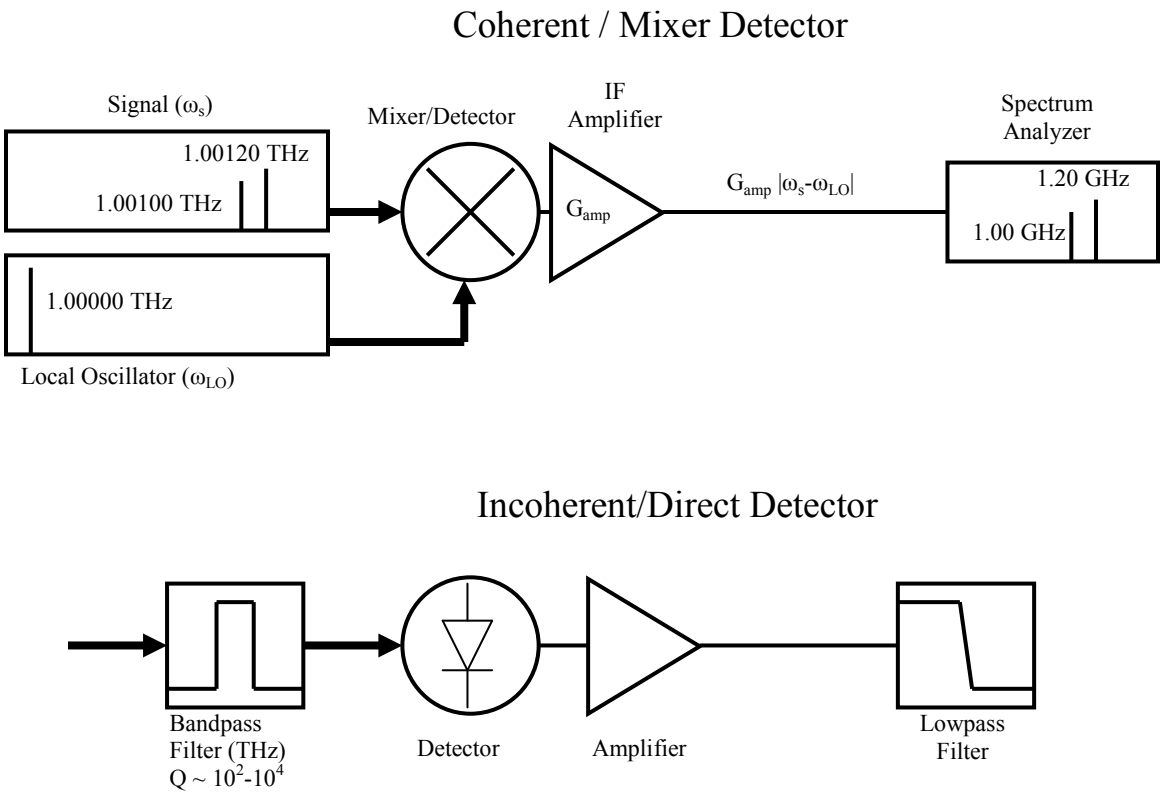

Figure 34 Block Diagrams of Coherent and Direct and Detectors [21]

The theoretically, detectors are bounded by the quantum limit, which the smallest detectable noise change and also be the residual background noise floor levels. These limits are set by nature and are essentially equal to the lowest noise temperature

achievable. Modern detectors, such as those used in radio telescopes and spacecraft receivers, approach these limits today. [Kraus: 172, Rogalski: 197, Siegel: 194, Zmuidzinas: 39]

The detailed performance characteristics of modern detectors types are outlined in Table 7. This table shows Response Time, Responsivity, NEP (noise equivalent power), and Frequency Range.

.

Detector Characteristics	
Coherent detection (indirect, heterodyne)	***Incoherent (direct) detection***
Narrow band, high resolution, high sensitivity and low noise	Better sensitivity in some devices, higher frequency limit, wideband, larger dynamic range.
Mixer down converter, but requires mmw local oscillator	For shorter wavelength, higher frequency
Accurate frequency resolution (high resolution spectroscopy)	Less stable

Incoherent (Direct) Detectors				
Type	**Frequency Range (μm)**	**Response Time**	**Responsivity (V/W)**	**NEP (W/√Hz)**
Si bolometer (4.2 K)	2-2,000	1 ms	1.5×10^4	2×10^{-12}
InSb 4,2 K	200-2000	10 μs	10^3	10^{-12}
Ge 4,2 K	30-1000	10 ms	2×10^4	2×10^{-11}
Schottky diode (zero bias)	1 THz	<1 ns-1 us	4,000-400	$\sim 10^{-10}$.10^{-12}
HEB bolometer Nb, NbN	5 THz	<1-10 ns	780	$10^{-12} \sim 10^{-16}$
Golay cell	20 to 1000μm	25 ms	$8\text{-}100 \times 10^3$	$\sim 10^{-10}$

Coherent Detectors (Indirect)				
Type	**Frequency Range (μm)**	**Response Time**	**Responsivity (V/W)**	**NEP (W/√Hz)**
Si bolometer (4.2 K)	2-2,000 (100THz)	1 ms	1.5×10^4	$\sim 10^{-13}$
Schottky mixer	Medium bandwidth	1 ns	1,000	$\sim 10^{-10}$
HEB bolometer mixer Nb, NbN	5 THz	5 ns		$10^{-12} \sim 10^{-16}$
SIS (tunneling)	<1.5 THz	10GHz	10^3	□4 10^{-13} W@4K - 30fW multiplex

Table 7 Detectors Characteristics compared

The four THz measurement instruments were used for this project had various types of detectors. The Fourier Transform Spectrometer detector used an IR Labs cooled silicon bolometer as the Golay cell was not sensitive enough. The TDS and VNA have their own very sensitive and highly optimized coherent detection systems.

The Picometrix T-Ray Series Time Domain Spectrometer (TDS) is a pulsed system. It has a receiver and transmitter and each has a collimating lens, an antenna, and an electro-optical converter using an Auston switch. [Auston:1]. This system also uses a femto-second laser in combination with the free-space electro-optic sampling unit which contains a semiconductor device acting as a high speed switching detector. The system is coherent system.

The THz Vector Network Analyzer (i.e., a VNA/ZVA with a THz Extender unit) uses up to three superheterodyne receivers (Through, Reference, Reflection ports) plus a tracking receiver that is internal to the VNA. The three receivers allow a full 2-port vector calibration and the output data is given in s-parameters. This setup allows direct extraction and normalization of the data when combined with various calibration schemes (SOLT, TRL, and GRL). The VNA has an internal calibration system and then there also a quasi-optical free space calibration system. Calibration kits are required for each process for best results. The free space calibration done at VDI and PSU was a simple one and still required normalization. The later systems now have a calibration system that integrates with the VNA making parameter extraction less complicated.

The Scalar Network Analyzer at the U of A, is part of a Defense University Research Instrumentation Program (Durip) and was custom developed by Virginia Diodes, Inc. (VDI). It can use various types of detectors depending on frequency band, signal levels, and speed. This system consists of a 5-band millimeter THz heterodyne down converter system with synthesizer, and a Golay cell detector. This detector is very broadband and requires no cooling and is incoherent. It produces a baseband signal that gets followed by a lock-in amplifier (an active filter) along with averaging to remove electrical and mechanical noise.

2.3.1.2 Detector Terminology

Detector: a device that recovers information from a modulated signal

Responsivity = detector transfer function, Output volts/Input power, [V/W]

Signal to Noise Ratio (SNR): Signal power / noise power, SNR (dB) = 10 log (SNR)

Noise Factor, F: (SNR)out / (SNR)in

Noise Figure, NF (dB) =10 log (F)

NEP = min power detectable for particular device; specifically it is that level which produces an SNR of 1, in a 1 Hz window. Mathematically this is given by:

$$NEP = \frac{Noise\ Voltage/\sqrt{Hz}}{R_r(\mathrm{Re}\,sponsivity)} \rightarrow W/\sqrt{Hz}\ @\ f_0$$

Filters can increase/improve SNR by reducing the bandwidth (BW)

Receiver noise Temperature $T_r = T_m + LT_{if}$

T_m = mixer noise; T_f = IF noise, L= mixer loss

Overall system noise figure:

F*tot* = $F_1 + (F_2 - 1)/ G_1 + \ldots.+ (Fn -1)/ (G_1 \ldots.G_{n-1})$,

Where G_1 = Gain of the 1st amplifier, F_1 = Noise Figure

Minimum detectable signal (MDS), noise floor, is the smallest detectable signal power that can be received and demodulated. It can be as a dimensionless ratio or it can be expressed in dB or dBm/Hz. This floor is typically -174dBm plus system noise.

Equivalent noise temperature compared to a matched resistor

$$N_0 = kT_eB$$

$$T_e = \frac{N_0}{kB}$$

Where, No = output noise (equivalent)

Te = equivalent noise temperature

k = Boltzmann's constant, $1.3806488 \times 10^{-23}$ m^2 kg s^{-2} K^{-1} or J/K

2.4 Methodology and Calibration Techniques

There are numerous calibration techniques that make use of various technologies to achieve this goal. For each type of system can use various combinations. At THz bands this process is still evolving. For some systems, direct calibration is used for others such as the THZ VNA, a low frequency calibration is used for the basic instrument and then a free space is added to the entire system.

Some of these combinations are shown in Table 8.

Instrument Technique	**Measurement Type**	**EM-Parameters**	**Material Param's**	**Calibration Technique**
Vector Network Analyzer (VNA, PNA, NVNA)	Vector, contacting or spatial	**Complex** permittivity	Loss tangent, Index of Refraction	SOLT, TRL, TRM, LRM, LRRM, GRL
Time Domain Spectrometer (TDS)	Spatial, non-contacting	**Complex** permittivity and permeability	Index of refraction, loss tangent	Spatial, SOLT, TRM, LRRM
Fourier Transform Spectrometer (FTS)	Spatial, non-contacting	**Scalar** absorption/relative loss and magnitude of dielectric constant	Scalar magnitude index of refraction	Thru or SOLT

Table 8: Extraction parameters and Calibration Techniques

2.4.1 Material Sample Holder and Test Fixtures

The material sample holder assembly in Figure 35 has a number of unique features. It can hold sheet samples of varying thickness and dimensions and the holder has spring loaded spacing screws, so the sample can be carefully removed or rotated without disturbing any positional settings or calibration. In this project the samples were rotated both 90 and 45 degrees. It also has a recess to accommodate rear mirrors for reflection measurements or dual pass transmission measurement. A recently developed adjustable commercial fixture is made by Swiss to 12, Inc. It uses waveguides and has an environmental chamber which can be sealed and is shown in Figure 36.

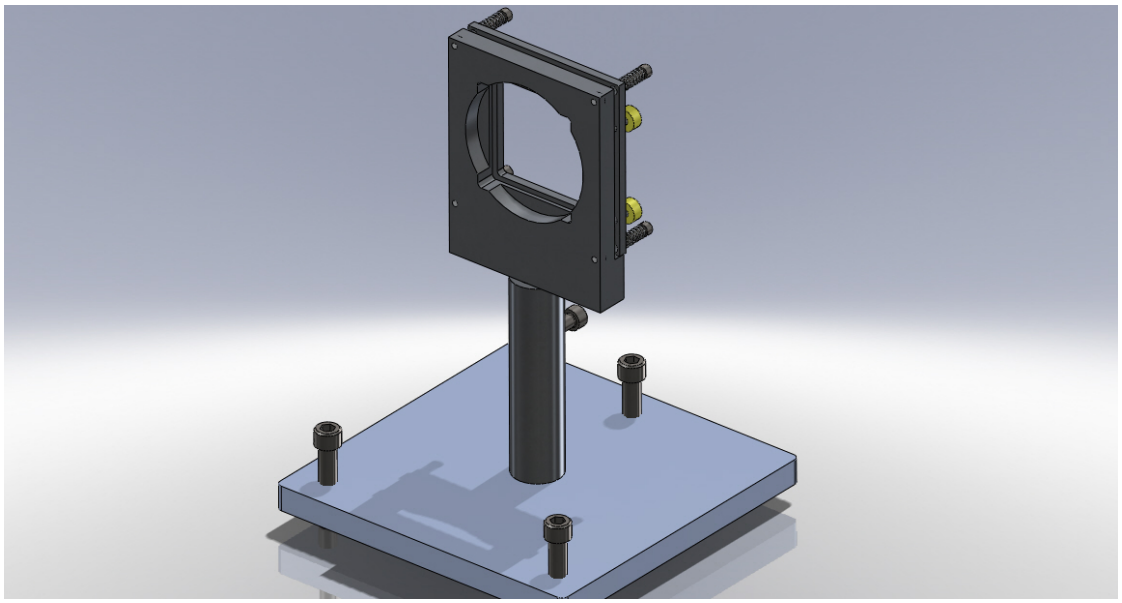

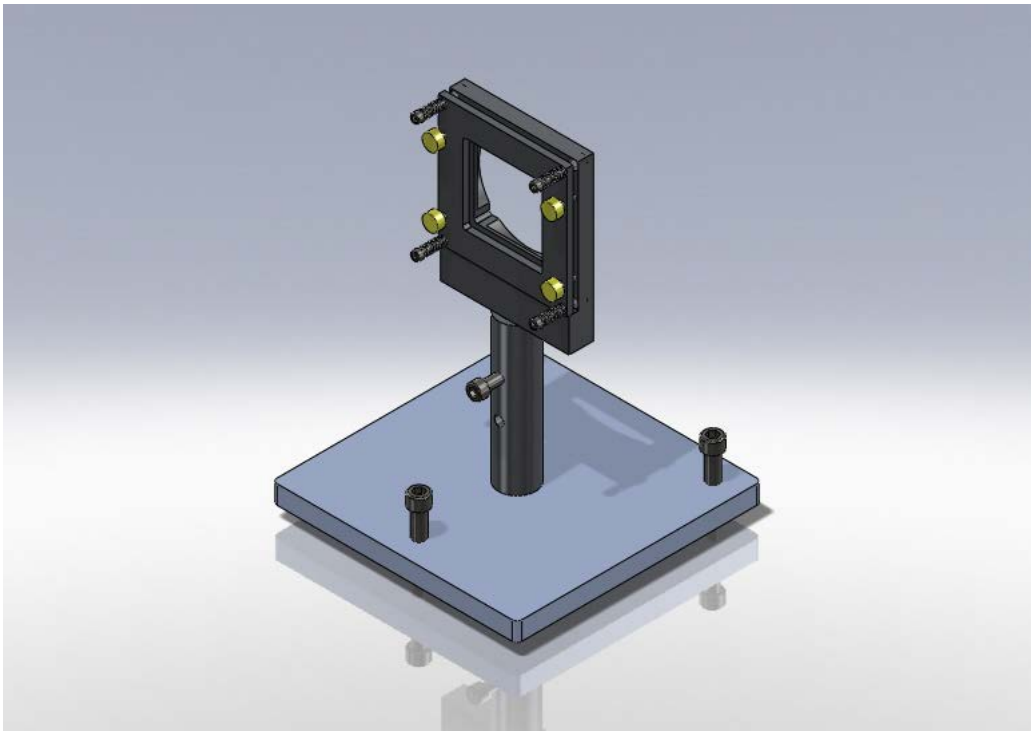

Figure 35: Precision Fixture fabricated by Steward Observatory Model shop and Universal Cryogenics, Tucson, AZ**.**

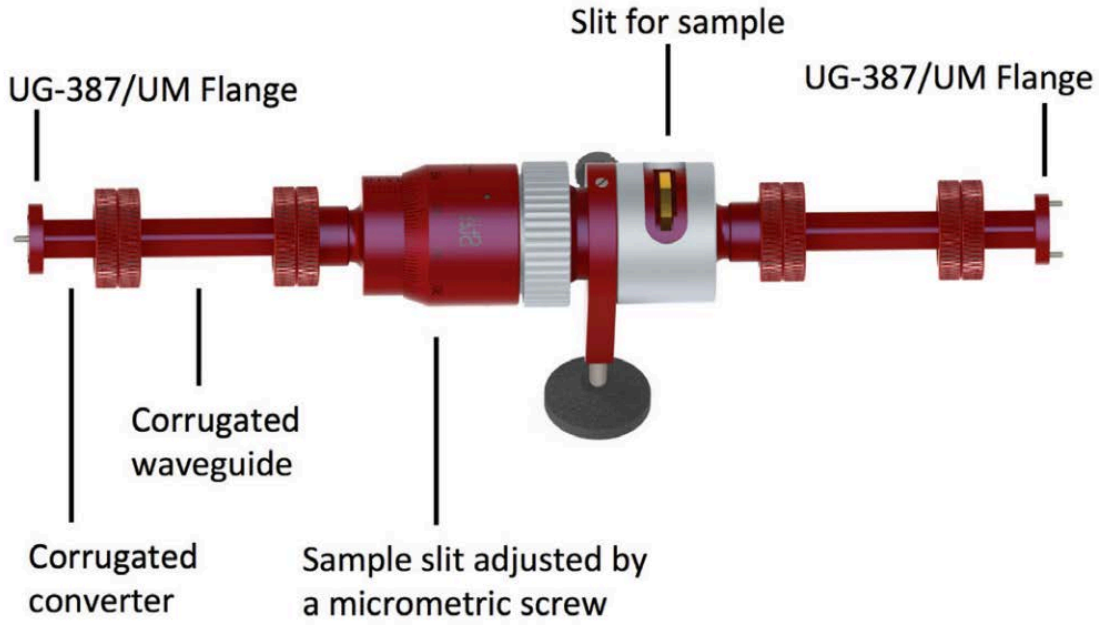

Figure 36: A Commercial Precision Waveguide Test Fixture (courtesy of Swiss to12)

3 MATERIAL CHARACTERIZATION METHODOLOGY

3.1 BASIC STRATEGY

3.2 Scalar Network Analyzer

This system does scalar loss measurements. It was found to have large reflections and no absolute parameter extraction was performed. However, relative loss was determined and compared to known data and was consistent with the material specifications and these results are presented in a later section. There was an inconsistency between different thicknesses for a given sample indicating reflections. An improved approach was developed for a later project which was to use a translation stage for the detector and surround the system by RF absorbent material to suppress reflections. This worked but was too late for my research. The Beer-Lambert law was used for direct computation and was compared to a reference run**.**

3.3 Fourier Transform Spectrometer (FTS)

Reference calibration sweeps were performed periodically. Then the FTS raw data runs were taken and stored for later normalization. The data was converted from the space domain- to the Frequency Domain using Fourier Transforms (FFTW). Then there is centering, apodization, and scaling to match range of lock-in amplifier. Normalization was accomplished by using the reference sweeps. This system produced relative sample loss. No polarization based anisotropy was observed since the source was not coherent.

This could possibly be done using polarization filters or a Wollaston prism. The performance was verified using Beer's Law.

3.4 Time Domain Spectrometer TDS (Vector system: T-Ray 4000)

This vector system gives amplitude and delay time through the sample. Results are averaged 6000 times per sweep within the TDS. Reference passes were taken periodically for normalization. The time domain data is converted to frequency domain via FFT, it was then normalized, scaled, and then extraction routines are employed. This process was done using a modified NEAR Lab MATLAB scripts. Two or three polarizations (H-V, and 45 degrees in some cases) were measured. [Dorney:55]

3.4.1.1 TDS Broadband Extraction (coarse estimate verification)

$$n = n_0 + \Delta n = 1 + c\Delta t/d, \qquad \text{and, } \Delta n = c/v = c/(\Delta s/\Delta t) = c/(d/\Delta t)$$

where Δt= time difference between largest peaks on TDS, d = sample thickness, c=1.1803E10 in/sec, and $\sqrt{\varepsilon_r'} = n, or\ \varepsilon_r' = n^2$.

Two samples with very different dielectric constants were checked with the following results, see Figure 37 and table below:

Sample/ID	Date	Thick(in)	Bkgnd	Delta_t	n	Er	Factory specification	freq(GHz)	loss
R3003_010_1	9/29/2011	0.01	bk05	6.92E-13	1.8169	3.301	3	10GHz	0.0013
		0.01	bk03	6.44E-13	1.76	3.0976			
TMM10_015_1	9/29/2011	0.15	bk03	2.90E-11	3.2799	10.7575	9.2	10GHz	0.0022

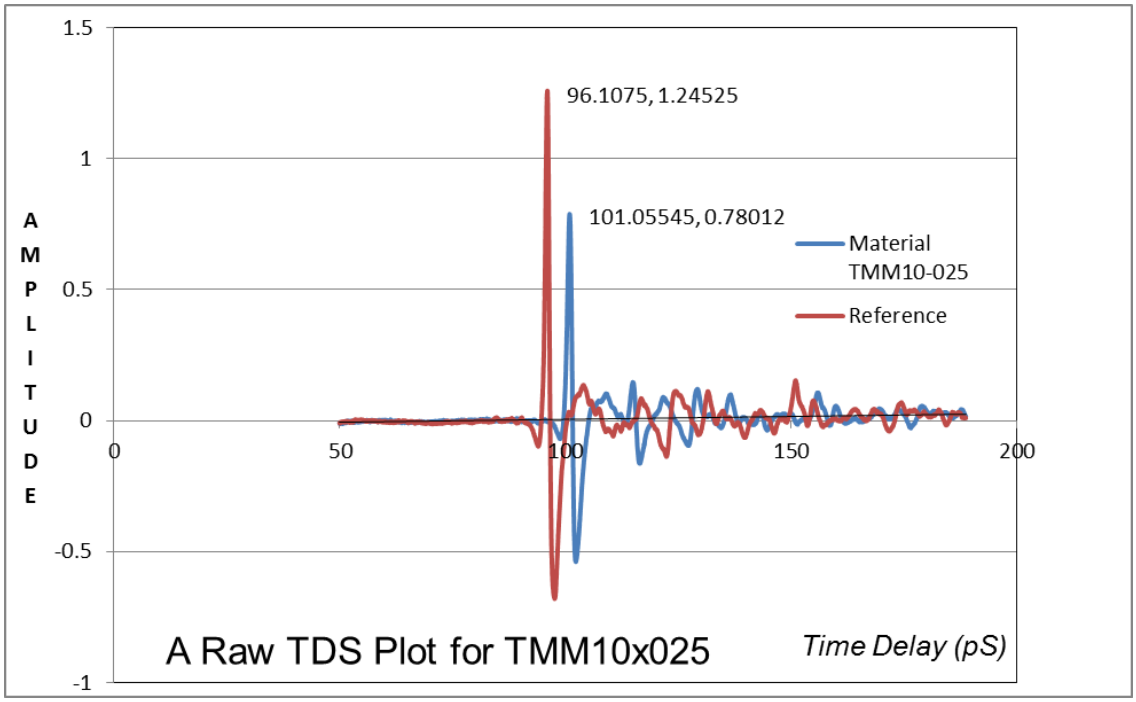

Figure 37 Raw TDS Data Plot for TMM10 Material

3.5 VNA Measurement Technique

3.5.1 VNA calibration and Data Collection

A two-step process is needed. First step is to set local reference planes on VNA by itself with manufacturer's calibration tools. Then the entire system including the THz Extender is connected together and a free space SOLT calibration is done on the complete setup using the VDI waveguide calibration standards, and then store data. A Reference sweep is performed and stored periodically. Then the measurement sweep is run for each sample and polarization and the s-parameters are stored in the VNA. Later, the results are normalized by the Reference run. Exaction routines were then used based on a modified differential phase technique using S21 (dB, and angle) rather than S21 plus S11 together, as in the NRW iterative process. Details are in the Appendix. Obtaining S11 uniquely is problematic in a free space setup. GRL is gradually replacing these calibrations. Numerous new algorithms are being developed.

3.6 Comparative Summary

The FTS/FTSIR has the widest bandwidth of any spectral system and can go to infrared wavelengths and has the multiplex advantage. However, it is scalar, was detector limited, and had reflections that were hard to eliminate, as the detector had be close to the output window. It was hard to observe polarization based anisotropy since the source is not polarized. Polarizers would be needed on the source which is inside the vacuum chamber

or somewhere in the transmission path, adding system loss. The beam splitters are relatively narrowband and must be changes thus requiring recalibration for different materials. The FTS gives excellent qualitative and relative information.

The VNA is also being used for free space spectral measurements and is evolving rapidly. Improved calibration routines are constantly being developed. It is the narrowest band system, but it can go down to much lower frequencies and it has the highest resolution. It can do anisotropic measurements, due to its coherent polarized source and detector but its beam is not very narrow. However, a lot of analysis is required and there is no standard extraction method. As a result, substrate manufacturers are still relying on lower frequency single frequency methods when using a VNA. More recently a new VNA system is being developed that has a beam focusing system and does a reflective measurement. Also this improves calibrations accuracy and a pulsed gated system has been added.

At this time, the TDS appears to be the most promising instrument for free space spectral material measurements. It is coherent, vector based, wideband (but less than an FTS), and has high dynamic range. It is also easy to calibrate, very stable, fast with high averaging capabilities, and does not require a vacuum chamber. Since it is coherent it is ideal for observing anisotropy. Its sensor heads can be moved at different angles. It has less resolution than a VNA, but on the other had is sees material defects and inhomogeneity that is not visible on the VNA. Both the VNA and TDS are limited by the

source power available and detector technology. There are some extraction procedures available for the TDS, but no standard as yet. It relies on amplitude and phase information, rather than s-parameters and since it is pulsed, it does not see some types interfering sources of reflection.

4 PERFORMANCE AND COLLECTION SUMMARY

The Summary Tables in Chapter 5 show the all the test results and demonstrate where the material sample test results overlapped for the different measurement systems. This consistency is an important part of this project.

4.1 DATA RESULTS AND DISCUSSION

This section discusses the different aspects of the data collection for each instrument.

4.1.1 FTS FS-720 Summary (Wide Bandwidth, 200 MHz – 3 THz, Scalar Measurement System, University of Arizona)

The FTS measurements established the relative loss of the samples. This type of FTS-IR (Beckman FS720, circa 1978) is a scalar system using a Michelson interferometer and a broad band source and a cooled detector. This instrument has very wide bandwidth (up to 3+ THz). The FTS makes use of the Fellgett Multiplex Advantage (all spectral elements are measured simultaneously) and the Jacquinot Throughput Advantage (no dispersive slits). Typical water lines were used to verify operation before the relative material loss was observed. The measurement accuracy was limited by inherent system positional coarseness and reflection issues. A number of modifications were made to the electro-optical mechanical servo positioning system of the FTS to improve its accuracy. The test fixture had sample position repeatability issues, so later a precision test fixture was developed and it was used successfully for the Vector and TDS measurements (see

figures). The discrete Fourier transform (DFT) conversion was accomplished using the MIT/FFTW software library.

4.1.1.1 FTS System Limitations and Methodology

This FTS instrument is a complex system (see figures in experimental section) and has electrical and mechanical components contributing to drift, variance in positional tolerances, environmental effects, FFT analysis, normalization, and computational error.

4.1.1.1.1 *FTS Specific sources of error*

1. There were positional and calibration errors due to the FTS mirror electro-optical servo mechanism and the test fixture. Each time a new sample was inserted, both the system and fixture had to be reassembled and realigned, so the calibration was disturbed. Reflections changed due to the repositioning of the fixture, but mirror alignment was not disturbed. Two different beam splitters were used depending on the sample properties (loss and dielectric constant). The high dielectric constant TMM10 material required a thinner, lower loss splitter/filter.

2. In-line reflections resulted from proximity of the source to the detector producing interference that could not be eliminated. This distance was limited by the detector sensitivity and noise. A cooled IR Labs bolometer (He @ 4.2K) detector was used for best results. An improved precision fixture eliminated some of these issues and it was used for the vector VNA and TDS measurements. (Figure36).

3. The FTS uses an incoherent (non-polarized) broadband arc-lamp source. It was not realized, at this time, that the some of the test materials were anisotropic, so polarizers were not employed to examine this behavior. Since the VNA and TDS are coherent systems anisotropy was easily observed and quantified at that time. Note that coherent systems are polarization sensitive due to the fact their sources are usually polarized and also they respond to the phase of the carrier wave and its envelope.

4. There was some uncompensated dispersive loss due the different characteristics of the interferometer filter/beam splitters. Normalization minimized this effect.

5. Instrument drift, both electrical and mechanical, was noticeable. There can be thermal and humidity issues. The detector was kept a constant temperature (4.2K) with a liquid helium dewar and a liquid nitrogen (77K) cooled radiation shield. Internally, there is a bolometer detector element and a low noise amplifier. Additionally, there are vacuum pumps for the detector and the FTS eliminating the air and moisture and also a cooler is required for the light source. (see the FTS experimental section).

6. Numerical Computational Error: Computational error is inherent due to rounding and the FFT numerical calculations, but system noise and performance limitations dominated, so these effects were negligible.

7. Experimental computational error is due manual centering of calibration reference signal and data signal plus jitter and noise on raw data. Triangular apodization reduced this effect but cannot eliminate it.

8. Source non-uniformity and instability are difficult to compensate for except by normalization and taking reference and sample measurements close together.

4.1.1.1.2 *FTS Measurement Methodology*

The FTS experimental process consisted of two scans (reference and sample measurement), an FFT conversion, centering, apodization, scaling, and normalizing. Note again that the spatial interference patterns from the interferometer in the FTS are converted to frequency domain using the FFTW routines.

4.1.2 TDS Summary (Wideband, 100 MHz – 1.5 THz), Picometrix T-Ray Series Instruments at Portland State University and The University Of Arizona)

The measurement and extraction techniques for the TDS were done in a similar way to the VNA, using the newly developed precision test fixture but the calibration process is very different. Insertion loss and time delay (phase) are the raw results of this process. . This is analogous to VNA s-parameters for transmission loss (VNA:dB_S21) and angle

(VNA: Phase_S21). The TDS data must first be converted from time domain to frequency domain. This was done using MATLAB's FFT library functions to perform the DFT. These results were then used to determine the material parameters. Fresnel and Fabry-Perot reflections were examined and were not a large contributor, as the index of refraction (permittivity) of most of the samples was relatively low. For the VNA, all reflections were taken into account to provide a comparison. The TDS does not see some reflections due its picosecond time slices. Fresnel effects were calculated.

The materials were evaluated using two different TDS systems (one at U of A and one at PSU). There were three groups of samples material types. The parameter extraction data presented herein was the data harvested at the NEAR Lab at Portland State University.

The TDS measurements were originally performed at the Physics Department, at the University of Arizona, using a Picometrix T-Ray 2000, Time Domain Spectrometer. This system was not integrated and had many separate components, which reduced calibration accuracy and performance. It was found that this equipment was too coarse for parameter extraction. It also had unresolvable positional and calibration issues and was decommissioned. Nevertheless, the relative loss measurements were in agreement with the results of the other systems used.

Successful parameter extraction was achieved using the newer Picometrix T-Ray 4000 instrument system located at PSU. This is a more advanced and fully integrated system

that has the positional accuracy needed for reliable parameter extraction. It also has much more sophisticated averaging techniques (UA=3, PSU=600+), which significantly reduced noise and systematic errors. This instrument operates from about 0.02 - 1.5 THz. The parameter extraction tool used was based on routines developed for the instrument at PSU [Ref: Kniffin, Dorney et al.] and they were modified for this application and implemented using MATLAB.

4.1.3 Vector Network Analyzers at Portland State University (PSU) and Virginia Diodes Incorporated (VDI) – (Rohde & Schwarz, ZVA-40, VNA, plus VDI THz Extender, 325-500 THz/PSU, 500-750 THz/VDI, in two bands)

This summary covers the portion of the data taken at PSU (325-500 GHz) and VDI (500-750 GHz) using their ZVA-40 VNA systems with VDI THz Extenders. The results compare well at both bands and also with correlated to the FTS (relative) results. The data compared closely to manufacturer specifications.

Polarization related anisotropy was most pronounced in the composite materials. Each sample was rotated 90 degrees (H-V polarization) and variations in loss were observed and correlated with the results from the different measurement systems. Some data was dropped due to recording errors or bad normalization files.

4.1.3.1 A Note On The Three Different Sample Types

The first group of samples types (designated '**ECE Samples**') consisted of *Photopolymers*, used in 3-D printing, and were supplied to the ECE Department by Stratosys, Inc. These polymers were isotropic and uniform and tests confirmed this, but over time, they changed thickness due to changes in temperature and humidity. The loss was consistent in all polarizations. The average dielectric constant (ε_r') ranged from 2.7 to 3.3, depending upon the sample and thickness. The Loss Tangent (Df, Tan delta = ε_r"/ ε_r') varied from .055 to 0.12. Due to the proprietary nature of the material, comparison data was not provided by the manufacturer, but values were typical for polymers per Stratosys catalog and data compiled by various researchers.

The second sample group consisted dielectric substrates consisting of circuit laminates and composite materials supplied by **Rogers Corporation**, Advanced Circuit Materials Division, in Chandler, Arizona. These materials were mildly anisotropic depending upon composition and thickness and wave polarization. The dielectric constant and loss tangent varied with polarization of the incident wave (0, 45, and 90 degrees, see summary table, section 5.3). The THz material parameters obtained were quite close to the manufacturer values, even though they are done at lower frequencies, (10-14 GHz) using the *IPC 650 TM 2-5-5-5, Stripline Test Method for Permittivity and Loss Tangent.*

The third group of materials (polyethylene and polymer plastics) consisted of low density (LDPE) and high density polymer (HDPE) and polyethylene sheets supplied by

McMaster-Carr, Inc. These materials were well behaved electrically and did not display any significant anisotropic behavior, but they are not mechanically suitable for packaging or substrates. Their average dielectric permittivity varied from 2.2 to 2.5 and the loss tangent varied from .001 to 0.013. This was consistent with values obtained by other researchers and systems.

Parameter extraction was done directly from the s-parameter data. This done was using a combination of a modified differential phase technique and the Method of Multiple Reflections was used to computer the Fresnel loss, (see Appendix 11).

4.1.4 VDI/DURIP Scalar Network Analyzer (100 TO 850 GHz)

Significant reflections were noted in this setup that could not be removed. While the system was coherent, the Golay detector is incoherent. Although it is wideband, it is subject to significant drift and not as sensitive as other detectors. The data was consistent in that the relative loss of the test materials agreed with specifications by the manufacturer. However, thicker materials did not always have more loss due to large reflections. Later, a technique was developed to reduce this error by the addition of a translation stage on the detector combined with averaging software. However, this setup was not yet available at the time the measurements were performed, so this data was held in abeyance. The relative loss computations were done using Beer's Law.

4.1.4.1 Scalar VDI System Notes

1. Large Reflections - both inline and external were observed. Inline reflections: the reflection between the source, the load, and the test fixture in the signal path.

2. External reflections – due to objects outside or near the signal path. That was mitigated by using a corrugated absorptive cover placed over the measurement setup, but variations were still noted. In the future, these reflections and noise could be mitigated by using a stepper motor on the detector stage and averaging, however, this equipment was not available at the time of these measurements.

The relative loss of the samples measured on the scalar system agreed with the relative loss of the samples measured on the vector systems. The scalar system results were sometimes inconsistent for different thickness materials due to uncompensated calibration and reflection errors. There was also drift of the Golay Cell detector and errors due to the manual range settings of the Stanford Lock-in Amplifier. The next generation of this measurement system used a stepping stage on the detector to improve accuracy, and absorptive shielding, but it was not available at the time my measurements were taken.

4.1.5 A Note on Material Thickness

All of the parameter extraction methods rely directly on the accuracy of the sample thickness and its location. Besides thickness varying as a function of temperature,

moisture, and age, there are also errors introduced by the accuracy by which the thickness is measured as well as the position on the sample. A digital caliper and a micrometer were used for this project. Thickness was then surface averaged and many times and sometimes it was different from the factory data. In some cases, a noticeably different result obtained by the two thickness methods when the surface was not exactly flat.

A number of new precision thickness measurement instruments have been developed and this is an emerging area. Some of these systems use terahertz Time Domain Spectrometers; THz Ellipsometers, and there are also nanoscale measurement systems such as those developed by Filmetrics, Inc., and Fischer Technology.

Small vector calibration errors are introduced relating to sample thickness, fixture offset, and the same errors are for the calibration shorting plate. The exact position of sources and detectors were maintained by locking everything on a Newport test stage. These types of calibration issues are currently addressed when using a new technique called Gated Reflect Line (GRL) calibration (Agilent/), which was not available for this project. [Bartley, Begley:44].

4.1.6 System Measurement Considerations and Sources of Error

4.1.6.1 General Sources of Error for all systems

The Fourier Transform Spectrometer is useful in establishing relative loss but has limited absolute accuracy. By incorporating a more sophisticated electronically controlled stage servo, the performance of the FTS could be improved. There are also limitations related to the beam splitters (dispersive loss) and arc lamp source (non-polarized).

The TDS gives a vector measurement by virtue of the fact that it gives both amplitude and time delay through the test material. However, the repeatability of the translation stage positioning and distance of travel, the pulse width of the laser, the optics, and the performance E/O transmit and receive modules limit accuracy. The measurements that were performed at Portland State University used a more sophisticated TDS to address these issues.

Network analyzers have inherent limitations relating to couplers and switches, calibration, frequency tracking, connector repeatability, jitter, and drift. These effects can be minimized by using proper measurement techniques. The network analyzer has greater sensitivity, higher dynamic range, better resolution, and possibly more accuracy than any of the other equipment available but less bandwidth and complicated extraction. Completely different programs were used to convert the s-parameter data to loss tangent than the ones used for TDS.

Specific Issues:

1. Reflections (3 types, external reflections, Fresnel, and internal Fabry-Perot)
2. Calibration, repeatability, and random errors

3. Electrical Component Drift: detectors (Golay and cryogenic), and sources (especially arc lamps and unleveled oscillators.
4. Mechanical drift and sample thickness changes
5. Diffraction and radiative loss
6. Dispersion
7. Scattering
8. Temperature changes
9. Systematic errors
10. Sample integrity
11. Source beam width to assure sample coverage without spill-over
12. Surface propagation effects and losses

4.1.6.2 TDS errors and limitations

1) Match beam diameter to area of target (can use iris or lens) or surface scan
2) Antenna bandwidth and loss on transmitter and detector heads (Auston switch assembly)
3) Bandwidth limited by laser pulse width, transmitter, and detector systems
5) Calibration routines
6) Software
7) Translation stage distance and positional accuracy and speed
8) Averaging routines (quite good)
9) Local reflections and diffraction (minimal)
10) Fresnel and Fabry-Perot reflections

11) Environmental (water vapor, temperature)
12) Surface finish and reflections

4.1.6.3 FTS Errors and Limitations

1) Bandwidth of beam splitter
2) Software Fourier transform and apodization routines
3) Source bandwidth and intensity and detector sensitivity
4) Integrity of parabolic source focusing mirror
5) Translation stage travel range
6) Translation stage positioning system (optical servo) and positional accuracy
7) Standing wave and Fresnel reflections
8) Manual index for stage has limited positional accuracy
9) Detector integrity: cooled silicon bolometer or Golay cell (less sensitive and less stable)
10) Residual water vapor (vacuum pump system) and other environmental factors
11) Sampling rate and sweep time
12) Lock-In Amplifier range and calibration

4.1.6.4 THz Network Analyzer (VNA/SNA with VDI-THz Extender)

1) VNA wave guide (WR kit) calibration and software
2) THz Quasi-optical (free space) calibration routine
3) Stability and drift of network analyzer and averaging

4) Added system noise of Extender assembly and instrument noise error
5) S-parameter firmware and software tools
6) Repeatability and random thermal error and jitter
7) Standing waves and Fresnel reflections
8) Stability and integrity of source, couplers, receiver, connectors and cables
9) Accuracy of reference path and beam coupling

4.1.6.4.1 *VNA Specific sources of error*

1) Switch Repeatability Errors
2) Connector Repeatability Errors
3) calibration standards
4) connector interface
5) Interconnecting cables
6) Coupler Directivity and match
7) Source Match
8) Frequency jitter and synthesizer noise
9) Frequency Response Reflection Tracking
10) Transmission measurements generate the following three systematic errors:
11) Isolation
12) Load Match
13) Frequency Response Transmission Tracking and jitter [Sternberg, Dvorak:94]

Experimental Related Computational Error

1. Manual Centering of calibration and reference sweeps plus jitter and noise on raw data adds random error. Apodization and normalization reduces this effect.
2. Errors in the reference sweep add small normalization error plus drift.

3. Computational round off errors on data evaluation.

4.1.6.5 FTS Data Summary Details

In the summary table in Chapter 5, five of the samples measured shown are manufactured by Rogers Corporation. These composite materials included TMM10, Theta, R4350B, R3003, and R6002. The relative loss correlated in all cases to data sheets. TMM10 had the most loss and R6002 had the least loss, as expected.

The range of the dielectric constants of these samples varied from 2.92 to 9.2. Two beam splitters/filters were used to cover this range. All samples were measured using the 7.4 mil splitter except for TMM10, which required the 1.1 mil splitter, due to its higher dielectric constant and loss.

4.1.6.6 Materials measured at Portland State University VNA - Summary details (see section 5.3-6 for tables).

A precision fixture was developed to eliminate positional issues for the VNA and TDS measurements, but there are still system calibration limitations and errors due to tolerances on the thickness of test material its positional offset from the reference plane in the fixture and the same is true for the shorting test plate.

The results for the Rogers materials, McMaster polyethylene, and the Stratosys (ECE) samples are presented in a Chapter 5 and they correlated well to the manufacturer's data.

The relative loss was consistent between the systems and frequency bands. Most measurements were taken in both horizontal and vertical polarizations planes (H-V). Anisotropic differences in dielectric constant and loss were observed for all test systems.

4.1.6.7 Material measured at Virginia Diodes, Inc. - VNA summary details

The results for the Rogers samples correlated well to their data sheets and relative loss was also consistent. The VDI data was taken in the horizontal and vertical polarizations and differences were tabulated. Data was also taken for some samples in the 45 degree polarization. These results agree closely with the data taken at PSU as shown on the summary table.

4.1.6.8 Material measured at Portland State University – TDS summary details.

The results are presented in a table for eight Rogers materials, two polyethylene samples (HDPE, LDPE), and three Stratosys (ECE) samples. Dielectric constant and loss correlated well to the manufacturer's published data. This data was taken in the horizontal and vertical polarization and differences were observed. These results agreed with the VNA data.

5 DATA TABLES AND PLOTS (see Chapter 4 and 6 for related discussions)

5.1 FTS Data Summary Table

FTS Data Summary using UA Astronomy Beckman FS720 Spectrometer								
Sample#	Mfgr (Thickness) caliper	Part/lot #	Description	Thickness (actual) Micrometer	ε_r / Loss [3]	Average Relative Level	Voltage (Scale factor) [1], [2] mV	*Scaled Average (mV)*
1	Rogers (0.0260)	2012159	**TMM10**	**0.025**/(0.0266)	9.2/**0.0022**	5.00	1.18	***5.90***
1, pol	Rogers (0.0510)	2011993	**TMM10**	**0.05**/(0.05085)	9.2/**0.0022**	2.50	1.58	***3.95***
1	Rogers (0.0195)	3025938	**Theta**	**0.02**/(0.0197)	4.01/**0.0118**	0.65	4.31	***2.80***
1	Rogers (0.0100)	3018414	**Theta**	**0.01**/(0.01055)	4.01/**0.0118**	0.50	11.60	***5.80***
1	Rogers (0.0205)	2007683	**R4350B**	**0.02**/(0.01995)	3.66/**0.0037**	0.50	12.30	***6.15***
1	Rogers (0.0100)	2007680	**R4350B**	**0.01**(0.0102)	3.66/**0.0037**	1.00	9.00	***9.00***
1	Rogers (0.0205)	3015151	**R3003**	**0.02**/(0.02045)	3.00/**0.0013**	0.80	13.00	***10.40***
1, pol	Rogers (0.0100)	3014902	**R3003**	**0.01**/(0.01015)	3.00/**0.0013**	0.70	18.00	***12.60***
1	Rogers (0.0205)	2020435	**R6002**	**0.02**/(0.02035)	2.94/**0.0012**	0.75	24.80	***18.60***
1	Rogers ((0.0105)	2010668	**R6002**	**0.01**/(0.01075)	2.94/**0.0012**	1.00	28.20	***28.20***
Samples arranged in order of Relative Loss and corresponding manufacturer data								
Notes								
(1) 1.1 mil Beam Splitter/Filter used for TMM10 Measurement (SF correction 3.5)								
(2) 7.4 mil Beam Splitter/Filter used and set as reference using R6002								
(3) Rogers Corp. Loss Tangent @ 10 GHz using method IPC-TM-650-2.5.5.5C (ipc.org)								
Er, using stripline resonant Method								
TMM™10 = thermoset microwave materials are ceramic, hydrocarbon, thermoset polymer composite								
THETA = MCL-HE-679G Laminate, GHA-679G Prepreg, Halogen Free (FR4 replacement)								
RO4350B™ = proprietary woven glass reinforced hydrocarbon/ceramic (replaces PTFE/woven glass)								
RO3003™ = high frequency circuit materials are ceramic-filled PTFE composites								
R6002 = RT/duroid™ Laminates								

Table 9 FTS Data Summary

This table shows the results of the FTS measurements. The samples tested were in pairs of two different thicknesses for comparison and to allow parameter extraction via Beer's Law. The relative loss of the samples tested came out in the same order as vendor specifications. The relative loss correlates to the data obtained on the other instruments.

5.2 FTS Data Plots Thickness Pairs (Theta, TMM10, R6002, R4350B, and R3003)

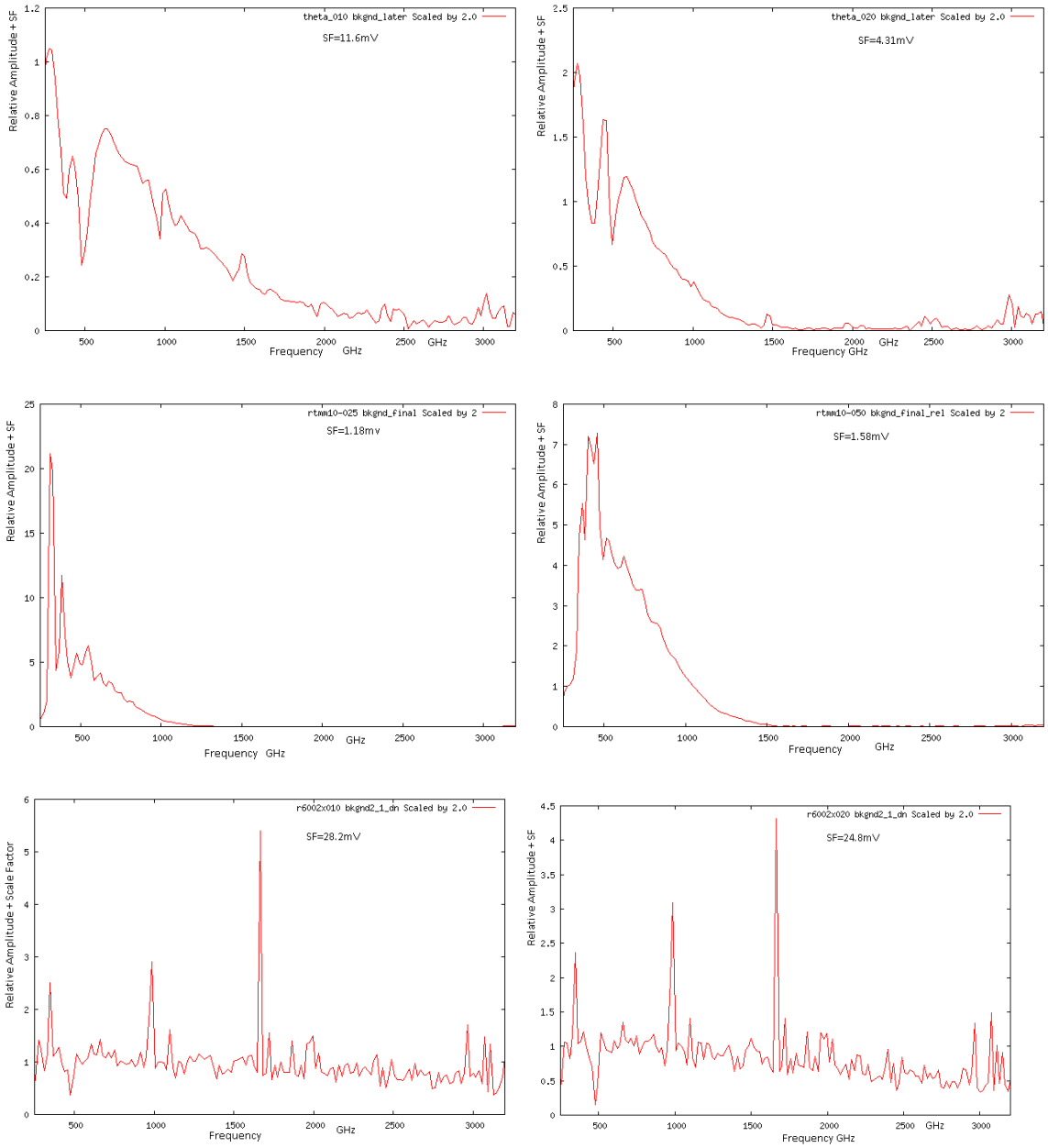

Figure 38 FTS Plots (continued)

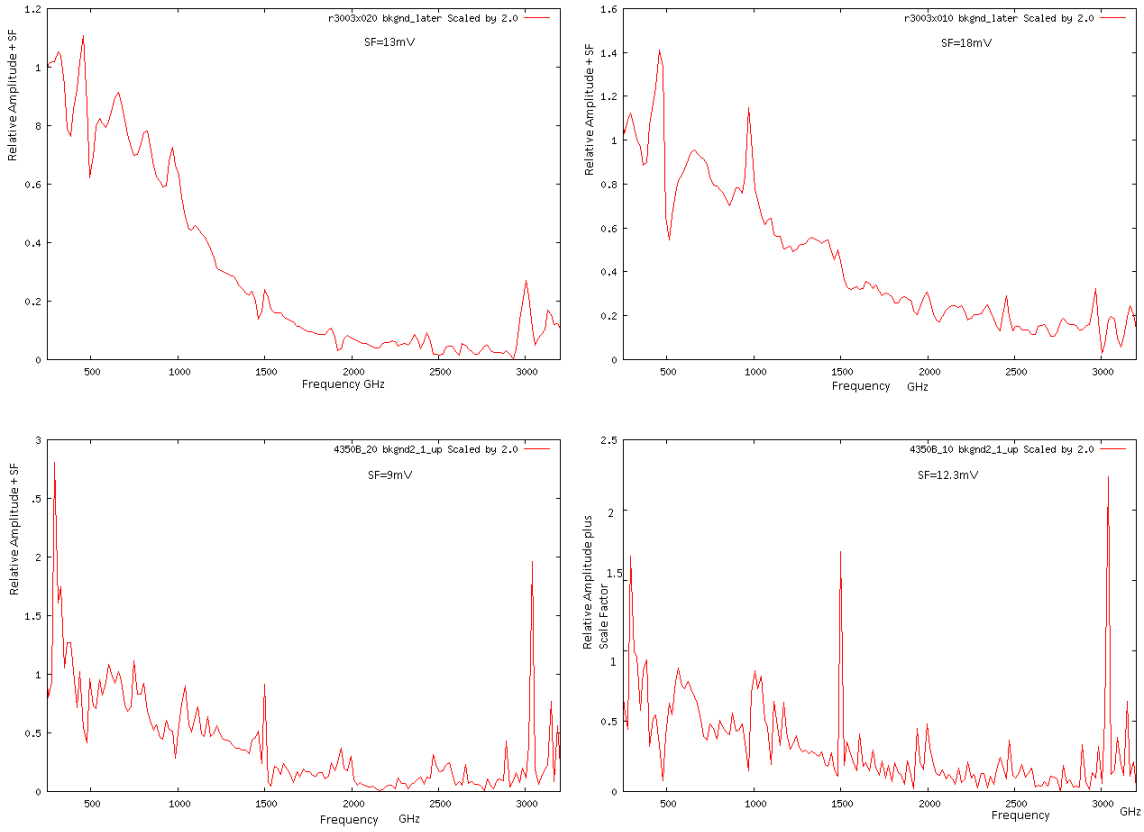

Figure 39 Show FTS Plots for R3003 and R4350B. A larger scale factor indicates lower loss since more signal will pass and it also passes more source noise.

The FTS plots show the water spectral lines, source and signal noise, reflections, and relative amplitude plus a scale factor (in mV) for the lock-in amplifier. Each plot is normalized by a background normalization file, indicated on the upper right area of each plot, along with the scale factor (SF) from the lock-in amplifier. Hence, the scales can be compared as done the Table 9. For the lower loss R6002 material, the response is relatively flat with source noise visible, while for the materials with more loss such as TMM10, levels drop off quite rapidly above 500 GHz, it has lower output voltage and the reflections are attenuated. Thicker materials will have more total loss.

These ratios and results were spot checked using two different thicknesses and the Beer-Lambert Law.

$I_n=I_0 \exp(-\alpha d_n)$, where I_n is Intensity (power, uW) or $(mV)^2$, d_n = sample thickness, and α= absorption coefficient, this is also designated by many authors as "k".

On the other hand, κ is used for extinction coefficient and they are slightly different. $\alpha = 4\pi f\kappa/c$. Beer's law assumes a monochromatic calculation for α, but an average value can be substituted for approximate results [Chan:86]. The attenuation constant values were also calculated at two frequencies: 500GHz and 1000 GHz.

From the ratio of intensity, for two different thicknesses of same material, one can determine α, the attenuation constant (similar to extinction coefficient). Each can be also compared to air. I_0 power and was calculated obtaining α. Since we are taking ratios, the I_0 Intensity term will initially cancel out. At frequencies above 500 GHz the loss get considerably larger as was also found on the vector systems.

Since the plots were averaged visually, and a non-monochromatic source was used, this is a coarse estimate, but it shows that the FTS data was fairly consistent, in spite of reflections, calibration variances between samples, and beam splitters. For a material, with a voltage ratioV_2/V_1, the intensity ratio (in power) will vary by the square, or a

voltage ratio of about 1.4, since intensity is a power quantity. This can be seen to be the case. Errors in actual thickness values and reflections account for some of this error. So for a thickness ratio of 2:1, we would expect a ratio of √2.

k or α= abs [ln (I_2)-ln (I_1) / (d_1-d_2)], (per length, inch), and $I_{1,2} = (V_{1,2})^2$, amplitude squared for each thickness.
$I_0 = I_{1,2} \exp(k*d_{1,2}) = (V_{1,2})^2 \exp(k*d_{1,2})$, for two different thicknesses of the same material.

5.3 VNA and TDS Data Summary Tables as discussed in Chapter 4

Materials Measured 6/5-2012 at Portland State University using VNA / ZVA 40										
Frequency (GHz)	Sample Description	Thickness (actual)	ε_r / Loss Tan (manufacturer) @10GHz	ε_r' (minimum) (H, V, 45)	ε_r' (maximum) (H, V, 45)	ε_r' (average) (H, V, 45)	ε_r" (average) (H, V, 45)	Loss tan (minimum) (H, V, 45)	Loss tan (maximum) (H, V, 45)	Loss tan (average) (H, V, 45)
325 - 500	ECE Blk 1mm	1mm (1.02mm)	no data	2.63, 2.66, ---	2.81, 2.79, ---	2.73, 2.73, ---	0.0948, 0.0948, ---	0.0302, 0.0302, ---	0.0381, 0.0381, ---	0.0347, 0.0347, ---
325 - 500	ECE Blk 2mm	2mm (2.00mm)	no data	2.70, 2.69, ---	2.79, 2.78, ---	2.74, 2.74, ---	0.0912, 0.0912, ---	0.0302, 0.0302, ---	0.0358, 0.0358, ---	0.0334, 0.0334, ---
325 - 500	ECE Clr 2mm	2mm (2.34mm)	no data	3.04, 3.03, ---	3.17, 3.16, ---	3.10, 3.10, ---	0.382, 0.382, ---	0.118, 0.118, ---	0.123, 0.123, ---	0.127, 0.127, ---
325 - 500	R3006 25mils	25.0mils	6.15 / 0.0020	6.65, 7.04, ---	7.46, 7.92, ---	7.14, 7.53, ---	0.122, 0.126, ---	0.0143, 0.0138, ---	0.0193, 0.0187, ---	0.0172, 0.0166, ---
325 - 500	R4350B 60mils	59.5mils	3.66 / 0.0037	3.65, 3.68, ---	3.80, 3.86, ---	3.75, 3.78, ---	0.0527, 0.0770, ---	0.0099, 0.0152, ---	0.0173, 0.0247, ---	0.0141, 0.0206, ---
325 - 500	R5870 31mils	31.0mils	2.33 / 0.0012	2.38, 2.37, ---	2.52, 2.50, ---	2.45, 2.43, ---	0.0094, 0.0094, ---	0.0038, 0.0038, ---	0.0039, 0.0039, ---	0.0038, 0.0038, ---
325 - 500	R6002 20mils	20.5mils	2.94 / 0.0012	2.77, 2.81, ---	3.03, 3.06, ---	2.90, 2.94, ---	0.0039, 0.0039, ---	0.0012, 0.0012, ---	0.0014, 0.0014, ---	0.0013, 0.0013, ---
325 - 500	R6002 30mils	29.5mils	2.94 / 0.0012	2.84, 2.83, ---	3.06, 3.03, ---	2.94, 2.93, ---	0.0039, 0.0039, ---	0.0012, 0.0012, ---	0.0014, 0.0014, ---	0.0013, 0.0013, ---
325 - 500	TMM10 25mils	26.0mils	9.2 / 0.0022	9.39, 9.73, ---	10.42, 10.69, ---	9.92, 10.26, ---	0.0901, 0.1525, ---	0.0060, 0.0120, ---	0.0111, 0.0174, ---	0.0089, 0.0151, ---
325 - 500	Theta 20mils	19.5mils	4.01 / 0.0118	3.80, 3.77, ---	4.68, 4.70, ---	4.13, 4.12, ---	0.1899, 0.1899, ---	0.0406, 0.0406, ---	0.0595, 0.0595, ---	0.0487, 0.0487, ---

Materials Measured 10/24-2012 at Virginia Diodes, Inc. using VNA/ZVA40										
Frequency (GHz)	Sample Description	Thickness (actual)	ε_r / Loss Tan (manufacturer) @10GHz	ε_r' (minimum) (H, V, 45)	ε_r' (maximum) (H, V, 45)	ε_r' (average) (H, V, 45)	ε_r" (average) (H, V, 45)	Loss Tan (minimum) (H, V, 45)	Loss Tan (maximum) (H, V, 45)	Loss Tan (average) (H, V, 45)
500 - 750	R3006 25mils	25.0mils	6.15 / 0.0020	7.17, 7.50, 7.19	7.93, 8.36, 8.04	7.61, 8.00, 7.63	0.3348, 0.3642, 0.3814	0.0077, 0.0118, 0.0153	0.0729, 0.0757, 0.0780	0.0446, 0.0480, 0.0509
500 - 750	R3003 10mils	10.0mils	3.00 / 0.0013	2.66, 2.71, ---	3.32, 3.38, ---	3.07, 3.10, ---	0.0055, 0.0183, ---	0.0018, 0.0055, ---	0.0019, 0.0066, ---	0.0019, 0.0062, ---
500 - 750	R3010 10mils	10.5mils	10.20 / 0.0027	11.28, 11.15, ---	14.06, 13.32, ---	13.19, 12.40, ---	0.1105, 0.0965, ---	0.0078, 0.0053, ---	0.0113, 0.0122, ---	0.0098, 0.0092, ---
500 - 750	R4350B 60mils	59.5mils	3.66 / 0.0037	3.67, 3.69, ---	3.83, 3.95, ---	3.75, 3.76, ---	0.1022, .1275, ---	0.0184, 0.0268, ---	0.0347, 0.0403, ---	0.0276, 0.0345, ---
500 - 750	R6002 20mils	20.5mils	2.94 / 0.0012	---, 2.81, ---	---, 3.17, ---	---, 2.97, ---	---, 0.0080, ---	---, 0.0008, ---	---, 0.0043, ---	---, 0.0028, ---
500 - 750	R6002 30mils	29.5mils	2.94 / 0.0012	---, 2.83, ---	---, 3.06, ---	---, 2.97, ---	---, 0.0088, ---	---, 0.0011, ---	---, 0.0045, ---	---, 0.0030, ---
500 - 750	TMM10 50mils	51.0mils	9.2 / 0.0022	10.82, 9.87, ---	11.21, 10.52, ---	11.06, 10.27, ---	0.1105, 0.1117, ---	0.0081, 0.0054, ---	0.0120, 0.0116, ---	0.0103, 0.0089, ---
500 - 750	Theta 20mils	19.5mils	4.01 / 0.0118	4.14, 4.11, 3.91	4.49, 4.46, 4.42,	4.30, 4.29, 4.27	0.2321, 0.2103, 0.2134	0.0324, 0.0382, 0.0410	0.0776, 0.0636, 0.0583	0.0580, 0.0526, 0.0508

Materials Measured 5/31-6/2/2012 at Portland State University Picometrix T-Ray 4000 Time Domain Spectrometer OFFSET=680pS, Tavg=6000										
Frequency (GHz)	Sample Description	Thickness (actual)	ε_r / Loss Tan (manufacturer) @10GHz	ε_r' (minimum) (H, V)	ε_r' (maximum) (H, V)	ε_r' (average) (H, V)	ε_r" (min,max,avg) (H, V)	Loss Tan (minimum) (H, V)	Loss Tan (maximum) (H, V)	Loss Tan (average) (H, V)
200 - 1600	ECE Blk 1mm	1mm (1.02mm)	proprietary	2.63	2.78	2.7	0.11, 0.2, 0.15	0.04 H=V	0.075 H=V	0.055 H=V
200 - 1600	ECE Blk 2mm	2mm (2.00mm)	proprietary	1.6	2.8	2.73	0.15, 0.205, 0.15	0.038	0.075	0.055
200 - 1600	ECE Clr 2mm	2mm (2.34mm)	proprietary	3.2	3.5	3.3	0.3, 0.41, 0.4	0.1	0.13	0.12
200 - 1600	R3003 20mils	20.5000	3.00 / 0.0013	V3.05 / H 3.0	V 3.12 / H 3.0	V3.06/ H 2.9	V: 0.05, 0.18, 0.075 H: 0.05, 0.16, 0.070	V 0.01 / H 0.01	V 0.065 / H 0.056	V 0.03 / H 0.02
200 - 1600	R3006 25mils	25.0 mils	6.15 / 0.0020	V 6.9 / H 6.9	V 8.2 / H 7.6	V 7.8 / H 7.4	V: 0.25, 1.9, 1.0 H: 0.25, 1.6, 0.8	V 0.025 / H 0.025	V 0.3 / H 0.22	V 0.20 / H 0.15
200 - 1600	R3850B 4mils	4.0/(3.7 mils)	2.90 / 0.0025	V 3.6 / H 3.8	V 4.65 / H 4.85	V 3.9 / H 4.1	V: 0.0, 0.4, 0.10 H: same	V 0.025 / H 0.02	V 0.01 / H 0.008	V 0.023 / H 0.021
200 - 1600	R4350B 60mils	59.5 mils	3.66 / 0.0037	V 3.7 / H 3.65	V 3.76 / H 3.8	V 3.73 / H 3.73	V: 0.075, 0.25, 0.16 H: 0.10, 0.23, 0.17	V 0.02 / H 0.03	V 0.07 / H 0.065	V 0.04 / H 0.045
200 - 1600	R5870 31mils	31.0 mils	2.33 / 0.0012	V 2.375 / H 2.43	V 2.475 / H 2.45	V 2.46 / H 2.44	V: 0.13, 0.3, 0.15 H: 0.03, 0.08, 0.05	V 0.05 / H 0.01	V 0.12 / H 0.035	V 0.07 / H 0.025
200 - 1600	R6002 20mils	20.5 mils	2.94 / 0.0012	V 2.93 / H 2.95	V 2.93 / H 2.95	V 2.93 / H 2.95	V: 0.020, 0.040, 0.028 H: 0.020, 0.040, 0.028	V 0.005 / H 0.005	V 0.014 / H 0.014	V 0.0075 / H 0.0075
200 - 1600	R6002 30mils	29.5 mils	2.94 / 0.0012	V 2.90 / H 2.90	V 2.95 / H 2.95	V 2.93 / H 2.93	V: 0.03, 0.08, 0.04 H: 0.03, 0.08, 0.04	V 0.008 / H 0.008	V 0.027 / H 0.028	V 0.013 / H 0.013
200 - 1600	TMM10 15mils	15.65 mils	9.2 / 0.0022	V 10.8 / H 10.25	V 11.4 / H 10.8	V 11.2 / H 10.6	V: 0.1, 0.5, 0.25 H: 0.1, 0.35, 0.23	V 0.015 / H 0.015	V 0.043 / H 0.032	V 0.025 / H 0.022
200 - 1600	Theta 20mils	19.5 mils	4.01 / 0.0118	V 4.13 / H 4.12	V 4.4 / H 4.4	V 4.25 / H 4.24	V: 0.2, 0.58, 0.35 H: 0.2, 0.57, 0.34	V 0.045 / H 0.040	V 0.14 / H 0.14	V 0.09 / H 0.085
200 - 1600	HDPE_K71_dull 30 mils	31.9 mils	2.25-2.35/.0003	V 2.47 / H 2.49	V 2.46 / H 2.48	V 2.465 / H 2.485	V: 0.010, 0.030, 0.018 H: 0.06, 0.035, 0.030	V 0.005 / H 0.025	V 0.010 / H 0.012	V 0.007 / H 0.013
200 - 1600	LDPE_K112_01 25, 125mils	125.5 mils	2.25-2.35/.0003	V 2.282/ H 2.282	V 2.286 / H 2.286	V 2.284 / H 2.284	V = H .0075, .003, .0025	V 0.0045 / H 0.0045	V 0.0015 / H 0.0015	V 0.001 / H 0.001

Table 10 Horizontal Table - VNA and TDS Data with Comparative Results

Materials Measured 6/5-2012 at PortlandState University using VNA / ZVA 40										
Frequency (GHz)	Sample Description	Thickness (actual)	εr / Loss Tan (manufacturer) @10GHz	εr ' (minimum) (H, V, 45)	εr ' (maximum) (H, V, 45)	εr ' (average) (H, V, 45)	εr " (average) (H, V, 45)	Loss tan (minimum) (H, V, 45)	Loss tan (maximum) (H, V, 45)	Loss tan (average) (H, V, 45)
325 - 500	ECE Blk 1mm	1mm (1.02mm)	no data	2.63, 2.66, ---	2.81, 2.79, ---	2.73, 2.73, ---	0.0948, 0.0948, ---	0.0302, 0.0302, ---	0.0381, 0.0381, ---	0.0347, 0.0347, ---
325 - 500	ECE Blk 2mm	2mm (2.00mm)	no data	2.70, 2.69, ---	2.79, 2.78, ---	2.74, 2.74, ---	0.0912, 0.0912, ---	0.0302, 0.0302, ---	0.0358, 0.0358, ---	0.0334, 0.0334, ---
325 - 500	ECE Clr 2mm	2mm (2.34mm)	no data	3.04, 3.03, ---	3.17, 3.16, ---	3.10, 3.10, ---	0.382, 0.382, ---	0.118, 0.118, ---	0.123, 0.123, ---	0.127, 0.127, ---
325 - 500	R3006 25mils	25.0mils	6.15 / 0.0020	6.65, 7.04, ---	7.46, 7.92, ---	7.14, 7.53, ---	0.122, 0.126, ---	0.0143, 0.0138, ---	0.0193, 0.0187, ---	0.0172, 0.0166, ---
325 - 500	R4350B 60mils	59.5mils	3.66 / 0.0037	3.65, 3.68, ---	3.80, 3.86, ---	3.75, 3.78, ---	0.0527, 0.0770, ---	0.0099, 0.0152, ---	0.0173, 0.0247, ---	0.0141, 0.0206, ---
325 - 500	RS870 31mils	31.0mils	2.33 / 0.0012	2.38, 2.37, ---	2.52, 2.50, ---	2.45, 2.43, ---	0.0094, 0.0094, ---	0.0038, 0.0038, ---	0.0039, 0.0039, ---	0.0038, 0.0038, ---
325 - 500	R6002 20mils	20.5mils	2.94 / 0.0012	2.77, 2.81, ---	3.03, 3.06, ---	2.90, 2.94, ---	0.0039, 0.0039, ---	0.0012, 0.0012, ---	0.0014, 0.0014, ---	0.0013, 0.0013, ---
325 - 500	R6002 30mils	29.5mils	2.94 / 0.0012	2.84, 2.83, ---	3.06, 3.03, ---	2.94, 2.93, ---	0.0039, 0.0039, ---	0.0012, 0.0012, ---	0.0014, 0.0014, ---	0.0013, 0.0013, ---
325 - 500	TMM10 25mils	26.0mils	9.2 / 0.0022	9.39, 9.73, ---	10.42, 10.69, ---	9.92, 10.26, ---	0.0901, 0.1525, ---	0.0060, 0.0120, ---	0.0111, 0.0174, ---	0.0089, 0.0151, ---
325 - 500	Theta 20mils	19.5mils	4.01 / 0.0118	3.80, 3.77, ---	4.68, 4.70, ---	4.13, 4.12, ---	0.1899, 0.1899, ---	0.0406, 0.0406, ---	0.0595, 0.0595, ---	0.0487, 0.0487, ---

Materials Measured 10/24-2012 at Virginia Diodes, Inc. using VNA/ZVA40										
Frequency (GHz)	Sample Description	Thickness (actual)	εr / Loss Tan (manufacturer) @10GHz	εr ' (minimum) (H, V, 45)	εr ' (maximum) (H, V, 45)	εr ' (average) (H, V, 45)	εr " (average) (H, V, 45)	Loss Tan (minimum) (H, V, 45)	Loss Tan (maximum) (H, V, 45)	Loss Tan (average) (H, V, 45)
500 - 750	R3006 25mils	25.0mils	6.15 / 0.0020	7.17, 7.50, 7.19	7.93, 8.36, 8.04	7.61, 8.00, 7.63	0.3348, 0.3642, 0.3814	0.0077, 0.0118, 0.0153	0.0729, 0.0757, 0.0780	0.0446, 0.0480, 0.0509
500 - 750	R3003 10mils	10.0mils	3.00 / 0.0013	2.66, 2.71, ---	3.32, 3.38, ---	3.07, 3.10, ---	0.0055, 0.0183, ---	0.0018, 0.0055, ---	0.0019, 0.0066, ---	0.0019, 0.0062, ---
500 - 750	R3010 10mils	10.5mils	10.20 / 0.0027	11.28, 11.15, ---	14.06, 13.32, ---	13.19, 12.40, ---	0.1105, 0.0965, ---	0.0078, 0.0053, ---	0.0113, 0.0122, ---	0.0098, 0.0092, ---
500 - 750	R4350B 60mils	59.5mils	3.66 / 0.0037	3.67, 3.69, ---	3.83, 3.95, ---	3.75, 3.76, ---	0.1022, 1275, ---	0.0184, 0.0268, ---	0.0347, 0.0403, ---	0.0276, 0.0345, ---
500 - 750	R6002 20mils	20.5mils	2.94 / 0.0012	--- 2.81, ---	--- 3.17, ---	--- 2.97, ---	--- 0.0080, ---	--- 0.0008, ---	--- 0.0043, ---	--- 0.0028, ---
500 - 750	R6002 30mils	29.5mils	2.94 / 0.0012	--- 2.83, ---	--- 3.06, ---	--- 2.97, ---	--- 0.0088, ---	--- 0.0011, ---	--- 0.0045, ---	--- 0.0030, ---
500 - 750	TMM10 50mils	51.0mils	9.2 / 0.0022	10.82, 9.87, ---	11.21, 10.52, ---	11.06, 10.27, ---	0.1105, 0.1117, ---	0.0081, 0.0054, ---	0.0120, 0.0116, ---	0.0103, 0.0089, ---
500 - 750	Theta 20mils	19.5mils	4.01 / 0.0118	4.14, 4.11, 3.91	4.49, 4.46, 4.42	4.30, 4.29, 4.27	0.2321, 0.2103, 0.2134	0.0324, 0.0382, 0.0410	0.0776, 0.0636, 0.0583	0.0580, 0.0526, 0.0508

Materials Measured 5/31-6/2/2012 at Portland State University Picometrix T-Ray 4000 Time Domain Spectrometer OPUS IT=680 pS, Tavg=6000									
Frequency (GHz)	Sample Description	Thickness (actual)	εr / Loss Tan (manufacturer) @10GHz	εr ' (minimum) (H, V)	εr ' (maximum) (H, V)	εr ' (average) (H, V)	εr " (min,max,avg) (H, V)	Loss Tan (minimum) (H, V)	Loss Tan (maximum)	Loss Tan (average)
200 - 1600	ECE Blk 1mm	1mm (1.02mm)	proprietary	2.63	2.78	2.7	0.11, 0.2, 0.15	0.04 H=V	0.075 H=V	0.055 H=V
200 - 1600	ECE Blk 2mm	2mm (2.00mm)	proprietary	1.6	2.8	2.73	0.15, 0.205, 0.15	0.038	0.075	0.055
200 - 1600	ECE Clr 2mm	2mm (2.34mm)	proprietary	3.2	3.5	3.3	0.3, 0.41, 0.4	0.1	0.13	0.12
200 - 1600	R3003 20mils	20.5000	3.00 / 0.0013	V 3.05 / H 3.0	V 3.12 / H 3.0	V 3.06 / H 2.9	V: 0.05, 0.18, 0.075 H: 0.05, 0.16, 0.070	V 0.01 / H 0.01	V 0.065 / H 0.056	V 0.03 / H 0.02
200 - 1600	R3006 25mils	25.0mils	6.15 / 0.0020	V 6.9 / H 6.9	V 8.2 / H 7.6	V 7.8 / H 7.4	V: 0.25, 1.9, 1.0 H: 0.25, 1.6, 0.8	V 0.025 / H 0.025	V 0.3 / H 0.22	V 0.20 / H 0.15
200 - 1600	R3850B 4mils	4.0(3.7mils)	2.90 / 0.0025	V 3.6 / H 3.8	V 4.65 / H 4.85	V 3.9 / H 4.1	V: 0.0, 0.4, 0.10 H: same	V 0.025 / H 0.02	V 0.01 / H 0.008	V 0.023 / H 0.021
200 - 1600	R4350B 60mils	59.5mils	3.66 / 0.0037	V 3.7 / H 3.65	V 3.76 / H 3.8	V 3.73 / H 3.73	V: 0.075, 0.25, 0.16 H: 0, 0.10, 0.23, 0.17	V 0.02 / H 0.03	V 0.07 / H 0.065	V 0.04 / H 0.045
200 - 1600	RS870 31mils	31.0mils	2.33 / 0.0012	V 2.375 / H 2.43	V 2.475 / H 2.45	V 2.46 / H 2.44	V: 0.13, 0.3, 0.15 H: 0.03, 0.08, 0.05	V 0.05 / H 0.01	V 0.12 / H 0.035	V 0.07 / H 0.025
200 - 1600	R6002 20mils	20.5mils	2.94 / 0.0012	V 2.93 / H 2.95	V 2.93 / H 2.95	V 2.93 / H 2.95	V: 0.020, 0.040, 0.028 H: 0.020, 0.040, 0.028	V 0.005 / H 0.005	V 0.014 / H 0.014	V 0.0075 / H 0.0075
200 - 1600	R6002 30mils	29.5mils	2.94 / 0.0012	V 2.90 / H 2.90	V 2.95 / H 2.95	V 2.93 / H 2.93	V: 0.03, 0.08, 0.04 H: 0.03, 0.08, 0.04	V 0.008 / H 0.008	V 0.027 / H 0.028	V 0.013 / H 0.013
200 - 1600	TMM10 15mils	15.65 mils	9.2 / 0.0022	V 10.8 / H 10.25	V 11.4 / H 10.8	V 11.2 / H 10.6	V: 0.1, 0.5, 0.25 H: 0.1, 0.35, 0.23	V 0.015 / H 0.015	V 0.043 / H 0.032	V 0.025 / H 0.022
200 - 1600	Theta 20mils	19.5 mils	4.01 / 0.0118	V 4.13 / H 4.12	V 4.4 / H 4.4	V 4.25 / H 4.24	V: 0.2, 0.58, 0.35 H: 0.2, 0.57, 0.34	V 0.045 / H 0.040	V 0.14 / H 0.14	V 0.09 / H 0.085
200 - 1600	HDPE_K71_dull 30 mils	31.9 mils	2.25-2.35/.0003	V 2.47 / H 2.49	V 2.46 / H 2.48	V 2.465 / H 2.485	V: 0.010, 0.030, 0.018 H: 0.06, 0.035, 0.030	V 0.005 / H 0.025	V 0.010 / H 0.012	V 0.007 / H 0.013
200 - 1600	LDPE_K112_01 25, 125mils	125.5 mils	2.25-2.35/.0003	V 2.282 / H 2.283	V 2.286 / H 2.286	V 2.284 / H 2.284	V = H .0075, .003, .0025	V 0.0045 / H 0.0045	V 0.0015 / H 0.0015	V 0.001 / H 0.001

Table 11 VNA and TDS Data with Comparative Results

Materials Measured 6/5-2012 at Portland State University using VNA / ZVA 40										
Frequency (GHz)	Sample Description	Thickness (actual)	ε_r / Loss Tan (manufacturer) @10GHz	ε_r' (minimum) (H, V, 45)	ε_r' (maximum) (H, V, 45)	ε_r' (average) (H, V, 45)	ε_r'' (average) (H, V, 45)	Loss tan (minimum) (H, V, 45)	Loss tan (maximum) (H, V, 45)	Loss tan (average) (H, V, 45)
325 - 500	ECE_Blk_1mm	1mm (1.02mm)	no data	2.63, 2.66, ---	2.81, 2.79, ---	2.73, 2.73, ---	0.0948, 0.0948, ---	0.0302, 0.0302, ---	0.0381, 0.0381, ---	0.0347, 0.0347, ---
325 - 500	ECE_Blk_2mm	2mm (2.00mm)	no data	2.70, 2.69, ---	2.79, 2.78, ---	2.74, 2.74, ---	0.0912, 0.0912, ---	0.0302, 0.0302, ---	0.0358, 0.0358, ---	0.0334, 0.0334, ---
325 - 500	ECE_Clr_2mm	2mm (2.34mm)	no data	3.04, 3.03, ---	3.17, 3.16, ---	3.10, 3.10, ---	0.382, 0.382, ---	0.118, 0.118, ---	0.123, 0.123, ---	0.127, 0.127, ---
325 - 500	R3006 25mils	25.0mils	6.15 / 0.0020	6.65, 7.04, ---	7.46, 7.92, ---	7.14, 7.53, ---	0.122, 0.126, ---	0.0143, 0.0138, ---	0.0193, 0.0187, ---	0.0172, 0.0166, ---
325 - 500	R4350B 60mils	59.5mils	3.66 / 0.0037	3.65, 3.68, ---	3.80, 3.86, ---	3.75, 3.78, ---	0.0527, 0.0770, ---	0.0099, 0.0152, ---	0.0173, 0.0247, ---	0.0141, 0.0206, ---
325 - 500	R5870 31mils	31.0mils	2.33 / 0.0012	2.38, 2.37, ---	2.52, 2.50, ---	2.45, 2.43, ---	0.0094, 0.0094, ---	0.0038, 0.0038, ---	0.0039, 0.0039, ---	0.0038, 0.0038, ---
325 - 500	R6002 20mils	20.5mils	2.94 / 0.0012	2.77, 2.81, ---	3.03, 3.06, ---	2.90, 2.94, ---	0.0039, 0.0039, ---	0.0012, 0.0012, ---	0.0014, 0.0014, ---	0.0013, 0.0013, ---
325 - 500	R6002 30mils	29.5mils	2.94 / 0.0012	2.84, 2.83, ---	3.06, 3.03, ---	2.94, 2.93, ---	0.0039, 0.0039, ---	0.0012, 0.0012, ---	0.0014, 0.0014, ---	0.0013, 0.0013, ---
325 - 500	TMM10 25mils	26.0mils	9.2 / 0.0022	9.39, 9.73, ---	10.42, 10.69, ---	9.92, 10.26, ---	0.0901, 0.1525, ---	0.0060, 0.0120, ---	0.0111, 0.0174, ---	0.0089, 0.0151, ---
325 - 500	Theta 20mils	19.5mils	4.01 / 0.0118	3.80, 3.77, ---	4.68, 4.70, ---	4.13, 4.12, ---	0.1899, 0.1899, ---	0.0406, 0.0406, ---	0.0595, 0.0595, ---	0.0487, 0.0487, ---
Materials Measured 10/24-2012 at Virginia Diodes, Inc. using VNA/ZVA40										
Frequency (GHz)	Sample Description	Thickness (actual)	ε_r / Loss Tan (manufacturer) @10GHz	ε_r' (minimum) (H, V, 45)	ε_r' (maximum) (H, V, 45)	ε_r' (average) (H, V, 45)	ε_r'' (average) (H, V, 45)	Loss Tan (minimum) (H, V, 45)	Loss Tan (maximum) (H, V, 45)	Loss Tan (average) (H, V, 45)
500 - 750	R3006 25mils	25.0mils	6.15 / 0.0020	7.17, 7.50, 7.19	7.93, 8.36, 8.04	7.61, 8.00, 7.63	0.3348, 0.3642, 0.3814	0.0077, 0.0118, 0.0153	0.0729, 0.0757, 0.0780	0.0446, 0.0480, 0.0509
500 - 750	R3003 10mils	10.0mils	3.00 / 0.0013	2.66, 2.71, ---	3.32, 3.38, ---	3.07, 3.10, ---	0.0055, 0.0183, ---	0.0018, 0.0055, ---	0.0019, 0.0066, ---	0.0019, 0.0062, ---
500 - 750	R3010 10mils	10.5mils	10.20 / 0.0027	11.28, 11.15, ---	14.06, 13.32, ---	13.19, 12.40, ---	0.1105, 0.0965, ---	0.0078, 0.0053, ---	0.0113, 0.0122, ---	0.0098, 0.0092, ---
500 - 750	R4350B 60mils	59.5mils	3.66 / 0.0037	3.67, 3.69, ---	3.83, 3.95, ---	3.75, 3.76, ---	0.1022, 1275, ---	0.0184, 0.0268, ---	0.0347, 0.0403, ---	0.0276, 0.0345, ---
500 - 750	R6002 20mils	20.5mils	2.94 / 0.0012	---, 2.81, ---	---, 3.17, ---	---, 2.97, ---	---, 0.0080, ---	---, 0.0008, ---	---, 0.0043, ---	---, 0.0028, ---
500 - 750	R6002 30mils	29.5mils	2.94 / 0.0012	---, 2.83, ---	---, 3.06, ---	---, 2.97, ---	---, 0.0088, ---	---, 0.0011, ---	---, 0.0045, ---	---, 0.0030, ---
500 - 750	TMM10 50mils	51.0mils	9.2 / 0.0022	10.82, 9.87, ---	11.21, 10.52, ---	11.06, 10.27, ---	0.1105, 0.1117, ---	0.0081, 0.0054, ---	0.0120, 0.0116, ---	0.0103, 0.0089, ---
500 - 750	Theta 20mils	19.5mils	4.01 / 0.0118	4.14, 4.11, 3.91	4.49, 4.46, 4.42,	4.30, 4.29, 4.27	0.2321, 0.2103, 0.2134	0.0324, 0.0382, 0.0410	0.0776, 0.0636, 0.0583	0.0580, 0.0526, 0.0508

Table 12 VNA DATA SUMMARY

Materials Measured 5/31-6/2/2012 at Portland State University Picometrix T-Ray 4000 Time Domain Spectrometer OFFSET=680pS, Tavg=6000										
Frequency (GHz)	Sample Description	Thickness (actual)	ε_r / Loss Tan (manufacturer) @10 GHz	ε_r ' (minimum) (H, V)	ε_r ' (maximum) (H, V)	ε_r ' (average) (H, V)	ε_r '' (min,max,avg) (H, V)	Loss Tan (minimum) (H, V)	Loss Tan (maximum) (H, V)	Loss Tan (average) (H, V)
200 - 1600	ECE_Blk_1mm	1mm (1.02mm)	proprietary	2.63	2.78	2.7	0.11, 0.2, 0.15	0.04 H=V	0.075 H=V	0.055 H=V
200 - 1600	ECE_Blk_2mm	2mm (2.00mm)	proprietary	1.6	2.8	2.73	0.15, 0.205, 0.15	0.038	0.075	0.055
200 - 1600	ECE_Clr_2mm	2mm (2.34mm)	proprietary	3.2	3.5	3.3	0.3, 0.41, 0.4	0.1	0.13	0.12
200 - 1600	R3003_20mils	20.5000	3.00 / 0.0013	V 3.05 / H 3.0	V 3.12 / H 3.0	V3.06/ H 2.9	V: 0.05, 0.18, 0.075 H: 0.05, 0.16, 0.070	V 0.01 / H 0.01	V 0.065 / H 0.056	V 0.03 / H 0.02
200 - 1600	R3006 25mils	25.0 mils	6.15 / 0.0020	V 6.9 / H 6.9	V 8.2 / H 7.6	V 7.8 / H 7.4	V: 0.25, 1.9, 1.0 H: 0.25, 1.6, 0.8	V 0.025 / H 0.025	V 0.3 / H 0.22	V 0.20 / H 0.15
200 - 1600	R3850B 4mils	4.0(3.7 mils)	2.90 / 0.0025	V 3.6 / H 3.8	V 4.65 / H 4.85	V 3.9 / H 4.1	V: 0.0, 0.4, 0.10 H: same	V 0.025 / H 0.02	V 0.01 / H 0.008	V 0.023 / H 0.021
200 - 1600	R4350B 60mils	59.5 mils	3.66 / 0.0037	V 3.7 / H 3.65	V 3.76 / H 3.8	V 3.73 / H 3.73	V: 0.075, 0.25, 0.16 H: 0.10, 0.23, 0.17	V 0.02 / H 0.03	V 0.07 / H 0.065	V 0.04 / H 0.045
200 - 1600	R5870 31mils	31.0 mils	2.33 / 0.0012	V 2.375 / H 2.43	V 2.475 / H 2.45	V 2.46 / H 2.44	V: 0.13, 0.3, 0.15 H: 0.03, 0.08, 0.05	V 0.05 / H 0.01	V 0.12 / H 0.035	V 0.07 / H 0.025
200 - 1600	R6002 20mils	20.5 mils	2.94 / 0.0012	V 2.93 / H 2.95	V 2.93 / H 2.95	V 2.93 / H 2.95	V: 0.020, 0.040, 0.028 H: 0.020, 0.040, 0.028	V 0.005 / H 0.005	V 0.014 / H 0.014	V 0.0075 / H 0.0075
200 - 1600	R6002 30mils	29.5 mils	2.94 / 0.0012	V 2.90 / H 2.90	V 2.95 / H 2.95	V 2.93 / H 2.93	V: 0.03, 0.08, 0.04 H: 0.03, 0.08, 0.04	V 0.008 / H 0.008	V 0.027 / H 0.028	V 0.013 / H 0.013
200 - 1600	TMM10 15mils	15.65 mils	9.2 / 0.0022	V 10.8 / H 10.25	V 11.4 / H 10.8	V 11.2 / H 10.6	V: 0.1, 0.5, 0.25 H: 0.1, 0.35, 0.23	V 0.015 / H 0.015	V 0.043 / H 0.032	V 0.025 / H 0.022
200 - 1600	Theta 20mils	19.5 mils	4.01 / 0.0118	V 4.13 / H 4.12	V 4.4 / H 4.4	V 4.25 / H 4.24	V: 0.2, 0.58, 0.35 H: 0.2, 0.57, 0.34	V 0.045 / H 0.040	V 0.14 / H 0.14	V 0.09 / H 0.085
200 - 1600	HDPE_K71_dull 30 mils	31.9 mils	2.25-2.35/.0003	V 2.47 / H 2.49	V 2.46 / H 2.48	V 2.465 / H 2.485	V: 0.010, 0.030, 0.018 H: 0.06, 0.035, 0.030	V 0.005 / H 0.025	V 0.010 / H 0.012	V 0.007 / H 0.013
200 - 1600	LDPE_K112_01 25, 125mils	125.5 mils	2.25-2.35/.0003	V 2.282 / H 2.282	V 2.286 / H 2.286	V 2.284 / H 2.284	V = H .0075, .003, .0025	V 0.0045 / H 0.0045	V 0.0015 / H 0.0015	V 0.001 / H 0.001

Table 13 TDS DATA SUMMARY

5.4 TDS Data Plots Rogers Low loss Composite Materials

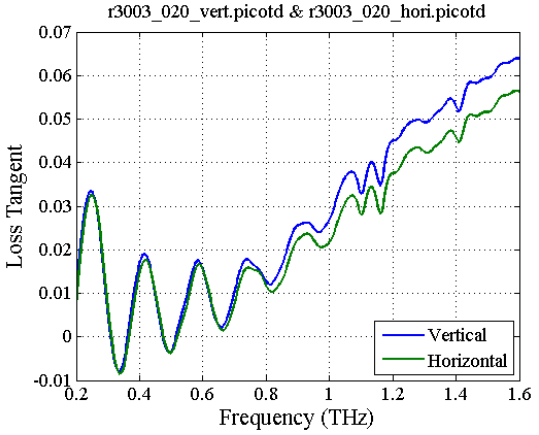

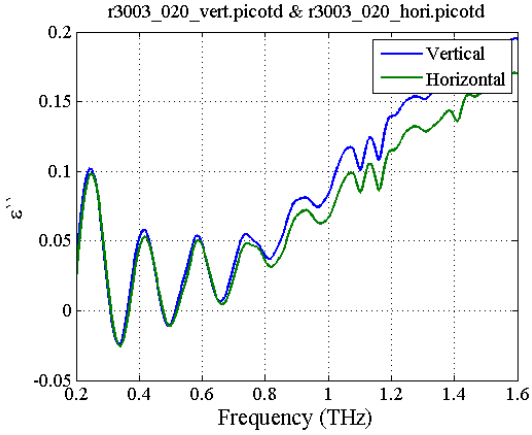

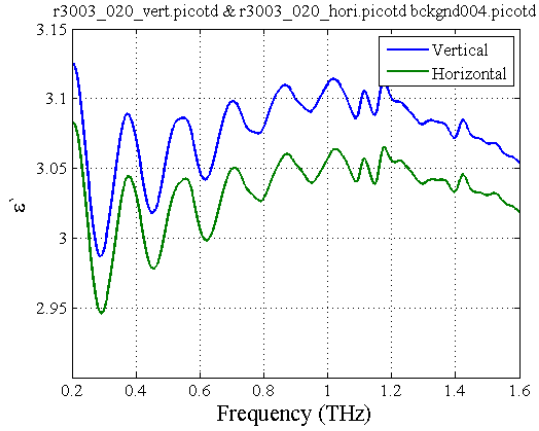

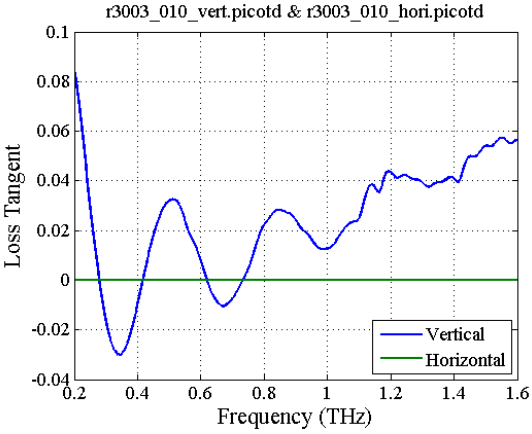

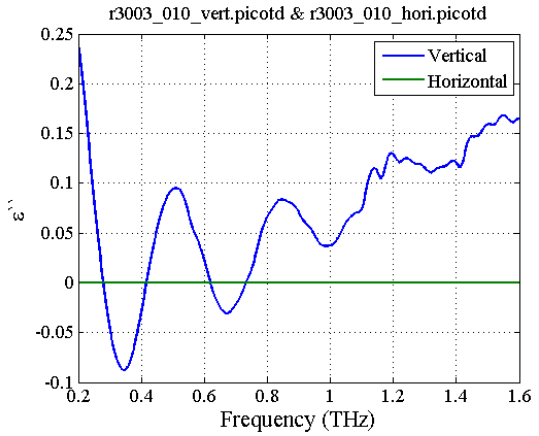

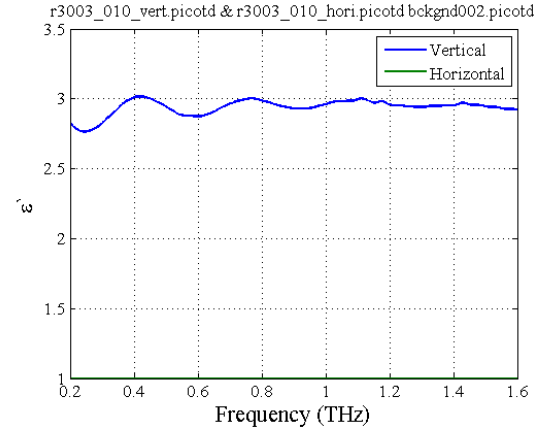

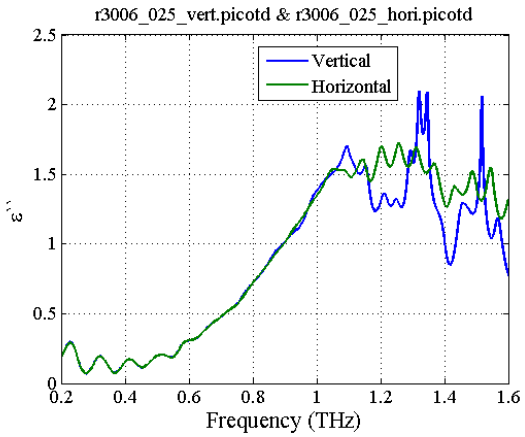
r3006_025_vert.picotd & r3006_025_hori.picotd
Vertical
Horizontal
ε``
Frequency (THz)

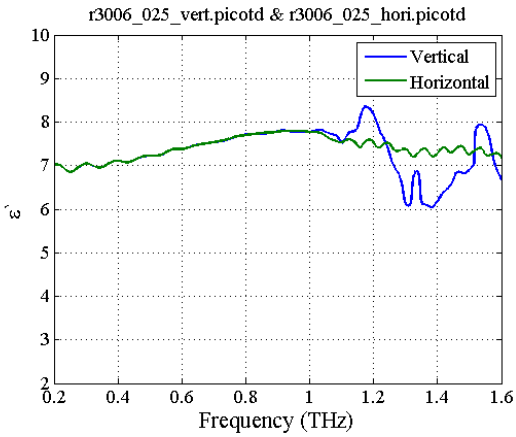
r3006_025_vert.picotd & r3006_025_hori.picotd
Vertical
Horizontal
ε`
Frequency (THz)

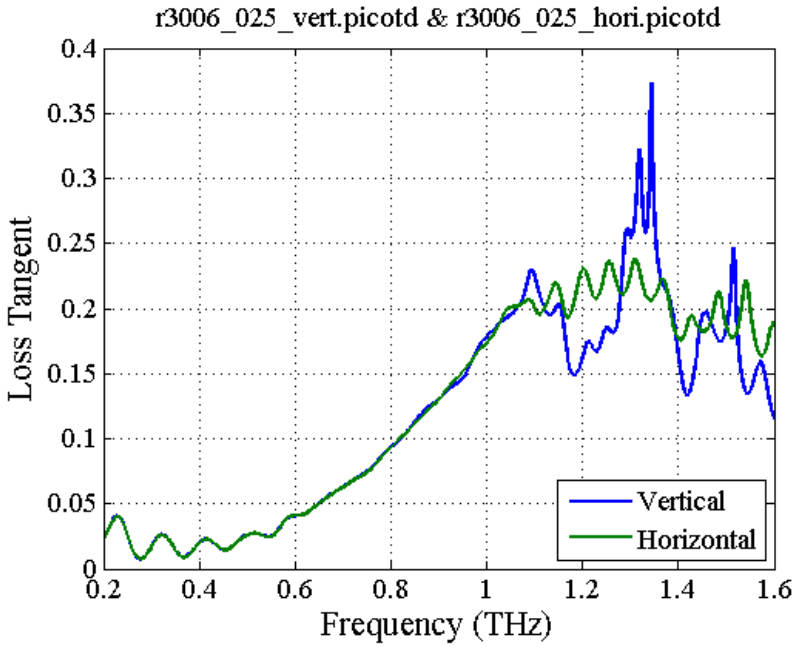
r3006_025_vert.picotd & r3006_025_hori.picotd
Loss Tangent
Vertical
Horizontal
Frequency (THz)

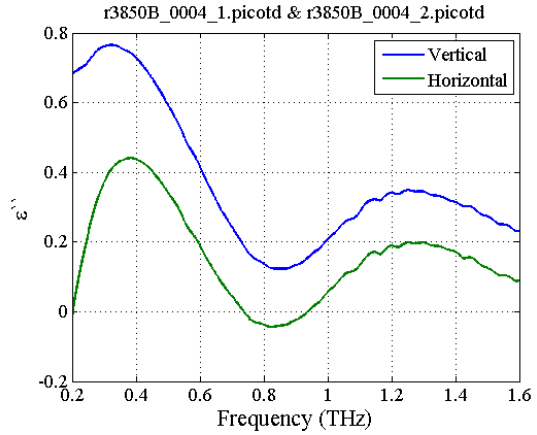
r3850B_0004_1.picotd & r3850B_0004_2.picotd
Vertical
Horizontal
ε``
Frequency (THz)

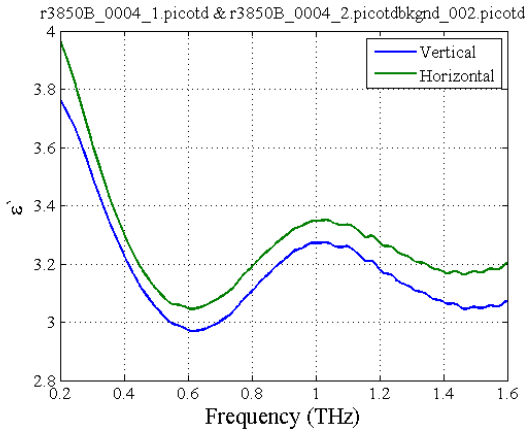
r3850B_0004_1.picotd & r3850B_0004_2.picotdbkgnd_002.picotd
Vertical
Horizontal
ε`
Frequency (THz)

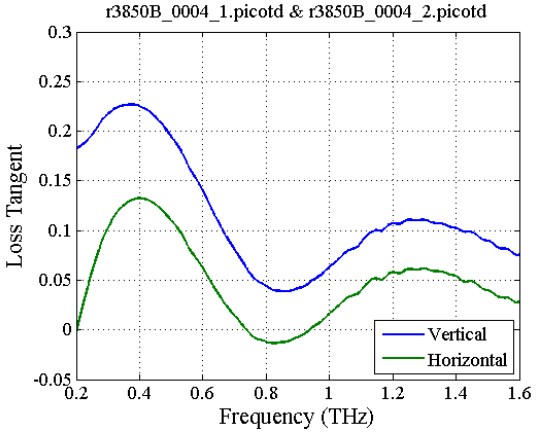
r3850B_0004_1.picotd & r3850B_0004_2.picotd
Loss Tangent
Vertical
Horizontal
Frequency (THz)

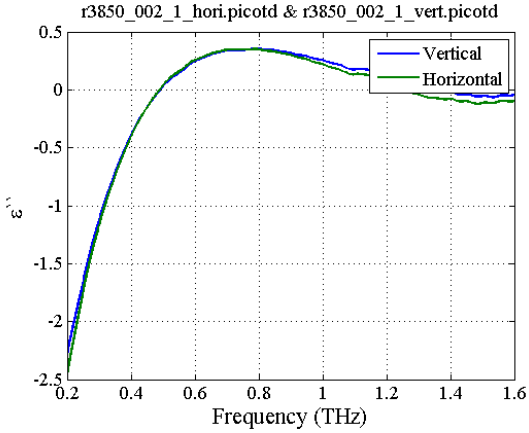
r3850_002_1_hori.picotd & r3850_002_1_vert.picotd
Vertical
Horizontal
ε``
Frequency (THz)

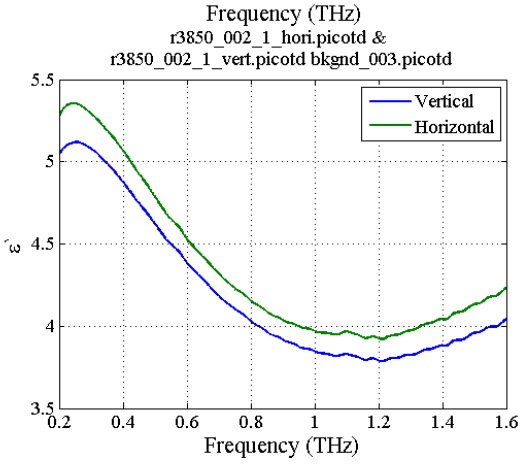
r3850_002_1_hori.picotd &
r3850_002_1_vert.picotd bkgnd_003.picotd
Vertical
Horizontal
ε`
Frequency (THz)

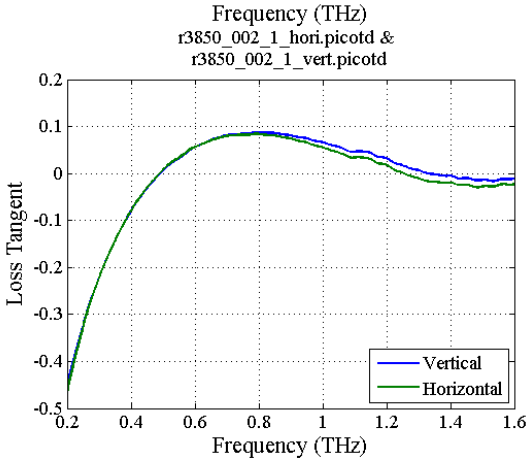
r3850_002_1_hori.picotd &
r3850_002_1_vert.picotd
Loss Tangent
Vertical
Horizontal
Frequency (THz)

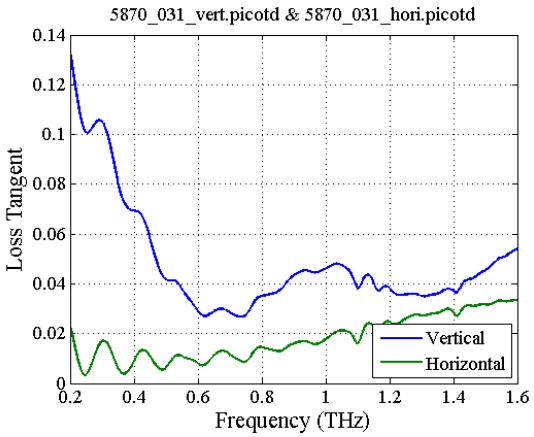
5870_031_vert.picotd & 5870_031_hori.picotd
Loss Tangent
Frequency (THz)
Vertical
Horizontal

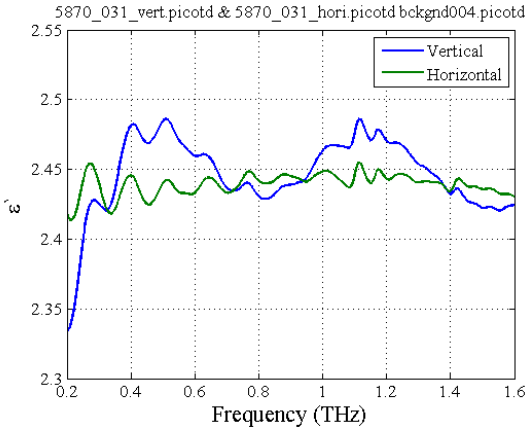
5870_031_vert.picotd & 5870_031_hori.picotd bckgnd004.picotd
ε'
Frequency (THz)
Vertical
Horizontal

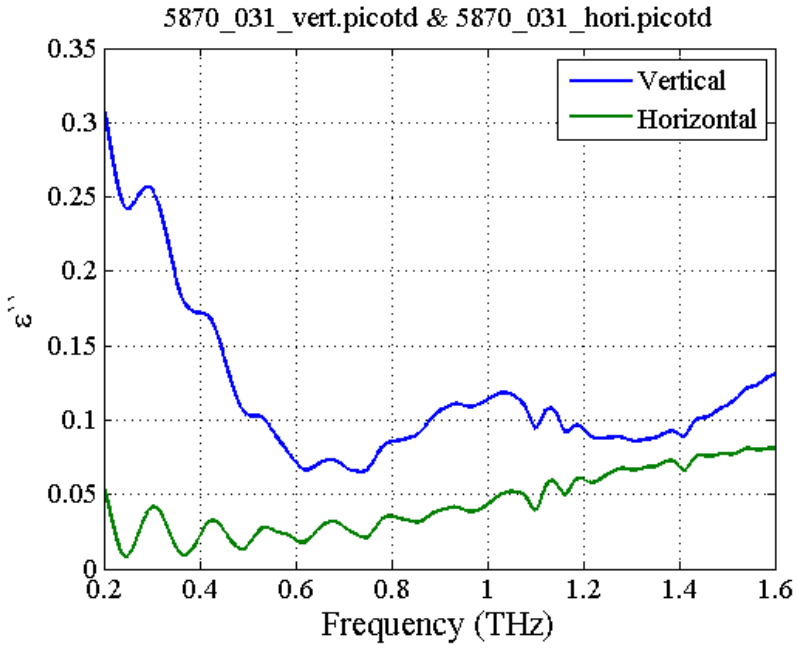
5870_031_vert.picotd & 5870_031_hori.picotd
ε''
Frequency (THz)
Vertical
Horizontal

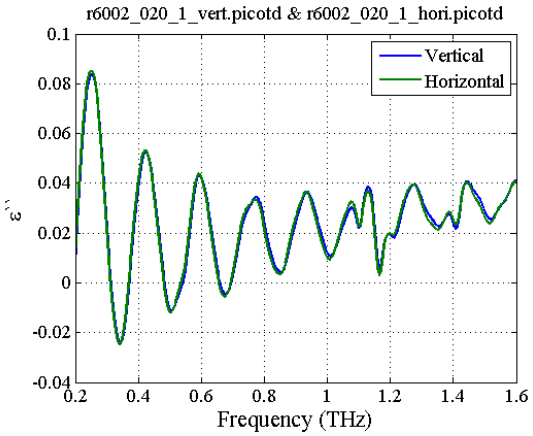
r6002_020_1_vert.picotd & r6002_020_1_hori.picotd
Vertical
Horizontal
ε''
Frequency (THz)

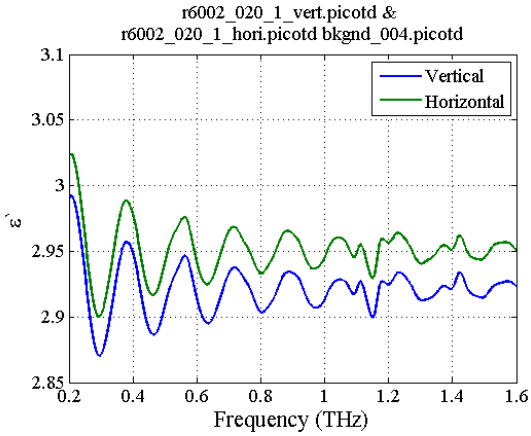
r6002_020_1_vert.picotd &
r6002_020_1_hori.picotd bkgnd_004.picotd
Vertical
Horizontal
ε'
Frequency (THz)

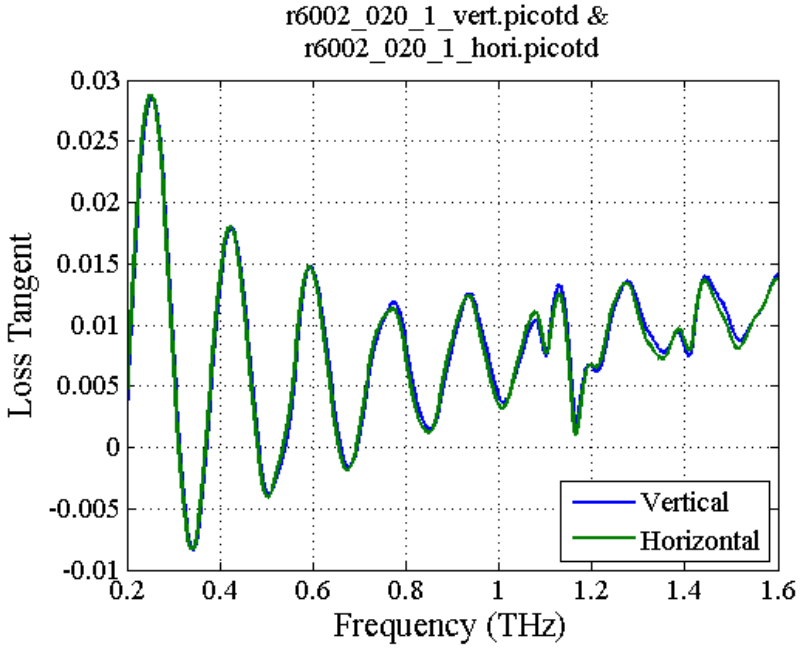
r6002_020_1_vert.picotd &
r6002_020_1_hori.picotd
Loss Tangent
Vertical
Horizontal
Frequency (THz)

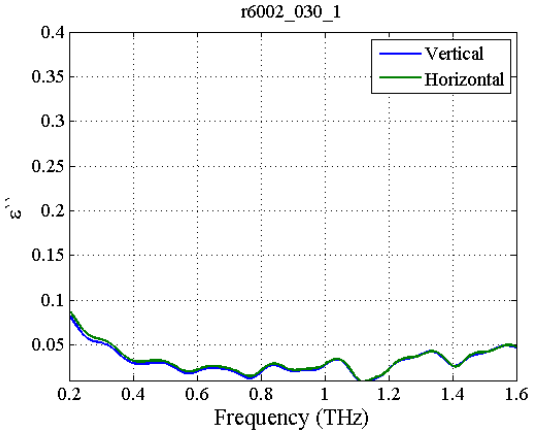
r6002_030_1
Vertical
Horizontal
ε''
Frequency (THz)

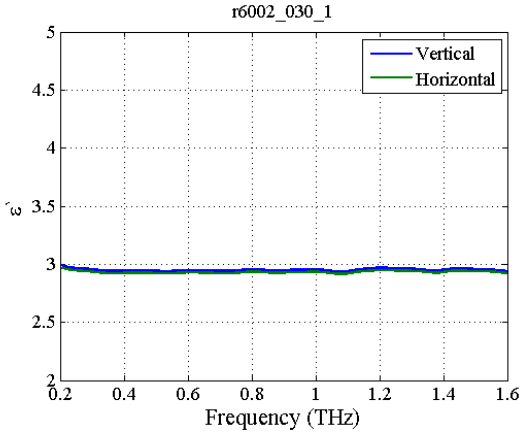
r6002_030_1
Vertical
Horizontal
ε'
Frequency (THz)

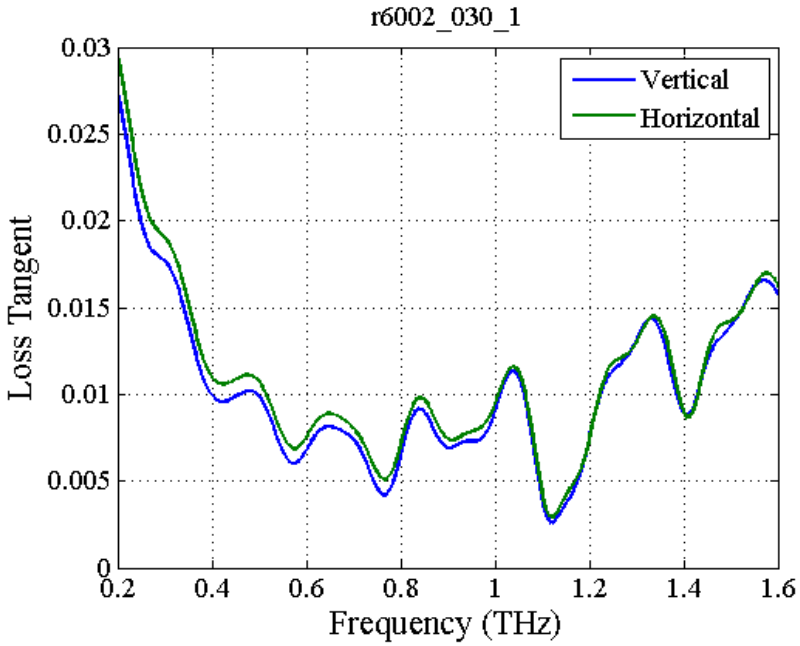
r6002_030_1
Vertical
Horizontal
Loss Tangent
Frequency (THz)

5.5 TDS Plots for Polymer and Polyethylene Plastics (Photo polymers, HDPE, LDPE)

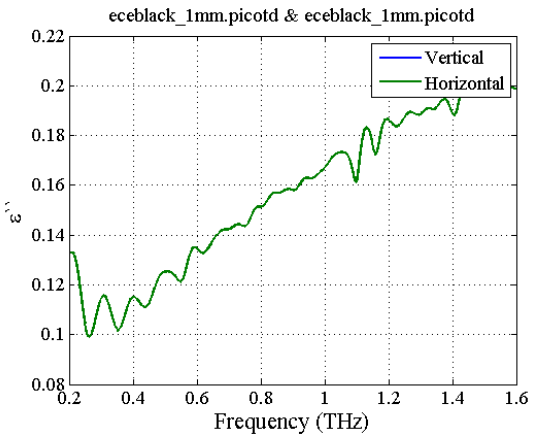

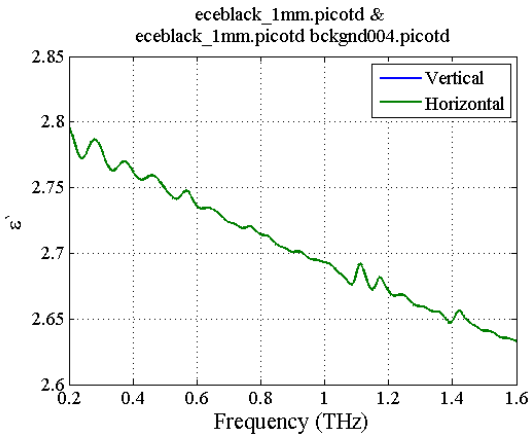

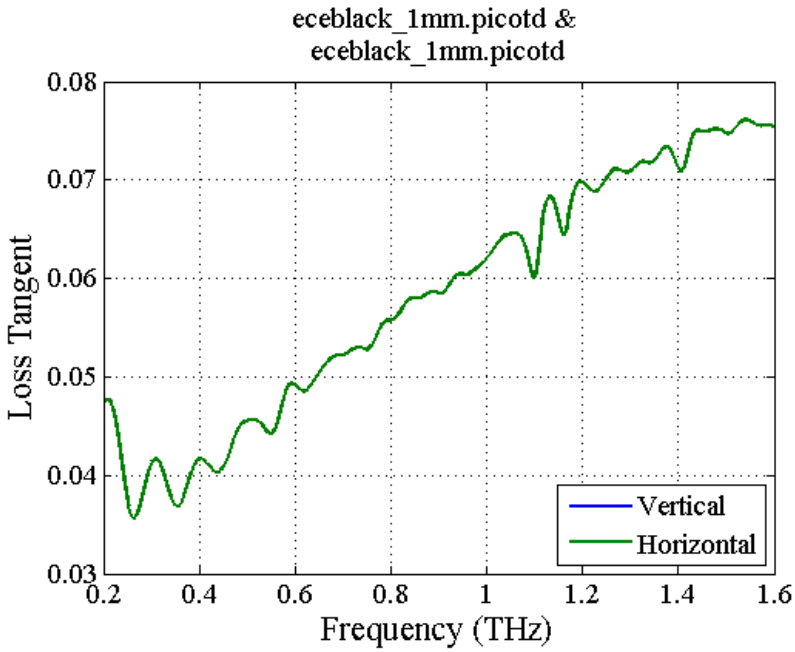

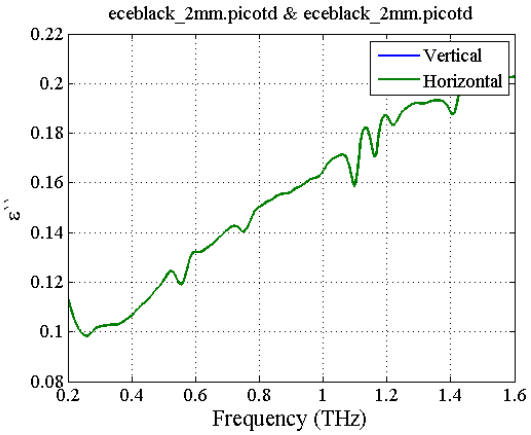
eceblack_2mm.picotd & eceblack_2mm.picotd
Vertical
Horizontal
ε''
Frequency (THz)

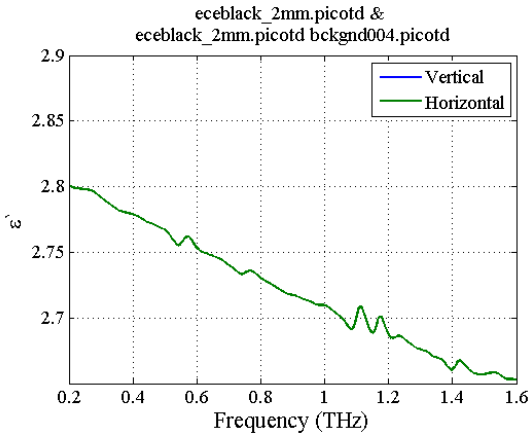
eceblack_2mm.picotd &
eceblack_2mm.picotd bckgnd004.picotd
Vertical
Horizontal
ε'
Frequency (THz)

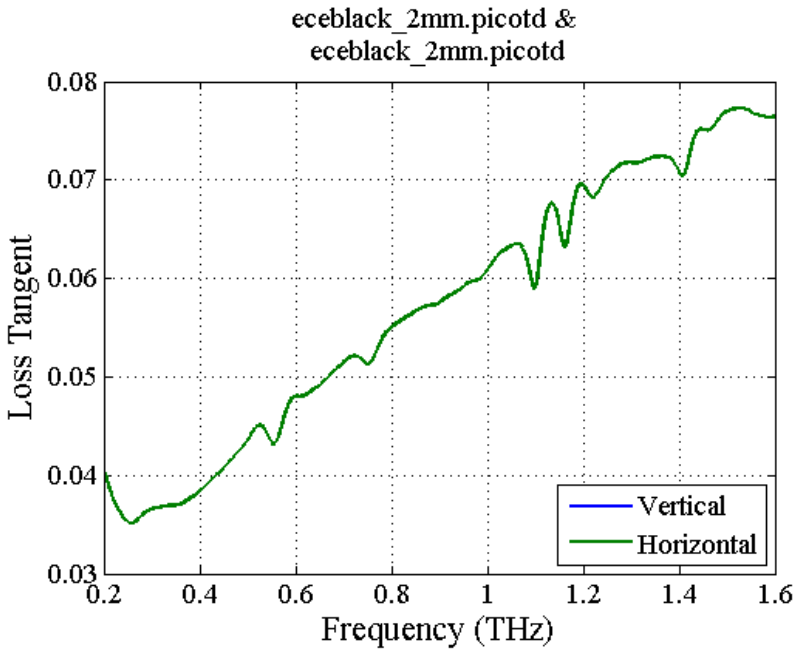
eceblack_2mm.picotd &
eceblack_2mm.picotd
Loss Tangent
Vertical
Horizontal
Frequency (THz)

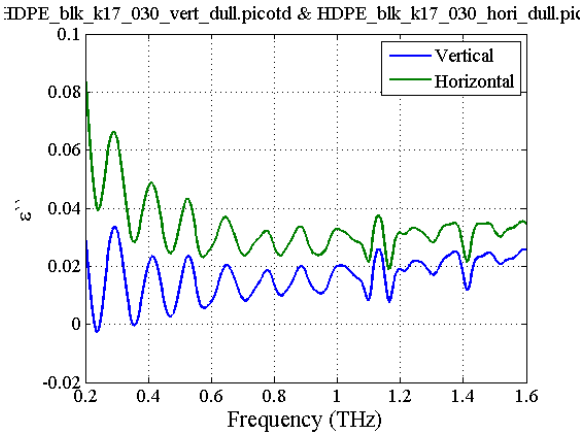
HDPE_blk_k17_030_vert_dull.picotd & HDPE_blk_k17_030_hori_dull.pic
Vertical
Horizontal
ε''
Frequency (THz)

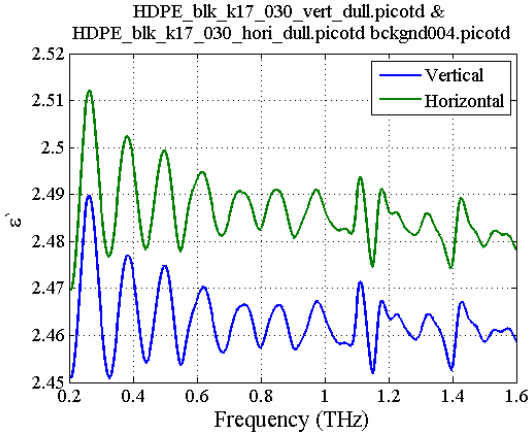
HDPE_blk_k17_030_vert_dull.picotd &
HDPE_blk_k17_030_hori_dull.picotd bckgnd004.picotd
Vertical
Horizontal
ε'
Frequency (THz)

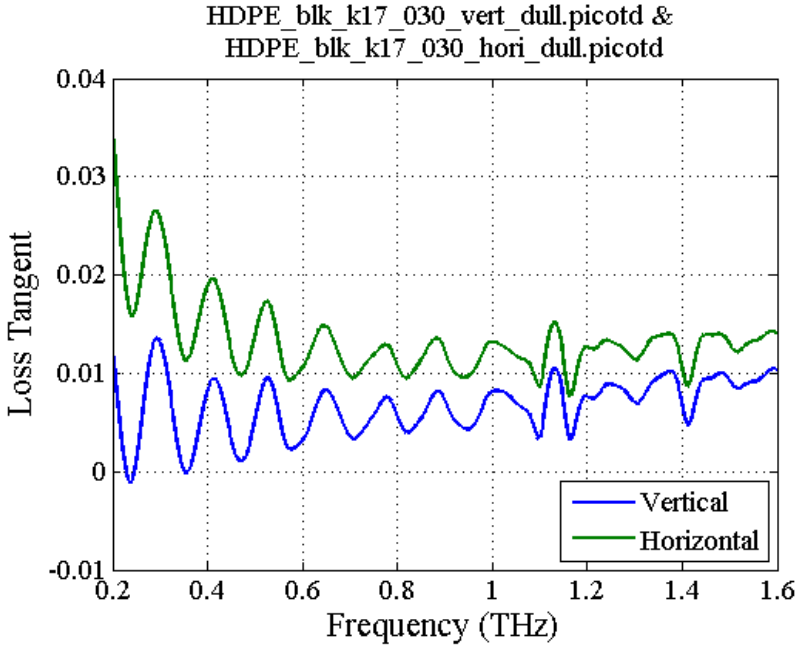
HDPE_blk_k17_030_vert_dull.picotd &
HDPE_blk_k17_030_hori_dull.picotd
Loss Tangent
Vertical
Horizontal
Frequency (THz)

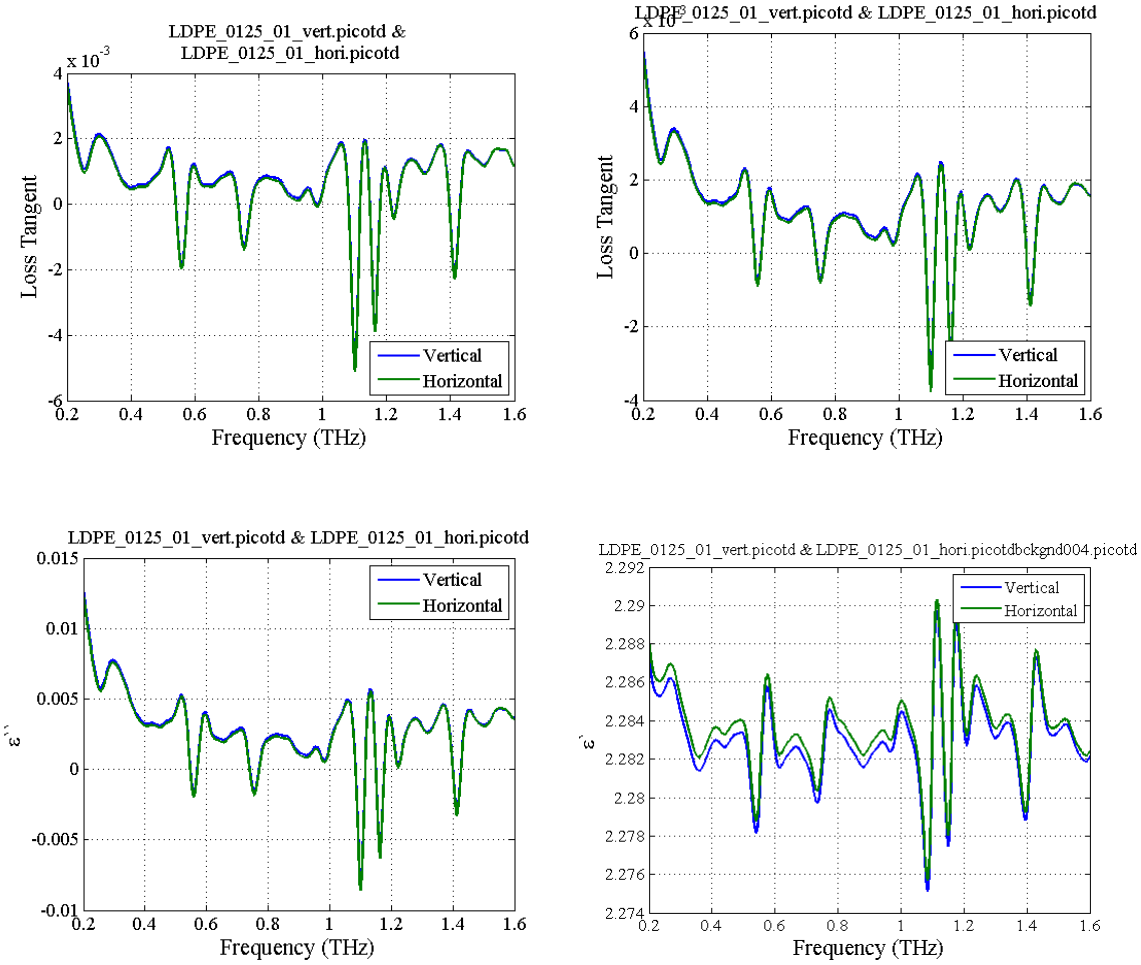

Figure 40 TDS Plots for Polymers and Polyethylene Plastics

There is a single curve, when both polarizations have the same response and table is also highly magnified. The ripple periods correlate to material thickness effects and scattering.

5.6 TDS Data Plots for Rogers higher loss and higher dielectric materials

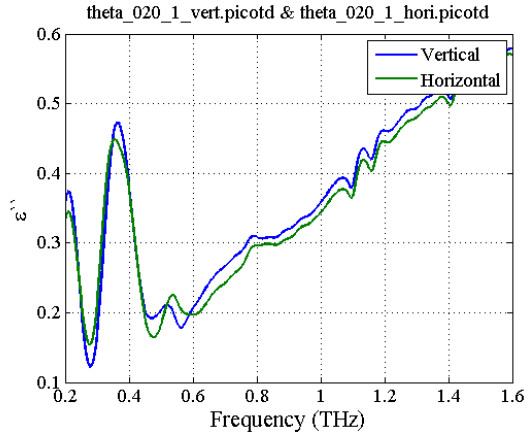

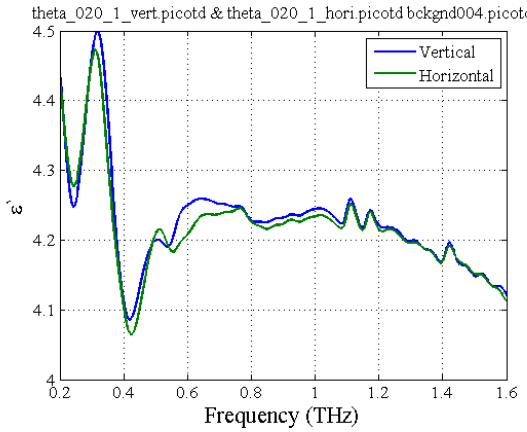

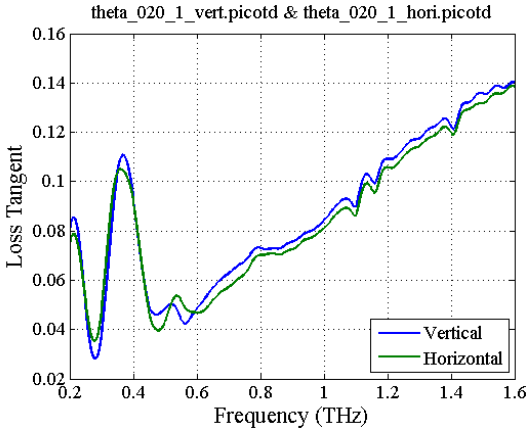

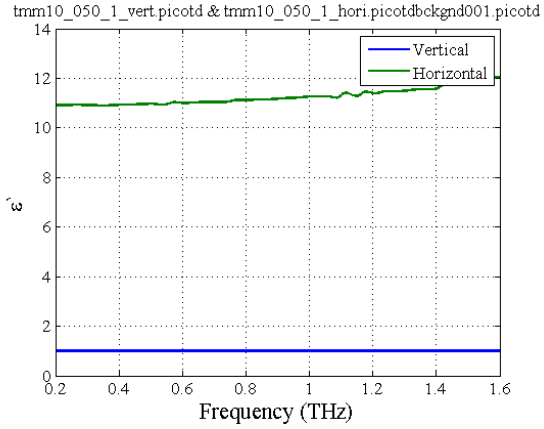

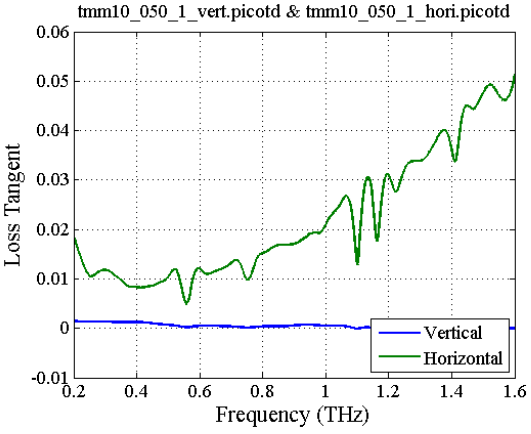

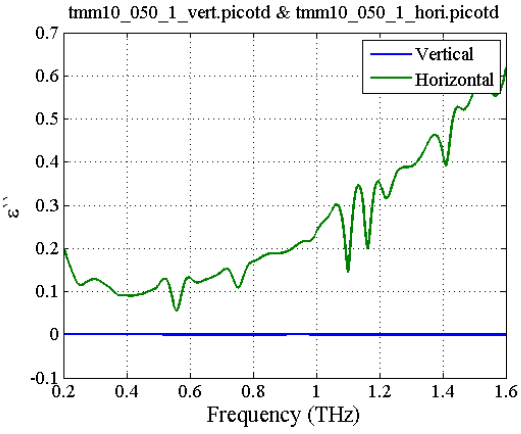

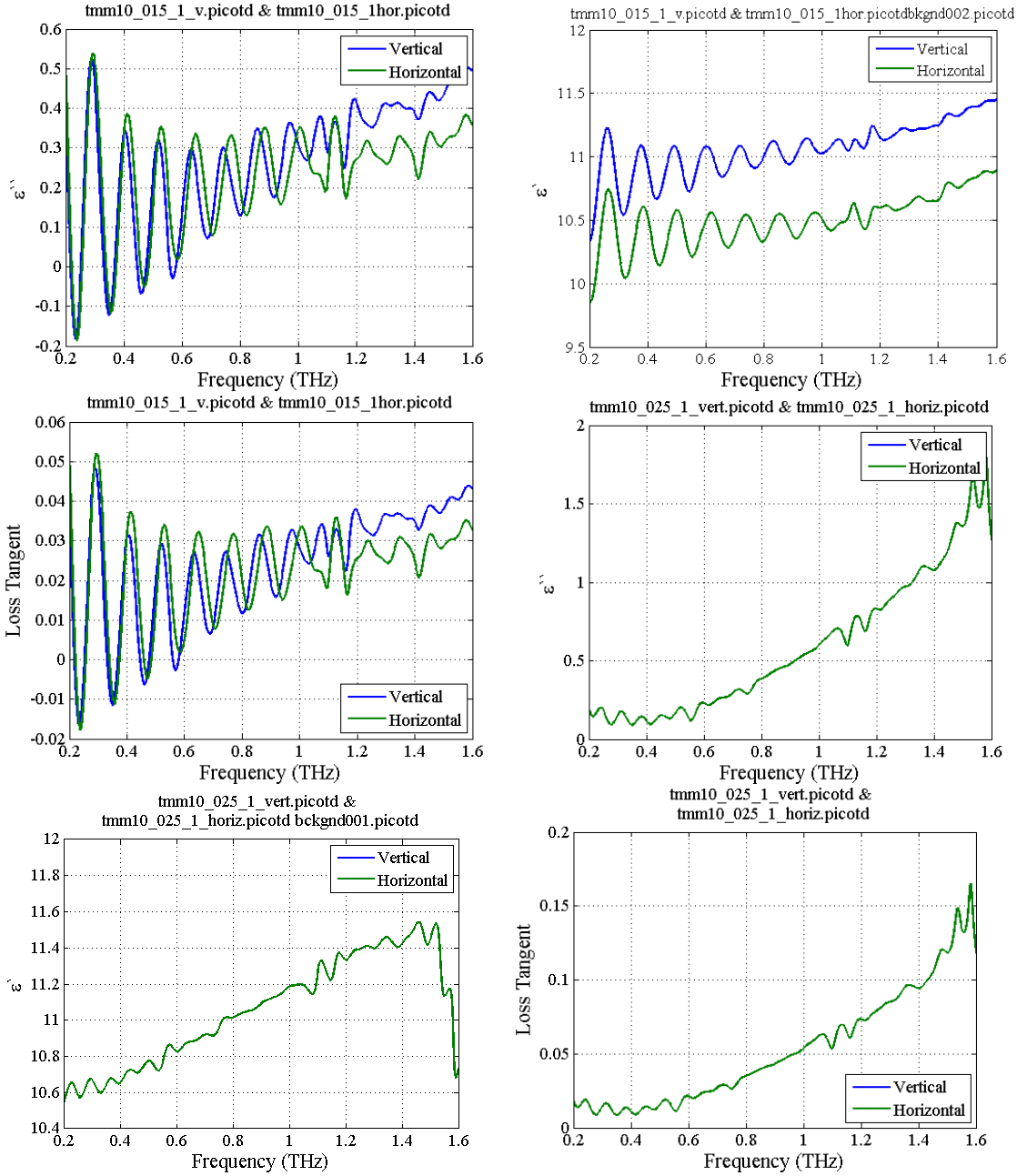

Figure 41 TDS Data Plots for Rogers' higher loss and higher dielectric Materials showing internal reflection ripples due to scattering.

6 RESULTS AND DISCUSSION

This section and supporting tables summarizes collection procedures, results, and error analysis. The errors in the test results for the VNA and TDS are presented in Figure 42.

Materials Measured 6/5-2012 at Portland State University using VNA / ZVA 40

Frequency (GHz)	Sample Description	Thickness (actual)	ε_r / Loss Tan (manufacturer) @10GHz	εr' (manufacturer) @10GHz	er' (avg) THz	er'(percent)	tand (mfgr @10GHz)	tand(avg) THz	tand (percent)	ε_r' (average) (H, V, 45)	ε_r" (average) (H, V, 45)	Loss tan (average) (H, V, 45)
325 - 500	ECE_Blk_1mm	1mm (1.02mm)	proprietary							2.73, 2.73, ---	0.0948, 0.0948, ---	0.0347, 0.0347, ---
325 - 500	ECE_Blk_2mm	2mm (2.00mm)	proprietary							2.74, 2.74, ---	0.0912, 0.0912, ---	0.0334, 0.0334, ---
325 - 500	ECE_Clr_2mm	2mm (2.34mm)	proprietary							3.10, 3.10, ---	0.382, 0.382, ---	0.127, 0.127, ---
325 - 500	R3006 25mils	24.5.0mils	6.15 / 0.0020	6.15	**7.335**	**-19.2683**	**0.0020**	**0.0169**	**-745.0000**	7.14, 7.53, ---	0.122, 0.126, ---	0.0172, 0.0166, ---
325 - 500	R4350B 60mils	59.5mils	3.66 / 0.0037	3.66	**3.765**	**-2.8689**	**0.0037**	**0.0116**	**-212.6126**	3.75, 3.78, ---	0.0527, 0.0770, ---	0.0141, 0.0206, ---
325 - 500	R5870 31mils	31.25mils	2.33 / 0.0012	2.33	**2.44**	**-4.7210**	**0.0012**	**0.0038**	**-216.6667**	2.45, 2.43, ---	0.0094, 0.0094, ---	0.0038, 0.0038, ---
325 - 500	R6002 20mils	20.35mils	2.94 / 0.0012	2.94	**2.92**	**0.6803**	**0.0012**	**0.0013**	**-8.3333**	2.90, 2.94, ---	0.0039, 0.0039, ---	0.0013, 0.0013, ---
325 - 500	R6002 30mils	29.75mils	2.94 / 0.0012	2.94	**2.935**	**0.1701**	**0.0012**	**0.0013**	**-8.3333**	2.94, 2.93, ---	0.0039, 0.0039, ---	0.0013, 0.0013, ---
325 - 500	TMM10 25mils	26.6mils	9.2 / 0.0022	9.2	**10.09**	**-9.6739**	**0.0022**	**0.0120**	**-445.4545**	9.92, 10.26, ---	0.0901, 0.1525, ---	0.0089, 0.0151, ---
325 - 500	Theta 20mils	19.7mils	4.01 / 0.0118	4.01	**4.125**	**-2.8678**	**0.0118**	**0.0487**	**-312.7119**	4.13, 4.12, ---	0.1899, 0.1899, ---	0.0487, 0.0487, ---

Materials Measured 10/24-2012 at Virginia Diodes, Inc. using VNA/ZVA40

Frequency (GHz)	Sample Description	Thickness (actual)	ε_r / Loss Tan (manufacturer) @10GHz	ε'_r (manufacturer) @10GHz	er' (avg) THz	er'(percent)	tand (mfgr) @10GHz	tand(avg) THz	tand (percent)	ε_r' (average) (H, V, 45)	ε_r" (average) (H, V, 45)	Loss Tan (average) (H, V, 45)
500 - 750	R3006 25mils	24.5mils	6.15 / 0.0020	6.15	**7.74666667**	**-25.9621**	**0.0020**	**0.0478**	**-2291.6667**	7.61, 8.00, 7.63	0.3348, 0.3642, 0.3814	0.0446, 0.0480, 0.0509
500 - 750	R3003 10mils	10.15mils	3.00 / 0.0013	3	**3.085**	**-2.8333**	**0.0013**	**0.0041**	**-211.5385**	3.07, 3.10, ---	0.0055, 0.0183, ---	0.0019, 0.0062, ---
500 - 750	R3010 10mils	10.5mils	10.20 / 0.0027	10.2	**12.795**	**-25.4412**	**0.0027**	**0.0095**	**-251.8519**	13.19, 12.40, ---	0.1105, 0.0965, ---	0.0098, 0.0092, ---
500 - 750	R4350B 60mils	59.5mils	3.66 / 0.0037	3.667	**3.755**	**-2.3998**	**0.0037**	**0.0311**	**-739.1892**	3.75, 3.76, ---	0.1022, .1275, ---	0.0276, 0.0345, ---
500 - 750	R6002 20mils	20.35mils	2.94 / 0.0012	2.94	**2.97**	**-1.0204**	**0.0012**	**0.0028**	**-133.3333**	---, 2.97, ---	---, 0.0080, ---	---, 0.0028, ---
500 - 750	R6002 30mils	29.75mils	2.94 / 0.0012	2.94	**2.97**	**-1.0204**	**0.0012**	**0.0030**	**-150.0000**	---, 2.97, ---	---, 0.0088, ---	---, 0.0030, ---
500 - 750	TMM10 50mils	50.85mils	9.2 / 0.0022	9.2	**10.665**	**-15.9239**	**0.0022**	**0.0096**	**-336.3636**	11.06, 10.27, ---	0.1105, 0.1117, ---	0.0103, 0.0089, ---
500 - 750	Theta 20mils	19.7mils	4.01 / 0.0118	4.01	**4.28666667**	**-6.8994**	**0.0118**	**0.0538**	**-355.9322**	4.30, 4.29, 4.27	0.2321, 0.2103, 0.2134	0.0580, 0.0526, 0.0508

Materials Measured 5/31-6/2/2012 at Portland State University Picometrix T-Ray 4000 Time Domain Spectrometer OFFSET=680pS, Tavg=6000

Frequency (GHz)	Sample Description	Thickness (actual)	ε_r / Loss Tan (manufacturer) @10GHz	ε'_r (manufacturer) @10GHz	er' (avg) THz	er'(percent)	tand (mfgr) @10GHz	tand(avg) THz	tand (percent)	ε_r' (average) (H, V)	ε_r" (min,max,avg) (H, V)	Loss Tan (average) (H, V)
200 - 1600	ECE_Blk_1mm	1mm (1.02mm)	proprietary	proprietary						2.7	0.11, 0.2, 0.15	0.055 H=V
200 - 1600	ECE_Blk_2mm	2mm (2.00mm)	proprietary	proprietary						2.73	0.15, 0.205, 0.15	0.055
200 - 1600	ECE_Clr_2mm	2mm (2.34mm)	proprietary	proprietary						3.3	0.3, 0.41, 0.4	0.12
200 - 1600	R3003_20mils	20.4500	3.00 / 0.0013	3	**2.98**	**0.6667**	**0.0013**	**0.0250**	**-94.8000**	V3.06/ H 2.9	V: 0.05, 0.18, 0.075 H: 0.05, 0.16, 0.070	V 0.03 / H 0.02
200 - 1600	R3006 25mils	24.5 mils	6.15 / 0.0020	6.15	**7.6**	**-23.5772**	**0.0020**	**0.1750**	**-98.8571**	V 7.8 / H 7.4	V: 0.25, 1.9, 1.0 H: 0.25, 1.6, 0.8	V 0.20 / H 0.15
200 - 1600	R3850B 4mils	4.0/(3.9 mils)	2.90 / 0.0025	2.9	**4**	**-37.9310**	**0.0025**	**0.0220**	**-88.6364**	V 3.9 / H 4.1	V: 0.0, 0.4, 0.10 H: same	V 0.023 / H 0.021
200 - 1600	R4350B 60mils	59.5 mils	3.66 / 0.0037	3.66	**3.73**	**-1.9126**	**0.0037**	**0.0425**	**-91.2941**	V 3.73 / H 3.73	V: 0.075, 0.25, 0.16 H: 0.10, 0.23, 0.17	V 0.04 / H 0.045
200 - 1600	R5870 31mils	31.25 mils	2.33 / 0.0012	2.332	**2.45**	**-5.0600**	**0.0012**	**0.0451**	**-97.3407**	V 2.46 / H 2.44	V: 0.13, 0.3, 0.15 H: 0.03, 0.08, 0.05	V 0.07 / H 0.025
200 - 1600	R6002 20mils	20.35 mils	2.94 / 0.0012	2.94	**2.94**	**0.0000**	**0.0012**	**0.0075**	**-84.0000**	V 2.93 / H 2.95	V: 0.020, 0.040, 0.028 H: 0.020, 0.040, 0.028	V 0.0075 / H 0.0075
200 - 1600	R6002 30mils	29.75 mils	2.94 / 0.0012	2.94	**2.93**	**0.3401**	**0.0012**	**0.0130**	**-90.7692**	V 2.93 / H 2.93	V: 0.03, 0.08, 0.04 H: 0.03, 0.08, 0.04	V 0.013 / H 0.013
200 - 1600	TMM10 15mils	15.65 mils	9.2 / 0.0022	9.2	**10.9**	**-18.4783**	**0.0022**	**0.0235**	**-90.6383**	V 11.2 / H 10.6	V: 0.1, 0.5, 0.25 H: 0.1, 0.35, 0.23	V 0.025 / H 0.022
200 - 1600	Theta 20mils	19.7mils	4.01 / 0.0118	4.01	**4.245**	**-5.8603**	**0.0118**	**0.0875**	**-86.5143**	V 4.25 / H 4.24	V: 0.2, 0.58, 0.35 H: 0.2, 0.57, 0.34	V 0.09 / H 0.085
200 - 1600	HDPE_K71_dull 30 mils	31.9 mils	2.25-2.35/.0003	2.3	**2.98**	**-29.5652**	**0.0003**	**0.0100**	**-97.0000**	V 2.465 / H 2.485	V: 0.010, 0.030, 0.018 H: 0.06, 0.035, 0.030	V 0.007 / H 0.013
200 - 1600	LDPE_K112_01 25, 125mils	124.5 mils	2.25-2.35/.0003	2.3	**2.284**	**0.6957**	**0.0003**	**0.0010**	**-70.0000**	V 2.284 / H 2.284	V = H .0075, .003, .0025	V 0.001 / H 0.001

Figure 42: Error Analysis of VNA and TDS Data

6.1 Data collection procedures, summary, and comments related to errors

All uncut samples were sliced up into three sections; each was one inch square, each coming from the same sheet. After contacting the manufacturers regarding the wide tolerance given for the physical and electrical parameters of their material, it was found that most of these firms have many different manufacturing facilities located worldwide. Therefore, a sample of one thickness may not be from the same plant as the exact same material of another thickness. This implies that testing different thicknesses of the same material may not produce the expected results. However, this was done and the results were all within 10% of one another and within 25% of most manufacturer specifications. Both the VNA and TDS produced well correlated results and the FTS showed similar relative results.

As discussed in Chapter 1, the three measurement techniques, VNA, TDS, and FTS, work over different frequency ranges; with the VNA working over the lowest and the FTS the highest. This makes it challenging to directly compare measurement results between all of them. However, Table 14 provides a direct comparison between measurement results for several commonly used dielectrics when VNA and TDS techniques are used. The table shows that the measured values for the real part of the permittivity, ε_r', of the samples are consistent with that provided by the manufacturer at 10 GHz. However, the imaginary part of the permittivity, ε_r", and therefore the loss tangent, tan δ, can vary by up to an order of magnitude from the 10 GHz data at high frequencies.

Table 14: Summary for three samples on VNA and TDS

Parameter	Sample	Mfgr value (10GHz)	VNA/PSU (325-500 GHz)	VNA/VDI (500-750GHz)	TDS (200-1.5 THz)
	R3006x25				
Er'		6.15	7.3	7.8	7.6
Er"		0.0123	0.124	0.358	0.25
Tan (d)		0.002	0.0169	0.0478	0.025
	TMM10				
Er'		9.2	10	10.63	10.9
Er"		0.0202	0.12	0.111	0.1
Tan (d)		0.0022	0.012	0.0096	0.015
	R6002				
Er'		2.94	2.92	2.97	2.93
Er"		0.00353	0.0039	0.008	0.02
Tan (d)		0.0012	0.0013	0.0028	0.008

Table 14 Summary for three samples on VNA and TDS, R3006, TMM10, and R6002

The error analysis computation for Loss Tangent (and ε_r") revealed that for the Rogers composites, their values were larger by about a factor of 6-10 times. The plastics were much closer to manufacturer data. This is apparently due to internal scattering and various intermolecular losses of the different materials used within the composite

substrates. **Users should be cognizant of this fact when designing circuits at high frequencies.**

While some of the substrates have a factory rated permittivity of about 3, they have alumina ceramic particles imbedded having a permittivity of 9.-10. The Terahertz waves can resolve these fine differences and may respond to the alumina depending on the relative dimensions to the material in the lattice. This will then change the value of ε_r" obtained on the TDS. To resolve this issue, a lower frequency setup would have to be used to see when the higher loss materials start to dominate.

Calibration probably cannot cancel out these effects, since they are real. These higher loss results were consistent with the findings of other experimenters, [Hejase:63], for the same exact materials. In a few cases, this data showed operational errors and those results are not always meaningful, but presented for completeness. In all cases, the results were consistent between the different measurements systems, therefore, these effects do, in fact, exist.

Relating to error analysis schemes, it was found that Rogers, Inc. uses the ANOVA Gauge Repeatability and Reproducibility measurement systems analysis technique for its IPC 10 GHz microwave stripline evaluation. This procedure requires data that is not available in this project. It is less meaningful in a free space system where samples are positioned into an immobile optical platform that cannot be moved once locked into

place, without causing major disruption to the setup and not deemed permissible by the equipment owner, in terms of stress to their system. For the TDS, each sample is averaged at least 6000 times and the incidence angle is not very critical once it is near 90 degrees. The samples were also rotated 0, 45, and 90 degrees. For the VNA, the data is averaged continuously. Typically, 1-3 samples of each type were tested and compared before storing the final test data. There were operational limits set by the equipment owners.

The thickness of each sample was measured three times and averaged using both a digital micrometer and a digital caliper. Each instrument had a tolerance of +/- 0.0005 per inch, which is below that which Rogers Corporation shows in their data sheets (+/- 10% typical). Their tolerances varied from 10-15 percent. This is due to external manufacturing tolerances, plus handling and processing. This is important since the results are directly proportional to material thickness. The one inch square samples were well within the tolerances physically attainable to contain 100% of the test signal wave.

A precision test fixture was developed and placed into the test apparatus which allowed precise positioning and rotation. The entire setup was aligned for a strongest signal, with the aid of the factory technicians, using a known sample. It was not practical to disassemble and reassemble the setup, as this could lead to excessive wear or damage to the equipment, as well as time constraints. The data plots are highly magnified and

therefore are showing very small changes that would be almost a straight line on a larger scale.

As mentioned, the TDS averages over 6000 times per measurement and the VNA runs continuously. Thus once a stable reading is achieved the data is captured. Since this is a free space measurement the physical errors are averaged out. Cubic spline smoothing was considered, but it was realized that the reflection ripples could and were used as a secondary method to confirm the sample thickness, since ε_r' was available. Further, the MATLAB plot tool used for the TDS data analysis partially smoothed each plot. The VNA data was averaged using visual and spreadsheet techniques described in the appendix very similar to least square approach.

VNA calibration was performed in two steps. First it was done using a standard local calibration kit plus a free space SOLT/reflection procedure similar to that used by Agilent. There are now newer Gated Reflect Line (GRL) calibration procedures available which require modifications to implement. The TDS is internally calibrated and reference sweeps are taken regularly in between sample test sweeps. The TDS is pulsed and therefore it does not see many type of reflective interference.

Microwave circuit material manufacturers are using the IPC-TM-650, 2.5.5.5 X-Band standard. This is a single frequency resonant stripline method, typically 10 GHz. A 14 GHz method called IPC standard. 2.5.5.5.1, is also used. After discussions with a plant

manufacturing engineer, it was found out that the IPC methods are hard to stabilize, but very accurate at one frequency, once locked in. They were anxious to have a consistent wideband technique that was more forgiving and had extended the test frequency range such as the TDS or VNA. While the TDS method may not be as accurate in absolute readings, it has a broader range of operation and much better consistency, since it is free space, thereby eliminating most mechanical and conductor related variables. Water spectral lines are easily detectable and therefore can be bypassed and samples were cleaned could be baked, except for the plastics which absorb moisture but are very temperature sensitive. Intermolecular scattering errors are hard to compensate for. The Rogers composite microwave grade, substrates were the primary test target and polymers/plastics were included for comparison and verification purposes. Plastics are less stable mechanically, but generally have lower loss and are homogeneous (isotropic).

The preliminary analysis and results from this project were evaluated by Rogers Corporation for integrity and considered to be a reasonable and within their tolerance range. Impact: A new broadband standard needs to be developed to get these types of measurements into the manufacturing sector and into the IPC Standards catalog.

Most project measurements were made off site at PSU and VDI. This was due to equipment functional and accuracy limitations locally. Hence, testing times were very limited for reruns and repeatability studies, nor were the facility owners in favor of this due to equipment stress issues. It was not recommended to disassemble and reassemble

their test setups due to possible damage. This generally is not done for experimental quasi-optical setups. It would be recommended for the IPC catalogue. However, this process would be very expensive and need to be undertaken by a manufacturer. Since multiple samples for each type were available, they were used to determine when the data was reproducible and the setup was deemed stable and then data was the recorded. Candidates were selected for the data sweeps based on previous measurements, and three samples of each were available for initial setup and integrity tests. Calibration and normalization runs were taken frequently. They used later for normalization and comparison calculations.

Thickness accuracy is an important issue. Currently there are a number of manufacturers working on Optical and Terahertz ellipsometers to get more accurate thickness dimensions of films and sheets. (e.g., Filmetrics, Inc.) Since anisotropy was observed, efforts were concentrated on comparing those particular samples on the different platforms. External limitations such as making sure all the radiation fields are contained within the sample and water lines were performed. Focusing was not needed but was considered.

When examining the TDS Data and VNA data, the results were very close among the same samples for both systems. The results were close to material data sheets for dielectric constant.

All project goals were achieved. Sample correlation data agreed with results reported by other experimenters. The purpose to this project was to demonstrate correlation among several broadband wideband quasi-optical THz measuring systems for characterization of various dielectric sheets and this was task was accomplished. Additionally, anisotropy was observed. A more detailed error analysis could have been possible if there was more sample data, but the primary scope of this project was comparative in nature.

6.2 SUMMARY AND CONCLUSIONS

- This Project used four THz Measurements systems (FTS, SNA, VNA, and TDS) to demonstrate the latest techniques in Materials Characterization. The results indicate that TDS is the instrument of choice for terahertz material characterization, for reasons previously stated.
- Extraction techniques produced consistent results with all systems which also agreed closely with manufacturer data, where available.
- Results were consistent over a wide range of frequency bands from 300 GHz to 1.5 THz, even though different instruments were used for the various bands.
- Polarization based anisotropy was observed in the high performance composite samples and those results were also consistent between the systems.
- Excellent correlation was achieved for the dielectric constant (ε_r').
- The values for Loss Tangent (tan δ, ε_r"/ε_r') obtained on all the instruments were considerably higher than the manufacturer data that is obtained at lower frequencies (10 GHz). However, these results correlated well to the results of other experimenters. These effects are real and are probably due intermolecular scattering as these materials are not homogeneous and were not designed for these bands.

- Plastics (HDPE, LDPE, polystyrene, and the ECE 3D Jet polymers) all were well behaved, low loss, but are not mechanically stable and cannot be used for packaging or substrates. The thickness of the Jet Polymers changed over time while the McMasters samples were more stable.

6.3 FUTURE RESEARCH AND IMPROVEMENTS

6.3.1 IMPROVEMENTS TO SAMPLES AND RELATED ELEMENTS

6.3.1.1 Better sample storage cleaning and handling techniques

- Accurate thickness measurement using THz ellipsometers
- Optional beam focusing and attenuator lens to be sure all energy is in the inside test sample and this can also be used to suppress reflections.
- Anisotropic measurements in numerous planes rather than just x-y plane.
- Advanced test fixtures such as the one by Swissto-12, Inc.; which can handle positional and environmental variations.
- Controlled measurement environment conditions (moisture and temperature, etc.)
- Translating motion stages to further cancel local reflections.
- A technique for evaluating scattering losses.

6.3.1.2 FTS Improvements

- Use modern FTS system with more precise stage control (Nicolet, Inc.)
- Better calibration routines for the different beam splitters and wider band splitters

- Better ways of minimizing local sample-to-detector reflections into account and keeping sample stage farther from the detector. This requires higher detector sensitivity and/or more source power. [Jarrah:109]
- FTMS (Fourier Transform Microwave Spectrometer) monochromatic measurements for gasses (Zikrs), Fabry-Perot system could be done for additional comparison, but packaging substrates were the project target.

6.3.1.3 TDS Improvements

6.3.1.3.1 Use a *T-Ray 5000*, a new integrated instrument, with advanced tools, including a better positioning system and better computational tools.

- T-Ray® 5000 ASR5001™ Spectroscopy Rail, new lenses, new Explorer ™ software
- Integrated Smart Data Acquisition™ and Stand-Alone Measurement Streaming system and an advanced Terahertz Control Unit.

6.3.1.3.2 Use Teralyzer © software (Menlo Systems) for analyzing thin films in more detail.

6.3.1.3.3 Consider using a Near Field TDS or AFM for more detailed studies as might be useful for nanoscale measurements.

6.3.1.3.4 Due to large distances in TDS measurements, be sure all energy is captured inside the test sample. Minimize sources of system loss and reflections and noise.

6.3.1.3.5 Improved sources and detectors will give more dynamic range and lower noise figures.

6.3.1.3.6 Access to a near field TDS system for observing surface details

6.3.1.4 VNA Improvements

- Better integration of the THz Extender with VNA, as is now done in the latest instruments, for improved performance.
- More advanced calibration systems such as Gated Reflect-Line (GRL) and pulsed techniques.
- Access to Precision Network Analyzer (PNA/X) with X-parameters and commercially proven extraction software for nonlinear measurements
- Higher frequencies and powers by using newer detectors and sources.

In conclusion, this project met or exceeded all its primary goals. Some new information and techniques were developed and used to demonstrate the feasibility of quasi-optical methodologies for wideband measurements of frequency dependent properties of dielectric materials. The TDS turned out to be the best instrument for characterizing materials at the terahertz frequency band. This work paves the way for commercialization of these processes, which are so very important to industry and national defense.

Thanks to all, JMS May 2015

7 BIBLIOGRAPHY

7.1 Detectors and Sources

1. Auston, D. H., K. P. Cheung, and P. R. Smith. “Picosecond Photoconducting Hertzian Dipoles.” *Applied Physics Letters* 45.3 (1984): 284–286. Web.
2. Busch, Kenneth W., and Marianna A. Busch. *Multielement Detection Systems for Spectrochemical Analysis*. Wiley-Interscience, 1990. Print.
3. Caves, Carlton M. “Quantum-Mechanical Radiation-Pressure Fluctuations in an Interferometer.” *Physical Review Letters* 45.2 (1980): 75–79. *APS*. Web. 1 Sept. 2012.
4. D.J, Benford, Hunter T.R, and Phillips T.G. “Noise Equivalent Power of Background Limited Thermal Detectors at Submillimeter Wavelengths.” Text. N.p., July 1998. Web. 12 Sept. 2012.
5. E, Jr Jones Charlie et al. “The Cooled Germanium Bolometer as a Far Infrared Detector.” *Applied Optics* 4.6 (1965): 683–685. Print.
6. Fellgett, Peter. “I. — Les Principes Généraux Des Méthodes Nouvelles En Spectroscopie Interférentielle - A Propos de La Théorie Du Spectromètre Interférentiel Multiplex.” *Journal de Physique et le Radium* 19.3 (1958): 187–191. *CrossRef*. Web. 11 Sept. 2012.
7. Giovannetti, Vittorio, Seth Lloyd, and Lorenzo Maccone. “Quantum-Enhanced Measurements: Beating the Standard Quantum Limit.” *Science* 306.5700 (2004): 1330–1336. *www.sciencemag.org*. Web. 1 Sept. 2012.
8. Golay, Marcel J. E. “Theoretical Consideration in Heat and Infra-Red Detection, with Particular Reference to the Pneumatic Detector.” *Review of Scientific Instruments* 18.5 (1947): 347–356. Web.
9. Golay, M. J. E. “Multislit Spectrometry.” *J. Opt. Soc. Am.* 39 (1949): 437–444. Print.
10. Grannan, S. M., P. L. Richards, and M. K. Hase. “Numerical Optimization of Bolometric Infrared Detectors Including Optical Loading, Amplifier Noise, and Electrical Nonlinearities.” *International Journal of Infrared and Millimeter Waves* 18.2 (1997): 319–340. Print.
11. Han, P. Y. et al. “A Direct Comparison between Terahertz Time-Domain Spectroscopy and Far-Infrared Fourier Transform Spectroscopy.” *Journal of Applied Physics* 89.4 (2001): 2357–2359. Print.

12. Hesler, J.L. et al. “The Development of Quasi-Optical THz Detectors.” *33rd International Conference on Infrared, Millimeter and Terahertz Waves, 2008. IRMMW-THz 2008*. N.p., 2008. 1 –2. *IEEE Xplore*. Web.
13. Hesler, J.L., and T.W. Crowe. “NEP and Responsivity of THz Zero-Bias Schottky Diode Detectors.” *Joint 32nd International Conference on Infrared and Millimeter Waves, 2007 and the 2007 15th International Conference on Terahertz Electronics. IRMMW-THz*. N.p., 2007. 844 –845. Print.
14. Jacquinot, P. “New Developments in Interference Spectroscopy.” *Reports on Progress in Physics* 23 (1960): n. pag. Print.
15. Jaekel, M. T, and S Reynaud. “Quantum Limits in Interferometric Measurements.” *Europhysics Letters (EPL)* 13.4 (1990): 301–306. *Institute of Physics*. Web. 1 Sept. 2012.
16. Khiabani, N., Yi Huang, and Yao-chun Shen. “Comparison of Ultra-Wideband THz Generation and Detection Systems.” *Proceedings of the 5th European Conference on Antennas and Propagation (EUCAP)*. N.p., 2011. 457 –461. Print.
17. Khosropanah, P. et al. “Analysis of NbN Hot Electron Bolometer Receiver Noise Temperatures Above 2 THz With a Quantum Noise Model.” *IEEE Transactions on Applied Superconductivity* 19.3 (2009): 274 –277. *IEEE Xplore*. Web.
18. Khosropanah, Pourya et al. “Fabrication and Noise Measurement of NbTiN Hot Electron Bolometer Heterodyne Mixers at THz Frequencies.” *Fourteenth International Symposium on Space Terahertz Technology*. Vol. -1. N.p., 2003. 20. *adsabs.harvard.edu*. Web. 19 Aug. 2012.
19. Kniffin, G.P., and L.M. Zurk. “Model-Based Material Parameter Estimation for Terahertz Reflection Spectroscopy.” *Terahertz Science and Technology, IEEE Transactions on* 2.2 (2012): 231 –241. *IEEE Xplore*. Web.
20. Kraus, J. D. *Radio Astronomy (Cygnus-Quasar Books): Powell*. N.p., 1986. Print.
21. Liu, Lei et al. “A Broadband Quasi-Optical Terahertz Detector Utilizing a Zero Bias Schottky Diode.” *IEEE Microwave and Wireless Components Letters* 20.9 (2010): 504 –506. *IEEE Xplore*. Web.
22. Lobanov, Y. et al. “Large-Signal Frequency Response of an HEB Mixer: From 300 MHz to Terahertz.” *IEEE Transactions on Applied Superconductivity* 21.3 (2011): 628–631. *IEEE Xplore*. Web.
23. Lobanov, Y. V. et al. “Microwave-Assisted Measurement of the Frequency Response of Terahertz HEB Mixers with a Fourier Transform Spectrometer.” *Twenty-First International Symposium on Space Terahertz Technology*. Vol. -1. N.p., 2010. 420–423. *adsabs.harvard.edu*. Web. 17 Aug. 2012.
24. Low, Frank J. “Low-Temperature Germanium Bolometer.” *J. Opt. Soc. Am.* 51.11 (1961): 1300–1304. Web.

25. Manohara, Harish M. et al. “Carbon Nanotube Schottky Diodes Using Ti−Schottky and Pt−Ohmic Contacts for High Frequency Applications.” *Nano Letters* 5.7 (2005): 1469–1474. *ACS Publications*. Web.
26. Nahata, Ajay et al. “Coherent Detection of Freely Propagating Terahertz Radiation by Electro-Optic Sampling.” *Applied Physics Letters* 68.2 (1996): 150 – 152. *IEEE Xplore*. Web.
27. Phillips, T. G. *Techniques of Submillimeter Astronomy*. Ed. R. D. Wolstencroft and W. B. Burton. in Millimeter and Submillimeter Astronomy, 1988. Print.
28. Richards, P. L. “Bolometers for Infrared and Millimeter Waves.” *Journal of Applied Physics* 76.1 (1994): 1–24. Print.
29. Rieke, George. *Detection of Light: From the Ultraviolet to the Submillimeter*. 2nd ed. Cambridge University Press, 2002. Print.
30. Schoenherr, D. et al. “Extremely Broadband Characterization of a Schottky Diode Based THz Detector.” *2010 35th International Conference on Infrared Millimeter and Terahertz Waves (IRMMW-THz)*. N.p., 2010. 1 –2. *IEEE Xplore*. Web.
31. Sizov, F. “THz Radiation Sensors.” *Opto-Electronics Review* 18.1 (2010): 10–36. *SpringerLink*. Web. 12 Sept. 2012.
32. Sizov, F., and A. Rogalski. “THz Detectors.” *Progress in Quantum Electronics* 34.5 (2010): 278–347. Print.
33. Song, Woo-Bin, and Joseph J Talghader. “Design and Characterization of Adaptive Microbolometers.” *Journal of Micromechanics and Microengineering* 16.5 (2006): 1073–1079. *Institute of Physics*. Web. 21 Aug. 2012.
34. Tittonen, I. et al. “Interferometric Measurements of the Position of a Macroscopic Body: Towards Observation of Quantum Limits.” *Physical Review A* 59.2 (1999): 1038–1044. *APS*. Web. 1 Sept. 2012.
35. Veksler, D. et al. “GaN Heterodimensional Schottky Diode for THz Detection.” *5th IEEE Conference on Sensors, 2006*. N.p., 2006. 323 –326. *IEEE Xplore*. Web.
36. Woolard, Dwight L., William R. Loerop, and Michael Shur. *Terahertz Sensing Technology*. 30, v. 32. River Edge, N.J.: World Scientific, 2003. Print.
37. Wu, Ziran et al. “Terahertz Electromagnetic Crystal Waveguide Fabricated by Polymer Jetting Rapid Prototyping.” *Optics Express* 19.5 (2011): 3962–3972. Print.
38. Yang, Xianbo, and P. Chahal. “Large-Area Low-Cost Substrate Compatible CNT Schottky Diode for THz Detection.” *Electronic Components and Technology Conference (ECTC), 2011 IEEE 61st*. N.p., 2011. 2158 –2164. *IEEE Xplore*. Web.

39. Zmuidzinas, J., and P.L. Richards. “Superconducting Detectors and Mixers for Millimeter and Submillimeter Astrophysics.” *Proceedings of the IEEE* 92.10 (2004): 1597 – 1616. *IEEE Xplore*. Web.
40. *International Symposium Digest: Antennas and Propagation (Cat. No. CH2435-6)* (1987): 1174–7 vol.27 vol.2. Print.
41. Jarrahi, M., and T.H. Lee. “High-Power Tunable Terahertz Generation Based on Photoconductive Antenna Arrays.” Microwave Symposium Digest, 2008 IEEE MTT-S International. N.p., 2008. 391–394. IEEE Xplore. Web.
42. Kloosterman, J. L. et al. “Hot Electron Bolometer Heterodyne Receiver with a 4.7-THz Quantum Cascade Laser as a Local Oscillator.” Applied Physics Letters 102.1 (2013): -. Web.
43. Mouret, G. et al. “Anomalous Dispersion Measurement in Terahertz Frequency Region by Photomixing.” Applied Physics Letters 88.18 (2006): 181105–181105–3. AIP. Web. 27 May 2013.

7.2 Dielectrics and Measurements

44. Bartley, P.G., and S.B. Begley. “A New Free-Space Calibration Technique for Materials Measurement.” Instrumentation and Measurement Technology Conference (I2MTC), 2012 IEEE International. N.p., 2012. 47–51. Web.
45. A. M. Nicolson, G. F. Ross, 'Measurement of the intrinsic properties of materials by time-domain techniques', *IEEE Trans. on Instrum. Meas*., vol. IM-19, Nov 1970, pp. 377-82
46. Weir, W.B. 'Automatic Measurement Of Complex Dielectric Constant And Permeability At Microwave Frequencies'. *Proc. IEEE* 62.1 (1974): 33-36. Web.
47. Green, Christopher, C. and J. M. Seligman. 'Method And Apparatus For Measuring And Characterizing The Frequency Dependent Electrical Properties Of Dielectric Materials'. US Patent 6,472,885. 29 Oct. 2002.
48. Engen, G. F. 'An improved circuit for implementing the six-port technique of microwave measurements'. *IEEE Trans. Microwave Theory Tech.*, Dec. 1977, vol. MTT-25, no. 12, p. 1080- 1083.
49. Janezic, M.D.; Jargon, J.A., "Complex permittivity determination from propagation constant measurements," *Microwave and Guided Wave Letters, IEEE* , vol.9, no.2, pp.76,78, Feb 1999.
50. Abernethy, C.E., A.C. Cangellaris, and J.L. Prince. “A Novel Method of Measuring Microelectronic Interconnect Transmission Line Parameters and Discontinuity Equivalent Electrical Parameters Using Multiple Reflections.”

Components, Packaging, and Manufacturing Technology, Part B: Advanced Packaging, IEEE Transactions on 19.1 (1996): 32 –39. Web.

51. Baker-Jarvis, J., E.J. Vanzura, and W.A. Kissick. "Improved Technique for Determining Complex Permittivity with the Transmission/reflection Method." Microwave Theory and Techniques, IEEE Transactions on 38.8 (1990): 1096–1103. Web.
52. Baker-Jarvis, J. et al. "Dielectric Characterization of Low-Loss Materials in the Range 1 GHz to 20 GHz: A Comparison of Techniques." *" IEEE Trans. Dielect. Elect. Insulation, vol. 5, no* 5.4 (1998): 571—577. Print.
53. Bartley, P.G., and S.B. Begley. "Improved Free-Space S-Parameter Calibration." In Instrumentation and Measurement Technology Conference, 2005. IMTC 2005. Proceedings of the IEEE, 1:372 –375, 2005.
54. Chen, Weiwu, Soshu Kirihara, and Yoshinari Miyamoto. "Fabrication of Three-Dimensional Micro Photonic Crystals of Resin-Incorporating TiO2 Particles and Their Terahertz Wave Properties." *Journal of the American Ceramic Society* 90.1 (2007): 92–96. Web.
55. Dorney, Timothy D., Richard G. Baraniuk, and Daniel M. Mittleman. "Material Parameter Estimation with Terahertz Time-Domain Spectroscopy." *Journal of the Optical Society of America A* 18.7 (2001): 1562–1571. *Optical Society of America*. Web. 20 Aug. 2012.
56. Elhawil, A. et al. "A Quasi-Optical Free-Space Method for Dielectric Constant Characterization of Polymer Materials in Mm-Wave Band." *Proc. Symp. IEEE/LEOS Benelux Chapter Brussels*. N.p., 2007. 187–190. *Google Scholar*. Web. 29 June 2014.
57. Ferguson, Bradley, and Xi-Cheng Zhang. "Materials for Terahertz Science and Technology." *Nature Materials* 1.1 (2002): 26–33. *www.nature.com*. Web. 26 Aug. 2012.
58. Green, C.C., Seligman, J.M. et al. "Characterization of Frequency Dependent Dielectric Packaging Media Using Differential and Multiple-Reflection Techniques on a Precision Stripline Test Structure." *IEEE 7th Topical Meeting on Electrical Performance of Electronic Packaging (Cat. No.98TH8370)*. New York, NY, USA: IEEE. 69–72 (1998). Print.
59. Green, C.C. et al. "Electrical Characterization of Integrated Circuit Molding Compound." *IEEE TRANSACTIONS ON ADVANCED PACKAGING* 22.3 (1999): 337–342. Web.
60. Guo, Zhonghai et al. "Broadband Characterization of Complex Permittivity for Low-Loss Dielectrics: Circular PC Board Disk Approach." *Antennas and Propagation, IEEE Transactions on* 57.10 (2009): 3126 –3135. Web.

61. Haggenmueller, R. et al. “Production and Characterization of Polymer Nanocomposites with Highly Aligned Single-Walled Carbon Nanotubes.” *Journal of Nanoscience and Nanotechnology* 3.1-2 (2003): 105–110. Web.
62. Hartley, Rick. “Base Materials for High. Speed, High Frequency PC Boards.” PCB&A (2002): n. pag. Print.
63. Hejase, J.A., P.R. Paladhi, and P. Chahal. “Terahertz Characterization of Dielectric Substrates for Component Design and Nondestructive Evaluation of Packages.” *IEEE Transactions on Components, Packaging and Manufacturing Technology* 1.11 (2011): 1685 –1694. *IEEE Xplore*. Web.
64. Hill, M.J., and L.E. Wojewoda. “A Study of Permittivity Measurement Reproducibility Utilizing the Agilent 4291B.” *Advanced Packaging, IEEE Transactions on* 29.4 (2006): 714 –718. Web.
65. J. Baker-Jarvis, R. Geyer, J. Grosvenor, M. Janezic, C. Jones, B. Riddle,C. Weil, and J. Krupka, “Dielectric characterization of low-loss materials in the range 1 GHz to 20 GHz: A comparison of techniques,” IEEE Trans. Dielectr. Electr. Insulation, vol. 5, no. 4, pp. 571—577, 1998.]
66. Janezic, M.D. et al. “Permittivity Characterization of Low-K Thin Films from Transmission-Line Measurements.” *Microwave Theory and Techniques, IEEE Transactions on* 51.1 (2003): 132 – 136. Web.
67. Jin, Yun-Sik, Geun-Ju Kim, and Seok-Gy Jeon. “Terahertz Dielectric Properties of Polymers.” Journal of the Korean Physical Society 49.2 (2006): 513–517. Print.
68. Jin, Yun-Sik, Geun-Ju Kim, and Seok-Gy Jeon. “Terahertz Dielectric Properties of Polymers.” *Journal Of The Korean Physical Society* 49.2 (2006): 513–517. Print.
69. Kaatze, Udo. *Techniques for Measuring the Microwave Dielectric Properties of Materials*. Vol. 47. N.p., 2010. Web. 2.
70. Kniffin, Gabriel Paul. “Model-Based Material Parameter Estimation for Terahertz Reflection Spectroscopy.” Thesis. N.p., 1 Jan. 2010. Web. 20 Aug. 2012.
71. Kniffin, G.P., and L.M. Zurk. “Model-Based Material Parameter Estimation for Terahertz Reflection Spectroscopy.” *Terahertz Science and Technology, IEEE Transactions on* 2.2 (2012): 231 –241. *IEEE Xplore*. Web.
72. Levitskaya, Tsylya M, and Ben K Sternberg. “Polarization Processes in Rocks: 1. Complex Dielectric Permittivity Method.” Radio Science 31.4 (1996): 755–779. Print.
73. Liang, Min et al. “Terahertz Characterization of Single-Walled Carbon Nanotube and Graphene On-Substrate Thin Films.” *Microwave Theory and Techniques, IEEE Transactions on* 59.10 (2011): 2719 –2725. Web.

74. M.J., and L.E. Wojewoda. “A Study of Permittivity Measurement Reproducibility Utilizing the Agilent 4291B.” Advanced Packaging, IEEE Transactions on 29.4 (2006): 714 –718.
75. Martens, Luc. *High-Frequency Characterization of Electronic Packaging*. Boston: Kluwer Academic Publishers, 1998. Print.
76. Sternberg, BK, and TM Levitskaya. “Measurement of Sheet-Material Electrical Properties: Extending Lumped-Element Methods to 10 GHz.” IEE Proceedings-Science, Measurement and Technology 152.3 (2005): 123–128. Print.
77. Sternberg, Ben K., and Tsylya M. Levitskaya. “Electrical Parameters of Soils in the Frequency Range from 1 kHz to 1 GHz, Using Lumped-circuit Methods.” Radio Science 36.4 PP. 709–719. Web. 28 Apr. 2012.]
78. Trambarulo, R., and H.S. Berger. “Conversion Loss and Noise Temperature of Mixers from Noise Measurements.” *Microwave Symposium Digest, 1983 IEEE MTT-S International*. N.p., 1983. 364 –365. *IEEE Xplore*. Web.
79. Wu, Ziran et al. “Microwave to Terahertz Characterization of Carbon Nanotube Materials.” *Silicon Monolithic Integrated Circuits in RF Systems (SiRF), 2011 IEEE 11th Topical Meeting on*. N.p., 2011. 181 –184. Web.
80. Xin, X. et al. “Terahertz Absorption Spectrum of Para and Ortho Water Vapors at Different Humidities at Room Temperature.” *Journal of Applied Physics* 100.9 (2006): 094905–094905–4. *SPIE-AIP*. Web. 27 Aug. 2012.
81. Zhu, Wanhua et al. “The Calculation of Dielectric Dispersive Models in THz Range with GA.” *Microwave and Optical Technology Letters* 49.10 (2007): 2540–2545. *onlinelibrary.wiley.com*. Web. 30 Apr. 2012.

7.3 FTS Related

82. “Fellgett’s Advantage - eNotes.com Reference.” N.p., n.d. Web. 17 Mar. 2012.
83. “Fourier Transform Infrared Spectroscopy - Wikipedia, the Free Encyclopedia.” N.p., n.d. Web. 5 Apr. 2015.
84. Bell, E.E. “Measurement of the Far Infrared Optical Properties of Solids with a Michelson Interferometer Used in the Asymmetric Mode: Part I, Mathematical Formulation∗.” *Infrared Physics* 6.2 (1966): 57–74. *Science Direct*. Web. 11 Sept. 2012.
85. Bell, Robert John. *Introductory Fourier Transform Spectroscopy*. Academic Press, 1972. Print.

86. Chan, George C.-Y., and WingTat Chan. “Beer’s Law Measurements Using Non-Monochromatic Light Sources—A Computer Simulation.” *Journal of Chemical Education* 78.9 (2001): 1285. *ACS Publications*. Web. 5 Dec. 2014.
87. CONNES, JANINE, and PIERRE CONNES. “Near-Infrared Planetary Spectra by Fourier Spectroscopy. I. Instruments and Results.” J. Opt. Soc. Am. 56.7 (1966): 896–910. Web.
88. Fellgett, Peter B. “(Multiplex Advantage).” University of Cambridge, 1949. Print.
89. Golay, M. J. E. “Multislit Spectrometry.” *J. Opt. Soc. Am.* 39 (1949): 437–444. Print.
90. Jacquinot, P. “New Developments in Interference Spectroscopy.” *Reports on Progress in Physics* 23 (1960): n. pag. Print.
91. Ziurys, L. M. et al. “A Millimeter/submillimeter Spectrometer for High Resolution Studies of Transient Molecules.” *Review of Scientific Instruments* 65.5 (1994): 1517–1522. Print.

7.4 Measurements and New Technologies and Extraction

92. Courtney, W.E. “Analysis and Evaluation of a Method of Measuring the Complex Permittivity and Permeability Microwave Insulators.” *IEEE Transactions on Microwave Theory and Techniques* 18.8 (1970): 476 – 485. *IEEE Xplore*. Web.
93. Crowe, T.W. et al. “VNA Frequency Extenders to 1.1 THz.” *Infrared, Millimeter and Terahertz Waves (IRMMW-THz), 2011 36th International Conference on*. N.p., 2011. 1. *IEEE Xplore*. Web.
94. Dvorak, S. L., and B. K. Sternberg. “Suppression of Phase-Noise Interference Due to Closely Spaced Data and Calibration Signals.” *IEEE TRANSACTIONS ON INSTRUMENTATION AND MEASUREMENT* 51 (2002): 1157–1162. Print.
95. Ghodgaonkar, D.K., V.V. Varadan, and Vijay K. Varadan. “A Free-Space Method for Measurement of Dielectric Constants and Loss Tangents at Microwave Frequencies.” *IEEE Transactions on Instrumentation and Measurement* 38.3 (1989): 789–793. *IEEE Xplore*. Web.
96. Guo, Zhonghai et al. “Broadband Characterization of Complex Permittivity for Low-Loss Dielectrics: Circular PC Board Disk Approach.” *Antennas and Propagation, IEEE Transactions on* 57.10 (2009): 3126 –3135. Web.
97. Haggenmueller, R. et al. “Production and Characterization of Polymer Nanocomposites with Highly Aligned Single-Walled Carbon Nanotubes.” *Journal of Nanoscience and Nanotechnology* 3.1-2 (2003): 105–110. Web.

98. Kim, Sung et al. “Effective Material Property Extraction Of A Metamaterial By Taking Boundary Effects Into Account At Te/Tm Polarized Incidence.” *Progress In Electromagnetics Research B* 36 (2012): 1–33. *CrossRef*. Web. 14 Dec. 2013.
99. Krupka, Jerzy et al. “A Dielectric Resonator for Measurements of Complex Permittivity of Low Loss Dielectric Materials as a Function of Temperature.” *Measurement Science and Technology* 9.10 (1998): 1751–1756. *Institute of Physics*. Web. 2 Aug. 2012.
100. Liang, Min et al. “Terahertz Characterization of Single-Walled Carbon Nanotube and Graphene On-Substrate Thin Films.” *Microwave Theory and Techniques, IEEE Transactions on* 59.10 (2011): 2719 –2725. Web.
101. Paquay, M., J. Hesler, and D. Kurtz. “Improvements on High Performance Solid State Frequency Extension Units for Full-Band Frequency Coverage at Mm-Wave Frequencies.” *Antenna Measurement Techniques Association Symposium (AMTA)*. N.p., 2007. 4–9. Print.
102. Saenz, E., L. Rolo, K. van’t Klooster, et al. “Accuracy Assesment of Material Measurements with a Quasi-Optical Free-Space Test Bench.” *2012 6th European Conference on Antennas and Propagation (EUCAP)*. N.p., 2012. 572 –576. *IEEE Xplore*. Web.
103. Saenz, E., L. Rolo, M. Paquay, et al. “Sub-Millimetre Wave Material Characterization.” *Proceedings of the 5th European Conference on Antennas and Propagation (EUCAP)*. N.p., 2011. 3183 –3187. Print.
104. Siegel, Peter, and Robert Dengler. “TERAHERTZ HETERODYNE IMAGING PART I: INTRODUCTION AND TECHNIQUES.” *International Journal of Infrared and Millimeter Waves* 27.4 (2006): 465–480. Print.
105. Wang, Lu et al. “Demetalization of Single-Walled Carbon Nanotube Thin Films with Microwave Irradiation.” *Applied Physics A: Materials Science & Processing* 102.2 (2011): 401–406. Print.
106. Wu, Ziran et al. “Microwave to Terahertz Characterization of Carbon Nanotube Materials.” *Silicon Monolithic Integrated Circuits in RF Systems (SiRF), 2011 IEEE 11th Topical Meeting on*. N.p., 2011. 181 –184. Web.
107. Zhang, Jianmin et al. “Extraction of Dispersive Material Parameters Using Vector Network Analyzers and Genetic Algorithms.” *Proceedings of the IEEE Instrumentation and Measurement Technology Conference, 2006. IMTC 2006*. N.p., 2006. 462–467. *IEEE Xplore*. Web.

7.5 THz Time Domain Spectrometry

108. Aschaffenburg, D. J. et al. “Efficient Measurement of Broadband Terahertz Optical Activity.” *Appl. Phys. Lett., 2012* 100 (2012): n. pag. Print.
109. Berry, Christopher W., and Mona Jarrahi. “Terahertz Generation Using Plasmonic Photoconductive Gratings.” *New Journal of Physics* 14.10 (2012): 105029. *Institute of Physics*. Web. 14 Mar. 2015.
110. Cook, David J., Brian K. Decker, and Mark G. Allen. “Quantitative THz Spectroscopy of Explosive Materials.” *Optical Terahertz Science and Technology*. Optical Society of America, 2005. MA6. *Optical Society of America*. Web. 13 Dec. 2013. Technical Digest (CD).
111. Duvillaret, Lionel, Frédéric Garet, and Jean-Louis Coutaz. “Highly Precise Determination of Optical Constants and Sample Thickness in Terahertz Time-Domain Spectroscopy.” *Applied Optics* 38.2 (1999): 409–415. *Optical Society of America*. Web. 13 Dec. 2013.
112. Holzman, J. F, F. E Vermeulen, and A. Y Elezzabi. “Ultrafast Photoconductive Self-Switching of Subpicosecond Electrical Pulses.” *IEEE Journal of Quantum Electronics* 36.2 (2000): 130–136. *IEEE Xplore*. Web.
113. Jarrahi, M., and T.H. Lee. “High-Power Tunable Terahertz Generation Based on Photoconductive Antenna Arrays.” *Microwave Symposium Digest, 2008 IEEE MTT-S International*. N.p., 2008. 391–394. *IEEE Xplore*. Web.
114. Jin, Yun-Sik, Geun-Ju Kim, and Seok-Gy Jeon. “Terahertz Dielectric Properties of Polymers.” *Journal Of The Korean Physical Society* 49.2 (2006): 513–517. Print.
115. Liang, Min et al. “Terahertz Characterization of Single-Walled Carbon Nanotube and Graphene On-Substrate Thin Films.” *Microwave Theory and Techniques, IEEE Transactions on* 59.10 (2011): 2719 –2725. Web.
116. Mickan, Samuel P et al. “Double Modulated Differential THz-TDS for Thin Film Dielectric Characterization.” *Microelectronics Journal* 33.12 (2002): 1033–1042. *Science Direct*. Web. 27 July 2013.
117. Siegel, P.H. “Terahertz Technology in Biology and Medicine.” *IEEE Transactions on Microwave Theory and Techniques* 52.10 (2004): 2438–2447. *IEEE Xplore*. Web.
118. Tonouchi, Masayoshi. “Cutting-Edge Terahertz Technology.” *Nat Photon* 1.2 (2007): 97–105. Web.
119. Yardimci, N.T. et al. “High-Power Terahertz Generation Using Large-Area Plasmonic Photoconductive Emitters.” *IEEE Transactions on Terahertz Science and Technology* 5.2 (2015): 223–229. *IEEE Xplore*. Web.

7.6 Packaging

120. Lau, John H., C. P. Wong, and J. L. Prince. *Electronic Packaging: Design, Materials, Process, and Reliability*. 1st ed. McGraw-Hill Professional, 1998. Print.
121. Seraphim, Donald P., Ronald. Lasky, and Che-Yu. Li. *Principles of Electronic Packaging*. New York: McGraw-Hill, 1989. Print.

7.7 Techniques and Standards

122. "Dielectric Relaxation in Solids." *Journal of Physics D-Applied Physics* 32.14 (1999): R57–R70. Print.
123. "Energy Criterion in the Interpretation of Dielectric-Relaxation." *Applied Physics A-Materials Science & Processing* 56.5 (1993): 405–408. Print.
124. "Low-Loss Dielectrics." *Journal of Materials Science* 34.13 (1999): 3071–3082. Print.
125. "Stripline Test for Complex Relative Permittivity of Circuit Board Materials to 14GHz - 2-5_2-5-5-5-1.pdf." N.p., n.d. Web. 5 Apr. 2015.
126. Afsar, M. N. et al. "The Measurement of the Properties of Materials." *Proceedings of the IEEE* 74.1 (1986): 183–199. Print.
127. al, L. B. Kong et. *Frequency Dependence of Effective Permittivity of Carbon Nanotube Composites*. Vol. 101. N.p., 2007. Web. 9.
128. and, J. Peyrelasse C Boned. *Automatic Measurement of Complex Permittivity (from 2 MHz to 8 GHz) Using Time Domain Spectroscopy*. Vol. 15. N.p., 1982. Web. 5.
129. Appleby, R., and H. B. Wallace. "Standoff Detection of Weapons and Contraband in the 100 GHz to 1 THz Region." *Antennas and Propagation, IEEE Transactions on* 55.11 (2007): 2944–2956. Print.
130. Balanis, Constantine A. *Advanced Engineering Electromagnetics*. New York: Wiley, 1989. Print.
131. Bell, Robert John. *Introductory Fourier Transform Spectroscopy*. Academic Press, 1972. Print.
132. Cole, Robert H. "Evaluation of Dielectric Behavior by Time Domain Spectroscopy. II. Complex Permittivity." *The Journal of physical chemistry* 79.14 (1975): 1469–1474. Print.

133. Cole, Robert H., Satoru Mashimo, and Paul Winsor. “Evaluation of Dielectric Behavior by Time Domain Spectroscopy. 3. Precision Difference Methods.” *The Journal of physical chemistry* 84.7 (1980): 786–793. Print.
134. Coonrod, John. "Apparent Dielectric Constant of High-frequency PCBs." Microwave Engineering Europe 1 Sept. 2011: 22-26. Print.
135. Coonrod, John. “Methods for Characterizing the Dielectric Constant of Microwave PCB Laminates.” Microwave Journal 54.5 (2011): 132–144. Print.
136. Czichos, Horst, T. Saito, and L. R. Smith. *Springer Handbook of Materials Measurement Methods*. Germany: Springer, 2006. Web.
137. Debye, Peter J. W. *Polar Molecules*. New York: Dover, 1929. Print.
138. Dejardin, Jean-Louis, and Jan Jadzyn. “Determination of the Nonlinear Dielectric Increment in the Cole-Davidson Model.” *The Journal of chemical physics.* 125.11 (2006): 114503. Print.
139. Dexheimer, Susan L. *Terahertz Spectroscopy :principles and Applications*. Vol. 131. Boca Raton: CRC Press, 2008. Print.
140. Dhawale, Mr Ravindra, and Prof Dr D. N. Raut. Evaluating Measurement Capabilities by Gauge R&R Using ANOVA for Reliability. N.p. Print.
141. E, Jr Jones Charlie et al. “The Cooled Germanium Bolometer as a Far Infrared Detector.” *Applied Optics* 4.6 (1965): 683–685. Print.
142. Fan, Wenhui. “Broadband Terahertz Spectroscopy (Invited Paper).” *Chin.Opt.Lett.* 9.11 (2011): 110008. Print.
143. Federici, J. F. et al. “THz Imaging and Sensing for Security Applications - Explosives, Weapons and Drugs.” *Semiconductor Science and Technology* 20.7 (2005): S266–S280. Print.
144. Federici, John et al. “Standoff Sensing of Explosives Using Terahertz Radiation.” *American Laboratory* 38.12 (2006): 28–+. Print.
145. Fellget, P. B. N.p., 1949. Print.
146. Fukunaga, K. et al. “Terahertz Spectral Database for Expanding Applications.” 34th International Conference on Infrared, Millimeter, and Terahertz Waves, 2009. IRMMW-THz 2009. N.p., 2009. 1–3. IEEE Xplore. Web.
147. Fukunaga, K. et al. “Terahertz Spectral Database for Expanding Applications.” *34th International Conference on Infrared, Millimeter, and Terahertz Waves, 2009. IRMMW-THz 2009*. N.p., 2009. 1–3. *IEEE Xplore*. Web.
148. Gaidis, M. C. et al. “A 2.5-THz Receiver Front End for Spaceborne Applications.” *Microwave Theory and Techniques, IEEE Transactions on* 48.4 (2000): 733–739. Print.

149. Gehm, Michael E. et al. “Static Two-Dimensional Aperture Coding for Multimodal, Multiplex Spectroscopy.” *Applied Optics* 45.13 (2006): 2965–2974. *Optical Society of America*. Web. 17 Mar. 2012.
150. Ghodgaonkar, D. K., V. V. Varadan, and V. K. Varadan. “A Free-Space Method for Measurement of Dielectric Constants and Loss Tangents at Microwave Frequencies.” *Instrumentation and Measurement, IEEE Transactions on* 38.3 (1989): 789–793. Print.
151. Gibson, Jerry D. *The Communications Handbook*. Boca Raton, Fla.; London: CRC, 2002. Print.
152. Goldsmith, Paul F., IEEE Microwave Theory, and Techniques Society. *Quasioptical Systems : Gaussian Beam Quasioptical Propagation and Applications*. Piscataway, NJ: IEEE Press, 1998. Print.
153. Grannan, S. M., P. L. Richards, and M. K. Hase. “Numerical Optimization of Bolometric Infrared Detectors Including Optical Loading, Amplifier Noise, and Electrical Nonlinearities.” *International Journal of Infrared and Millimeter Waves* 18.2 (1997): 319–340. Print.
154. Grischkowsky, D., and Soren Keiding. “THz Time-Domain Spectroscopy of High T[sub C] Substrates.” *Applied Physics Letters* 57.10 (1990): 1055–1057. Print.
155. Han, P. Y. et al. “A Direct Comparison between Terahertz Time-Domain Spectroscopy and Far-Infrared Fourier Transform Spectroscopy.” *Journal of Applied Physics* 89.4 (2001): 2357–2359. Print.
156. Harrington, Roger F. *Time-Harmonic Electromagnetic Fields.* New York: McGraw-Hill, 1961. Print.
157. Hattori, Toshiaki. “Classical Theory of Two-Dimensional Time-Domain Terahertz Spectroscopy.” *The Journal of chemical physics* 133.20 (2010): 204503. Print.
158. Hippel, A. R. von. “The Dielectric Relaxation Spectra of Water, Ice, and Aqueous Solutions, and Their Interpretation. I. Critical Survey of the Status-Quo for Water.” *Electrical Insulation, IEEE Transactions on* 23.5 (1988): 801–816. Print.
159. Hippel, A. R. Von. *Dielectrics and Waves*. First. New York: John Wiley & Sons, 1954. Print.
160. Hippel, Arthur R. Von. *Dielectric Materials and Applications; Papers by Twenty-Two Contributors.* [Cambridge; New York: published jointly by the Technology Press of M.I.T. and Wiley, 1954. Print.

161. Horn III, Allen F et al. “The Influence of Test Method, Conductor Profile and Substrate Anisotropy on the Permittivity Values Required for Accurate Modeling of High Frequency Planar Circuits.” Circuit World 38.4 (2012): 219–231. Print.
162. Horowitz, Paul, and Winfield Hill. *The Art of Electronics*. Cambridge University Press, 1980. Print.
163. IPC-TM-650, TM 2.5.5.5C, Stripline Test for Permittivity and Loss Tangent (Dielectric Constant and Dissipation Factor) at X-Band-3/98, Web. 5 Apr. 2015
164. J. Coonrod, J. Horn, A. "Understanding dielectric constant for microwave PCB materials" High Frequency Electronics, vol. 18, no23 (2011).
165. Janezic, M. D. “Nondestructive Relative Permittivity and Loss Tangent Measurements Using a Split-Cylinder Resonator.” University of Colorado at Boulder, 2003. Print.
166. Jin, Yun-Sik, Geun-Ju Kim, and Seok-Gy Jeon. “Terahertz Dielectric Properties of Polymers.” *Journal of the Korean Physical Society* 49.2 (2006): 513–517. Print.
167. Jonscher, A. K. “A New Understanding of the Dielectric-Relaxation of Solids.” *Journal of Materials Science* 16.8 (1981): 2037–2060. Print.
168. Jonscher, A. K. “Relaxation of Polarization.” *Applied Physics A-Materials Science & Processing* 55.2 (1992): 135–138. Print.
169. Jonscher, A. K., and S. Bozdemir. “All Forms of Relaxation Take Place in Fractal Time.” *Electrical Insulation Magazine, IEEE* 11.2 (1995): 30–33. Print.
170. Kaatze, Udo, and Christof Hubner. *Electromagnetic Techniques for Moisture Content Determination of Materials*. Vol. 21. N.p., 2010. Web. 8.
171. Kaatze, Udo. *Techniques for Measuring the Microwave Dielectric Properties of Materials*. Vol. 47. N.p., 2010. Web. 2.
172. Kraus, John Daniel. *Radio Astronomy : 2nd Edition*. Durham: Cygnus-Quasar Books, 2004. Print.
173. Lamb, Willis E. “Theory of a Microwave Spectroscope.” *Physical Review* 70.5-6 (1946): 308. Print.
174. Li, JiuSheng, and JianRui Li. “Dielectric Properties of Silicon in Terahertz Wave Region.” *Microwave and Optical Technology Letters* 50.5 (2008): 1143–1146. Print.
175. Liang, Min et al. “Terahertz Characterization of Single-Walled Carbon Nanotube and Graphene On-Substrate Thin Films.” *Microwave Theory and Techniques, IEEE Transactions on* 59.10 (2011): 2719 –2725. Web.
176. Liu, Hai-Bo et al. “Terahertz Spectroscopy and Imaging for Defense and Security Applications.” *Proceedings of the IEEE* 95.8 (2007): 1514–1527. Print.

177. M, Sun, Apponi AJ, and Ziurys LM. “Fourier Transform Microwave Spectroscopy of HZnCN(X 1Sigma+) and ZnCN(X 2Sigma+).” *The Journal of chemical physics* 130.3 (2009): n. pag. Print.
178. Ma, Ying-Zhong et al. “Femtosecond Spectroscopy of Optical Excitations in Single-Walled Carbon Nanotubes: Evidence for Exciton-Exciton Annihilation.” *Physical Review Letters* 94.15 (2005): 157402. Print.
179. Mahafza, Bassem R. *Radar Systems Analysis and Design Using MATLAB*. 2nd ed. Boca Raton, FL: Chapman & Hall/CRC, 2005. Print.
180. Martens, Luc. *High-Frequency Characterization of Electronic Packaging*. Boston: Kluwer Academic Publishers, 1998. Print.
181. Mittleman, D. M. et al. “Recent Advances in Terahertz Imaging.” *Applied Physics B-Lasers and Optics* 68.6 (1999): 1085–1094. Print.
182. O. P. Thakur, A. K. Singh. “Analysis of Dielectric Relaxation in Water at Microwave Frequency.” *Adv. Studies Theor. Phys.* Vol. 2.no. 13-16 (2008): 637. Print.
183. Palik, Edward D. Handbook of Optical Constants of Solids II. Vol. 2. Boston: Academic Press, 1991. Print.
184. Peden, I. C., and J. C. Rogers. “An Experiment for Determining the VLF Permittivity of Deep Antarctic Ice.” *Geoscience Electronics, IEEE Transactions on* 9.4 (1971): 224–233. Print.
185. Peyghambarian, Nasser, S. W. Koch, and Andre Mysyrowicz. *Introduction to Semiconductor Optics*. Englewood Cliffs, N.J.: Prentice Hall, 1993. Print.
186. Pozar, David M. *Microwave Engineering*. New York; Chichester: Wiley, 1998. Print.
187. Pulliam, R. L. et al. “The Sub-Millimeter and Fourier Transform Microwave Spectrum of HZnCl (X 1Σ+).” *Journal of Molecular Spectroscopy* 257.2 (2009): 128–132. Print.
188. Raju, Gorur G. *Dielectrics in Electric Fields*. New York: Marcel Dekker, 2003. Web.
189. Rekanos, I. T., and T. G. Papadopoulos. “An Auxiliary Differential Equation Method for FDTD Modeling of Wave Propagation in Cole-Cole Dispersive Media.” *Antennas and Propagation, IEEE Transactions on* 58.11 (2010): 3666–3674. Print.
190. Richards, P. L. “Bolometers for Infrared and Millimeter Waves.” *Journal of Applied Physics* 76.1 (1994): 1–24. Print.
191. Rudd, J. V., J. L. Johnson, and D. M. Mittleman. “Quadrupole Radiation from Terahertz Dipole Antennas.” *Optics Letters* 25.20 (2000): 1556–1558. Print.

192. Rudd, J. Van, and Daniel M. Mittleman. “Influence of Substrate-Lens Design in Terahertz Time-Domain Spectroscopy.” *J.Opt.Soc.Am.B* 19.2 (2002): 319–329. Print.
193. Seligman, J.M., E.S. Gillespie, and M. Ryken. “A Quasi-Lumped Planar Balun for Printed Circuit Antennas.” *AP-S International Symposium 1987. 1987*
194. Siegel, P. H. “Terahertz Technology.” *Microwave Theory and Techniques, IEEE Transactions on* 50.3 (2002): 910–928. Print.
195. Simmons, J. H., and Kelly S. Potter. *Optical Materials*. San Diego: Academic Press, 2000. Print.
196. Simon, J. M., and M. C. Simon. “Wollaston Prism as a Beam Splitter in Convergent Light.” *Appl. Opt.* 17.21 (1978): 3352–3353. Web.
197. Sizov, F., and A. Rogalski. “THz Detectors.” *Progress in Quantum Electronics* 34.5 (2010): 278–347. Print.
198. Skolnik, Merrill I. *Introduction to Radar Systems*. 2d ed. New York: McGraw-Hill, 1980. Print.
199. Stuchly, Maria A., and Stanislaw S. Stuchly. “Coaxial Line Reflection Methods for Measuring Dielectric Properties of Biological Substances at Radio and Microwave Frequencies-A Review.” *Instrumentation and Measurement, IEEE Transactions on* 29.3 (1980): 176–183. Print.
200. T.C, Dotson et al. “Cole-Davidson Dynamics of Simple Chain Models.” *J Chem Phys Journal of Chemical Physics* 130.2 (2009): n. pag. Print.
201. Teixeira, F. L. “Time-Domain Finite-Difference and Finite-Element Methods for Maxwell Equations in Complex Media.” *Antennas and Propagation, IEEE Transactions on* 56.8 (2008): 2150–2166. Print.
202. Townes, C. H., and A. L. Schawlow. *Microwave Spectroscopy*. New York: Dover, 1975. Print.
203. US Department of Commerce, NIST. “NIST Atomic Spectra Database.” N.p., n.d. Web. 5 Apr. 2015.
204. Vanexter, M., C. Fattinger, and D. Grischkowsky. “Terahertz Time-Domain Spectroscopy of Water-Vapor.” *Optics Letters* 14.20 (1989): 1128–1130. Print.
205. Wang, F., R. Pottel, and U. Kaatze. “Dielectric Properties of Alkanediol/Water Mixtures.” *The Journal of Physical Chemistry B* 101.6 (1997): 922–929. Print.
206. Wang, Lu et al. “Demetalization of Single-Walled Carbon Nanotube Thin Films with Microwave Irradiation.” *Applied Physics A: Materials Science & Processing* 102.2 (2011): 401–406. Print.
207. Wang, Yung-Cheng, Lih-Horng Shyu, and Chung-Ping Chang. “The Comparison of Environmental Effects on Michelson and Fabry-Perot

Interferometers Utilized for the Displacement Measurement.” *Sensors* 10.4 (2010): 2577–2586. Print.

208. Woolard, Dwight L., William R. Loerop, and Michael Shur. *Terahertz Sensing Technology*. 30, v. 32. River Edge, N.J.: World Scientific, 2003. Print.
209. Engheta, N, and Richard W. Ziolkowski. *Metamaterials: Physics and Engineering Explorations*. Hoboken, N.J: Wiley-Interscience, 2006. Print.
210. Benford, Dominic J., Jacob W. Kooi, and E. Serabyn. "Spectroscopic measurements of optical components around 1 terahertz." *Proc. Ninth Intl. Symp. Space Terahertz Tech*. 1998
211. Reese, Matthew Owen. *Superconducting Hot Electron Bolometers for Terahertz Sensing,* N.p., 2006. Print.
212. Ahmed, O.S.; Swillam, M.A.; Bakr, M.H.; Xun Li, "Efficient Optimization Approach for Accurate Parameter Extraction With Terahertz Time-Domain Spectroscopy," *Lightwave Technology, Journal of* , vol.28, no.11, pp.1685,1692, June1, 2010.
213. Han, P. Y. et al. 'A Direct Comparison Between Terahertz Time-Domain Spectroscopy And Far-Infrared Fourier Transform Spectroscopy'. *J. Appl. Phys.* 89.4 (2001): 2357. Web.
214. Ramo, Simon, John R. Whinnery, and Theodore Van Duzer. *Fields and Waves in Communication Electronics*. 3rd ed. John Wiley & Sons, Inc., 1994

8 APPENDICES

8.1 APPENDIX 1: DIELECTRIC LOSS TANGENT

Propagation constant from the plane wave solution to Maxwell's equations:

$$\gamma = j\omega\sqrt{\mu\varepsilon}\sqrt{(1 - j\sigma/\omega\varepsilon)} = \alpha + j\beta$$

Complex dielectric constant

$$\varepsilon = \varepsilon' - j\varepsilon'' \tag{A1.1}$$

Loss Tangent: $\tan\delta = \varepsilon''/\varepsilon'$ (A1.2)

$$\alpha_D = \frac{\pi\sqrt{\varepsilon_r'}}{\lambda_o}\tan\delta = \frac{\pi\sqrt{\varepsilon_r'}}{c/f}\tan\delta \text{ (see appendix: Polarization, Loss Tangent)} \tag{A1.3a}$$

$$\alpha_D = \frac{\pi f\sqrt{\varepsilon_r'}}{c}\tan\delta, \text{ Np/meter} \tag{A1.3b}$$

$$\alpha_D = \frac{\pi f}{v_p}\tan\delta, \text{ Np/meter} \tag{A1.3c}$$

To covert to dB: 1 Neper = 8.686 dB (or 20/ln10)

$$\log_e x = \log_{10} x \log_e 10 \rightarrow \log_{10} x = \frac{\log_e x}{\log_e 10} \tag{A1.4}$$

$$dB = 20\log_{10} R = 20\frac{\log_e x}{\log_e 10} = \frac{20}{\ln 10}\ln x \tag{A1.5a}$$

$$dB = 8.68\ln x \tag{A1.5b}$$

$$\alpha_{dB/Meter} = 8.68\alpha_D = 8.68\frac{\pi}{c}\sqrt{\varepsilon_r'}\, f \tan\delta \text{ , dB/meter} \quad \text{(A1.6a)}$$

$$\alpha_{dB/M} = \left(\frac{20}{\ln(10)} \times \frac{\pi}{c}\right) f\sqrt{\varepsilon_r'} \tan\delta \quad \text{dB/meter} \quad \text{(A1.6b)}$$

$$\alpha_{dB/M} = \underbrace{\left(\frac{20}{\ln(10)} \times \frac{\pi}{c}\right)}_{91.0214} f\sqrt{\varepsilon_r'} \tan\delta \quad \text{dB/meter} \quad \text{(A1.6c)}$$

$$\alpha_{dB/M} = 91.024 f(GHz)\sqrt{\varepsilon_r'} \tan\delta \quad \text{dB/Meter} \quad \text{(A1.6d)}$$

$$\alpha_{dB/IN} = \alpha_{dB/M} / 39.37 in/m \; f(GHz)\sqrt{\varepsilon_r'} \tan\delta \text{ , dB/in} \quad \text{(A1.6e)}$$

Finally:

$$\alpha_{dB/IN} = 2.31 f(GHz)\sqrt{\varepsilon_r'} \tan\delta \quad \text{dB/in.}$$

and, (A1.6f)

$$\alpha_{nepers/in} = 0.2662\, f(GHz) \tan(\delta) \left(\varepsilon_r'\right)^{1/2} \text{, nepers/in.}$$

Dielectric Material Parameters

For a linear media, the intrinsic constants are:

$$k = \omega\sqrt{\mu\varepsilon} \text{ , (wavenumber)} \quad \text{(A1.7)}$$

$$\eta = \sqrt{\frac{\mu}{\varepsilon}} = \sqrt{\frac{\hat{z}}{\hat{y}}}, \quad \text{(wave impedance)} \quad \text{(A1.8)}$$

$\hat{z} = j\omega\mu$, $\hat{y} = j\omega\varepsilon$, $\sigma = 0$ (lossless conductor)

$$k = \sqrt{-\hat{z}\hat{y}} \,. \quad \text{(A1.9)}$$

For a good dielectric (low loss criteria, $\varepsilon'' << \varepsilon'$) :

$\hat{z} = j\omega\mu$, $\hat{y} = j\omega\varepsilon = \omega\varepsilon'' + j\omega\varepsilon'$, with $\varepsilon' >> \varepsilon''$

$$\hat{k} = \omega\sqrt{\mu\varepsilon'\left(1 - j\frac{\varepsilon''}{\varepsilon'}\right)} \approx \omega\sqrt{\mu\varepsilon'}\left(1 - \frac{j}{2}\frac{\varepsilon''}{\varepsilon'}\right) = \omega\sqrt{\mu\varepsilon'} - j\frac{\omega\varepsilon''}{2}\sqrt{\frac{\mu}{\varepsilon'}} \quad \text{(A1.10)}$$

$$\hat{\eta} \approx \sqrt{\frac{\mu}{\varepsilon'}}\left(1 + j\frac{\varepsilon''}{2\varepsilon'}\right) = \sqrt{\frac{\mu}{\varepsilon'}} + j\frac{\varepsilon''}{2\varepsilon'}\sqrt{\frac{\mu}{\varepsilon'}} \quad \text{(A1.11)}$$

For a good conductor:

$\hat{z} = j\omega\mu$, $\hat{y} = \sigma + j\omega\varepsilon$, with $\sigma >> \omega\varepsilon$

$$k = \sqrt{-j\omega\mu(\sigma - j\omega\varepsilon)} \approx \sqrt{-j\omega\mu\sigma} = \sqrt{\frac{\omega\mu\sigma}{2}}(1 + j) \quad \text{(A1.12)}$$

$$\eta = \sqrt{\frac{j\omega\mu}{\sigma}}. \quad \text{(A1.13)}$$

Optical Quantities

The refractive index of a material, scalar n, is defined as the ratio of the speed of light in a vacuum to the speed of light in that material (phase velocity). That is:

$\tilde{n} = c/(v_p) = \sqrt{(\mu_r\varepsilon_r)} = \sqrt{(\varepsilon_r)}$, (pure dielectric, $\mu_r = 1$) = n -j κ (vector)

For complex ε_r, $\varepsilon'_r = (n^2 - k^2) \rightarrow n^2$ and $\varepsilon''_r = 2n\kappa$, where κ is called the extinction coefficient, and absorption $\alpha = 2\omega\kappa/c = 4\pi f\kappa/c = \pi f \tan(\delta)\,(\varepsilon'_r)^{1/2}/c$

8.2 APPENDIX 2 DIELECTRIC RELAXATION MODELS

[Debye:137, Raju:188, VonHippel:159, 160]

Debye Model: $\hat{\varepsilon} = \varepsilon_\infty + \frac{\Delta\varepsilon}{1 + j\omega\tau}$; $\Delta\varepsilon = \varepsilon_s - \varepsilon_\infty$ (simple relaxation) (A2.1)

Cole-Cole: $\hat{\varepsilon} = \varepsilon_\infty + \frac{\Delta\varepsilon}{1 + (j\omega\tau)^\alpha}$ (A2.2)

Davidson-Cole: $\hat{\varepsilon} = \varepsilon_\infty + \frac{\Delta\varepsilon}{1 + (j\omega\tau)^{1-\alpha}}$ (A2.3)

Havriliak-Negami: $\hat{\varepsilon} = \varepsilon_\infty + \frac{\Delta\varepsilon}{\left(1 + (j\omega\tau)^\alpha\right)^\beta}$ (A2.4)

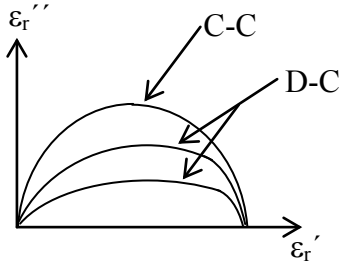

Alternate Forms

Debye: $\frac{\hat{\varepsilon} - \varepsilon_\infty}{\varepsilon_s - \varepsilon_\infty} = \frac{1}{1 + j\omega\tau_D}$, (A2.5)

$\tau_D = \frac{1}{\omega_0}$, relaxation time constant, ω_0 = relaxation frequency.

Cole-Cole: $\frac{\hat{\varepsilon} - \varepsilon_\infty}{\varepsilon_s - \varepsilon_\infty} = \frac{1}{1 + (j\omega\tau_D)^\alpha}$ (A2.6)

Davidson-Cole: $$\frac{\hat{\varepsilon}-\varepsilon_\infty}{\varepsilon_s-\varepsilon_\infty}=\frac{1}{1+\left(j\omega\tau_D\right)^{\alpha-1}} \tag{A2.7}$$

Havriliak-Negami: $$\frac{\hat{\varepsilon}-\varepsilon_\infty}{\varepsilon_s-\varepsilon_\infty}=\frac{1}{\left[1+\left(j\omega\tau_D\right)^{\alpha}\right]^{\beta}} \tag{A2.8}$$

8.2.1 Additional Dispersive Models [Ahmed:212, Zhu:81].

The *Debye Dispersion Model* can be modified to include conductor loss. When the conductor loss term is neglected, it can be used to extract the parameters of high density polyethylene slabs and other plastics.

$$\varepsilon(\omega)=\varepsilon_\infty+\frac{\Delta\varepsilon}{1+(j\omega t)}+\frac{\sigma}{j\varepsilon_0\omega} \tag{A2.9}$$

The *Cole-Cole Model* can be used for a wide variety of materials. When including conductor loss, it is useful for multiwall carbon nanotubes (MWCNTs) and carbon black (CB) materials.

$$\varepsilon(\omega)=\varepsilon_\infty+\frac{\Delta\varepsilon}{1+(j\omega t)^{\alpha}}+\frac{\sigma}{j\varepsilon_0\omega} \tag{A2.10}$$

The *Lorentz Model* is useful for biological materials in the THz regime:

$$\varepsilon=\varepsilon_0+\frac{S\omega_0^2}{(\omega_0^2-\omega^2)-j\Gamma\omega}. \tag{A2.11}$$

ε_0, is the low-frequency permittivity, ω_0 is the center frequency, S is the oscillator strength, and Γ is the oscillation damping factor.

The *Drude model* is shown below. This relation can be used for analysis of dispersion in semiconductor materials.

$$\varepsilon = \varepsilon_\infty - \frac{\omega_p^2}{\omega(\omega + j\Gamma)} \tag{A2.12}$$

Where: ε_∞ is the frequency-independent part of the dielectric constant, Γ is the damping rate, and ω_p^2 is the plasma angular frequency.

When there are several different relaxation processes, the *Havriliak-Negami formula* can be written as:

$$\hat{\varepsilon} = \varepsilon_\infty + \sum_{j=1}^{N} \frac{\Delta\varepsilon}{\left(1 + \left(j\omega\tau_j\right)^{\alpha j}\right)^{\beta j}} + \frac{\sigma}{j\varepsilon_0\omega} \tag{A2.13}$$

Where N is the number of different relation processes and the **σ** term has been added for considering conduction processes.

8.3 APPENDIX 3: DISPERSIVE DIELECTRIC MECHANISMS

[Balanis:130, Potter:195]

Dielectric polarization of a material varies with applied electric field intensity and direction, frequency, temperature, and the state of the material. Dielectric Relaxation is the result of (delayed) movement of dipoles and electric charges due to an applied alternating field and is usually in the frequency range of $10^2 – 10^{10}$ Hz. Relaxation mechanisms are slow compared to electronic or molecular transitions and they occur at frequencies > 10^{12} Hz. These mechanisms result in a variation of dispersion and the refractive index which therefore affects absorption and transmission. The materials characterized in this project are solids that are linear, isotropic, and homogeneous. There are three-four different behavioral regions: Ionic and/or Dipolar Polarization (lowest frequency), Atomic Polarization (mid, microwave frequencies), and Electronic Polarization (THz). The transitions joining these domains may be regions of anomalous dispersion.

Electronic Polarization occurs when an applied electric field displaces electronic density relative to the nucleus. This is a very fast effect, usually observed at THz frequencies above 10^{12} Hz.

Atomic Polarization: Electronic cloud deformation results from the forces included by an applied field, so that a negative and positive space charge region is formed. This is a resonant process happens at microwave frequencies, 10^9-10^{12} Hz.

Relaxation Effects

Dipole Relaxation (Dipolar oriental polarization): Covalent polar molecules with permanent and induced dipoles align to an applied electric field. Without a field present, the dipoles are not aligned due to thermal noise and relaxation. Dipole relaxation is temperature dependent. This is a mid-low frequency effect, 10^6-10^9 Hz.

Ionic Polarization-Relaxation: Ionic bonds and small space charge shifts occur when an electric field is applied. This effect dominates at lower frequencies, $< 10^6$ Hz. Interfacial relaxation can occur when charge carriers are trapped at interfaces, 10^3-10^6 Hz.

8.4 APPENDIX 4: COMPLEX DIELECTRIC CONSTANT USING THE DEBYE MODEL

Complex dielectric constant definition:

$\hat{\varepsilon} = \varepsilon' - j\varepsilon''$, $\Delta\varepsilon = \varepsilon_s - \varepsilon_\infty$, and $\varepsilon_s > \varepsilon_\infty$, simple, linear, homogeneous, isotropic, media.

Debye relation: [Debye:137*]*

$$\frac{\hat{\varepsilon} - \varepsilon_\infty}{\varepsilon_s - \varepsilon_\infty} = \frac{1}{1 + j\omega\tau} = \frac{1 - j\omega\tau}{1 + \omega^2\tau^2} = \frac{1}{1 + \omega^2\tau^2} - j\left(\frac{\omega\tau}{1 + \omega^2\tau^2}\right) \tag{A4.1}$$

$$\hat{\varepsilon} = \varepsilon_\infty + \frac{\varepsilon_s - \varepsilon_\infty}{1 + \omega^2\tau^2} - j\frac{\omega\tau(\varepsilon_s - \varepsilon_\infty)}{1 + \omega^2\tau^2}, \tag{A4.2a}$$

$$\hat{\varepsilon} = \frac{\varepsilon_\infty + \varepsilon_\infty\omega^2\tau^2 + \varepsilon_s - \varepsilon_\infty}{1 + \omega^2\tau^2} - j\frac{\omega\tau(\varepsilon_s - \varepsilon_\infty)}{1 + \omega^2\tau^2}. \tag{A4.2b}$$

Simplifying the real and imaginary parts:

$$\hat{\varepsilon} = \underbrace{\left[\frac{\varepsilon_\infty\omega^2\tau^2 + \varepsilon_s}{1 + \omega^2\tau^2}\right]}_{\varepsilon'} - j\underbrace{\left[\frac{\omega\tau(\varepsilon_s - \varepsilon_\infty)}{1 + \omega^2\tau^2}\right]}_{\varepsilon''}. \tag{A4.2c}$$

So that

$$\varepsilon' = \left[\frac{\varepsilon_\infty\omega^2\tau^2 + \varepsilon_s}{1 + \omega^2\tau^2}\right] \tag{A4.2d}$$

and

$$\varepsilon'' = \left[\frac{\omega\tau(\varepsilon_s - \varepsilon_\infty)}{1 + \omega^2\tau^2}\right]. \tag{A4.2e}$$

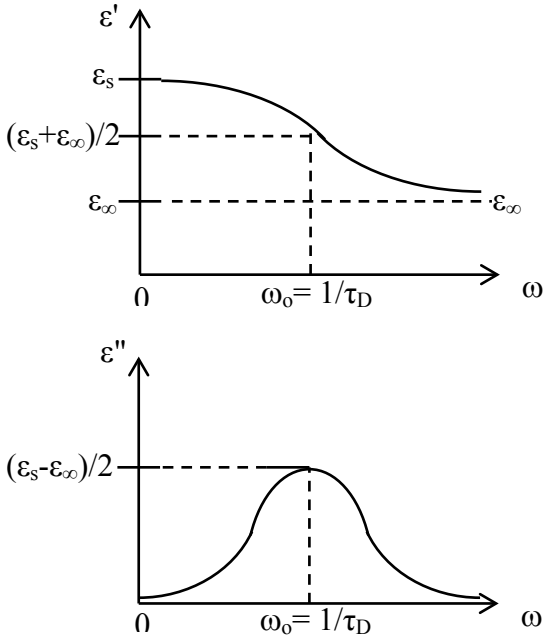

Figure x.yy: Plot of Epsilon vs Frequency

$$\varepsilon''_{\max}\left(\omega_0 = \frac{1}{\tau_D}\right) = \frac{\varepsilon_s - \varepsilon_\infty}{1+1} = \frac{\varepsilon_s - \varepsilon_\infty}{2} \text{ (maximum value)} \tag{A4.3}$$

$$\varepsilon'\left(\omega_0 = \frac{1}{\tau_D}\right) = \frac{\varepsilon_s + \varepsilon_\infty}{2} \tag{A4.4}$$

Dielectric Constant Dispersion Limits - Debye Model	
$\varepsilon'(\omega \to \infty) = \varepsilon_s$	$\varepsilon'(\omega \to 0) = \varepsilon_\infty$
$\varepsilon''(\omega \to 0) = 0$	$\varepsilon''(\omega \to \infty) = 0$
$\varepsilon'\left(\omega_0 = \frac{1}{\tau}\right) = \frac{\varepsilon_s + \varepsilon_\infty}{2}$	$\varepsilon''_{\max}\left(\omega_0 = \frac{1}{\tau}\right) = \frac{\varepsilon_s - \varepsilon_\infty}{2}$
$\hat{\varepsilon}(\omega \to 0) = \varepsilon_s$	$\hat{\varepsilon}(\omega \to \infty) = \varepsilon_\infty$

The dielectric resonance and time constant for ε'' can be found by noting that at the point where there is a maximum, the slope is zero.

$$\varepsilon'' = \frac{\omega\tau(\varepsilon_s - \varepsilon_\infty)}{1+\omega^2\tau^2} = \frac{\omega\left[\tau\overbrace{(\varepsilon_s - \varepsilon_\infty)}^{\Delta\varepsilon}\right]}{1+\omega^2\tau^2} \tag{A4.5a}$$

$$\varepsilon'' = \frac{\omega\tau\Delta\varepsilon}{1+\omega^2\tau^2} = \frac{\tau(\omega\Delta\varepsilon)}{1+\omega^2\tau^2} \tag{A4.5b}$$

$$\frac{d\varepsilon''}{d\omega}\max = \frac{(1+\omega^2\tau^2)(\Delta\varepsilon) - \omega\tau\Delta\varepsilon(2\omega\tau)}{(1+\omega^2\tau^2)^2} = 0 \tag{A4.6}$$

$$= 1+\omega^2\tau^2 - \omega 2\omega\tau^2 = 0\,.$$

$$1 = \omega^2\tau^2 \rightarrow \omega_0 = {}^{1}\!/_{\tau_D}$$

While the resonance frequency appears independent of temperature, this is not the case as the time constant is temperature dependent. The loss tangent will have similar resonances.

A simple relationship is obtained by rearranging terms and dividing the expression for the imaginary and real parts of the dielectric constant.

$$\frac{\varepsilon''}{\varepsilon' - \varepsilon_\infty} = \omega\tau \tag{A4.7}$$

Loss tangent is most generally defined as:

$$\tan\delta = \frac{\omega\varepsilon'' + \sigma}{\omega\varepsilon'} = \frac{1}{Q} \rightarrow \frac{\varepsilon''}{\varepsilon'} \text{ (no conductor loss).} \tag{A4.8}$$

It tracks the behavior of permittivity and attenuation, but the resonant frequencies are shifted slightly.

By following the procedure used previously for the dielectric dipole resonance, and again setting the slope to zero at the maximum value point, similar relationships are found.

$$\frac{d(\tan\delta)}{d(\omega\tau)} = \frac{d(\frac{\varepsilon''}{\varepsilon'})}{d(\omega\tau)} = 0 \tag{A4.9}$$

These yields:

$$\omega^2\tau^2 = \frac{\varepsilon_s}{\varepsilon_\infty}, \quad \omega\tau = \sqrt{\frac{\varepsilon_s}{\varepsilon_\infty}} \rightarrow \omega_0 = \frac{\sqrt{\frac{\varepsilon_s}{\varepsilon_\infty}}}{\tau_{\delta\max}} > 1, \tag{A4.10}$$

This value is then inserted into the previous relationships to find the values of the complex dielectric constant at this frequency.

$$\varepsilon' = \frac{2\varepsilon_s\varepsilon_\infty}{\varepsilon_s + \varepsilon_\infty}, \text{ and} \tag{A4.11}$$

$$\varepsilon''_{\max} = \frac{(\varepsilon_s - \varepsilon_\infty)\sqrt{\varepsilon_s\varepsilon_\infty}}{\varepsilon_s + \varepsilon_\infty} \ . \tag{A4.12}$$

Loss tangent maximum is obtained by taking the ratio of these two expressions:

$$\tan\delta_{\max} = \frac{(\varepsilon_s - \varepsilon_\infty)}{2\sqrt{\varepsilon_s \varepsilon_\infty}} \ . \qquad \text{(A4.13)}$$

Since ε_s *and* ε_∞, ($\varepsilon_s > \varepsilon_\infty$) are typically very close in value, the above expressions will be numerically close to the previous expressions for the components of the dielectric constant.

Maximum Values			
Time Constant at max value	ε'	$\varepsilon''_{\max}$	**Loss Tangent**
$\omega_0\tau = 1$ (max dielectric loss)	$\frac{\varepsilon_s + \varepsilon_\infty}{2}$	$\varepsilon''_{\max} = \frac{(\varepsilon_s - \varepsilon_\infty)}{2}$	$\frac{\varepsilon''}{\varepsilon'} = \frac{\varepsilon_s - \varepsilon_\infty}{\varepsilon_s + \varepsilon_\infty}$
$\omega_0\tau = \sqrt{\frac{\varepsilon_s}{\varepsilon_\infty}} > 1$ (max loss tangent)	$\varepsilon' = \frac{2\varepsilon_s\varepsilon_\infty}{\varepsilon_s + \varepsilon_\infty}$	$\varepsilon''_{\delta\max} = \frac{(\varepsilon_s - \varepsilon_\infty)\sqrt{\varepsilon_s\varepsilon_\infty}}{\varepsilon_s + \varepsilon_\infty}$	$\tan\delta_{\max} = \frac{(\varepsilon_s - \varepsilon_\infty)}{2\sqrt{\varepsilon_s\varepsilon_\infty}}$

There are new modified expressions for the Debye formula and there also are expressions which include anomalous dispersion and resonant absorption, but they were not included in this work.

8.5 APPENDIX 5: POLARIZATION, DIELECTRIC CONSTANT, AND LOSS TANGENT

[Pozar:186, Harrington:156, Balanis:130]

$\vec{D} = \varepsilon_o \vec{E} + \vec{P}$, total displacement field vector (A5.1)

$\vec{E}$, electric field vector

$\vec{P} = \varepsilon_o \chi_e \vec{E}$, electric polarization vector (A5.2)

χ_e = electric susceptibility.

Then $\vec{D} = \varepsilon_o (1 + \chi_e)\vec{E} = \varepsilon \vec{E}$ (A5.3)

where $\varepsilon = \varepsilon_o (1 + \chi_e) = \varepsilon' - j\varepsilon'' = \hat{\varepsilon}$, complex permittivity (A5.4)

ε' = stored energy component

ε'' = dipole vibration damping loss component

$\varepsilon_o = 8.85 \times 10^{-12}$ F/m is the permittivity of free space - vacuum.

$\vec{J} = \sigma \vec{E}$ (Ohm's Law), σ = conductivity (A5.5)

$\hat{\varepsilon} = \varepsilon' - j\varepsilon''$, complex dielectric constant (A5.6)

Constitutive relationships are

$\vec{D} = \varepsilon \vec{E}, \quad \vec{B} = \mu \vec{H}$, and $J=\sigma E$. (A5.7)

The relative dielectric constant/permittivity is related to free space parameters as follows:

$\varepsilon = \varepsilon_o \varepsilon_r$, (A5.8)

$\varepsilon'' = \varepsilon_o \varepsilon_r''$, (A5.9)

$$\varepsilon' = \varepsilon_o \varepsilon_r' \ . \tag{A5.10}$$

And then

$\hat{\varepsilon} = \varepsilon' - j\varepsilon''$ becomes $\hat{\varepsilon}_r = \varepsilon_r' - j\varepsilon_r''$, relative dielectric constant.

Using Maxwell's Equations and Ohm's Law:

$$\vec{\nabla} \times \vec{H} = j\omega\vec{D} + \vec{J} \ \text{(Ampère's Law)} \tag{A5.11a}$$

$$\vec{\nabla} \times \vec{H} = (j\omega\varepsilon + \sigma)\vec{E} \ \text{(Ampère's Law and Ohm's Law)} \tag{A5.11b}$$

$$\vec{\nabla} \times \vec{H} = [j\omega(\varepsilon' - j\varepsilon'') + \sigma]\vec{E} \tag{A5.11c}$$

$$\vec{\nabla} \times \vec{H} = j\omega[\varepsilon' - j(\varepsilon'' + \frac{\sigma}{\omega})]\vec{E} \tag{A5.11d}$$

$$\vec{\nabla} \times \vec{H} = j[\omega\varepsilon' - j(\omega\varepsilon'' + J)]\vec{E} \tag{A5.11e}$$

$$\vec{\nabla} \times \vec{H} = j\omega\varepsilon'[1 - j(\frac{\omega\varepsilon'' + \sigma}{\omega\varepsilon'})]\vec{E} \ \approx j\omega\varepsilon'[1 - j(\frac{\varepsilon''}{\varepsilon'})]\vec{E}\,, \tag{A5.11f}$$

$\sigma = 0$, no conductor loss.

Loss Tangent is then defined as:

$$\tan\delta = \frac{\omega\varepsilon'' + \sigma}{\omega\varepsilon'} = \frac{1}{Q} \rightarrow \frac{\varepsilon''}{\varepsilon'}\text{, for large } \omega\text{, low loss} \tag{A5.12}$$

Where, Q = 1/D = (stored energy) / (dissipated energy-loss).

Then

$$\hat{\varepsilon} = \varepsilon' - j\varepsilon'' = \varepsilon'(1 - \tan\delta)\,. \tag{A5.13}$$

For a pure dielectric material with no conductor loss, $\sigma = 0$. and, $\omega\varepsilon^{"} >> \sigma$.

For a low loss dielectric: $\frac{\varepsilon''}{\varepsilon'} << 1$ or $\varepsilon' >> \varepsilon''$.

Formulation for Plane Waves in Lossy Media

$\nabla \times \vec{E} = j\omega\mu\vec{H}$ (Faraday's Law) (A5.14)

$\nabla \times \vec{H} = (j\omega\varepsilon + \sigma)\vec{E}$ (Ampère's law) (A5.15)

Combining the above, yields the wave equation

$\nabla^2 \vec{E} + \omega^2 \mu\hat{\varepsilon}(1 - j\sigma / \omega\hat{\varepsilon})\vec{E} = 0$ (A5.16)

$\nabla^2 \vec{E} + k^2 \vec{E} = \nabla^2 \vec{E} - \gamma^2 \vec{E} = 0$. (A5.17)

With:

$k^2 = -\gamma^2 = \omega^2 \mu\varepsilon(1 - j\sigma / \omega\varepsilon), \quad \gamma = jk$, (A5.18)

and

$\gamma = jk$ is the propagation constant.

Thus,

$\gamma = j\omega\sqrt{\mu\varepsilon}\sqrt{(1 - j\sigma / \omega\varepsilon)} = \alpha + j\beta$. (A5.19)

Where

α = attenuation constant

$\beta = 2\pi / \lambda$, phase constant (wavenumber).

A plane wave solution is given by:

$E_x(z) = E^+ e^{-\gamma z} + E^- e^{\gamma z}$ (A5.20)

$H_y(z) = (E^+ e^{-\gamma z} - E^- e^{\gamma z}) / \eta$. (A5.21)

The wave is of the form:

$e^{-\gamma z} = e^{-\alpha z} e^{-\beta z} \leftrightarrow e^{-\alpha z} \cos(\omega t - \beta z)$ (A5.22)

$$\gamma = j\hat{k} = j(k' - jk'') = k'' + jk' = \alpha + j\beta \tag{A5.23}$$

Then,

$$\alpha = \mathrm{Re}(\gamma) = k'' = \mathrm{Im}(k) \tag{A5.24}$$

$$\beta = \mathrm{Im}(\gamma) = k' = \mathrm{Re}(k)\,. \tag{A5.25}$$

In a nonmagnetic material:

$\mu = \mu_0, \quad \varepsilon' = \varepsilon_o \varepsilon_r', \quad c = 1/\sqrt{\mu_0 \varepsilon_o}$., μ_r=1.

So,

$$\hat{k} = \omega\sqrt{\mu\varepsilon'}(1 - j\frac{\varepsilon''}{\varepsilon'})^{1/2} \tag{A5.26}$$

$\hat{k} \approx \omega\sqrt{\mu\varepsilon'}(1 - j\frac{\varepsilon''}{2\varepsilon'})$ (Expanded using 1st order approximation)

$$k'' = \alpha = \omega\sqrt{\mu\varepsilon'}\left(\frac{\varepsilon''}{2\varepsilon'}\right) = \left(\omega\sqrt{\mu\varepsilon'}\,\frac{\tan\delta}{2}\right), \quad \tan\delta = \frac{\varepsilon''}{\varepsilon'}. \tag{A5.27a}$$

$$k'' = \alpha = \omega\sqrt{\mu_0\varepsilon_o\varepsilon_r'}\left(\frac{\varepsilon''}{2\varepsilon'}\right) \tag{A5.27b}$$

$$k''_{(1)} = \frac{\omega}{c}\sqrt{\varepsilon_r'}\left(\frac{\varepsilon''}{2\varepsilon'}\right) = \frac{\omega}{2c}\sqrt{\varepsilon_r'}\tan\delta = \frac{\pi f}{c}\sqrt{\varepsilon_r'}\tan\delta\,. \text{ (1st order, attenuation, } \alpha) \tag{A5.28}$$

A second order solution for attenuation can be formulated as per Harrington, [156].

$$k'' \approx \frac{\omega\varepsilon''}{2}\sqrt{\frac{\mu}{\varepsilon'}}\left(1 - \frac{1}{8Q^2}\right), \tag{A5.29}$$

$Q = \dfrac{\omega\varepsilon'}{\sigma + \omega\varepsilon''} \to \dfrac{\varepsilon'}{\varepsilon''}$, (pure dielectric $\sigma \to 0$, Q>>1)

$$k'' = \frac{\omega\varepsilon''}{2}\frac{\sqrt{\mu\varepsilon'}}{\varepsilon'}\left(1-\frac{1}{2}\left(\frac{\varepsilon''}{2\varepsilon'}\right)^2\right) = \frac{\omega}{2}\frac{\sqrt{\mu\varepsilon'}}{1}(\tan\delta)\left(1-\frac{1}{2}\left(\frac{\tan\delta}{2}\right)^2\right) \quad \text{(A5.30)}$$

$$k''_{(2)} = \frac{\omega\varepsilon''}{2\varepsilon'}\frac{\sqrt{\varepsilon'_r}}{c}\left[1-\frac{1}{2}\left(\frac{\varepsilon''}{2\varepsilon'}\right)^2\right] \quad (2^{\text{nd}} \text{ order, attenuation, } \alpha) \quad \text{(A5.31a)}$$

$$k''_{(2)} = \frac{\omega}{2}\tan\delta\frac{\sqrt{\varepsilon'_r}}{c}\left[1-\frac{1}{2}\left(\frac{\tan\delta}{2}\right)^2\right] \quad \text{(A5.31b)}$$

Equivalently,

$$k''_{(2)} = k''_{(1)}\left[1-\frac{1}{2}\left(\frac{\varepsilon''}{2\varepsilon'}\right)^2\right] = k''_{(1)}\left[1-\frac{1}{2}\left(\frac{\tan\delta}{2}\right)^2\right]. \quad \text{(A5.31c)}$$

For low loss material, $\varepsilon' >> \varepsilon''$, and therefore both approximations are almost equivalent. Knowing these relationships, combined with the fact that the dielectric constant (ε') changes slowly with frequency, allows the use of a perturbation technique to iteratively determine values of ε''. Other methods may prove impractical. A combination of quasi-lumped models could also be used [seligman:193]. Some common external forms of error would include material thickness, non-uniformity, interatomic (rotational) absorption and scattering, systematic error, random error, calibration limitations, environmental factors, reflections/radiation, beam focusing characteristics (diameter), and noise. Magnetic effects were neglected (μ_r=1).

Similarly for the phase constant (in a nonmagnetic dielectric)

$$k'_{(1)} = \beta = \omega\sqrt{\mu\varepsilon'} = \omega\sqrt{\mu_0\varepsilon_0\varepsilon'_r} = \frac{\omega}{c}\sqrt{\varepsilon'_r} = 2\pi/\lambda_m \ (1^{\text{st}} \text{ order approximation}) \quad \text{(A5.32)}$$

Again using a 2nd order approximation

$$k'_{(2)} \approx \omega\sqrt{\mu\varepsilon'}\left(1+\frac{1}{8Q^2}\right), \quad Q=\frac{\omega\varepsilon'}{\sigma+\omega\varepsilon''} \rightarrow \frac{\varepsilon'}{\varepsilon''}, \text{ (pure dielectric } \sigma\rightarrow 0, \text{ Q>>1)} \qquad \text{(A5.33a)}$$

This will reduce to:

$$k'_{(2)} = \omega\sqrt{\mu\varepsilon'}\left(1+\frac{1}{2}\left(\frac{\varepsilon''}{2\varepsilon'}\right)^2\right) = \omega\sqrt{\mu\varepsilon'}\left(1+\frac{1}{2}\left(\frac{\tan\delta}{2}\right)^2\right) \qquad \text{(A5.33b)}$$

$$k'_{(2)} = \frac{\omega}{c}\sqrt{\mu\varepsilon'_r}\left(1+\frac{1}{2}\left(\frac{\varepsilon''}{2\varepsilon'}\right)^2\right) = \frac{\omega}{c}\sqrt{\mu\varepsilon'_r}\left(1+\frac{1}{2}\left(\frac{\tan\delta}{2}\right)^2\right) \qquad \text{(A5.33c)}$$

$$k'_{(2)} = k'_{(1)}\left(1+\frac{1}{2}\left(\frac{\varepsilon''}{2\varepsilon'}\right)^2\right) = k'_{(1)}\left(1+\frac{1}{2}\left(\frac{\tan\delta}{2}\right)^2\right) \qquad \text{(A5.33d)}$$

8.6 APPENDIX 6 - KRAMERS KRONIG RELATIONS

Circuit Parameter Relationships:

$$X = \frac{2}{\pi}\int_0^\infty \frac{R(u)}{u^2-\omega^2}du + X_o(\omega) \tag{A6.1}$$

$$R(\omega) = \frac{-2}{\pi}\int_0^\infty \frac{uX(u)}{u^2-\omega^2}du + R_o \tag{A6.2}$$

Material Parameter Relationships:

$$\varepsilon'(\omega) = \varepsilon_o + \frac{2}{\pi}\int_0^\infty \frac{u\varepsilon''(u)}{u^2-\omega^2}du \tag{A6.3}$$

$$\varepsilon''(\omega) = \frac{-2\omega}{\pi}\int_0^\infty \frac{\varepsilon'(u)-\varepsilon_o}{u^2-\omega^2}du \tag{A6.4}$$

[Ramo, Simon, John R. Whinnery, and Theodore Van Duzer. *Fields and Waves in Communication Electronics*. 3rd ed. John Wiley & Sons, Inc., 1994.:214]

8.7 APPENDIX 7: BREWSTER ANGLES FOR VARIOUS MATERIAL INDEXES OF REFRACTION WITH AIR

Brewster Angle for various Index of Refractions with Air					
n(index)	eps(diel)	refl-normal	trans-normal	Brewster(deg)	refl-Brewster
1	1	0	1	45	0
1.1	1.21	0.04761905	0.952380952	47.72631099	0.0090293
1.2	1.44	0.09090909	0.909090909	50.19442891	0.03251814
1.3	1.69	0.13043478	0.869565217	52.43140797	0.06579511
1.4	1.96	0.16666667	0.833333333	54.46232221	0.10518627
1.5	2.25	0.2	0.8	56.30993247	0.14792899
1.6	2.56	0.23076923	0.769230769	57.99461679	0.19202121
1.7	2.89	0.25925926	0.740740741	59.53445508	0.23606109
1.8	3.24	0.28571429	0.714285714	60.9453959	0.27910288
1.9	3.61	0.31034483	0.689655172	62.2414594	0.32053774
2	4	0.33333333	0.666666667	63.43494882	0.36
2.1	4.41	0.35483871	0.64516129	64.53665494	0.39729603
2.2	4.84	0.375	0.625	65.55604522	0.43235129
2.3	5.29	0.39393939	0.606060606	66.50143432	0.46517171
2.4	5.76	0.41176471	0.588235294	67.38013505	0.49581597
2.5	6.25	0.42857143	0.571428571	68.19859051	0.52437574
2.6	6.76	0.44444444	0.555555556	68.96248897	0.55096185
2.7	7.29	0.45945946	0.540540541	69.67686317	0.5756947
2.8	7.84	0.47368421	0.526315789	70.34617594	0.59869782
2.9	8.41	0.48717949	0.512820513	70.97439396	0.62009349
3	9	0.5	0.5	71.56505118	0.64
3.1	9.61	0.51219512	0.487804878	72.1213034	0.65852996
3.2	10.24	0.52380952	0.476190476	72.64597536	0.67578931
3.3	10.89	0.53488372	0.465116279	73.14160123	0.69187697
3.4	11.56	0.54545455	0.454545455	73.61045967	0.70688466
3.5	12.25	0.55555556	0.444444444	74.0546041	0.72089712
3.6	12.96	0.56521739	0.434782609	74.475889	0.73399233
3.7	13.69	0.57446809	0.425531915	74.87599269	0.74624194
3.8	14.44	0.58333333	0.416666667	75.25643716	0.75771162
3.9	15.21	0.59183673	0.408163265	75.61860541	0.76846152
4	16	0.6	0.4	75.96375653	0.77854671
4.1	16.81	0.60784314	0.392156863	76.293039	0.78801757
4.2	17.64	0.61538462	0.384615385	76.60750225	0.79692019
4.3	18.49	0.62264151	0.377358491	76.90810694	0.80529674
4.4	19.36	0.62962963	0.37037037	77.19573393	0.81318584
4.5	20.25	0.63636364	0.363636364	77.47119229	0.82062284
4.6	21.16	0.64285714	0.357142857	77.73522627	0.82764014
4.7	22.09	0.64912281	0.350877193	77.98852161	0.83426744

4.8	23.04	0.65517241	0.344827586	78.23171107	0.840532
4.9	24.01	0.66101695	0.338983051	78.46537935	0.84645886
5	25	0.66666667	0.333333333	78.69006753	0.85207101
1.5167	2.300379	0.20530854	0.794691461	56.60209022	0.15524307
1.3991	1.957481	0.16635405	0.833645951	54.44489378	0.10481327
1.5608	2.436097	0.21899406	0.781005936	57.35243186	0.17467735
www.dorotek.de/cms/upload/pdf/optik/englisch/8Polarizers.pdf					
rs(brewster) = sin^2 (2 αB – 90°) , rp = 0					
Normal as per Pozar:186					

8.8 APPENDIX 8: FRESNEL REFLECTIONS

SECTION 1: FRESNEL EQUATIONS AND SIMPLE FRESNEL REFLECTION

Fresnel equations are the result of meeting a set of boundary conditions, arising from Maxwell's equations, which specify continuity of tangential E and H fields at a purely dielectric interface. No surface currents exist. For simple Fresnel reflections of plane waves, incident on a uniform dielectric slab, the reflection and transmission at the first material interface is the largest contributor. The waves may be normal or oblique to the interface. In this project, all systems were setup for normal incidence. This is easily established. The surface reflection formulae are not directly frequency dependent but the elements are, such as index of refraction. There are higher order internal and compound reflections that depend on the material thickness and therefore are dispersive and frequency dependent. Standing waves are formed between the source and the material under test (MUT) and between the MUT and the detector as well as inside the material. These (Fabry-Perot) type reflections are both frequency and thickness dependent and are usually smaller in amplitude with each pass. Reflections can be dealt with in several ways: 1) numerically averaging (eg, cubic spline, least square); they will appear as small ripples, or alternately calibrating them out. However, those ripples can be used to check material thickness once the dielectric constant is determined. 2) using attenuator/deflectors sheets such as two thin (typical: 1/8 in x 3in dia) quartz slabs placed

at an angle to the signal path on either side of the MUT to break up the standing waves, 3) using a translation stage for the detector and performing sweeps or multiple runs to average out the reflections. For a VNA, another common option is to add a Reference and a reflection receiver and then divide out the reflection.

When materials are irradiated at a glancing angle with a polarized plane wave source, as in guided wave system (VNA, TDS), the reflections may also be a function of the polarization of the E-Field and plus incidence angle. For perpendicular incidence, propagation is polarization invariant except when the material is anisotropic. This effect was shown to occur in some of the materials measured. There is also the Brewster Angle (P-plane only) to consider.

S-Polarization (E field is perpendicular to incident plane)

Reflection and transmission coefficients:

$$r_{\perp} = \frac{n_i \cos(\theta_i) - n_t \cos(\theta_t)}{n_i \cos(\theta_i) + n_t \cos(\theta_t)}$$

$$t_{\perp} = \frac{2n_i \cos(\theta_i)}{n_i \cos(\theta_i) + n_t \cos(\theta_t)}$$

Notation:

$\theta i = \theta_1$, the incident wave in medium 1

$\theta_t = \theta_2$, the transmitted wave into medium 2

P-Polarization (E is parallel to incident plane, reflection and transmission coefficients):

$$r_{\parallel} = \frac{n_i \cos(\theta_t) - n_t \cos(\theta_i)}{n_i \cos(\theta_t) + n_t \cos(\theta_i)}$$

$$t_{\parallel} = \frac{2n_i \cos(\theta_i)}{n_i \cos(\theta_t) + n_t \cos(\theta_i)}$$

And, for both polarizations (Snell):

$$n_i \sin(\theta_i) = n_t \sin(\theta_t)$$

Page 15, bottom formula only

Reflectance (R), Reflected = Power / Incident Power

$$R = r^2$$

Transmittance (T), T = Transmitted Power / Incident Power

$$T = \left[\frac{(n_t \cos(\theta_t))}{(n_i \cos(\theta_i))}\right] t^2$$

For reflection and transmission at normal (perpendicular) incidence, $\theta_i = \theta_t = 0$, and the Fresnel equations reduce to:

$$r = \frac{n_i - n_t}{n_i + n_t} \; ; \; t = \frac{2n_i}{n_i + n_t}, \; T = \left[\frac{(n_t)}{(n_i)}\right] t^2$$

And therefore:

$$R = \left(\frac{n_t - n_i}{n_t + n_i}\right)^2$$

$$T = \frac{4n_t n_i}{(n_t + n_i)^2}$$

And conservation of energy dictates that

R = T = 1

Simple Reflection Fresnel Loss Calculator for Normal Incidence R+T=1						
ε_r	n, index	r, E-reflect	t, E-trans/opt	R, power=r^2	T, power	t, E-trans/ece
1.0000	1.0000	0.0000	1.0000	0.0000	1.0000	1.00000
2.0000	1.4142	0.1716	0.8284	0.0294	0.9706	0.82843
2.2500	1.5000	0.2000	0.8000	0.0400	0.9600	0.80000
2.5000	1.5811	0.2251	0.7749	0.0507	0.9493	0.77485
3.0000	1.7321	0.2679	0.7321	0.0718	0.9282	0.73205
3.5000	1.8708	0.3033	0.6967	0.0920	0.9080	0.69666
4.0000	2.0000	0.3333	0.6667	0.1111	0.8889	0.66667
4.5000	2.1213	0.3592	0.6408	0.1291	0.8709	0.64075
5.0000	2.2361	0.3820	0.6180	0.1459	0.8541	0.61803
5.5000	2.3452	0.4021	0.5979	0.1617	0.8383	0.59787
6.0000	2.4495	0.4202	0.5798	0.1766	0.8234	0.57980
6.5000	2.5495	0.4365	0.5635	0.1906	0.8094	0.56346
7.0000	2.6458	0.4514	0.5486	0.2038	0.7962	0.54858
7.5000	2.7386	0.4650	0.5350	0.2163	0.7837	0.53496
8.0000	2.8284	0.4776	0.5224	0.2281	0.7719	0.52241
8.5000	2.9155	0.4892	0.5108	0.2393	0.7607	0.51079
9.0000	3.0000	0.5000	0.5000	0.2500	0.7500	0.50000
9.5000	3.0822	0.5101	0.4899	0.2602	0.7398	0.48993
10.0000	3.1623	0.5195	0.4805	0.2699	0.7301	0.48051
10.5000	3.2404	0.5283	0.4717	0.2791	0.7209	0.47166
11.0000	3.3166	0.5367	0.4633	0.2880	0.7120	0.46332
11.5000	3.3912	0.5445	0.4555	0.2965	0.7035	0.45546
12.0000	3.4641	0.5520	0.4480	0.3047	0.6953	0.44802
12.5000	3.5355	0.5590	0.4410	0.3125	0.6875	0.44096
13.0000	3.6056	0.5657	0.4343	0.3201	0.6799	0.43426
13.5000	3.6742	0.5721	0.4279	0.3273	0.6727	0.42788
14.0000	3.7417	0.5782	0.4218	0.3343	0.6657	0.42179
14.5000	3.8079	0.5840	0.4160	0.3411	0.6589	0.41598
15.0000	3.8730	0.5896	0.4104	0.3476	0.6524	0.41043

SECTION 2: COMPOUND FRESNEL REFLECTIONS

For this situation, at least three reflections points are considered. There is a reflection at each side of the dielectric slab interface plus the internal reflections between each interface. These higher order reflections are all summed up. The final result is the total reflection loss, which will be higher than the simple case and is a function of angle, thickness (path length), and frequency.

Other factors are the Brewster (polarization) angle (for P-polarization only), and the angle for total internal reflection (when n1>n2), Snell's law, dispersive loss, and standing waves.

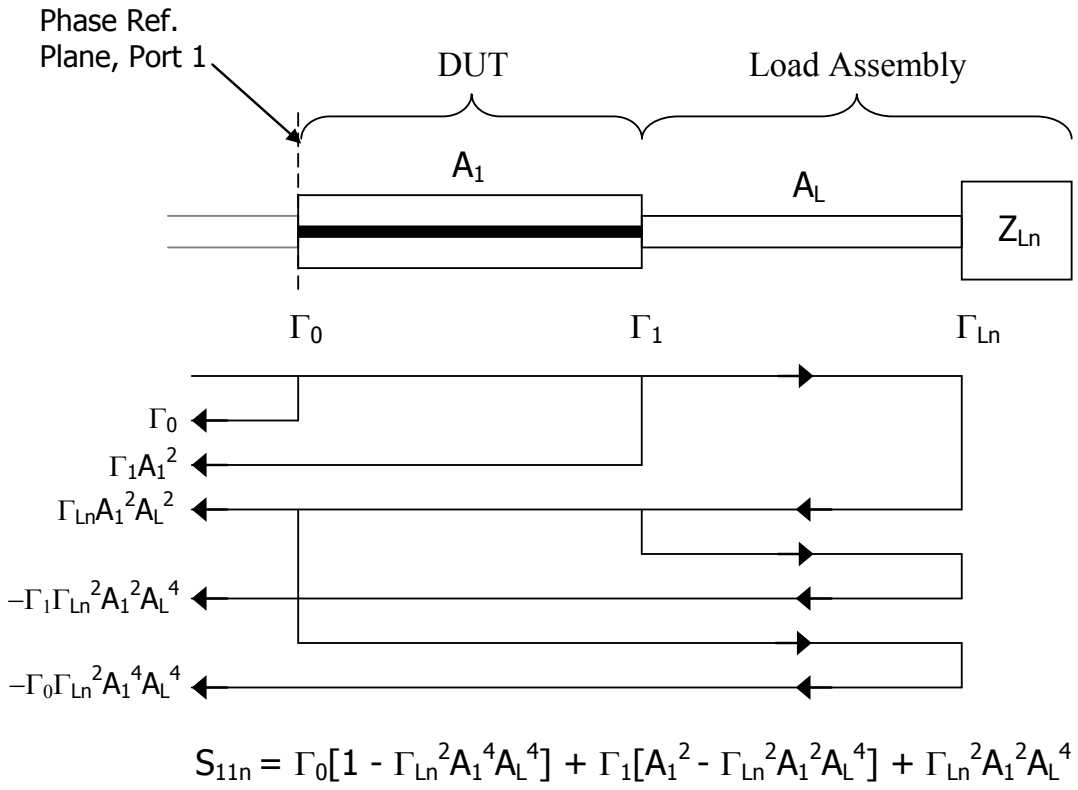

$$S_{11n} = \Gamma_0[1 - \Gamma_{Ln}^2 A_1^4 A_L^4] + \Gamma_1[A_1^2 - \Gamma_{Ln}^2 A_1^2 A_L^4] + \Gamma_{Ln}^2 A_1^2 A_L^4$$

A Method of Multiple Reflections (MMR), Reflection Diagram - the load corresponds to a second medium. *(US Patent 6,472,885. 29 Oct. 2002)*

8.9 APPENDIX 9: DATA SHEETS FOR INFRARED LABS SILICON BOLOMETER AND MICROTECH DETECTOR

INFRARED LABORATORIES
1808 E. 17th Street
Tucson, AZ 85719-6560 USA

Silicon Bolometer Unit#2912

External view of IR Labs Silicon Bolometer Dewar Assembly (Courtesy IR Labs, Tucson, AZ)

BOLOMETER CHARACTERISTICS DATE TESTED: 1/3/2001

UNIT#:	2912	G [μW/K]=	16.23
AREA:	2.5mm diameter diamond	Ro [Mohm]=	14.0
FILTER:	C103	S [V/W]=	2.46E+05
TEMP. [K]:	4.2	NEP[W/Hz1/2]=	1.40E-13

DC LOAD CURVE DATA

R-load [Mohm] Bias Battery
10 22.5

Vbias[V]	Vs[V]	Eb [V]	Ib [μA]
0.0	0.811	0.000	0.000
1.0	1.394	0.583	0.042
2.0	1.937	1.126	0.087
4.0	2.866	2.055	0.195
6.0	3.618	2.807	0.319
8.0	4.240	3.429	0.457
10.0	4.761	3.950	0.605
12.0	5.207	4.396	0.760
14.0	5.591	4.780	0.922
16.0	5.929	5.118	1.088
18.0	6.224	5.413	1.259
20.0	6.488	5.677	1.432
25.0	7.032	6.221	1.878
30.0	7.455	6.644	2.336
35.0	7.788	6.977	2.802
40.0	8.053	7.242	3.276

NOISE: Vn [nV/Hz1/2]

	FREQUENCY		
BIAS [μA]	20 Hz	80 Hz	200 Hz
2.25	44.8	34.3	33.6

FREQUENCY RESPONSE

f [Hz]	OUTPUT [% DC]
40	100
100	100
200	100
300	100
400	100
500	94

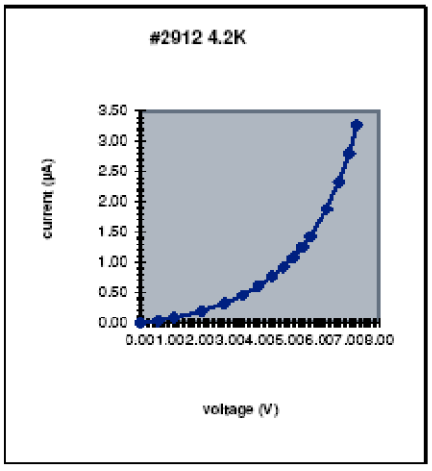

Performance Data for IR Labs Silicon Bolometer

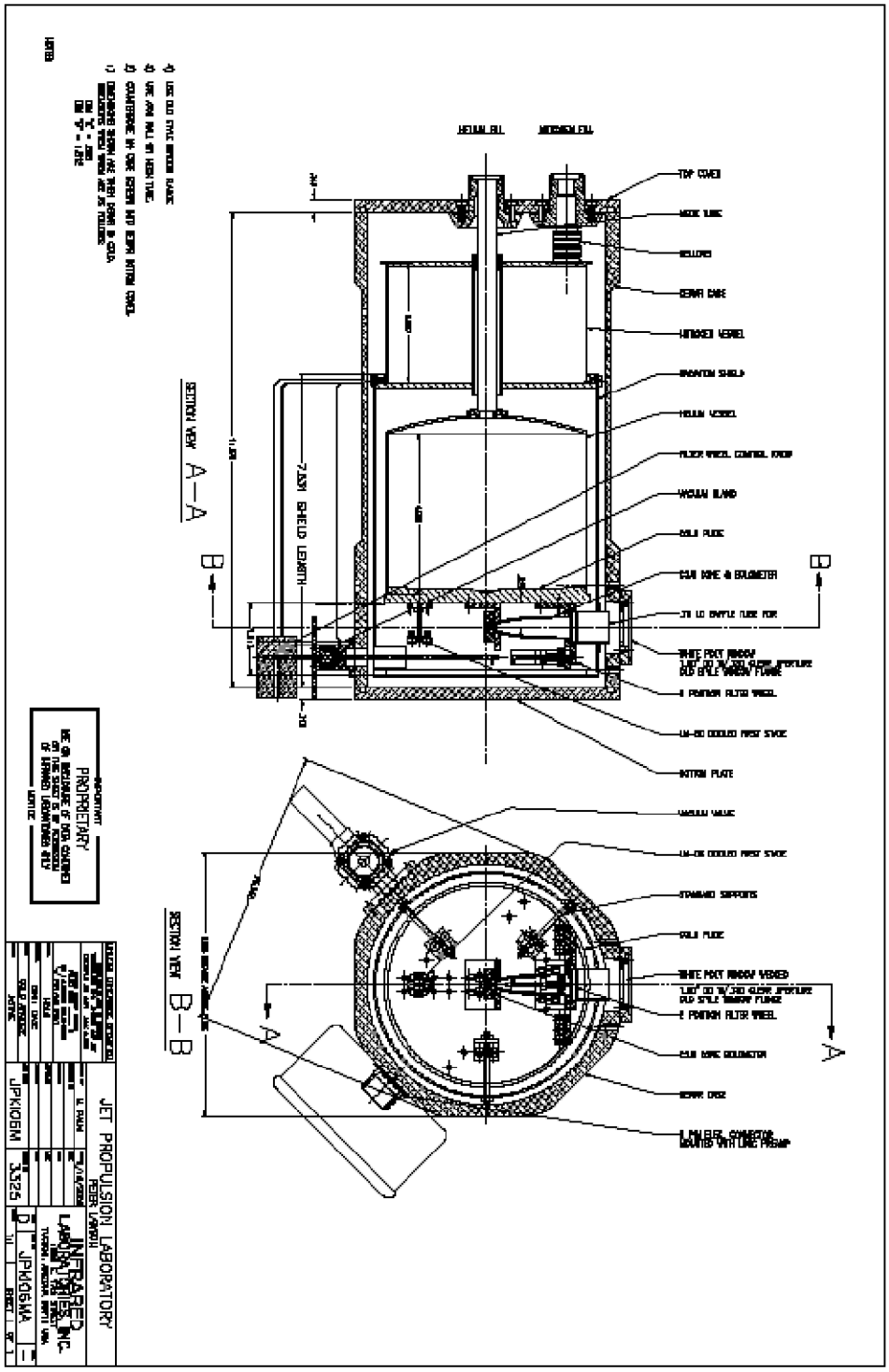

Diagram: IR Labs Silicon Bolometer Layout

Golay Cell – Manual (SN: 160724)

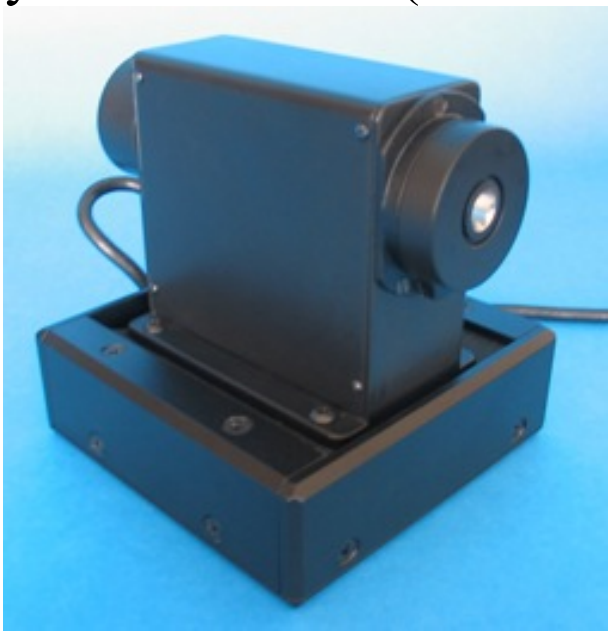

www.mtinstruments.com

Technical Description

This detector was invented by M.J.E. Golay in 1947. It quickly came to wide use because it operates at room temperature and is sensitive, with good efficiency, to a wide range of wavelengths.

The Golay Cell detector is a sensitive photo-acoustic device coupled to the input beam via a 6mm diameter polyethylene window. It is designed to respond to signals at wavelengths in the ranger from 20μm up to a few millimeters. Alternative window materials can also be used to extend the wavelength range to approximately 1μm.

The unit contains a sealed, gas-filled absorbing chamber, and optical microphone section, and a preamplifier. A sketch showing the optical arrangement is given in **Figure 2**. The basic

component parts of the detector are numbered in figure 2 – the following notes on basic operation refer to this numbering system.

Figure 2

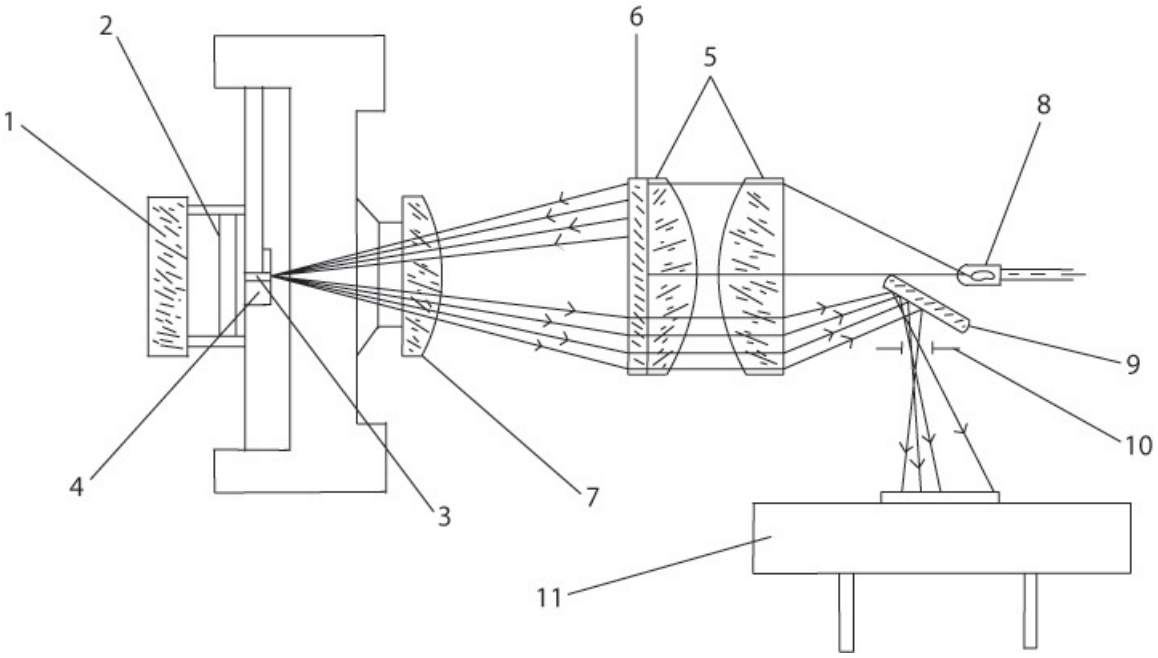

Modulated signal incident upon the window of the device **(1)** passes onto a semi-transparent film **(2)** located in the center of a sealed chamber. The energy absorbed in the film serves to heat the gas in the chamber, causing the pressure to rise. The pressure changes distort the shape of the membrane forming the wall of the chamber **(4)**.

A light emitting diode (LED) **(8)** emits through re-focussing optics **(5)** and onto the mirrored back surface of the chamber containing the absorbing membrane. This radiation is reflected back through the lower half of the optics via a grating **(10)**; as shown in the diagram and re-focussed onto a photodiode **(11)**. The degree of illumination of the photodiode by radiation from the LED is a function of the shape of the front chamber.

A preamplification circuit is included in the device. This is based on an operational amplifier and double FET circuit which converts the output from the photodiode into a useful AC voltage output.

Product Description and Specifications

Golay Cell is an opto-acoustic detector designed for operation in the spectral range 0.2-20 THz

It is equipped with a 6 mm diameter polyethylene input window that provides for high transparency at frequencies up to 20 THz.

Golay Cell includes a build-in preamplifier.

Operation of a Golay Cell requires a three-unit power supply delivering the following: +15 V, - 15 V and 32 mA. Such a power supply is also available as an option

Performance of Golay Cells is detrimentally affected by mechanical vibrations. In order to reduce the impact of mechanical vibrations, Golay Cells can be mounted on vibration-isolation bases.

Technical Specifications:

Parameter	**Value**
Responsivity, V/W	see calibration data on the next page
Sensitivity, W/Hz$^{1/2}$	~10^{-10}
Maximum modulation frequency	50 Hz
Dynamic range	3 μW- 112.5 μW
Rise time, ms	25
Maximum output voltage, V	1.5
Input window diameter, mm	6
Dimensions, mm	135x115x120

Operating Conditions:

Parameter	**Value**
Temperature, ^{o}C	+15 to +25
Pressure, Pa	$8.4x10^4$ to 10.7×10^4
Humidity, %	45 - 80

Calibration Data for Golay Cell SN160724

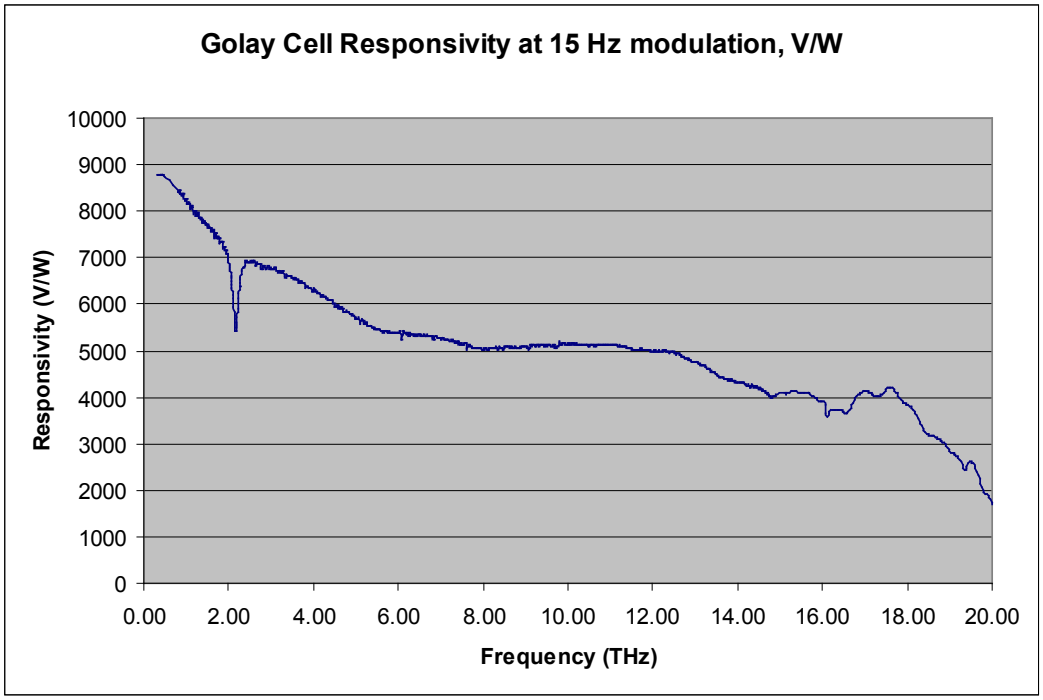

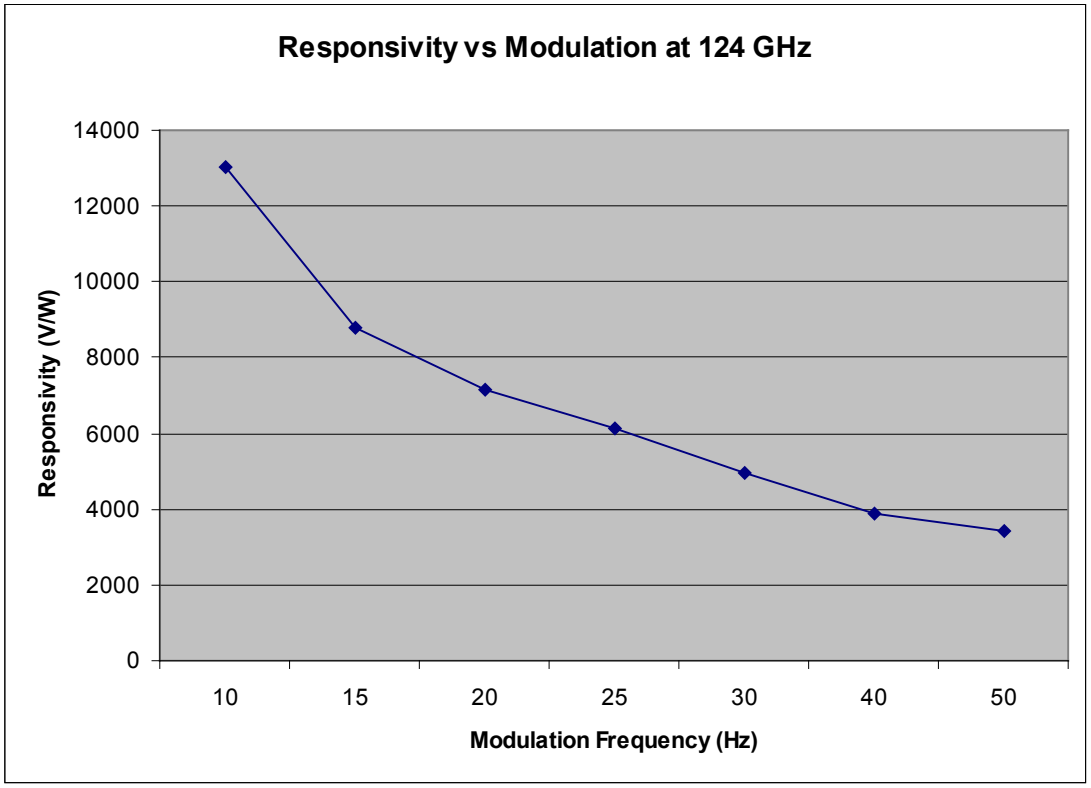

8.10 APPENDIX 10: VNA EXTRACTION FLOW PROCESS - FOR COMPUTING ε_r' AND ε_r" FROM S_{21}

STEP 1:Compute ε_r' not accounting for reflections (internal & external) (1st Iteration)

- Normalize S21 data and calculate the change in the number of zero crossings, N, of the phase shift due to the addition of the sample
- Calculate the increase in total phase shift in S_{21} ($\Delta\Phi$) due to the addition of the sample
- Calculate the number of wavelengths in the sample (appendix)
- Calculate $V_p = f\lambda_m$
- Calculate ε_r' based on the Vp and number of wavelengths in the
- $\varepsilon_r' \approx \varepsilon_r = c^2 / v_p^2 = (\tilde{n})^2$

STEP 2:Compute ε_r'' not accounting for reflections (internal & external)

- Relate the attenuation constant α to $\tan\delta$ (Appendix for derivation)
- $\alpha_D = \dfrac{\pi f\sqrt{\varepsilon_r'}}{c}\tan\delta$, and $\alpha\ (dB/in) = S_{21}(dB)\,normalized / t\,(in)$
- Calculated α, ε_r' from normalized S21 measurement results and material thickness. (note Nepers and inches)
- Knowing α and ε_r' (from Step 1), calculate ε_r'' from direct computation

$$\varepsilon_r'' = \frac{S_{21}(dB)\,normalized\sqrt{\varepsilon_r'}}{2.31t\ freq(GHz)}, \quad t = \text{sample thickness, (appendix)}$$

STEP 3: Compute ε_r'' accounting for reflections (internal & external)

- Determine the equations for the Transmission & Reflection Coefficients of the material by constructing a material transmission-reflection diagram (Fresnel/external plus Fabry-Perot/internal)
- Use equation for the total Transmitted wave, taking into account 8 different reflections (5 total terms)
- Relate the Log Magnitude of the total transmitted wave to the Normalized S21 log magnitude data
- Write out the equation for the total amplitude of the transmitted wave, taking into account 8 different reflections (5 total terms, appendix)
- Plot the Normalized S21 log magnitude data and graphically solve for α. Set the value for the phase constant $\beta = 2\pi/\lambda_m = 2\pi*f*(\sqrt{\varepsilon_r'}) / c$
- Use direct equation (see Hartley, Appendix) to relate α to ε_r'' to compute ε_r''

Future: Alternate method to check ε_r' accounting for reflections (internal & external)

- Write out the equation for the sum of the real parts and the equation for the sum of the imaginary parts for the total Transmitted wave coefficient
- Rewrite the equation for the phase of the total transmitted wave based on the real and imaginary parts
- Relate the normalized phase data S_{21} phase to the phase of the total transmitted wave
- Plot the Normalized S_{21} phase data and graphically solve for β (similar to least square). Set the value for the attenuation constant α to the value obtained previously.
- Again use the equation $\beta = 2\pi/\lambda_m = 2\pi*f*\varepsilon_r'^{\wedge}0.5 / c$ to compute the value for ε_r' (appendix)
- Repeat STEP 3 and STEP 4 as many times as desired to further converge on $\varepsilon_r'$and ε_r''

This is not required in most cases, as the delay through the material is not masked by

8.11 APPENDIX 11: - PERMITTIVITY AND LOSS TANGENT VNA COMPUTATION

(this section goes to previous flow Charts)

VNA Extraction Process Summary

* Determine ε_r' using differential phase scheme with a combination graphical and algebraic techniques by determining the time difference passing thru the sample compared to air. This technique uses magnitude and phase of S_{21} rather than relying on all S-parameters as required in NRW technique. This eliminated dependence on positional calibration, which is difficult on a free space setup, but it means that reflections must be accounted for manually.

- Use these results to obtain ε_r" from V_p and loss tangent relationships
- Then iterate between the two and apply 4 pass Fresnel corrections

ε_r', ε_r'' Equations, Without Taking Into Account Reflections (1st iteration)

This computation uses a differential phase technique combined with a graphical approach to determine the number of zero crossings. When the sample is inserted in the test path, the phase change is noted and then number of wavelengths in the material is calculated

from the s-parameter zero crossings. This is determined by averaging the phase differences over frequency and then calculating the remainder term. Then wavelength in the material is calculated using a relation between thickness, and number of wavelengths. This is then used to calculate phase velocity and ε_r'.

ε_r': For low loss materials, the real part of ε_r' is approximately equal to the total dielectric constant, ε_r, since $\varepsilon_r' >> \varepsilon_r''$. The computation of ε_r is performed by computing the change in the phase shift of S_{21} when the sample is placed between the two test ports when compared to air. The time delay ΔT, (related to $\Delta\phi = \Delta$ phase of S_{21}) is determined by knowing the number of wavelengths inside the sample and this can then be used to get absolute phase change. This result gives the phase velocity, $Vp=c/n=\omega/k$. Then ε_r can be calculated, since $n = c/v_p = (\mu r\ \varepsilon_r^{1/2}) = (\varepsilon_r^{1/2})$ (non-magnetic). There will be a correctable error due to Fabry-Perot reflections within the sample, and the Fresnel reflections at the interface. The amount of reflection loss also depends on the incidence angle (90 degrees in this project) and the value of the index of refraction compared to air.

Note: The S_{21} (phase), i.e., angle(S_{21}) and its slope are obtained from the THz VNA data for the number data points, *(b)*, across the swept frequency range, with and without the sample present. The difference between these two data sets is the normalized value of the phase of S_{21}.

S_{21} phase normalized = S_{21} phase (with sample present) – S_{21} phase (without sample present)

The slope of S_{21} phase with respect to frequency is negative. This because as frequency/time increases, wavelength decreases and delay gets larger, and the wavelength gets smaller, so the slope is negative in order to give positive delay. Therefore, the actual phase shift is 360 – S_{21} (phase) normalized. Then the total phase shift ($\Delta\Phi$) due to the addition of the sample will be this phase shift plus a multiple (N) of 360 degrees, depending on the number of zero crossings. Thus:

$\Delta\Phi$ = (360 – S_{21} phase normalized) + 360*N

The number of zero crossings, N_k, is the average slope of the phase shift divided by the frequency.

$$Average\left(\frac{dtheta}{dfreq}\right) = \left[\sum_{k=1}^{b-1}\left(\frac{theta_{k+1} - theta_k}{freq_{k+1} - freq_k}\right)\right] \div (b-1)$$

$$N_k = Round\left[\left\{\left(freq_k \times -Average\left(\frac{dtheta}{dfreq}\right) \div 360\right) - \left(\left(360 - S_{21,k}\ phase\,normalized\right) \div 360\right)\right\}, 0\right]$$

where k is the kth frequency point, theta = S_{21} (phase) normalized, b is the total number of points, and the ", 0]" denotes rounding the value to an integer or to the 0^{th} decimal place. Since Round [value, 0] = Int [value + 0.5], the equation can also be written as:

$$N_k = Int\left[\left(freq_k \times -Average\left(\frac{dtheta}{dfreq}\right) \div 360\right) - \left(\left(360 - S_{21,k}\ phase\,normalized\right) \div 360\right) + 0.5\right]$$

Before the addition of the material sample, the phase shift Φ_{fs} in free space the same thickness (t) of the material sample is:

Φ_{fs} = (# of wavelengths in free space) * 360

$\Phi_{fs} = (t / \lambda_{fs}) * 360$

$\Phi_{fs} = (t * f / c) * 360$

After the addition of the material sample, the phase in the sample Φ_m (in the distance t) is:

$\Phi_m = \Phi_{fs} + \Delta\Phi$

Where $\Delta\Phi$ (as defined before) is the difference between the phase when the material is present and when it is not present. The wavelength (λ_m) inside the material is:

$\lambda_m = t / [\Phi_m / 360]$

And the phase velocity, v_p inside the sample (at the kth frequency point) is:

$\mathbf{v_p = \omega/k = 2\pi f /*(2\pi/ \lambda_m) = f/ \lambda_m}$

and ε_r' is:

$\mathbf{\varepsilon_r' \approx \hat{\varepsilon_r} = c^2 / v_p^2 = (\tilde{n})^2}$

Where, $\tilde{n} = n + i\kappa$, is the complex index of refraction and κ corresponds to absorption (extinction) coefficient. More generally

$\mathbf{\hat{\varepsilon_r} = \varepsilon_r' - j\, \varepsilon_r''} = \tilde{n}^2 = (n + i\kappa)^2$

Hence,

$\mathbf{\varepsilon_r'} = n^2 - \kappa^2$, and $\mathbf{\varepsilon_r''} = 2 n \kappa$.

ε_r'': The calculation of ε_r'' is based a simple units conversion procedure described in the Appendix [*Hartley:62]*. The end result is:

$$\alpha\ (dB/in) = 2.31 freq(GHz)\sqrt{\varepsilon_r^{'}}\tan\delta$$

This comes from the relation:

$$\alpha_D = \frac{\pi f\sqrt{\varepsilon_r'}}{c}\tan\delta\ ,\ \text{Np/meter},\ \text{with}\ \tan\delta = \varepsilon''/\varepsilon' \qquad \text{(A1.3b)}$$

$$\alpha_{dB/Meter} = 8.68\alpha_D = 8.68\frac{\pi}{c}\sqrt{\varepsilon_r'}f\tan\delta\ ,\ \text{dB/meter} \qquad \text{(A1.6a)}$$

This gets converted to dB/inch and frequency in GHz. The attenuation constant,

$\alpha\ (dB/in) = S_{21}(dB)\,normalized/t\,(in)$ and thus,

$$\varepsilon_r^{"} = \frac{S_{21}(dB)\,normalized\sqrt{\varepsilon_r^{'}}}{2.31 t\ freq(GHz)}, \quad t = \text{sample thickness}$$

The error in the calculation of ε_r" is directly dependent on the value of both S_{21} (dB) and S_{21} (phase), since sqrt (ε_r') ~ (1/ v_p)~ (1 / λ) ~ # wavelengths in the sample ~ $\Delta\Phi$ ~ S_{21} (phase). The amplitude error in S_{21} (dB) can be partially masked by Fresnel and Fabry-Perot reflections in the S_{21} (phase) terms.

Calculating ε_r' & ε_r'' (taking reflections into account – 2nd iteration)

ε_r'': The computation of ε_r'' is first performed in the 2nd iteration (as opposed to ε_r' in the 1st iteration). It takes into account the primary transmission and four different secondary transmissions/reflections (due to Fresnel reflections). The primary transmission passes through the sample one time before exiting the material. The

secondary transmission reflects off the air-material interface of the sample two times before exiting the material and thus passes through the material a total of 3 times. The third transmission reflects off the air-material interface four times before exiting the material and passes through the material a total of 5 times and so forth. The calculated value of ε_r' from the 1st iteration is used as a starting point in this calculation.

The total wave amplitude through the material is the sum of the primary transmission through the material plus secondary transmission passes: (four passes chosen here, 5 in total). (See figure below)

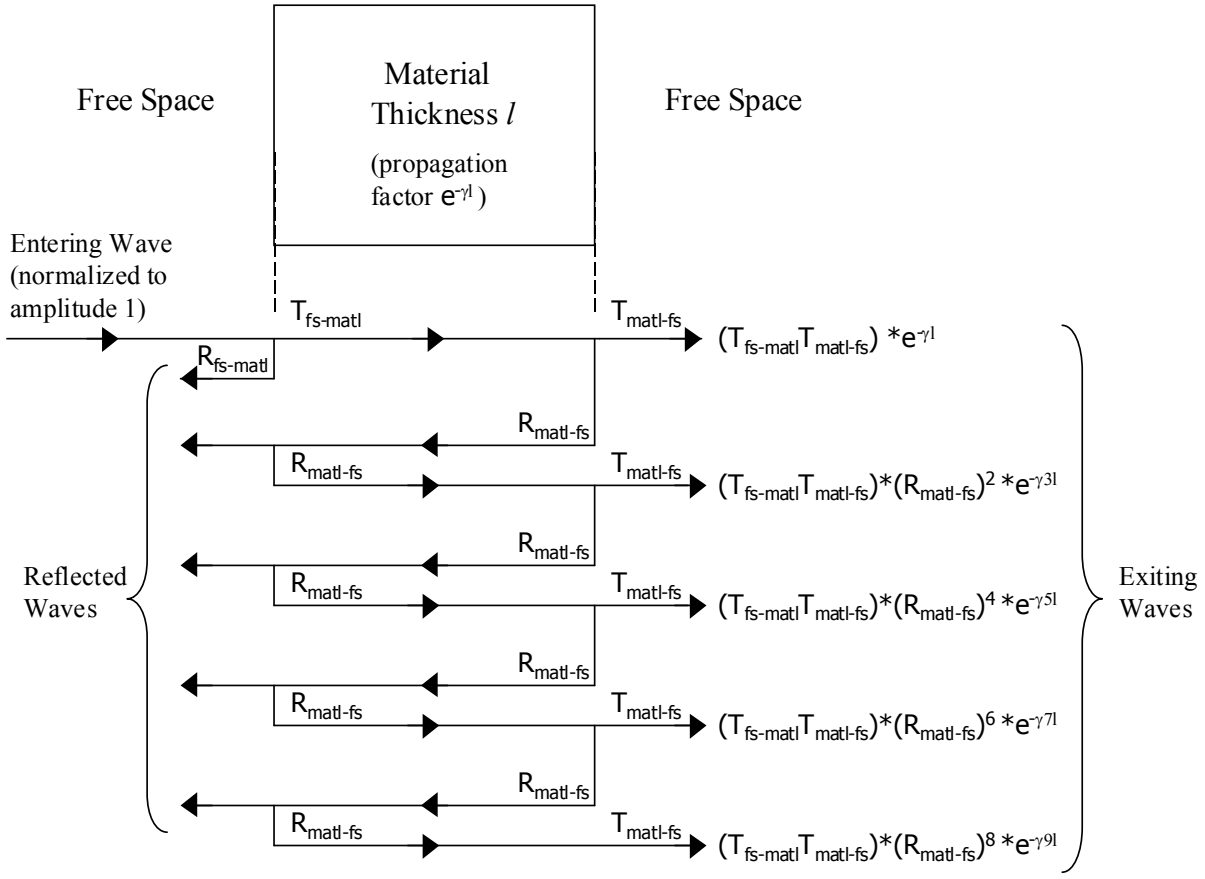

Material Transmission-Reflection Diagram

$$A_1 e^{-\gamma l} + A_2 e^{-\gamma 3l} + A_3 e^{-\gamma 5l} + A_4 e^{-\gamma 7l} + A_5 e^{-\gamma 9l} = C = Ae^{-ql}$$

T and R are reflection coefficients

$\gamma = \alpha + j\beta$, propagation constant.

α = attenuation constant (due to dielectric loss of the material)

β = phase constant = $2\pi / \lambda = 2\pi * \text{freq} * \sqrt{(\varepsilon_r')} / c$ (equation for β)

(*the value of ε_r' used in computing β is from the first iteration*)

$l = t$ = the thickness of the material sample

C = amplitude of the exiting wave (taking into account five components). C is a complex number.

A_1, A_2, A_3, A_4, and A_5 are the wave components which are dependent on the Fresnel Transmission and Reflection Equations for normal incidence on a dielectric.

The reflection equations passing through the sample, thickness (l, or t) are as follows:

$T = 2n_2/(n_1+n_2)$ where n = sqrt (mag(ε_r)),

$$T_{fs-matl} = \frac{2*1}{1+n} = \frac{2}{1+\sqrt{\varepsilon_r}}$$

$$T_{matl-fs} = \frac{2*n}{n+1} = \frac{2\sqrt{\varepsilon_r}}{\sqrt{\varepsilon_r}+1}$$

$$R_{matl-fs} = \frac{n-1}{n+1} = \frac{\sqrt{\varepsilon_r}-1}{\sqrt{\varepsilon_r}+1}$$

$$R_{fs-matl} = \frac{1-n}{1+n} = \frac{1-\sqrt{\varepsilon_r}}{1+\sqrt{\varepsilon_r}}$$

The variable n, in these equations, represents the (index of refraction) dielectric constant of air. The value of ε_r used is taken from the first iteration approximation.

The coefficients A_1, A_2, A_3, A_4, and A_5 of the transmitted waves through the material (due to Fresnel Transmission and Reflections) are as follows (See reflection diagram):

$A_1 = (T_{fs\text{-}matl} * T_{matl\text{-}fs})$

$A_2 = (T_{fs\text{-}matl} * T_{matl\text{-}fs}) * (R_{matl\text{-}fs})^2$

$A_3 = (T_{fs\text{-}matl} * T_{matl\text{-}fs}) * (R_{matl\text{-}fs})^4$

$A_4 = (T_{fs\text{-}matl} * T_{matl\text{-}fs}) * (R_{matl\text{-}fs})^6$

$A_5 = (T_{fs\text{-}matl} * T_{matl\text{-}fs}) * (R_{matl\text{-}fs})^8$

To solve for ε_r'', one must first solve for α in the total equation in previous. $\alpha + j\beta$ can be substituted for γ and the terms can be expressed in sines and cosines. The solution process was done graphically by trial and error directly on the data plots. However the equations below describe the computational process.

$$A_1 e^{-\alpha l}\cos(\beta l) + A_2 e^{-\alpha 3l}\cos(\beta 3l) + A_3 e^{-\alpha 5l}\cos(\beta 5l) + A_4 e^{-\alpha 7l}\cos(\beta 7l) + A_5 e^{-\alpha 9l}\cos(\beta 9l)$$

$$-jA_1e^{-\alpha l}\sin(\beta l)-jA_2e^{-\alpha 3l}\sin(\beta 3l)-jA_3e^{-\alpha 5l}\sin(\beta 5l)-jA_4e^{-\alpha 7l}\sin(\beta 7l)-jA_5e^{-\alpha 9l}\sin(\beta 9l)=C$$

Again, C is the complex amplitude of the exiting wave. 20 log of the magnitude of C in dB is the same as the normalized S21 log magnitude in dB from the normalized data sets:

20 Log {Mag(C)} (dB) = {S21 (dB)} normalized

Therefore,

$$20\log\{mag[(A_1e^{-\alpha l}\cos(\beta l)+A_2e^{-\alpha 3l}\cos(\beta 3l)+A_3e^{-\alpha 5l}\cos(\beta 5l)+A_4e^{-\alpha 7l}\cos(\beta 7l)+A_5e^{-\alpha 9l}\cos(\beta 9l))$$
$$-j(A_1e^{-\alpha l}\sin(\beta l)+A_2e^{-\alpha 3l}\sin(\beta 3l)+A_3e^{-\alpha 5l}\sin(\beta 5l)+A_4e^{-\alpha 7l}\sin(\beta 7l)+A_5e^{-\alpha 9l}\sin(\beta 9l))]\}=S21\,(dB)$$

α can be obtained graphically using the above equation. Rather than using a solver, the user is prompted to find the starting value of α from the basic equations in 1st Iteration, and fine tuning it by trial and error. While this method worked, it is not as substantial technique as using a totally computational approach, such as NRW, but they are mostly iterative as well. There is also the ½ wavelength cancellation issue to check for. Once α is obtained, Tan δ is computed from α using by modifying the direct equation used previously. ε_r'' is the product of Tan δ and ε_r'.

$$Tan\,\delta=\varepsilon r''/\varepsilon r'=\alpha\,(dB/m)\Big/\left[91.024\cdot freq(GHz)\cdot\sqrt{\varepsilon_r'}\right]$$

And α (dB/m) = 8.686 α (Np/m). Then,

$$Tan\,\delta=8.686\cdot\alpha\,(Np/m)\Big/\left[91.024\cdot freq(GHz)\cdot\sqrt{\varepsilon_r'}\right]$$

And also by definition,

$$\varepsilon_r''=Tan\,\delta\cdot\varepsilon_r'.$$

Taking 5 terms into account was arbitrary, after the first two terms, most error is negligible.

Future: Verifying ε_r' by an alternate method

ε_r' and β can now be solved for in a 2nd iteration in a similar way as solving for ε_r'' and α, which takes into account reflections. The calculated value for ε_r'' and α from the 2nd iteration are used as the starting point. Note that ε_r' depends primarily on the thickness of the sample and reflections only have a slight effect on this value.

First, the phase of the wave exiting the material must be computed, taking into account multiple components as before where:

$$A_1 e^{-\gamma l} + A_2 e^{-\gamma 3l} + A_3 e^{-\gamma 5l} + A_4 e^{-\gamma 7l} + A_5 e^{-\gamma 9l} = C \text{ (complex wave)}$$

The real and imaginary parts are:

$$Sum\ \mathrm{Re} = A_1 e^{-\alpha l}\cos(\beta l) + A_2 e^{-\alpha 3l}\cos(\beta 3l) + A_3 e^{-\alpha 5l}\cos(\beta 5l) + A_4 e^{-\alpha 7l}\cos(\beta 7l) + A_5 e^{-\alpha 9l}\cos(\beta 9l)$$
$$Sum\ \mathrm{Im} = -A_1 e^{-\alpha l}\sin(\beta l) - A_2 e^{-\alpha 3l}\sin(\beta 3l) - A_3 e^{-\alpha 5l}\sin(\beta 5l) - A_4 e^{-\alpha 7l}\sin(\beta 7l) - A_5 e^{-\alpha 9l}\sin(\beta 9l)$$

and

$$Sum\ \mathrm{Re} + jSum\ \mathrm{Im} = C\,.$$

The computed phase of the wave exiting the material sample is:

$$Phase(C) = \left(\frac{180}{\pi}\right)\tan^{-1}\left(\frac{Sum\,\mathrm{Im}}{Sum\,\mathrm{Re}}\right)$$

Where, $\tan^{-1}$ is in radians (from 0 to 2π). It is critical that the correct quadrant is selected for the value of $\tan^{-1}$ based on the polarity of the real and imaginary components. The ATAN2(x,y) function accomplishes this task.

The phase of C for the wave exiting the material is directly related to S_{21} phase normalized. S_{21} phase normalized is again the difference between the data with the material sample and the data without the material sample (just free space).

S_{21} phase normalized = S_{21} phase (with sample present) – S_{21} phase (without sample present)

However, the total phase shift in the material sample is the phase shift due to the addition of the sample ($\Delta\Phi$= (360 – S_{21} phase normalized) + 360*n), plus the phase shift in free space in that material distance *l*:

$$Phase(C) = \Delta\Phi + \frac{l}{\lambda} \cdot 360 \quad \text{or,}$$

$$Phase(C) = \Delta\Phi + \frac{freq \cdot l}{c} \cdot 360$$

Therefore, the overall equation becomes:

$$\left(\frac{180}{\pi}\right)\tan^{-1}\left(\frac{Sum\,\mathrm{Im}}{Sum\,\mathrm{Re}}\right) = \Delta\Phi + \frac{freq \cdot l}{c} \cdot 360$$

or

$$\left(\frac{180}{\pi}\right)\tan^{-1}\left(\frac{Sum\,\mathrm{Im}}{Sum\,\mathrm{Re}}\right) = \left(360 - S_{21}\ phase\,normalized\right) + 360 \times n + \frac{freq \cdot l}{c} \cdot 360$$

β can be solved iteratively for the Sum Im and Sum Re equations and substituted into the above equation. Once β is determined, ε_r' can be computed.

$$\beta = \frac{2\pi}{\lambda} = \frac{2\pi\, freq\sqrt{\varepsilon_r'}}{c}$$

or

$$\varepsilon_r^{'} = \left[\frac{c\beta}{2\pi\, freq} \right]^2$$

Additional iterations can be performed with ε_r' and ε_r'' from the previous result.